ROTORCRAFT FLIGHT SIMULATION WITH AEROELASTIC ROTOR AND IMPROVED AERODYNAMIC REPRESENTATION. VOLUME I. ENGINEER'S MANUAL

John M. Davis, et al

Bell Helicopter Company

Prepared for:

Army Air Mobility Research and Development Laboratory

June 1974

Unclassified

SECURITY CLASSIFICATION OF THIS PAGE (When Data Entered)

AD-782854

REPORT DOCUMENTATION PAGE

READ INSTRUCTIONS BEFORE COMPLETING FORM

1. REPORT NUMBER: USAAMRDL-TR-74-10A	2. GOVT ACCESSION NO.
3. RECIPIENT'S CATALOG NUMBER	
4. TITLE (and Subtitle): ROTORCRAFT FLIGHT SIMULATION WITH AEROELASTIC ROTOR AND IMPROVED AERODYNAMIC REPRESENTATION, Volume I, Engineer's Manual	5. TYPE OF REPORT & PERIOD COVERED: Final Technical Report
	6. PERFORMING ORG. REPORT NUMBER: 299-099-813
7. AUTHOR(s): John M. Davis, Richard L. Bennett, Barney L. Blankenship	8. CONTRACT OR GRANT NUMBER(s): DAAJ02-72-C-0098
9. PERFORMING ORGANIZATION NAME AND ADDRESS: Bell Helicopter Company, P. O. Box 482, Fort Worth, Texas 76101	10. PROGRAM ELEMENT, PROJECT, TASK AREA & WORK UNIT NUMBERS
11. CONTROLLING OFFICE NAME AND ADDRESS: Eustis Directorate, U.S. Army Air Mobility Research and Development Laboratory, Fort Eustis, Virginia 23604	12. REPORT DATE: June 1974
	13. NUMBER OF PAGES: 248
14. MONITORING AGENCY NAME & ADDRESS (if different from Controlling Office)	15. SECURITY CLASS. (of this report): Unclassified
	15a. DECLASSIFICATION/DOWNGRADING SCHEDULE

16. DISTRIBUTION STATEMENT (of this Report)

Approved for public release, distribution unlimited.

17. DISTRIBUTION STATEMENT (of the abstract entered in Block 20, if different from Report)

18. SUPPLEMENTARY NOTES

19. KEY WORDS (Continue on reverse side if necessary and identify by block number)

Aerodynamics	Flight Simulation	Dynamics
Aeroelasticity	Helicopters	Structural Properties
Rotors	Control	
Computer Programs	Numerical Analysis	
Digital Computers	Rotary Wing Aircraft	

20. ABSTRACT (Continue on reverse side if necessary and identify by block number)

This report consists of three volumes and documents the current version in the C81 family of rotorcraft flight simulation programs developed by Bell Helicopter Company. This current version of the digital computer program is referred to as AGAJ73.

DD FORM 1 JAN 73 1473 EDITION OF 1 NOV 65 IS OBSOLETE

Unclassified

SECURITY CLASSIFICATION OF THIS PAGE (When Data Entered)

Block 20. Continued

The new, revised, or alternate mathematical models incorporated into the program during the current contract are listed below:

(1) Fuselage aerodynamic forces and moments (revised)

(2) Aerodynamic surfaces (revised with two surfaces added)

(3) External stores/aerodynamic brakes (new)

(4) Rotor blade airfoil section distribution (new)

(5) Rotor-induced velocity distribution (alternate)

(6) Rotor unsteady aerodynamics (alternate)

(7) Rotor wake effect at aerodynamic surfaces (alternate)

(8) Method for numerically integrating rotorcraft equations of motion (alternate)

This first volume, the Engineer's Manual, presents an overview of the computer program capabilities plus discussions for the background and development of the principal mathematical models in the program. The models discussed include those developed under the current contract as well as two previous contracts.

Volume II, the User's Manual, contains the detailed information necessary for setting up an input data deck and interpreting the computed data. Volume III, the Programmer's Manual, includes cross-references of FORTRAN COMMON BLOCK variables, a catalog of subroutines, and a discussion of programming considerations. The listings and related software for the computer programs documented in this report are unpublished data which are on file at the Eustis Directorate, U. S. Army Air Mobility Research and Development Laboratory (USAAMRDL), Fort Eustis, Virginia.

PREFACE

This report and its accompanying computer program were developed under Contract DAAJ02-72-C-0098 awarded in June 1972 by the Eustis Directorate of the U.S. Army Air Mobility Research and Development Laboratory (USAAMRDL). In addition to the work performed under this contract, the report and computer program include the documentation and program features developed under USAAMRDL Contracts DAAJ02-70-C-0063 and DAAJ02-73-C-0086. The contractor and USAAMRDL have agreed that the computer program documented herein is the new master version of the program. Hence, this report supersedes all previous versions of the C81 program and documentation.

Technical program direction was provided by Mr. E. E. Austin of USAAMRDL. Principal Bell Helicopter personnel associated with the current contract were Messrs. B. L. Blankenship, J. M. Davis, P. Y. Hsieh, and Dr. B. T. Waak. In addition, Dr. R. L. Bennett and Mr. B. J. Bird assisted in coordinating the work and documentation prepared under the two previous contracts noted above with that prepared under this contract.

TABLE OF CONTENTS

LIST OF ILLUSTRATIONS

LIST OF TABLES

1. INTRODUCTION

1.1 BACKGROUND

In the early 1960's Bell Helicopter Company began development of a rotorcraft flight simulation program for digital computers. The original program was identified as C81. This identification has since become the family name for many different versions developed over the years. To minimize confusion as to which version of the program is being used or referenced, the more recent versions of the C81 program have been identified by four letters and the year in which they became production programs; e.g., AGAJ71 was developed in 1971, AGAJ72 in 1972. This report documents the current version of C81, AGAJ73.

The early history and basic analysis of C81 are given in Reference 1. The simulation for that study included a rigid body fuselage in three dimensions, coupled with two rotors, for a total of eleven degrees of freedom. The eleven degrees of freedom were:

Six rigid body (total rotorcraft)

Fore-and-aft and lateral flapping for two rotors

Rotor-engine torsional system

A variety of maneuvers were simulated by modeling control motions and external disturbances such as gusts. The program used a quasi-static rotor analysis. Aeroelastic feedback was represented by iteration through a rotor blade dynamic analysis.

The stop-fold rotor simulation study reported in Reference 2 delineates later additions to the program. The resulting computer program (ASAJ01) contained an uncoupled stability analysis which used the trim solutions and partial derivative computations available in the earlier version. Provisions were made to compute stability roots during maneuvers as well as at the trim point. The rotor mathematical model was modified to include the stop-fold rotor concepts. Both the tilt-forward-trail-aft and horizontal-stop-fold configurations were included. The rotor analysis in ASAJ01 was time-variant, but did not contain aeroelastic effects.

The next major expansion of the mathematical model was performed under Contract DAAJ02-70-C-0063 awarded by the Eustis Directorate of the U. S. Army Air Mobility Research and Development Laboratory (USAAMRDL). This AGAJ71 version of the program included the addition of a time-variant-aeroelastic rotor analysis (TVAR), rotor pylon degrees of freedom, unsteady rotor aerodynamic considerations, and a generalized automatic control stability package. The TVAR allowed calculation of time histories of the deflection, shear bending moment, and aerodynamic loading along each individual blade. In combination with the TVAR, the pylon degree of freedom model calculated the linear and angular displacements of each rotor hub.

The unsteady aerodynamic package computed increments to the lift, drag, and pitching moment aerodynamic coefficients in both stalled and unstalled flow as functions of blade bending and pitching velocities and accelerations. The automatic control stability package consisted of a Stability and Control Augmentation System (SCAS), an Automatic Pilot Simulator (APS), and an expanded stability analysis subroutine. Subsequently, under USAAMRDL Contract DAAJ02-71-C-0045, a second mathematical model for unsteady rotor aerodynamics was developed and incorporated in the trim portion of AGAJ71.

Two undocumented versions of the AGAJ72 program were delivered to the Eustis Directorate of USAAMRDL. The first AGAJ72 version included many minor refinements to the AGAJ71 version, while the second, developed under Contract DAAJ02-72-C-0086, included two major additions: an alternate trim procedure and expanded data printout. These two features were primarily incorporated to increase the versatility of the program in simulating wind tunnel tests. The alternate trim procedure provided for locking the rotor flapping angles at their input values and then iterating on control positions to trim the rotor. The additional printout, referred to as the optional trim page, provided data in a form that was most useful when correlating with wind tunnel data (e.g., dimensional and nondimensional force and moment data, a summary of rotor parameters, and test conditions).

Under the most recent USAAMRDL Contract (DAAJ02-72-C-0098), improvements to all aerodynamic representation in the program were developed. Specifically, the following aerodynamic-related modifications and additions were made to the program:

(1) A more accurate and complete representation of fuselage aerodynamic forces and moments.

(2) A single generalized representation for up to five aerodynamic surfaces with control surfaces (one wing and four stabilizing surfaces).

(3) The capability of representing external stores and/or aerodynamic brakes.

(4) The capability of representing up to five different airfoils along the span of the rotor blades.

(5) The capability of representing the induced velocity distribution across the rotor disc as a Fourier series that is a function of advance ratio, inflow ratio, blade station, and blade azimuth.

(6) The capability of representing the rotor wake at each aerodynamic surface as a Fourier series that is a function of rotor advance ratio, inflow ratio, and blade azimuth.

In addition to the above six tasks, the following features were also incorporated:

(7) An alternate method for numerically integrating the rotorcraft equations of motion in maneuvers.

(8) The unsteady aerodynamic model developed under Contract DAAJ02-71-C-0045 modified to work in maneuver as well as trim.

(9) The alternate trim procedure and expanded output developed under Contract DAAJ02-72-C-0086.

In the process of incorporating these eight features, the input format to the program was significantly revised to make the increased versatility of the program easier to use. The benefits of the current aerodynamic representations are discussed below.

1.2 DISCUSSION OF RECENT ADDITIONS

The current mathematical model for the fuselage aerodynamic forces and moments provides very accurate simulation of wind tunnel data, when it is available, but is easily adaptable to analytical estimates of such data when test results are not available. It also makes possible simulation of forces and moments at all possible aerodynamic angles, i.e., pitch between $\pm$ 90 degrees and yaw between $\pm$180 degrees, with a single set of inputs to the program. The representation consists of three models: one for the relatively low angles where the vast majority of flight takes place; a second for the very high angles encountered in such tasks as rearward, sideward, and vertical flight; and a third to provide a smooth transition between the other two models.

The current representation of aerodynamic surfaces provides for simulation of up to four generalized stabilizing surfaces and a wing as compared to two stabilizing surfaces and a wing in previous versions of the program. The restriction that the stabilizing surfaces must lie in a horizontal or vertical plane of the body was removed, thereby allowing simulation of canted fins, V-tails, horizontal stabilizers with dihedral or anhedral, etc. The current model simulates the change in lift, drag, and pitching moment of each surface with control surface deflection and the effects of the fuselage on the flow field at each surface. In addition, either equations or data tables can be used to compute the aerodynamic coefficients.

The capability of simulating external stores and/or aerodynamic brakes has been added to the current version of C81. The input group consists of four identical subgroups, each of which may represent either a store or a brake independently of the other subgroups. This model includes a representation of aerodynamic forces on the store or brake which is similar to the model for the fuselage. When running a maneuver, it is possible to selectively jettison stores and deploy brakes. In the case of store jettison, the aircraft gross weight, center of gravity and inertias are recalculated at the instant of release.

Previously, C81 required that each rotor be simulated with a single airfoil section from root to tip. It is now possible to input to the program the lift, drag, and pitching moment characteristics of up to five airfoil sections and assign any section to any of the twenty segments of the blades of either rotor. The user has the option of simulating each airfoil section with a set of closed-form equations or with data tables.

In earlier versions of C81, the induced velocity distribution over the rotor disc was defined by an equation which included only a first harmonic variation with blade azimuth angle and had all but one of its coefficients defined within the program. The single coefficient which the user could input only affected the distribution on the outboard 30 percent of the blade at predetermined azimuth angles. The program now includes the option of defining the distribution for each rotor with a data table. Each table contains the coefficients of Fourier-series curve-fit of a distribution generated external to C81. With such tables, the effects of inflow ratio and higher harmonic variations on the distribution, which were ignored in the built-in equation, can be included.

The effect of the rotor wake acting at aerodynamic surfaces is represented by superimposing on the flow field at the surface a velocity vector whose magnitude is equal to a factor times the average induced velocity across the rotor disk. In previous versions of the program, this factor was input as either a constant or a linear function of airspeed. In AGAJ73, an option has been added to input tables from which the factor can be computed as a function of advance ratio, inflow ratio, and rotor blade azimuth location. These tables are similar to the rotor induced velocity distribution tables in that they contain the coefficients of a Fourier-series curve-fit of wake data generated external to C81. Each table contains the data for the effect of a part cular rotor on a particular surface.

Several internal changes made to C81 caused the unsteady aerodynamic model developed under Contract DAAJ02-71-C-0045 to become incompatible with the current version of the program. Also, this model could be used only during time-variant trims, not in maneuver. Hence, the model was updated and modified to function in both time-variant trims and maneuvers.

In addition to these changes to the aerodynamic representations in the program, Hamming's predictor-corrector method of numerical integration was installed as an option to the four-cycle Runge-Kutta method previously used. In all, ten methods of numerical integration, including Hamming's and Runge-Kutta, were evaluated in the study which led to the incorporation of Hamming's method. At present, Hamming's method is strictly a programmer rather than a user option in AGAJ73. The detailed reasons for this course of action are discussed in Section II of this volume. It is sufficient to say here that the method did not perform as well within the C81 structure in terms of run time as the study had indicated it would. However, the method does not take significantly more time than the Runge-Kutta method and shows enough promise that its run time can be reduced that it has been retained in the program.

Incorporation of the features developed under Contract DAAJ02-72-C-0086 provides the AGAJ73 user with all the features and options which are currently being maintained in the master version of C81.

1.3 DOCUMENTATION CONSIDERATIONS AND ORGANIZATION

This report has been prepared under Contract DAAJ02-72-C-0098 awarded by the Eustis Directorate of USAAMRDL. However, it also includes documentation prepared under Contract DAAJ02-70-C-0063 and, as noted previously, the features developed under Contracts DAAJ02-70-C-0063, DAAJ02-71-C-0045, and DAAJ02-72-C-0086. The intent of combining the work performed under these four contracts is to provide the user of C81 with a single document to explain the background, development, and current operation of the master version of the computer program.

This volume of the report, Volume I, has been prepared with the following ideas in mind: to document those analyses which are important to understanding the program but not necessary for its execution; to provide background information and the rationale for selecting certain mathematical models over other models; and to suggest areas in which further development of the program is warranted.

Volume II, the User's Manual, provides the information necessary to set up a data deck to successfully execute the simulation, and to interpret the results. Volume III, the Programmer's Manual, contains the information required for setting up the program on the user's computer; brief descriptions of the subroutines are included.

2. COMPUTER PROGRAM ORGANIZATION

The logic of the computer program is organized into three major operations: determination of an equilibrium flight condition, computation of the time history of a prescribed maneuver, and stability analysis. The heart of each operation is the mathematical model of the rotorcraft. The following five subsections present general discussions of the rotorcraft model, the rotor analyses available, and each of the three major operations. Although the general organization of the program is essentially the same as documented in Reference 2, virtually every model and operation in the program has been expanded or revised since the publication of Reference 2.

2.1 MATHEMATICAL MODEL OF THE ROTORCRAFT

The currently programmed mathematical model of the rotorcraft provides for detailed simulation of the following rotorcraft configurations: single main rotor, tandem rotors, and side-by-side (or tilting prop) rotors. The model is broken down into the following major components, each of which is discussed in detail in the indicated section:

(1) Rotors (maximum of two, each with up to seven blades); Section 3

(2) Fuselage (valid in all flight regimes); Section 4

(3) Aerodynamic surfaces (one wing and up to four stabilizing surfaces); Section 5

(4) External stores or aerodynamic brakes (any combination of up to four stores and brakes); Section 6

(5) Auxiliary propulsion (up to two jet thrust vectors); Section 7

(6) Control system (including control of each rotor, aerodynamic surface, and jet; plus a Stability and Control Augmentation System and Automatic Pilot Simulator); Section 8

Since each model is general enough to be adapted to any one of the three rotorcraft configurations, each can provide very detailed simulation of any one configuration.

2.2 ROTOR ANALYSES

Two independent and mutually exclusive rotor analyses are programmed into AGAJ73: quasi-static and time-variant. When development of C81 began in the early sixties, the entire program was predicated on the quasi-static rotor analysis. As part of the contract documented in Reference 2, the time-variant rigid blade rotor analysis was added as an option. Subsequently, under Contract DAAJ02-70-C-0063, an aeroelastic blade representation based on the modal technique was added for use with both types of rotor analyses. Definitions of these two rotor analyses are given below.

2.2.1 Quasi-Static Rotor Analysis

The quasi-static rotor analysis is frequently called the "Frisbee" analysis. This nickname evolved from the fact that a rotor which is termed quasi-static is somewhat analogous to a rotating disk which generates dynamic and aerodynamic forces and moments, like the plastic-disk toy called a Frisbee. A more mathematical definition of the quasi-static analyses is that at any instant in time the frequency of rotor flapping is exactly one per revolution (1/rev). This situation requires that the path of each blade tip during one rotor revolution define a single plane, or disk. Since the locus of the blade tips defines a plane, the orientation of the rotor disk with respect to the rotor shaft can then be defined by two angles: the fore-and-aft and lateral flapping angles. These flapping angles are the dependent variables in the equations of motion of the rotor. Note that the quasi-static analysis does not require that the blades be rigid, but does require that the frequency of any elastic displacements be at 1/rev. Hence, the quasi-static rotor analysis is best suited to teetering or gimbaled rotor systems where the dominant blade motions are at 1/rev and where, for most performance and flying qualities investigations, other flapping frequencies can be neglected. However, the analysis is also suitable for first-order approximations of rigid rotors (where the blade beamwise stiffness is represented in a flapping spring chosen to simulate the blade elastic properties) and articulated rotors (where the flapping hinge offset is represented by a flapping spring chosen to reproduce the flapping natural frequency).

The major limitation of the quasi-static analysis is that only the static and 1/rev component of the blades response are calculated. Consequently, accurate computation of blade loads is not possible. Blade load calculations and printout are bypassed whenever the quasi-static rotor analysis is used.

Computationally, any rotor which uses the quasi-static analysis is in effect modeled as a twelve-bladed rotor at each time (computation) point. The input or computed pair of flapping angles are used to define the orientation of a single representative blade at each twelve equally spaced azimuth angles (30-degree increments). The dynamic and aerodynamic forces and moments are then calculated at each blade station for each azimuth, numerically integrated, and multiplied by the ratio of the actual number of blades to the 12 blades of the computational rotor. Another analogy which may help visualize the quasi-static analysis is to think of each calculation as a time-lapse photograph where the image is that of the forces and moments acting on the rotor when the shutter is left open for exactly one rotor revolution.

2.2.2 Time-Variant Rotor Analysis

The time-variant rotor analysis is predicated on the modal technique of representing rotor blade dynamics. It is this technique, described in detail in Section 3.2, which permits the simulation of an aeroelastic

rotor (i.e., a rotor where the shape and motion of each blade at any instant in time are functions of the aerodynamic loading and the elastic properties of the blade). In the time-variant rotor analysis, each blade is free to respond to aerodynamic and dynamic forces and moments of all frequencies, not just 1/rev, at each instant in time. To continue with the photographic analogy used in the discussion of the quasi-static analysis, each calculation in a time-variant analysis is a snapshot with the same force and moment image, but with the blades frozen in position at the time point. Since the blades are free to respond at all frequencies, the concepts of a tip-path plane and its associated fore-and-aft and lateral flapping angles used in the quasi-static analysis are not meaningful in the time-variant analysis; the meaningful parameters are the angle between the hub and mast plus the inplane, out-of-plane, and torsional displacements, velocities, and accelerations along the span of each blade.

The time-variant analysis is suitable for all types of rotors and should be used whenever possible, particularly for rigid or articulated rotors. It must be used when blade load data are desired.

Computationally, the forces and moments acting on each segment of each individual blade at its instantaneous position are calculated at each time point in the time-variant analysis. The resulting accelerations and current velocities are then numerically integrated to determine the velocities and displacements of each segment of each individual blade at the next time point (azimuth position).

2.3 DETERMINATION OF THE EQUILIBRIUM FLIGHT CONDITION

The technique used to determine the equilibrium, or trimmed, flight condition in AGAJ73 is an enlargement of the technique described in Reference 2. The additional considerations are those required to represent the steady-state solution of the elastic rotor equations and the hub motion and mast windup equations. The technique which had previously been used to trim the rigid blade has been modified to apply to any blade mode that has a natural frequency at or near one per rev.

The standard trim procedure determines the following quantities at each iteration: pilot control positions; angular orientation of the aircraft in space; and a harmonic analysis through one per rev of the participation factor for each mode (maximum of six) for each blade for each rotor, fore-and-aft and lateral hub motion, and mast windup for each rotor. The effects of the elastic blade and hub motions are included in the overall trim procedure to effect a coupled aeroelastic trim solution.

In addition, this standard trim procedure has been modified so that the user can in effect delete the airframe from the procedure and trim an isolated rotor, e.g., a wind tunnel simulation. This added path through the trim procedure allows the user two alternatives: to command the rotor

feathering angles and trim the rotor by iterating on flapping angles, or to command the flapping angles and iterate on the feathering angles. The mathematical techniques used in the standard and alternate trim procedures are discussed in Section 9.

2.4 STABILITY ANALYSIS

The stability analysis in this program is an enlargement of that presented in Reference 2. In the previous analysis, the procedure was based on two uncoupled 3 x 3 sets of equations of motion. In this stability analysis, the following 14 equations of motion can be considered:

(1) Six Rigid Body (total rotorcraft)

(2) Fore-and-Aft and Lateral Pylon Motion for 2 rotors

(3) Fore-and-Aft and Lateral Flapping for 2 rotors

The analysis may be performed for the trimmed flight condition or at specified times during a maneuver. The three stability matrices generated by the analysis can then be punched on cards for additional analysis external to C81.

The derivation of the current stability analysis is predicated on a quasi-static rotor analysis, and is not compatible with the time-variant rotor analysis. Hence, only the steady and one-per-rev response of elastic blades are included in this analysis. The complete equations of motion and the numerical techniques associated with the stability analysis are contained in Section 10.

2.5 MANEUVERS

Compared to the version of C81 documented in Reference 2, the capabilities of the program for computing the time history of a maneuver have been greatly enhanced. The current fully coupled analysis includes the user options of quasi-static or time-variant rotor analyses, rigid or aero-elastic blades, and over thirty different types of variations of control positions, control mechanisms, rotorcraft configuration, etc. In addition, a programmer option is included whereby the equations of motion may be numerically integrated by either the four-cycle Runge-Kutta technique or Hamming's fourth-order predictor-corrector method. The study which lead to the incorporation of Hamming's method is discussed in Section 11.

The program includes three options for reducing the data generated by the maneuver portion of the program. These options include plotting, harmonic analysis, and vector analysis. Each set of reduced data may be output on the printer or a CALCOMP plotter. The data which may be reduced consist of every parameter printed as part of the maneuver time history plus detailed rotor loads and elastic response data, for a total of more than 1300 variables. These 1300 variables may also be stored on magnetic tape and reloaded at a later date for additional analysis.

Another feature of the maneuver portion of the program is the restart capability which permits a long continuous run to be made in several passes. This procedure causes each item on the output page and many intermediate variables to be written also on a magnetic tape, which is saved. Then on subsequent runs, the start time can be any point on the saved tape. In addition, the maneuver cards can be changed on each run.

2.6 PROGRAMMING CONSIDERATIONS

The current program includes a program logic group as the first group of input data. This group allows the user many options as to the data to be read in and the analyses to be performed. In view of the large number of cards required to use every capability of the mathematical models, these logic controls can greatly reduce the size of a deck when a particular option is not to be used.

The contractor's version of the program includes a data library which permits the storage of complete rotorcraft configurations, or individual components (input groups) on magnetic disk. These data may then be called from storage by the first card of each input group. This feature greatly reduces the number of cards which must be included in the input deck and assures consistency in at least the initial input data when many people are making runs with the same configuration. Any parameter in most of the groups stored in the data library may be changed during read-in if the user so desires.

During the latest major revision to the program, the output formats for the trim iterations, trimmed flight condition page, and the maneuver-time-point page were revised as a result of user suggestions. In particular, formats for the trim and maneuver pages were greatly expanded and made quite similar to each other. All data printed by previous versions of the program have been retained and much has been added.

3. ROTOR MATHEMATICAL MODEL

3.1 INTRODUCTION

The Rotorcraft Flight Simulation Program uses the identical mathematical model for both rotors. The only major restrictions on the currently programmed model are that for a given rotor the number of blades must be between two and seven inclusive, the physical properties of each blade must be identical, and the rigid body feathering axes of the blades must be equally spaced around the rotor azimuth.

Some of the most useful features of the model are the options for inputting any of the following blade properties as distributions along the span of the blade rather than single values: twist, chord, airfoil section, mass, mass moments of inertia, and elasticity (aeroelastic mode shapes). These distributions contain data either for twenty blade segments or at twenty-one radial stations. Other blade parameters in the model include tip sweep, hub drag, precone angle, a lead-lag damper, flapping restraint and stops, and pitch-flap coupling. The possibilities for the rotor hub model include teetering (or gimbaled), articulated, and rigid. Also, undersling, the vertical distance between the flapping and feathering axes, may be simulated for teetering or gimbaled rotors.

Each rotor shaft (mast) may be given any desired orientation with respect to the airframe and can have torsional degree of freedom. In addition, a nonisotropic dynamic pylon model is included to simulate the mounting of the transmission/rotor shaft or gearbox/shaft system to the airframe.

The above model features relate primarily to the physical properties of the rotor systems and, hence, are used in the dynamic analysis of the rotor. The model also includes detailed aerodynamic analysis. This analysis is divided into two subanalyses: steady-state and unsteady aerodynamics. The steady-state aerodynamics are determined from sets of either equations or data tables. The choice of equations or tables is a user option. The option may be exercised for either an entire blade or each of the twenty blade segments.

The user also has the option of either an equation or a data table for computing the induced velocity distribution over the rotor disc. The table contains coefficients of a Fourier-series curve fit of wake data computed external to C81. The table is tri-variant with arguments of advance ratio, inflow ratio, and blade station. The aerodynamic analysis also includes two methods for computing increments to the steady-state aerodynamic coefficients due to time derivatives of the blade angle of attack. These methods, referred to as the BUNS and UNSAN unsteady aerodynamic options, and their accompanying models for yawed flow are independent and mutually exclusive. That is, the user may activate either the BUNS or UNSAN option

with or without its respective yawed flow models; alternatively, both unsteady models can be deactivated, and one or none of the yawed flow models can be activated.

This section of the report contains the dynamic and aerodynamic analyses incorporated into the rotor mathematical model. The next subsection discusses the dynamic analysis with emphasis on the modal technique used to simulate blade elasticity. Following the dynamic discussion, the aerodynamic analysis is presented with emphasis on the procedure for computing the angles of attack, Mach number, and dimensional forces and moments at a blade station and on the two models for unsteady aerodynamic effects. The model for calculating the steady-state coefficients is discussed in detail in Section 3.5 of Volume II; only selected information is repeated or expanded on in this volume.

3.2 DYNAMICS

3.2.1 General

The rotor analysis in the previous version of the Rotorcraft Flight Simulation Program ASAJ01 (Reference 2) is based on the rigid blade assumption and is therefore incapable of describing the time-variant aeroelastic behavior of the rotor blade. Because of the improved and enlarged digital computer facilities, and the desire for a more refined rotor analysis, a time-variant aeroelastic rotor analysis based on the modal technique has been added to ASAJ01. The resulting computer program is AGAJ73.

3.2.2 Differential Equations of Motion and Solution Techniques

The inclusion of a time-variant aeroelastic rotor analysis in a helicopter flight simulation program requires:

(1) Aeroelastic Rotor Analysis

- (a) Derivation of differential equations of motion
- (b) Solution technique for differential equations of motion

(2) Helicopter Flight Simulation Program

- (a) Representation of gross helicopter behavior
- (b) Determination of equilibrium flight conditions
- (c) Ability to integrate numerically equations of motion

(3) Interface between Rotor Analysis and Flight Simulation Program

- (a) Effect of rotor behavior on helicopter behavior
- (b) Effect of helicopter behavior on rotor behavior

The first step in developing an aeroelastic rotor analysis is the derivation of the differential equations of motion. The differential equations of motion for the combined inplane, out-of-plane, and torsional deformations of a twisted nonuniform rotating rotor blade were derived by Houbolt and Brooks (Reference 3).

These equations include the effect of the noncoincidence of the mass and elastic axes which produces the coupling between the inplane and torsional deformations, and between the out-of-plane and torsional deformations. The coupling between the inplane and out-of-plane deformations is caused by the unsymmetric bending of the cross section. The equations by Houbolt and Brooks adequately describe the dynamic considerations which influence the blade response; however, only passing attention is devoted to defining the aerodynamic and aeroelastic effects which also influence the blade response. If these aerodynamic forces are taken to be zero, then the equations for free vibration result.

There are several techniques for solving the free vibration equations of an elastic structure. Most outstanding among these techniques are the Rayleigh-Ritz, Stodola, and the Myklestad methods (Reference 4). The solution to the free vibration equations can be represented as a set of natural frequencies, and associated with each natural frequency, a corresponding mode shape. These natural frequencies and mode shapes are essential to the solution technique used to describe the time-variant aeroelastic rotor behavior.

The differential equations derived by Houbolt and Brooks do not lend themselves to closed-form solution technique for all possible combinations of the externally applied loads. Oette (Reference 5) shows how the separation of variables technique can be applied to the Houbolt equations. If the independent variables are assumed to be time t, and location along the blade x, then it is possible to write

$$\begin{bmatrix} Y(x,t) \\ Z(x,t) \\ \theta(x,t) \end{bmatrix} = \sum_{n=1}^{NM} \begin{bmatrix} Y_n(x) \\ Z_n(x) \\ \theta_n(x) \end{bmatrix} \delta_n(t) \qquad (3\text{-}1)$$

where Y, Z, and θ are the total elastic deformation of the blade; Y_n, Z_n, and θ_n are the components of the n^{th} normalized mode shape; and $\delta_n(t)$ is the participation factor associated with the n^{th} mode shape; Y and Y_n

refer to the inplane deformation; Z and Z_n refer to the out-of-plane deformation; θ and θ_n refer to the torsional deformation of the blade. Let it be assumed that at any point along the blade at a distance x from the hub centerline, and at any point in time t, the externally applied inplane force is F_y, the out-of-plane force is F_z, and the moment tending to twist the blade is M_θ. Oette demonstrates that

$$\ddot{\delta}_n + \omega_n^2 \delta_n = \frac{\int_o^R (F_y \cdot Y_n + F_z \cdot Z_n + M_\theta \cdot \theta_n) dx}{I_n} \qquad (3\text{-}2)$$

where ω_n is the natural frequency of the n^{th} mode of free vibration, and I_n is the generalized inertia of the n^{th} mode shape. For small amounts of viscous damping ζ_n, Equation (3-2) can be written

$$\ddot{\delta}_n + 2\zeta_n \dot{\delta}_n \omega_n + \omega_n^2 \delta_n = \frac{F_n}{I_n} \qquad (3\text{-}3)$$

where F_n is shown in Equation (3-2). There will be an equation of the above type for each mode included in the response analysis.

The development by Oette assumes the helicopter to be in unaccelerated flight, so only the externally applied aerodynamic forces would be included in F_n. Any nonuniform motion of the blade reference coordinate system would produce inertial type forces acting on the blade. These inertial forces should be included in F_n. Examples of the inertial forces would be the "gyroscopic effects" produced by the fuselage angular rates and accelerations. Likewise, the linear accelerations of the hub would also produce inertial forces to be included in F_n.

As indicated by Oette another source of terms to be included in F_n is any elastic velocity dependent dynamic terms deleted from the calculation of the blade natural frequencies and mode shapes. A classic example of these terms is the Coriolis accelerations dependent on the product of blade displacement and blade velocity, which are typically left out of the mode calculations.

The set of modal equations, Equation (3-3), is sufficient to describe the time-variant aeroelastic response of a rotor blade because: (a) the effects of the blade's mass, elastic, and geometric properties are included in the natural frequencies and mode shapes, and (b) the aerodynamic and aeroelastic effects are included in F_n.

The Rotorcraft Flight Simulation Program (C81) has been modified to include a time-variant aeroelastic rotor representation based on the modal

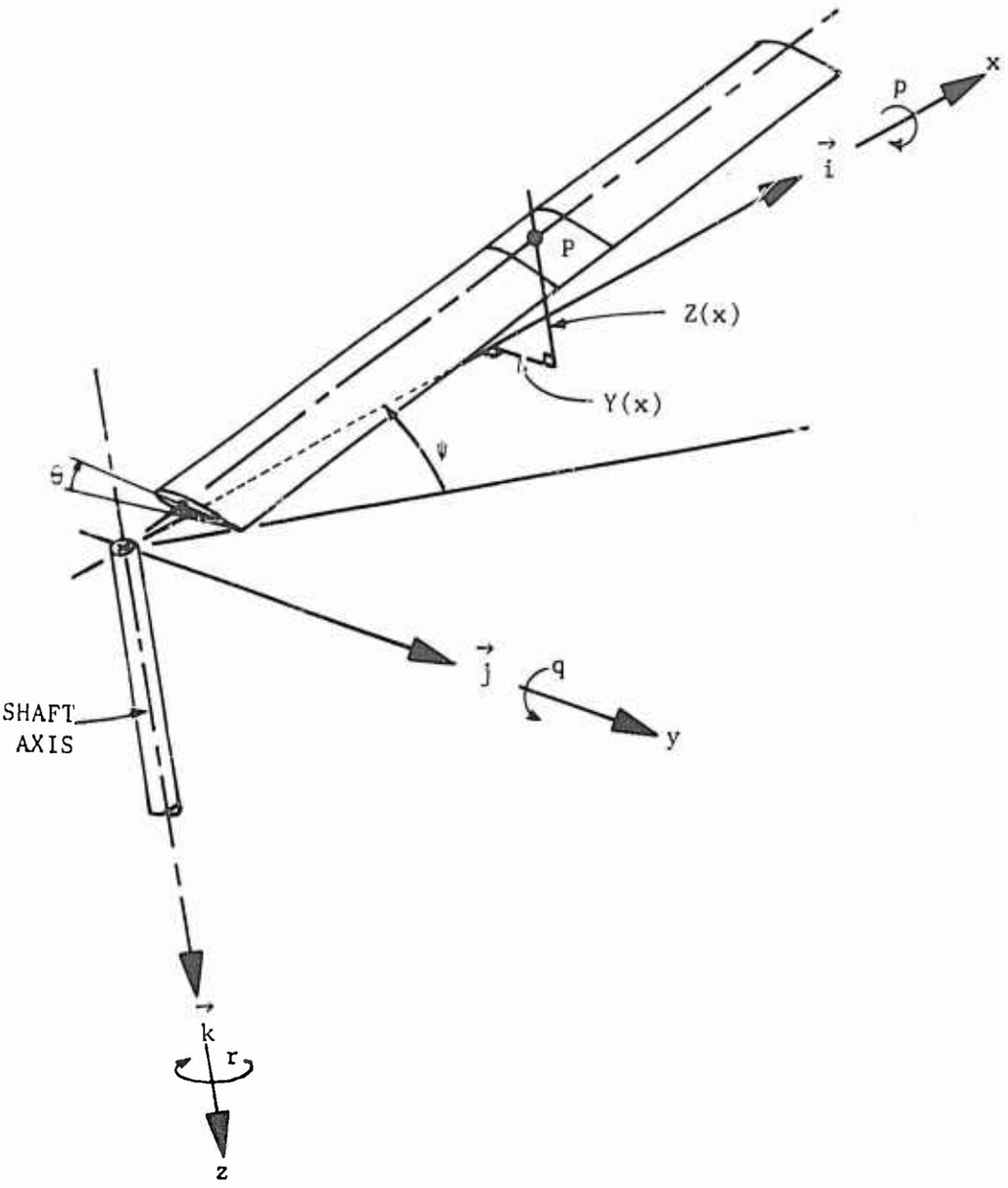

Figure 3-1. Reference System for Rotor Analysis.

techniques with the provision that the blade natural frequencies and mode shapes will be supplied as input data.

Since the derivation of the differential equations of motion and a practical method of solution of the equations have been fully described in the literature, they will not be repeated in this document. What will be emphasized is how these methods are included in the C81.

3.2.3 Reference Coordinate System

The dynamic analysis is performed in the shaft reference coordinate system shown in Figure 3-1. For the particular blade under consideration, the unit vector $\vec{I}$ is perpendicular to the shaft and positive out along the blade radial axis. The unit $\vec{J}$ is perpendicular to the shaft and perpendicular to the unit vector $\vec{I}$. The positive $\vec{J}$ vector is pointed toward the trailing edge of the blade. The unit vector $\vec{k}$ is pointed down along the shaft. The location of any point on the blade relative to the hub can be expressed as

$$\vec{\rho} = X\vec{I} + Y\vec{J} + Z^*\vec{k} \tag{3-4}$$

where X, Y, and Z* are the magnitudes of the displacements. Since it is convenient to consider upward blade displacements as positive, the relationship $Z = -Z^*$ is used throughout this analysis; hence,

$$\vec{\rho} = X\vec{I} + Y\vec{J} - Z\vec{k} \tag{3-5}$$

The angular velocity, ω_b, of this reference frame, relative to an inertial reference system, is given by

$$\vec{\omega}_b = p_b\vec{I} + q_b\vec{J} + r_b\vec{k} \tag{3-6}$$

where p_b, q_b and r_b are the three components which include such items as rotor speed, angular velocities of the rigid body fuselage and the mast angle.

3.2.4 Application of Modal Technique

The displacement $\begin{bmatrix} Y(x,t) \\ Z(x,t) \\ \theta(x,t) \end{bmatrix}$ of any point on the blade relative to its undeflected position at a radial distance x and at time t is approximated by

$$\begin{bmatrix} Y(x,\ t) \\ Z(x,\ t) \\ \theta(x,\ t) \end{bmatrix} = \sum_{n=1}^{NM} \begin{bmatrix} Y_n(x) \\ Z_n(x) \\ \theta_n(x) \end{bmatrix} \delta_n(t) \tag{3-7}$$

where $\begin{bmatrix} Y_n(x) \\ Z_n(x) \\ \theta_n(x) \end{bmatrix}$ is the n^{th} normalized mode of free vibration, NM is the total number of mode shapes to be used, and $\delta_n(t)$ is the participation factor or generalized coordinate associated with the n^{th} mode shape. The functional notation is used to emphasize the fact that the displacement of the blade element is a function of both the radial distance x, and time t.

To implement the modal technique in the computer program, the following assumptions have been made:

(1) The blade is divided into 20 equal radial segments for aerodynamic and dynamic calculations.

(2) Each of the 21 segment faces has three degrees of freedom: out-of-plane (Z), inplane (Y), and angular orientation of chordline about the positive x axis (θ).

(3) The user will supply up to six normalized mode shapes which describe Z_n, Y_n, and θ_n for each of the 21 segment faces for each mode shape.

(4) Linear interpolation can be used to define Z_n, Y_n, and θ_n between two adjacent faces.

(5) All spanwise integrals are to be taken in the Stieltjes sense.

(6) The maximum number of blades per rotor is seven.

(7) The maximum number of input mode shapes per rotor is six.

(8) The maximum number of rotors is two.

It is important to note that any assumptions made in the derivation of the mode shapes will also be applicable to the entire analysis.

As indicated, the program is structured to handle fully coupled mode shapes, which means that each blade element can have three degrees of freedom: vertical Z, inplane Y, and torsional θ.

$$MS_n(x) = \begin{bmatrix} Y_n(x) \\ Z_n(x) \\ \theta_n(x) \end{bmatrix} \tag{3-8}$$

where $\theta_n(x)$ is the radial distribution of the angular orientation of the chordline and is positive leading edge up. $Y_n(x)$ is the inplane displacement and is positive toward the trailing edge. $Z_n(x)$ is the out-of-plane displacement of the blade element and is positive in the direction of conventional positive aerodynamic lift. Any component (vertical, inplane, or torsional) of a mode can be deleted from the analysis by having the particular deflection distribution set to zero.

The mode shapes given by Equation (3-8) have several important attributes:

(1) Each one is a solution to the coupled differential equations of free vibration (obtained by deleting all velocity dependent terms) of the total system (see Reference 3).

(2) Associated with each mode shape is a natural frequency ω_n.

(3) Each mode shape must satisfy a set of physical boundary conditions that could exist on the blade.

(4) The collection of mode shapes forms an orthogonal set of functions.

This set of attributes makes possible the modal method of structural analysis. The boundary conditions are a function of the hub type, and must describe the physical constraints for the inplane, out-of-plane, and torsional behavior at the hub. To simplify the discussion, the mode shapes will be arbitrarily labeled either cyclic, collective, or scissor. These definitions and the selection of blade mode type are discussed in more detail in Section 3.2.10.

The inplane boundary condition is closely related to whether or not the mast is free to "wind up" in response to the total inplane torque. A cantilever inplane boundary condition is equivalent to assuming the mast to be infinitely stiff in torsion, while a pinned inplane condition is compatible with a mast with zero torsional stiffness.

A second, entirely different, method of describing the mast "windup" behavior is to write a completely separate differential equation for the mast "windup." If this additional differential equation is to be used, then all reference to the "mast windup" in the mode shapes must be eliminated; i.e., all inplane boundary conditions must be cantilever. The primary advantage of the mast windup differential equation is that it permits any degree of inplane fixity rather than the idealized conditions used in the definition of the mode shape.

The selection of which mode shape--cyclic, collective, or scissor--is a function of the hub type, and whether or not a separate differential equation is used to describe the mast windup. The selection processes are described in detail in Section 3.2.10.

The input mode shapes must be combined to give the elastic response of the blade according to Equation (3-7). The differential equation describing the response of each mode is

$$\ddot{\delta}_n(t) = \frac{F_n}{I_n} - \omega_n\left(2\zeta\dot{\delta}_n(t) + \omega_n\delta_n(t)\right) \qquad (3\text{-}9)$$

where ω_n is the natural frequency of the n^{th} mode shape and ζ_n is the structural damping factor. The term I_n is the generalized inertia associated with the n^{th} mode shape and is defined by Oette (Reference 5) to be

$$I_n = \int_o^R \left\{ M\left[Y_n^2 + Z_n^2 + 2\ell\, Y_n\theta_n \sin\theta_p - 2\ell\, Z_n\theta_n \cos\theta_p\right] + \left[\rho I_b + \rho I_c\right]\theta_n^2 \right\} dx \qquad (3\text{-}10)$$

where at a radial distance x,

M is the blade mass per unit length.

ℓ is the distance from the blade shear center to the reference axis.

ρI_c is the blade cross-sectional mass moment of inertia about the chord line per unit length.

ρI_b is the blade cross-sectional mass moment of inertia per unit length about an axis perpendicular to the chord line and intersecting at the quarter chord.

θ_p is the geometric pitch.

Since the terms containing ℓ are small in comparison with the other terms, they have been deleted in the calculation of the generalized inertia.

The term F_n in Equation (3-9) is described as the virtual work done by all of the externally applied aerodynamic forces and inertial forces associated with the nonuniform frame of reference, if these forces were to act through a virtual displacement equal to the input mode shape.

Thus,

$$F_n = \int_o^R \left| F_y \cdot Y_n + F_z \cdot Z_n + M_\theta \cdot \theta_n \right| dx \qquad (3\text{-}11)$$

where at a radial distance x,

F_y is the externally applied force in the Y direction (+ aft)

F_z is the externally applied force in the Z direction (+ up)

M_θ is the externally applied pitching moment (+ nose up)

Furthermore,

$$\begin{aligned} F_y &= A_y + I_y \\ F_z &= A_z + I_z \\ M_\theta &= A_\theta + I_\theta \end{aligned} \qquad (3\text{-}12)$$

It is important to note that F_y in Equation (3-12) is the sum of the externally applied aerodynamic forces A_y, given by Equation (3-142) plus the inertial forces I_y due to the nonuniform motion of the reference frame as described by Equations (3-28). F_z is the sum of the aerodynamic forces A_z shown by Equation (3-143) and the inertial forces given by Equation (3-29). The term M_θ includes the aerodynamic pitching moment A_θ as given by Equation (3-144) plus the inertial load due to the feathering acceleration as given by Equation (3-30). As will be seen in a later section, the inertial forces I_y and I_z are modified to account for externally applied mechanical forces produced by the precone effect given by Equation (3-31); the flapping spring, Equation (3-35); the flapping stop, Equation (3-34); and the lead-lag damper, Equation (3-38). In this manner, the rotor dynamic behavior reflects both the rotor aerodynamic

effects plus the dynamic effects of the rotor support system. The solution of Equation (3-11) in conjunction with Equation (3-9) leads to the time-variant behavior of the rotor blade. Equation (3-7) can be differentiated with respect to time to give the velocity of the blade segment, and is given by

$$\begin{bmatrix} \dot{Y}(x,t) \\ \dot{Z}(x,t) \\ \dot{\theta}(x,t) \end{bmatrix} = \sum_{n=1}^{NM} \begin{bmatrix} Y_n(x) \\ Z_n(x) \\ \theta_n(x) \end{bmatrix} \dot{\delta}_n(t) \qquad (3\text{-}13)$$

and the acceleration is given by

$$\begin{bmatrix} \ddot{Y}(x,t) \\ \ddot{Z}(x,t) \\ \ddot{\theta}(x,t) \end{bmatrix} = \sum_{n=1}^{NM} \begin{bmatrix} Y_n(x) \\ Z_n(x) \\ \theta_n(x) \end{bmatrix} \ddot{\delta}_n(t) \qquad (3\text{-}14)$$

The blade element displacement, velocity and acceleration as given by Equations (3-7), (3-13) and (3-14) are with respect to the reference coordinate system. As described in Section 3.3, the aerodynamic calculations have included the effects of the blade element displacements, velocities, and accelerations, so that the dynamic analysis becomes an aeroelastic analysis. The technique used for solving the basic modal equation depends on the character of F_n. If F_n can be accurately expressed as a Fourier series, then Equation (3-9) can be solved in closed form for the particular solution of the differential equation. That is precisely the technique used in the "elastic trim" procedure as described in Section 9, because in steady-state flight, F_n can be accurately expressed in terms of integer rotor harmonics.

During the maneuver portion of the program, Equation (3-9) for each blade for each mode for each rotor is numerically integrated using a four-cycle Runge-Kutta technique. Thus, at each time point, F_n must be evaluated to define the total aerodynamic and inertial forces. The numerical solution to Equation (3-9) gives both the particular solution which will be in terms of the rotor harmonics, as well as the complementary solution which will be a function of the input natural frequencies. The program is structured so that during the trim procedure, the steady-state response or particular solution for Equation (3-9) is obtained. Once the steady-state solution is known, the initial values for $\delta_n(0)$, $\dot{\delta}_n(0)$, and $\ddot{\delta}_n(0)$ can be obtained. The use of these initial values tends to smooth out any

discrepancies in entering the maneuver. It also tends to suppress the complementary solution for a steady-state maneuver.

3.2.5 Inertial Force Distribution on Blade

In Equation (3-12), it was shown that the forcing function F_n contains the distribution inertial forces associated with the nonuniform motion of the frame of reference. From basic kinematics, it can be shown that the total acceleration $\vec{a}_p$ of any point on the blade, relative to an inertial coordinate system, is given by

$$\vec{a}_p = \ddot{\vec{R}}_H + \ddot{\vec{\rho}} + \left[\vec{\omega}_b \times \left(\vec{\omega}_b \times \vec{\rho}\right)\right] + \left[\dot{\vec{\omega}}_b \times \vec{\rho}\right] + \left[2\vec{\omega}_b \times \dot{\vec{\rho}}\right] + l_F \ddot{a}_F + l_L \ddot{a}_L + x\ddot{\psi}_T \tag{3-15}$$

where $\vec{R}_H$ is the rigid fuselage linear acceleration of the origin of the moving coordinate system and $\vec{\rho}$ and $\vec{\omega}_b$ have been defined by Equations (3-5) and (3-6), respectively. The last three terms are the blade accelerations produced by the elastic hub motions and the mast windup as discussed in Section 3.2.9. Each mass point on the blade, when multiplied by $\vec{a}_p$ as given by Equation (3-15), would produce a force that must be accounted for in the elastic rotor analysis. There is also an inertial moment due to cyclic feathering acceleration that would tend to twist the blade.

It is necessary to consider each term in Equation (3-15) in one of the following manners:

(1) Included in the calculation of the blade natural frequencies mode shapes

(2) Included in the externally supplied forcing function as indicated by Equation (3-12), or

(3) Assumed small in comparison with other terms present and thus may be neglected.

The first term in Equation (3-15) is linear acceleration of the hub relative to ground as expressed in the rotating coordinate system. This term includes the linear acceleration of and the angular acceleration about the fuselage cg, and these terms have been considered in previous versions of the program (see Reference 2). The only modification that has been made to this term in the present version is the addition of the elastic pylon motion which is discussed in Section 3.2.9. All terms relating to

$\ddot{\vec{R}}_H$ must be treated as externally applied distributed inertial forces.

All inertial forces associated with the second term, $\ddot{\vec{\rho}}$, in Equation (3-15) have been included in the calculation of the blade mode shapes and natural frequencies because $\ddot{\vec{\rho}}$ is the mass point acceleration in the shaft axis system and cannot be used to describe the nonuniform motion of the reference axis system.

The third term in Equation (3-15) gives rise to some interesting terms. Using Equations (3-5) and (3-6),

$$\vec{\omega}_b \times \left(\vec{\omega}_b \times \vec{\rho}\right) = \vec{i}\left[q_b p_b Y - x q_b^2 - x r_b^2 - p_b Z r_b\right] + \vec{j}\left[+ q_b Z r_b - Y r_b^2 - p_b^2 Y + x p_b q_b\right] + \vec{k}\left[p_b x r_b + p_b^2 Z + q_b^2 Z + Y q_b r_b\right] \qquad (3\text{-}16)$$

Now let it be assumed that the product of any blade displacement times any fuselage rate is small in comparison to the other terms. Thus,

$$\vec{\omega}_b \times \left(\vec{\omega}_b \times \vec{\rho}\right) = -r_b^2 x \vec{i} + x p_b r_b \vec{k} - r_b^2 Y \vec{j} \qquad (3\text{-}17)$$

The $\vec{i}$ component of Equation (3-17) is the centripetal acceleration term which has been included in the calculation of the blade natural frequencies and mode shapes. The term Yr_b^2 is assumed to have been included in the calculation of the normal modes. Now let it be assumed that $r_b = -\Omega$ is the rotor speed. Then the $\vec{k}$ component of Equation (3-17) becomes

$$\vec{\omega}_b \times \left(\vec{\omega}_b \times \vec{\rho}\right) = -\Omega p_b x \vec{k} \qquad (3\text{-}18)$$

which is one component of the gyroscopic terms mentioned in Reference 2 and which must be treated as externally applied distributed inertial forces.

If the centripetal acceleration and the term Yr_b^2 are not included in the calculation of the blade natural frequencies and mode shapes, then the inertial force due to these effects must be treated as an externally applied force on the response calculation. This condition would correspond

to the use of nonrotating natural frequencies and mode shapes. It is assumed in this analysis that the centripetal acceleration has been included in the natural frequencies, and can thus be neglected in the externally applied forcing function.

The fourth term in Equation (3-15) can be written as

$$\dot{\vec{\omega}}_b \times \vec{\rho} = \vec{i}\left[+\dot{q}_b Z - Y\dot{r}_b\right] + \vec{j}\left[x\dot{r}_b + \dot{p}_b Z\right] + \vec{k}\left[\dot{p}_b Y - \dot{q}_b x\right] \tag{3-19}$$

Again, it is assumed that all products involving the elastic displacement of the blade times an angular velocity at the fuselage are small, so that Equation (3-19) can be written

$$\dot{\vec{\omega}}_b \times \vec{\rho} = x\dot{r}_b\vec{j} - \dot{q}_b x\vec{k} \tag{3-20}$$

or

$$\dot{\vec{\omega}}_b \times \vec{\rho} = -x\dot{\Omega}\vec{j} - \dot{q}_b x\vec{k} \tag{3-21}$$

The $\vec{j}$ component is the result of the mast windup differential equation mentioned in the discussion of the input mode shape. This component is most important in its relationship to the Coriolis forces. The $\vec{k}$ component is the second part of the gyroscopic terms discussed in Reference 2. The inertial terms produced by Equation (3-21) must be treated as externally applied distributed inertial forces.

The last term in Equation (3-15) produces the Coriolis terms and may be written

$$2\vec{\omega}_b \times \dot{\vec{\rho}} = 2\left[\vec{i}\left(-\dot{Z}q_b - \dot{Y}r_b\right) + \vec{j}\left(\dot{x}r_b + p_b\dot{Z}\right) + \vec{k}\left(p_b\dot{Y} - \dot{x}q_b\right)\right] \tag{3-22}$$

or, to be consistent with the previous assumptions,

$$2\vec{\omega}_b \times \dot{\vec{\rho}} = -2\dot{x}\Omega\vec{j} \quad -2\dot{Y}r_b\vec{i} \tag{3-23}$$

To better understand the first term on the right side of Equation (3-23), refer to Figure 3-2, where from the geometry it can be written

$$x = \sqrt{r^2 - (Z-h)^2} \tag{3-24}$$

where r is the radial distance from the origin to the point P, which can be differentiated to give

$$\dot{x} = \frac{-\dot{Z}(Z-h)}{\sqrt{r^2 - (Z-h)^2}} \tag{3-25}$$

where h is the underslinging.

Equation (3-25) can then be combined with Equation (3-23) to give

$$2\vec{\omega}_b \times \dot{\vec{\rho}} = \frac{2\Omega\dot{Z}(Z - h)}{\sqrt{r^2 - (Z-h)^2}} \tag{3-26}$$

which is usually referred to as the Coriolis acceleration and must be treated as an externally applied distributed inertial force. The term h is the underslinging. The location of the axis of constant rotational speed has a significant effect on the Coriolis acceleration term. If the inercia of the rotor is large in comparison to the mast stiffness, and the rotor is free to flap, then the axis of constant rpm will be perpendicular to the tip-path plane. Conversely, the axis of constant rpm would be along the mast. These conditions are approximated by removing the rigid blade component, if any, from Z and $\dot{Z}$ prior to calculating the Coriolis term. A more complete discussion of underslinging is given in Reference 6. The second term on the right side of Equation (3-23) is the Coriolis acceleration due to the change in centripetal acceleration generated by the inplane elastic velocity. This term has a significant effect on the elastic hub motion. Now it becomes possible to rewrite Equation (3-15) in the following form:

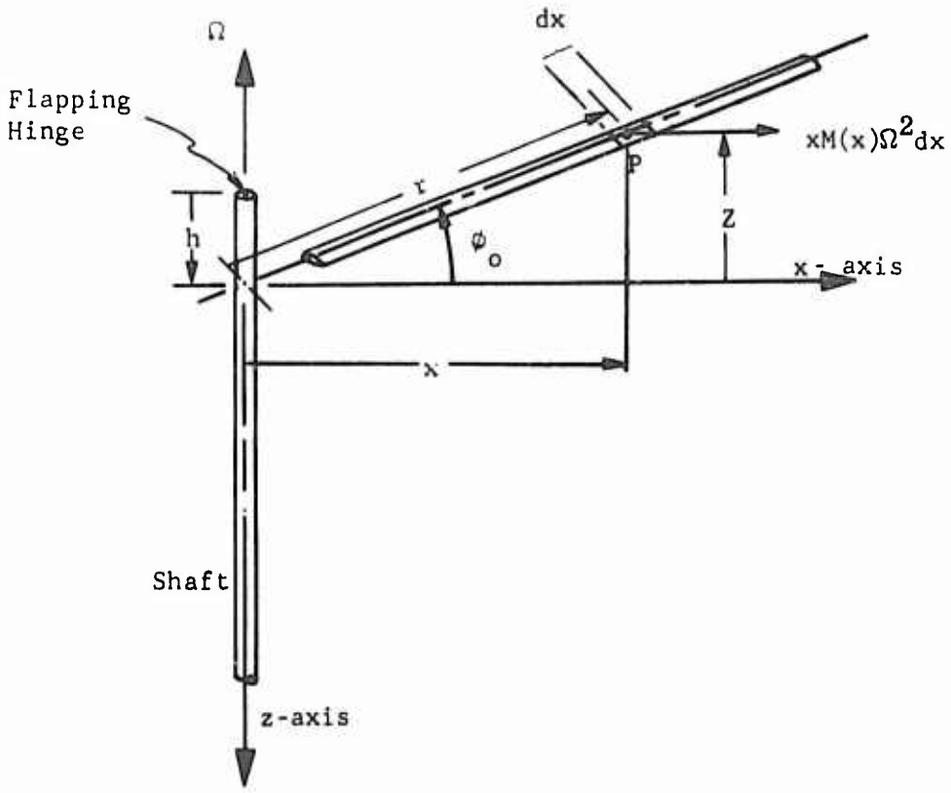

Figure 3-2. Undersling and Precone Effect.

$$\vec{a}_p = \ddot{\vec{R}}_H \qquad \text{(rigid hub acceleration)}$$

$$+ l_F\ddot{a}_F + l_L\ddot{a}_L \qquad \text{(elastic hub acceleration)}$$

$$- \Omega p_b x\vec{k} \qquad \text{(gyroscopic)}$$

$$- \dot{q}_b x\vec{k} \qquad \text{(gyroscopic)}$$

$$- \ddot{\psi}_T x\vec{j} \qquad \text{(mast windup)}$$

$$+\left(\frac{2\Omega\dot{Z}(Z-h)}{\sqrt{r^2-(Z-h)^2}}\right)\vec{j} \qquad \text{(Coriolis)}$$

$$- 2\dot{Y}\Omega\vec{i} \qquad \text{(Coriolis)} \qquad (3\text{-}27)$$

where the terms without the unit vector are calculated in the fixed coordinate system and must be transformed into the rotating coordinate system. In Equation (3-27) the first six terms on the right-hand side account for the nonuniform motion of the blade reference coordinate system. The last two terms represent the velocity dependent dynamic terms which have been left out of the mode shape calculation.

In keeping with the previously introduced notation, the inertial components from Equation (3-27) may be written as

$$I_y = \left[\left(\ddot{R}_{H_y} + l_L\ddot{a}_L\right)\cos\psi - \left(\ddot{R}_{H_x} + l_F\ddot{a}_F\right)\sin\psi + x\ddot{\psi}_T + \frac{2\Omega\dot{Z}(Z-h)}{\sqrt{r^2-(Z-h)^2}}\right] M \qquad (3\text{-}28)$$

$$I_z = \left(-\dot{q}_b x - \Omega p_b x\right) M \qquad (3\text{-}29)$$

and $$I_\theta = -\ddot{\theta}_c(\rho I_b + \rho I_c) - \theta_c\Omega^2(\rho I_b - \rho I_c) \qquad (3\text{-}30)$$

In Equation (3-30), the first term on the right side is the moment produced by the cyclic acceleration of the blade, while the second term is the incremental centrifugal twisting moment due to the cyclic pitch, θ_c. The tennis-racket moment due to the collective pitch is included in the blade natural frequencies and mode shape.

Since both the aerodynamic forces (see Section 3.3) and the distributed inertial forces are now known, it is possible to define the total forcing function F_n for each modal equation as given in Equation (3-11), which can then be used to calculate the time-variant aeroelastic response of the rotor system.

3.2.6 Precone Effects

If the precone angle ϕ_o has not been considered during the calculation of the rotor natural frequencies, then precone must be included as an externally applied forcing function. This can be done in the following manner:

(1) Let it be assumed that the equilibrium position for all mode shapes is the preconed position.

(2) The centrifugal force term $xM\Omega^2$ can then be broken into two components: $xM\Omega^2 \sin\phi_o$, which is perpendicular to the blade, and $xM\Omega^2 \cos\phi_o$, which is along the blade (see Figure 3-2).

(3) Prior to calculating the forcing function for each mode shape, the externally applied air loads should be modified by the precone force $xM\Omega^2 \sin\phi_o$ in the following manner:

$$\Delta I_z = xM\Omega^2 \sin\phi_o \qquad (3\text{-}31)$$

ΔI_z as given by Equation (3-31) should be added to the right side of Equation (3-29).

3.2.7 Flapping Springs, Flapping Stops, and Lead-Lag Dampers

Some rotor configurations can be equipped with hardware that generate mechanical forces that must be considered in an elastic rotor analysis. Among these items are flapping springs, flapping stops, and lead-lag dampers. To consider the first two items, refer to Figures 3-3 and 3-4. Let it be assumed that the flapping stop is placed at some angle β_{stop}, and that there is an associated spring with a spring rate k_1 in.-lb/rad. The flapping stop is simulated by a nonzero value of β_{stop}, and a much larger spring rate (k_2).

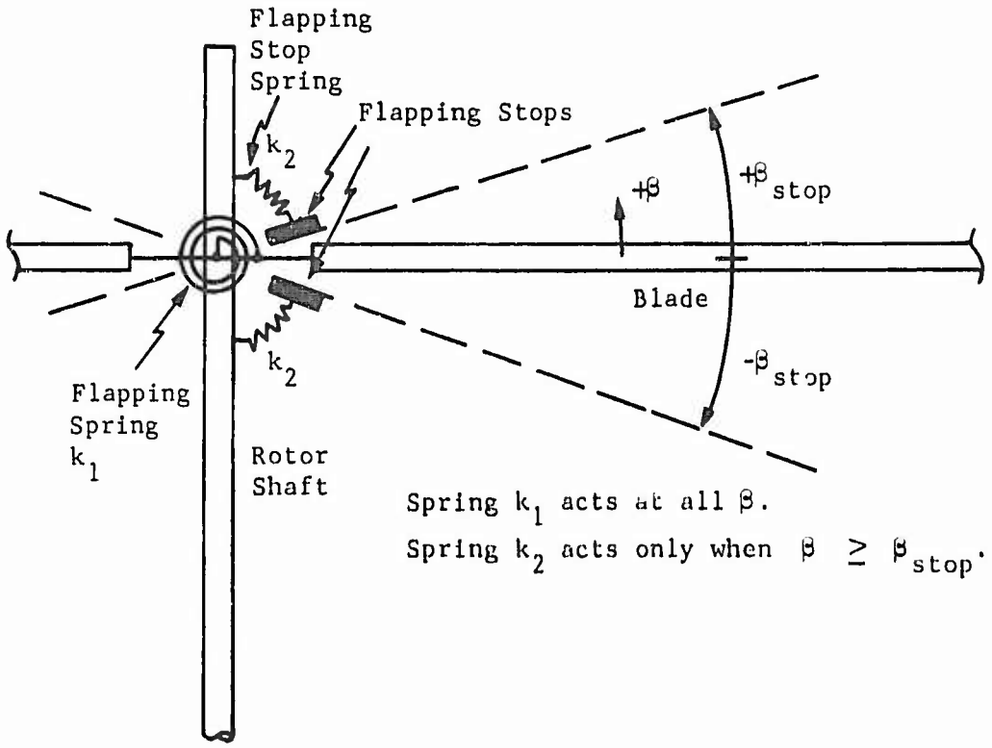

Figure 3-3. Schematic Diagram of Flapping Spring and Stops.

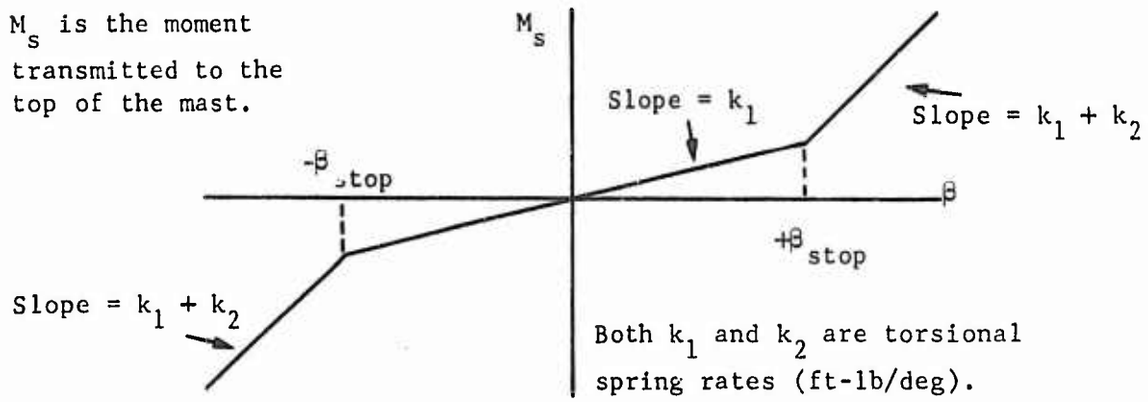

Figure 3-4. Spring Rates Representing Flapping Spring and Stops.

The blade root flapping angle $\beta(t)$ is defined at each time point in the maneuver. The moment transmitted to the top of the mast is given by

$$M_s = (M_s)_{spring} + (M_s)_{stop} \tag{3-32}$$

The two components of M_s are defined as follows:

$$(M_s)_{spring} = \begin{cases} k_1 \beta & \text{if } |\beta| < \beta_{stop} \\ k_1 \beta_{stop} \text{ sign } (\beta) & \text{if } |\beta| \geq \beta_{stop} \end{cases} \tag{3-33}$$

and

$$(M_s)_{stop} = \begin{cases} 0.0 & \text{if } |\beta| < \beta_{stop} \\ k_2 (|\beta| - \beta_{stop}) \text{ sign } (\beta) & \text{if } |\beta| \geq \beta_{stop} \end{cases} \tag{3-34}$$

Figure 3-4 is a plot of M_s based on Equations (3-32), (3-33), and (3-34).

That same moment M_s can be used in calculating the work done by the externally-applied loads acting through the n^{th} mode shape. Let it be assumed that ϕ_n is the slope at the hub in the vertical plane associated with the n^{th} mode shape; the incremental out-of-plane component F_z of the forcing function F_n for the n^{th} mode shape becomes

$$\Delta I_z = -M_s \phi_n \tag{3-35}$$

This increment to I_z should then be added to the right side of Equation (3-29) to account for flapping springs and stops.

Lead-lag dampers are handled in a fashion similar to that shown in Figure 3-5. It is assumed that at some radial point, r_1, a viscous damper (with damping rate c lb/ft/sec) is attached inplane. The inplane velocity of the attachment point is given by

$$\dot{Y}(r_1) = \sum_{n=1}^{NM} \dot{\delta}_n(t)\, Y_n(r_1) \tag{3-36}$$

which would then produce a damper force, F_{damp}, given by

$$F_{damp} = \dot{Y}(r_1)c \tag{3-37}$$

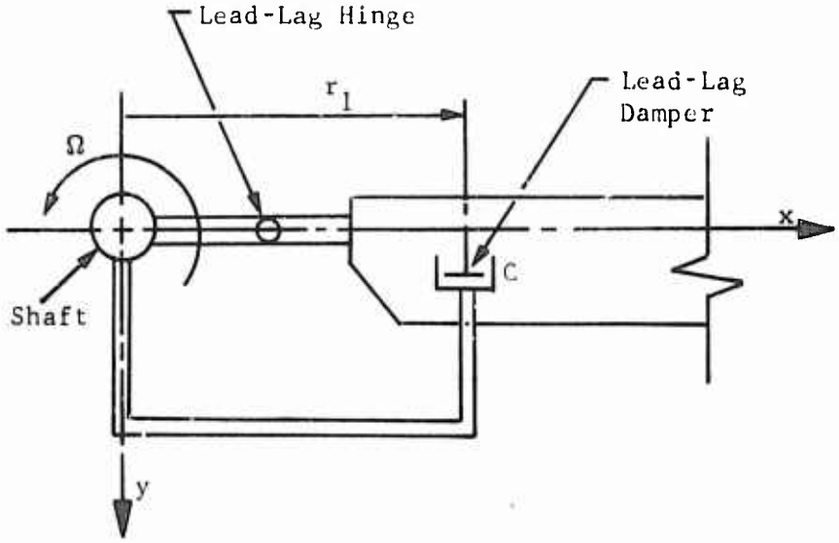

Figure 3-5. Schematic of Lead-Lag Hinge and Damper.

This damper force is included in the elastic rotor analysis. Recalling the basic definition of the inplane component F_y of the forcing function F_n of the modal equation,

$$\Delta I_y = [\dot{Y}(r_1)]\,[Y_n(r_1)]c \tag{3-38}$$

where r is defined in the program to be 0.1 R.

3.2.8 Rotor Bending Moments

By use of the modal technique, it is possible to show that

$$\begin{bmatrix} Y(x,t) \\ Z(x,t) \\ \theta(x,t) \end{bmatrix} = \sum_{n=1}^{NM} \begin{bmatrix} Y_n(x) \\ Z_n(x) \\ \theta_n(x) \end{bmatrix} \delta_n(t) \tag{3-39}$$

where $\begin{bmatrix} Y_n(x) \\ Z_n(x) \\ \theta_n(x) \end{bmatrix}$ is the n^{th} input mode shape and $\delta_n(t)$ is the participation factor associated with that mode. It is possible to write the following equations to describe the time-variant rotor loads at any point x_o on the blade at any time t:

(1) Total Out-of-Plane Bending Moment

$$VBM_T(x_o,t) = \sum_{n=1}^{NM} VBM_n(x_o)\delta_n(t) \tag{3-40}$$

(2) Total Out-of-Plane Shear

$$VS_T(x_o,t) = \sum_{n=1}^{NM} VS_n(x_o)\delta_n(t) \tag{3-41}$$

(3) Total Inplane Bending Moment

$$IBM_T(x_o,t) = \sum_{n=1}^{NM} IBM_n(x_o)\delta_n(t) \tag{3-42}$$

(4) Total Inplane Shear

$$IS_T(x_o,t) = \sum_{n=1}^{NM} IS_n(x_o)\delta_n(t) \tag{3-43}$$

(5) Total Torsional Moment

$$TBM_T(x_o,t) = \sum_{n=1}^{NM} TBM_n(x_o)\delta_n(t) \tag{3-44}$$

where NM is the total number of modes.

The load coefficients $VBM_n(x_o)$, $VS_n(x_o)$, $IBM_n(x_o)$, $IS_n(x_o)$, and $TBM_n(x_o)$ are functions of the input blade mode shape, mass and inertial distribution, rotor speed, and the natural frequency of the mode.

The Euler beam equation (Reference 4) shows that the out-of-plane bending moment $VBM_T(x_o)$ is given by

$$VBM_T(x_o) = EI_z \left.\frac{d^2Z}{dx^2}\right|_{x=x_o} \tag{3-45}$$

where Z is the total out-of-plane displacement and EI_z is the blade out-of-plane stiffness. Combining out-of-plane components of the two previous equations, it follows that

$$VBM_T(x,t) = EI_z \frac{d^2}{dx^2}\left[\sum_{n=1}^{NM} Z_n \cdot \delta_n(t)\right] \tag{3-46}$$

but since $\delta_n(t)$ is independent of x,

$$VBM_T(x_o,t) = \sum_{n=1}^{NM}[\delta_n(t)]EI_z \left.\frac{d^2Z_n}{dx^2}\right|_{x=x_o} \tag{3-47}$$

which can be written as

$$VBM_T(x_o,t) = \sum_{n=1}^{NM} \delta_n(t)\ VBM_n(x_o) \tag{3-48}$$

where

$$VBM_n(x_o) = EI_z \left.\frac{d^2Z_n}{dx^2}\right|_{x=x_o} \tag{3-49}$$

It can be seen that $VBM_n(x_o)$ is independent of time and can be calculated prior to calculating the elastic response. Just as $Z_n(x_o)$ describes the out-of-plane displacements of the n^{th} mode shape, $VBM_n(x_o)$ describes the out-of-plane bending moment associated with the n^{th} mode shape. To avoid difficulties in differentiating the mode shapes twice, the out-of-plane bending moment $VBM_n(x_o)$ associated with the n^{th} mode at radial station x_o can also be defined by

$$VBM_n(x_o) = \int_{x_o}^{R} \{[M\omega_n^2 Z_n(x)] (x-x_o) - (M\Omega^2) [Z_n(x)-Z_n(x_o)]\} dx \quad (3\text{-}50)$$

which is the moment produced by all forces outboard of x_o, as shown by Figure 3-6. The forces on Figure 3-6 can be obtained by making the following assumptions:

(1) Each point on the blade is executing pure harmonic motion, whose amplitude is given by the n^{th} mode shape.

(2) The harmonic motion occurs at the natural frequency ω_n.

(3) The rotor speed is Ω.

(4) There are no externally applied air loads.

Figure 3-6 shows the load distribution associated with the out-of-plane motion subject to the above four conditions.

In a similar manner it can be shown that the vertical shear force associated with the n^{th} mode at any point x_o can be

$$VS_n(x_o) = \frac{d}{dx} [VBM_B(x_o)]\Big|_{x=x_o} \quad (3\text{-}51)$$

or

$$VS_n(x_o) = [\frac{d}{dx} (EI_z \frac{d^2 Z_n}{dx^2})]\Big|_{x=x_o} \quad (3\text{-}52)$$

But $VS_n(x_o)$ can also be obtained by summing the out-of-plane forces, associated with the n^{th} mode shape, outboard of station x_o as shown by Figure 3-6. Thus,

$$VS(x_o) = \int_{x_o}^{R} MZ_n(x)\ \omega_n^2\ dx \quad (3\text{-}53)$$

Following the same reasoning, the inplane coefficients can be deduced from the load distribution shown in Figure 3-7.

$$IBM_n(x_o) = \int_{x_o}^{R} \{[M\ Y_n(x)\ (\omega_n^2 + \Omega^2)](x - x_o) - [M\ x\Omega^2][Y_n(x) - Y_n(x_o)]\}\ dx \qquad (3\text{-}54)$$

and the inplane shear $IS_n(x_o)$ is

$$IS_n(x_o) = \int_{x_o}^{R} M\ Y_n(x)\ (\omega_n^2 + \Omega^2)\ dx \qquad (3\text{-}55)$$

The torsional moment at any point x_o can be derived by observing the n^{th} mode shape shown in Figure 3-8.

The mass moments of inertia of the cross section about the principal axis of inertia are $\rho I_b(x)$ and $\rho I_c(x)$, where $\rho I_b(x)$ is significantly greater than $\rho I_c(x)$. The torsional moment is then given by

$$TBM_n(x_o) = \int_{x_o}^{R} \{(\rho I_b + \rho I_c)\ \theta_n(x)\ \omega_n^2 - (\rho I_b - \rho I_c)\ \Omega^2 \theta_n(x)\}\ dx \qquad (3\text{-}56)$$

If the blade stiffness distribution were input data to this program, the load coefficients could be obtained by combining the stiffness distribution with certain spatial derivatives of the mode shapes. Since the mode shapes are defined at only twenty-one points along the blade radius, performing the spatial derivatives can lead to numerical difficulties.

As mentioned in the description of the mathematical model, in the elastic trim procedure (discussed in Section 9) the harmonic representation of $\delta_n(t)$ is obtained. Using these values of the harmonic components, the rotor loads (beam, chord, and torsional bending moment) at twenty equally spaced radial stations are calculated. The beam and chord bending moments are obtained from the inplane and out-of-plane bending moments by a transformation through the geometric pitch angle (except for the inboard 10 percent of the blade which is assumed not to feather).

During the maneuver portion of the program, the rotor bending moments at any particular radial station can be printed. The maneuver output also prints the three components (fore-and-aft, lateral, and vertical) of the shear forces at the top of the mast. These shear forces, in the fixed coordinate system, are used to drive the hub motion equations as described in the next section.

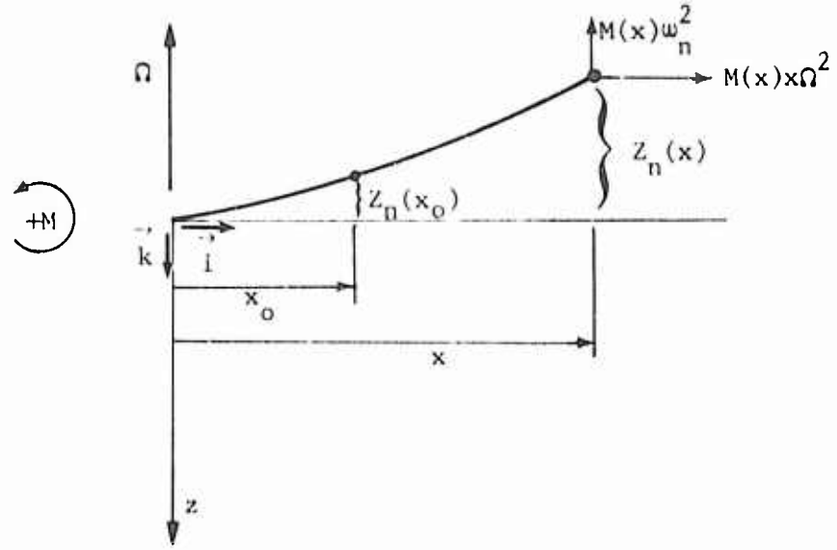

Figure 3-6. Vertical Inertial Forces on Rotor Blade.

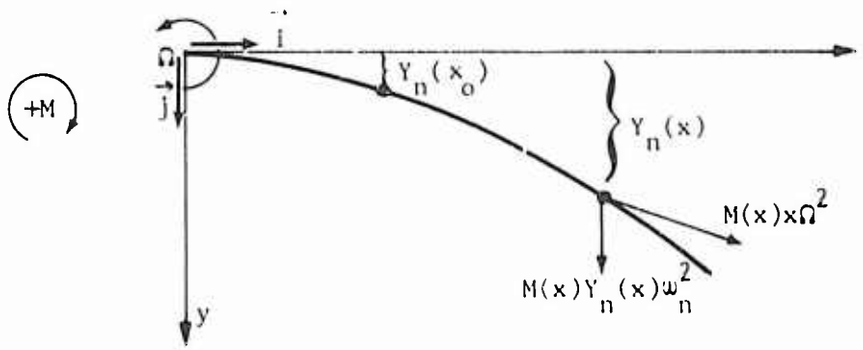

Figure 3-7. Inplane Inertial Forces on Rotor Blade.

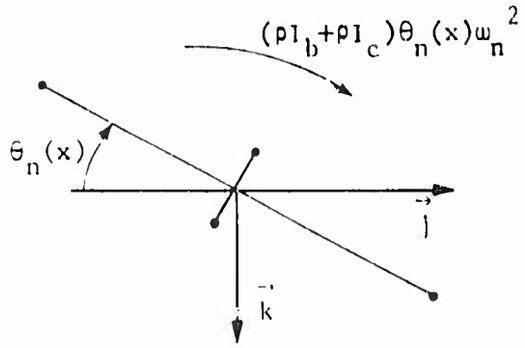

Figure 3-8. Torsional Inertial Moments on Rotor Blade.

3.2.9 Pylon Motion and Mast Windup

The behavior of the elastic rotor is dependent on the hub restraint imposed on the blade which is modeled by three independently actuated equations. The first two describe the fore-and-aft and the lateral motion of the pylon, while the third equation is related to the mast windup. The free-body diagrams associated with the fore-and-aft and lateral pylon motion are shown in Figures 3-9 and 3-10 respectively. The fore-and-aft and lateral pylon spring rates are k_F and k_L respectively. The same subscripting convention is used for all applicable pylon variables. The effective pylon lengths (l_F and l_L) are defined as the distance from the pivot point or focal point to the center of the rotor hub. The mass moments of inertia of the pylon alone, without any rotor mass, about the focal point are I_F and I_L.

The top view of the pylon motion is shown in Figure 3-11. The linear acceleration of the hub in the fore-and-aft direction is $l_F\ddot{a}_F$, and in the lateral direction is $l_L\ddot{a}_L$. The hub accelerations will produce the inertial forces on the blade mass M as shown by the dotted arrows on Figure 3-11. The inertial force perpendicular to the blade is accounted for in Equation (3-28), and thus may be eliminated from this discussion. The inertial force acting in the radial direction has not been treated previously. The inertial force in the radial direction can be resolved into components in the fore-and-aft and lateral directions and integrated over all the blades to give a fore-and-aft inertial force F_F

$$F_F = -M_{blade}\sum_{i=1}^{NM}\left(l_F\ddot{a}_F\cos^2\psi_i - l_L\ddot{a}_L\sin\psi_i\cos\psi_i\right) \tag{3-57}$$

and a lateral inertial force F_L

$$F_L = -M_{blade}\sum_{i=1}^{NB}\left(l_F\ddot{a}_F\sin\psi_i\cos\psi_i - l_L\ddot{a}_L\sin^2\psi_i\right) \tag{3-58}$$

These inertial forces must be treated in the pylon equations.

Referring to the model for the fore-and-aft pylon motion shown in Figure 3-9, it can be seen that

$$I_{F_o}\ddot{a}_F = -k_Fa_F - c_F\dot{a}_F - PMOM + l_FS_X + l_FF_F + I_{F_o}\dot{q} \tag{3-59}$$

and from the model for the lateral pylon motion shown in Figure 3-10,

$$I_{L_o}\ddot{a}_L = -k_La_L - c_L\dot{a}_L + RMOM + l_LS_y + l_LF_L - l_L(\dot{p}\cos a_m + \dot{i}\sin a_m) \tag{3-60}$$

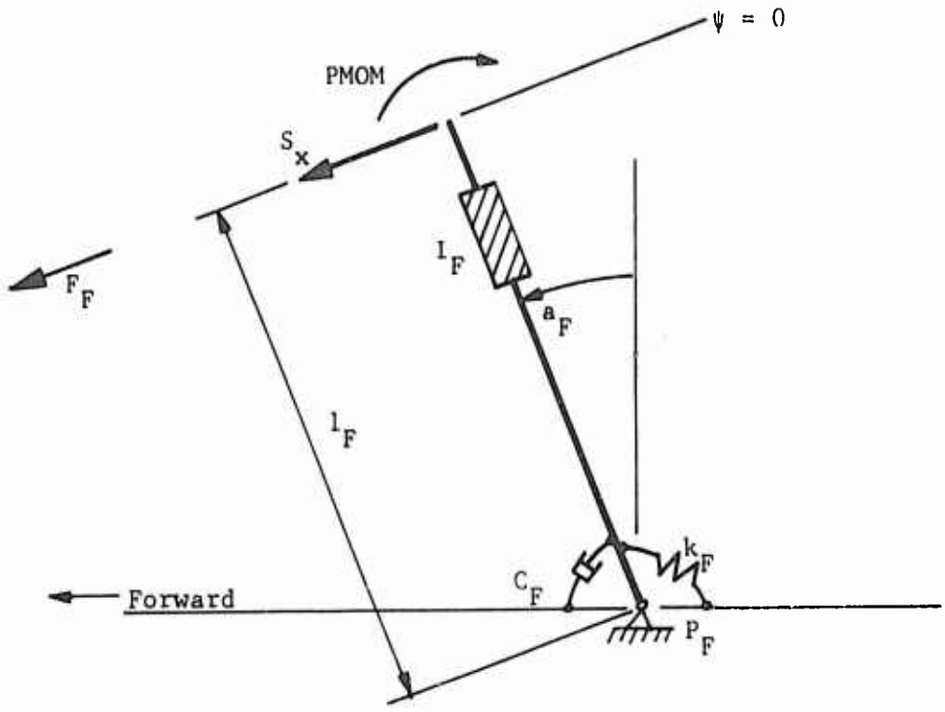

Figure 3-9. Model for F/A Pylon Motion.

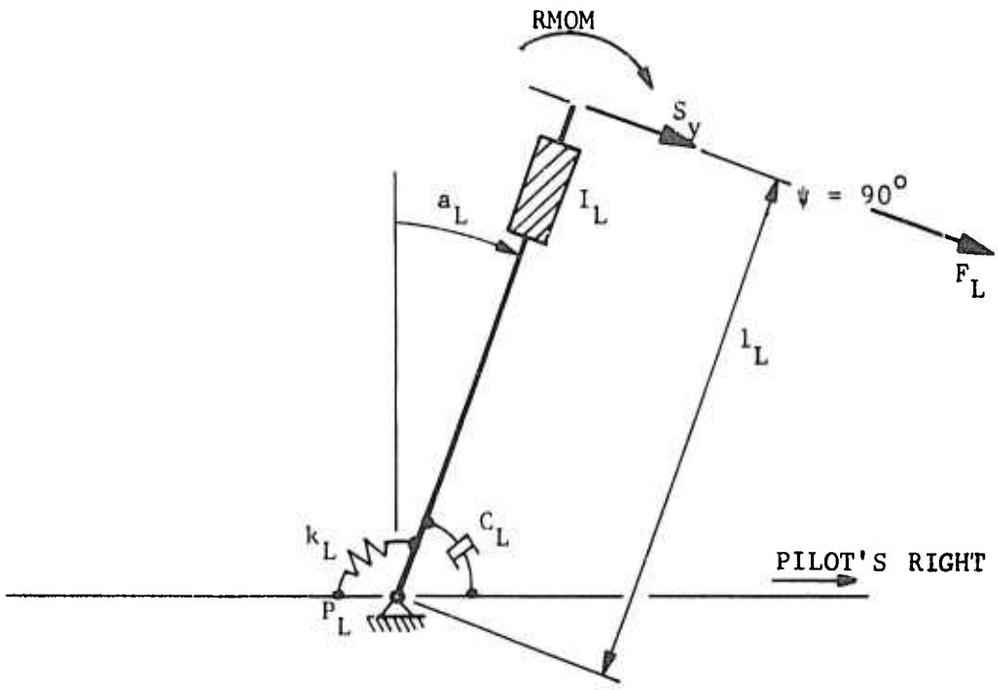

Figure 3-10. Model for Lateral Pylon Motion.

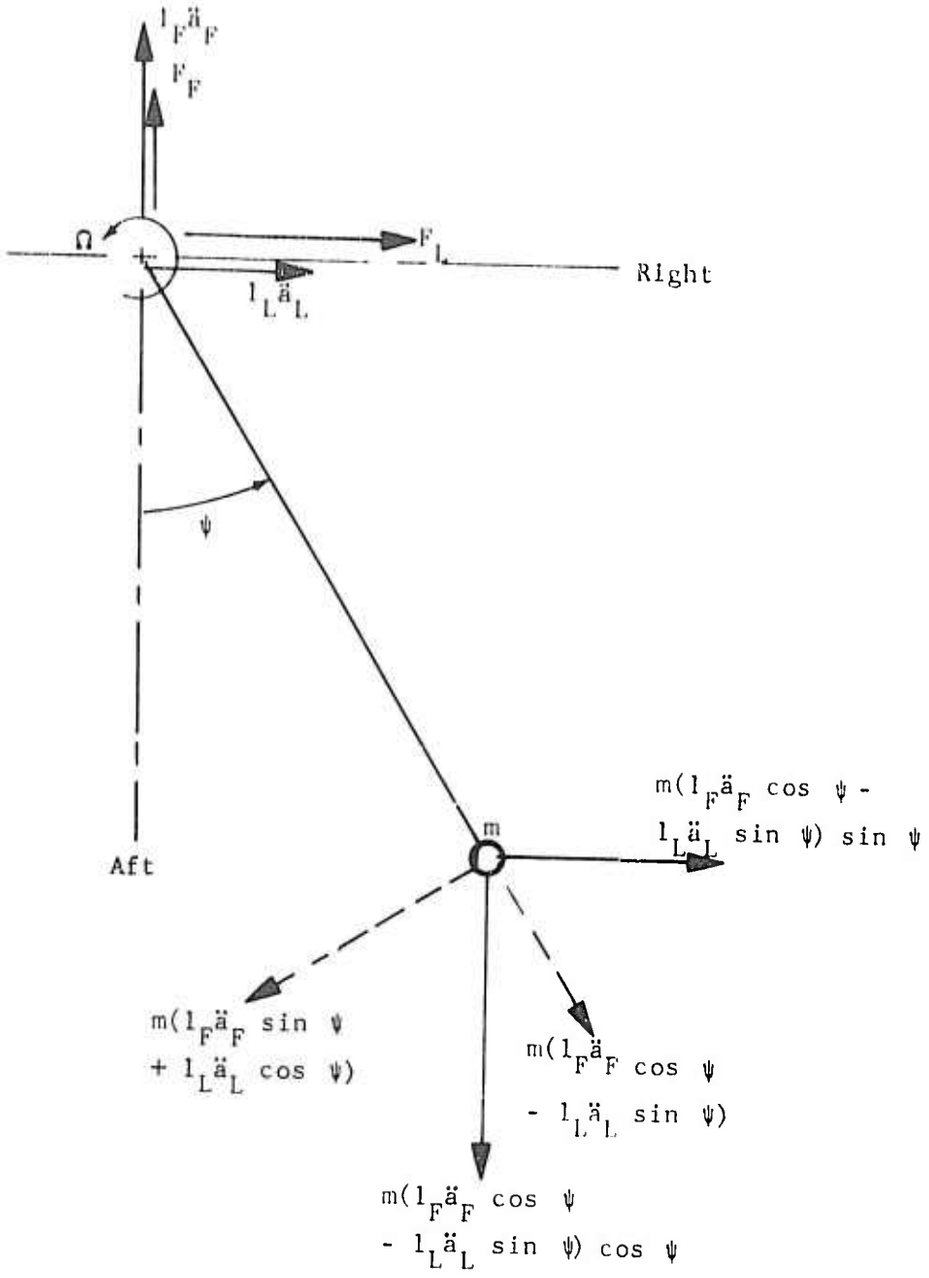

Figure 3-11. Top View of Pylon Motion.

In the above equations, S_x and S_y are the components in the fixed coordinate system of the inplane hub shear as defined by Equation (3-43) and the integrated change in centrifugal force produced by the change in effective rotor speed as defined by the second term in Equation (3-23). Likewise, PMOM and RMOM are the components of the total out-of-plane bending moment as given by Equation (3-40). The conventional angular rates of the rigid body fuselage are p, q, r, while a_m is the total mast tilt angle.

There are two other major effects of the elastic pylon motion which must be included in the analysis. The first is the effect of the elastic pylon velocity on the blade element velocity in the blade aerodynamic calculations. This effect is shown in Equation (3-101) given in Section 3.3.3. The second major effect is the coupling between the elastic pylon displacement and the geometric pitch of the blade. This coupling is accounted for in the following manner:

$$\begin{bmatrix} \theta_o \\ \theta_{F/A} \\ \theta_{Lat} \end{bmatrix} = \begin{bmatrix} \theta_o \\ \theta_{F/A} \\ \theta_{Lat} \end{bmatrix} + \begin{bmatrix} \frac{\partial\theta_o}{\partial a_F} & \frac{\partial\theta_o}{\partial a_L} \\ \frac{\partial\theta_{F/A}}{\partial a_F} & \frac{\partial\theta_{F/A}}{\partial a_L} \\ \frac{\partial\theta_{Lat}}{\partial a_F} & \frac{\partial\theta_{Lat}}{\partial a_L} \end{bmatrix} \times \begin{bmatrix} a_F \\ aL \end{bmatrix} \qquad (3\text{-}61)$$

where the elements of partial derivative matrix are input parameters.

The elastic mast windup can be represented by a differential equation. Referring to Figure 3-12, it is assumed that at the bottom of the shaft, an infinite inertia (I_∞) which turns at a constant angular speed, ω_t, is present. At the top of the shaft is a concentrated inertia (I_s) which is equal to the combined inertia of the rotor-pylon system and the rotating components of the control system. Connecting the two inertias is a flexible shaft of stiffness k_s. It now becomes possible to write

$$\ddot{\psi}_T = \frac{\sum_{j=1}^{NB} IBM_T(0)_j}{I_s} - \omega_{n_T}\left[2\xi_T\dot{\psi}_T + \omega_{n_T}\psi_T\right] \qquad (3\text{-}62)$$

where the forcing function is defined by Equation (3-42) in Section 3.2.8 and ω_{n_T} is given by

$$\omega_{n_T} = \sqrt{\frac{k_s}{I_s}} \qquad (3\text{-}63)$$

where k_s is an input parameter.

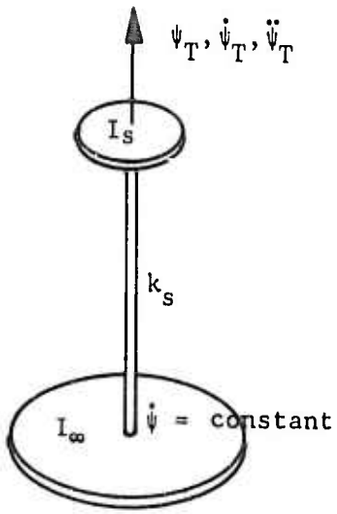

Figure 3-12. Mast Windup Motion.

Equation (3-62) describes the mast windup in response to externally applied rotor loads. The inertial effects due to the mast windup on the blade loads have been previously discussed. The inertial loads on the blade produced by the mast windup acceleration are represented by the fifth term in Equation (3-28). The calculation of the blade aerodynamics includes the incremental blade velocities caused by the mast windup velocity.

The gross rotor forces (H force, Y force, and thrust) and rotor moments, as obtained from the integration of the aerodynamic forces acting on the rotor, are used in the fuselage equations of motion. The hub shears and moments, as calculated from the elastic rotor response, are used as forcing function to the pylon motion and mast windup differential equations. Both sets of forces and moments are assumed to be acting at the top of the mast. The use of the effective pylon lengths in the pylon equations simulates the dynamic effects of the focused pylon concept. The accelerations, velocities and displacements from the pylon motion and mast windup are used in the evaluation of the aerodynamic and inertial forces on the rotor.

When only the rigid blade mode is used, the gross rotor forces are used in conjunction with the hub restraint equations. This path, which permits the use of hub restraint equations with a rigid blade, is used in the stability analysis portion of the program.

3.2.10 Blade Mode Type Selection

The rotor hub has the ability to act as an attenuator, filter, or amplifier with reference to the transmissibility of the externally applied loads. Gessow and Myers (Reference 7) show the response of various hub configurations to forces with various harmonic excitation frequencies. This unique behavior of the rotor hub can be related to the behavior of the mode shapes used to describe the total rotor system. The boundary conditions used to calculate and describe the blade modes are given in Table 3-1.

TABLE 3-1. BLADE BOUNDARY CONDITIONS AT ROOT

Mode Type	Out of Plane	Inplane	Torsion
Collective	Cantilever	Pinned	Cantilever
Cyclic	Pinned	Cantilever	Cantilever
Scissor	Cantilever	Cantilever	Cantilever

The proper selection of which blade mode types (cyclic, collective, or scisser) should be used is essential to an accurate rotor simulation. The purpose of this section is to describe the technique used to ascertain which mode types should be used to represent various hub types. The next section describes how the input blade modes are combined into rotor modes which are used in the computer program.

The first step in selecting which type blade modes--collective, cyclic, or scissor--should be used in the rotor simulation is to define the hub boundary conditions that can exist for each blade. The hub boundary conditions are a function of the type hub--gimbaled, teetering, hingeless, or articulated. For the latter two--hingeless or articulated--each blade's behavior is independent of any other blade's behavior. However, for the gimbaled or teetering hub there is moment carry-over across the hub, so it is possible for any one blade to affect the behavior of the other blades.

The hub boundary conditions for a rotor blade must include the out-of-plane, inplane, and torsional end restraint. The out-of-plane boundary condition for all blades on a hingeless or rigid hub is cantilever; i.e., out-of-plane slope is zero. See Table 3-2 for these boundary conditions and their corresponding mode types.

TABLE 3-2. BLADE BOUNDARY CONDITIONS AND MODE TYPES FOR HINGELESS OR ARTICULATED HUBS

Mast Torsional Stiffness	Boundary Condition			Blade Mode Type
	Inplane	Out of Plane	Torsional	
Zero	Pinned	Cantilever	Cantilever	Collective
Nonzero	Cantilever	Cantilever	Cantilever	Scissor

The selection of mode types for hubs with moment carry-over, i.e., teetering or gimbaled, is somewhat more difficult than for the hingeless or articulated hubs. The first step is to determine the actual boundary conditions that are compatible with the blade's response to integer-per-rev harmonic forcing functions. The four-bladed gimbaled rotor displays all the possible characteristics of the hubs with moment carry-over, and will therefore be used as an example. Let it be assumed that positive out-of-plane bending (compression in top of blade) is accompanied by positive inplane bending (tension in leading edge). Figure 3-13 shows that for the 0 or 4-per-rev response, each blade tip moves up and aft. Thus, the out-of-plane boundary condition is cantilever. The inplane boundary condition depends on the mast torsional stiffness. For zero mast torsional stiffness, the inplane boundary conditions would be pinned, which would require the use of collective blade modes. For the nonzero mast torsional stiffness, the scissor blade modes would be used to describe the response at

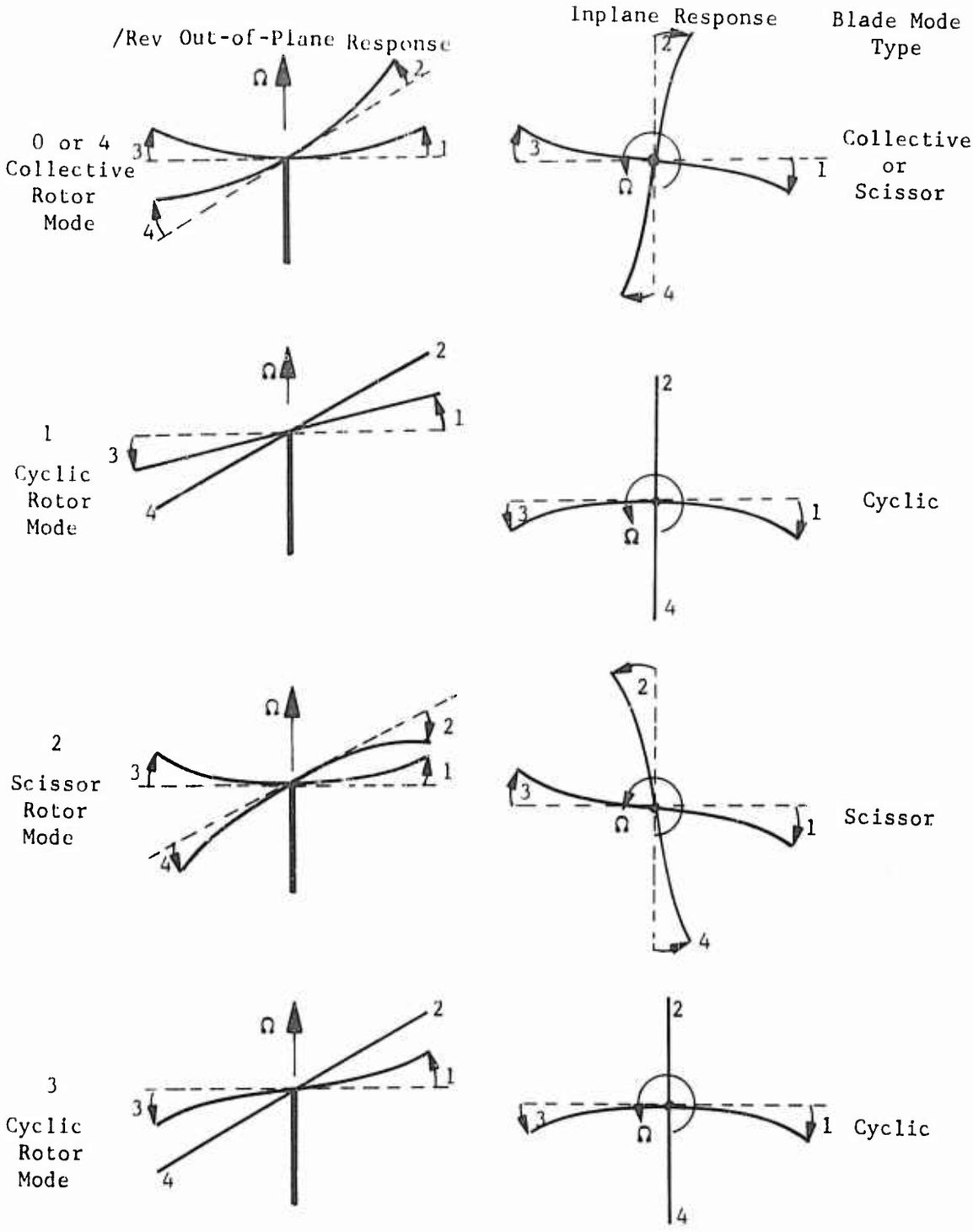

Figure 3-13. Response of 4-Bladed Gimbaled Rotor to Harmonic Forcing Functions.

0-per-rev or 4-per-rev. The 1-per-rev and 3-per-rev are very similar. In both cases, the out-of-plane boundary condition is pinned and the inplane is cantilever, regardless of the mast torsional stiffness. For the 2-per-rev blade response, blades 1 and 3 move up and aft; blades 2 and 4 move down and forward. The out-of-plane boundary condition is cantilever (the out-of-plane slope is zero). The hub inplane 2-per-rev moment produced by blade 1 is equal and opposite to that produced by blade 2; likewise, for blades 3 and 4. Thus, the total hub moment from the four blades is zero, so there is no hub moment tending to wind up the mast (regardless of the mast torsional stiffness). This condition is compatible with the cantilever inplane boundary condition.

The procedure described for the four-bladed gimbaled rotor can be applied to any rotor system with moment carry-over. The resulting blade boundary conditions associated with any integer per-rev response n, for any number of blades b, and the corresponding mode types are summarized in Table 3-3.

TABLE 3-3. BLADE BOUNDARY CONDITIONS AND MODE TYPES FOR GIMBALED OR TEETERING HUBS

Mast Torsional Stiffness	Harmonic Per Rev	Boundary Condition			Blade Mode Type
		Inplane	Out of Plane	Torsional	
Zero	nb	Pinned	Cantilever	Cantilever	Collective
	b(n-½)	Cantilever	Cantilever	Cantilever	Scissor*
	all other	Cantilever	Pinned	Cantilever	Cyclic
Nonzero	nb	Cantilever	Cantilever	Cantilever	Scissor
	b(n-½)	Cantilever	Cantilever	Cantilever	Scissor*
	all other	Cantilever	Pinned	Cantilever	Collective

n = integer per-rev response

b = number of blades

*Only meaningful for gimbaled rotor systems with four or six blades

The order in which the mode shapes are arranged in the input data in terms of natural frequencies (ascending or descending) is unimportant except for one condition: the mode shape that has a natural frequency closest to one per rev must be the first input mode shape. It is not required that the mode shapes have adjoining frequencies; i.e., certain mode shapes can be replaced with mode shapes with higher natural frequencies. Once the natural frequencies and their corresponding mode shapes are known, the only other modal input required is the structural damping coefficient, which should be taken as approximately 2 percent critical for all modes except the rigid-body mode, for which it is zero.

A flow chart for selecting the proper blade modes to simulate any conventional hub is shown in Figure 3-14.

Based on these input blade modes, the computer program must have a logic network to combine the blade modes in the proper manner. The logic network will be described in the next section.

3.2.11 Hub Transfer Coefficient Matrix

The approach of the modal technique is sufficiently general to handle any particular combination of hub type and/or number of blades. The principal problems arise from the fact that the normal modes of vibration and the natural frequencies are calculated for the individual blades while the modal equations are written for rotor modes. Some blade modes can be combined to form a rotor mode that can be described by one equation--consider a collective blade mode for a gimbaled rotor where all blades go up and down together. Other blade modes are combined to form a rotor mode that requires two independent modal equations to define its position--consider a cyclic blade mode for a gimbaled rotor which could move about two perpendicular axes (fore-and-aft flapping and lateral flapping).

The number of independent rotor modal equations required to describe a given blade mode is as follows: For all rotors where there is moment carry-over at the hub, two equations are required to described each cyclic mode and one equation to describe each collective or scissor blade mode; for all rotors where there is no moment carry-over at the hub, one independent equation must be written for each mode for each blade. Thus, the total number of independent equations required to describe any combination of hub type and number of blades is difficult to express in general terms. It can be shown, however, that the number of dependent equations is b times NM where there are b blades and NM the number of input mode shapes. These dependent equations can be used to describe all conventional hub types (hingeless, articulated, gimbaled, or teetering) for any number of blades. It is required that each input blade mode shape be designated as to whether it is to be formed into independent, cyclic, collective, or scissor rotor mode shapes. The independent rotor modes are associated with those rotor hubs without moment carry-over, and are thus capable of responding at all integer multiples of the rotor speed. The cyclic, collective and scissor rotor modes are associated with hubs with moment carry-over. Collective rotor modes respond at nb/rev; scissor rotor modes respond at b(n-1/2)/rev; and cyclic rotor modes respond at all other harmonics where b is the number of blades, and n can be any nonnegative integer. Scissor rotor modes are associated only with gimbaled hubs with 4 or 6 blades.

The Hub Transfer Coefficient (HTC) matrix is used to represent the interdependency of hub type and mode type. The HTC matrix will be derived for several different combinations. For each case, the input mode shape will be MS(x), the generalized inertia of one blade will be I_n, and the

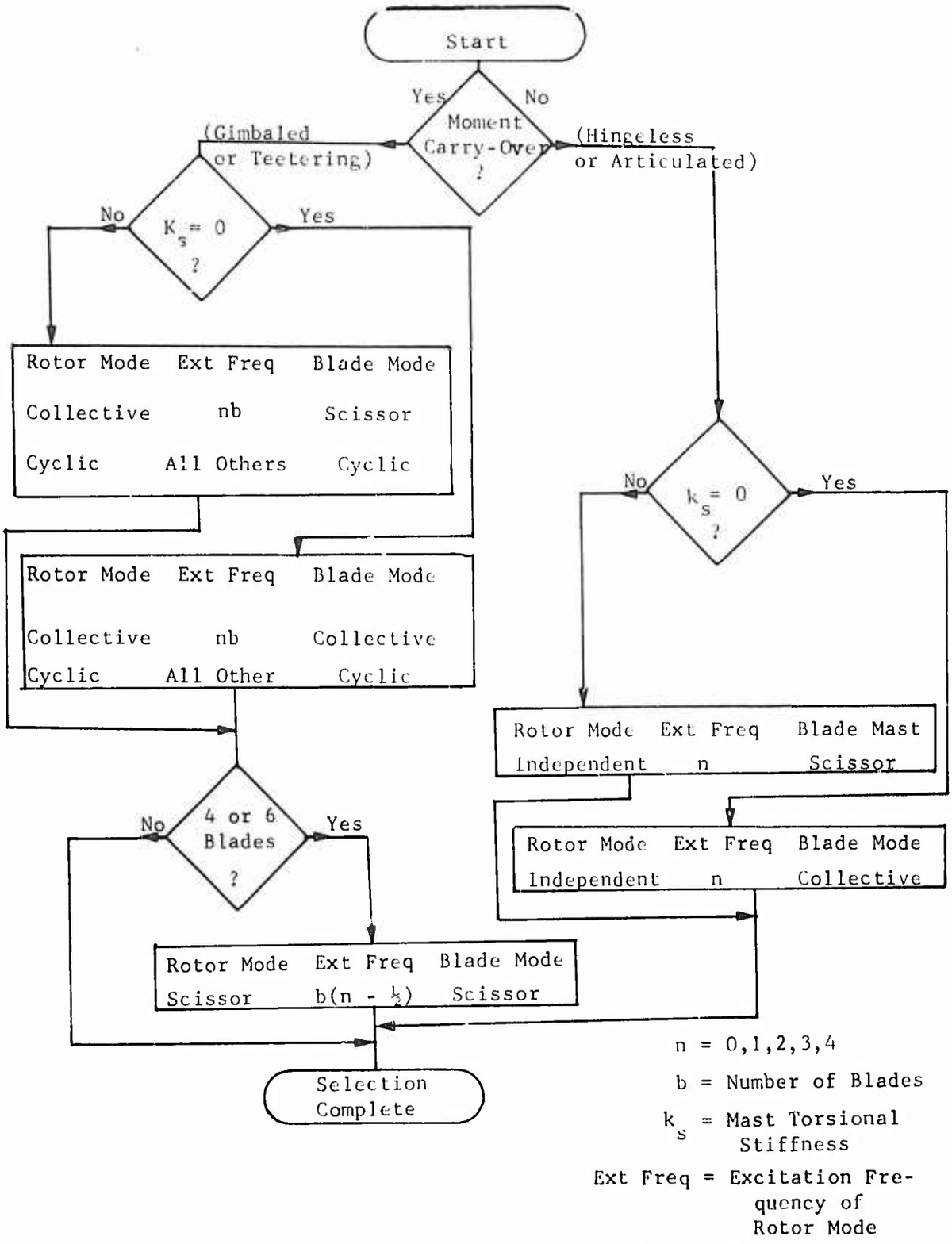

Figure 3-14. Guide for Selection of Blade Mode Types To Simulate Various Hub Types.

externally applied loads on blade j will be $A_j(x)$, with components F_{Y_j}, F_{Z_j}, and M_{θ_j} as given by Equation (3-12).

The first case will be the cyclic mode for a four-bladed gimbaled rotor. From the input blade mode shape MS(x), two independent rotor modes can be written:

	MODE SHAPE			
Mode No.	Blade 1	Blade 2	Blade 3	Blade 4
1	MS(x)	0	-MS(x)	0
2	0	MS(x)	0	-MS(x)

The inertia of each mode would be $2I_n$. The virtual work done by the externally applied air loads acting through the n^{th} mode shape would be for the first independent rotor mode

$$W_1 = \int_0^R \Big| \Big| F_{Z_1}(x) \cdot Z_n(x) + F_{Y_1}(x) \cdot Y_n(x) + M_{\theta_1}(x) \cdot \theta_n(x) \Big| - \Big| F_{Z_3}(x) \cdot Z_n(x) + F_{Y_3}(x) \cdot Y_n(x) + M_{\theta_3}(x) \cdot \theta_n(x) \Big| \Big| \, dx \qquad (3\text{-}64)$$

or

$$W_1 = \int_0^R \Big| MS_n(x) \cdot A_1(x) - MS_n(x) \cdot A_3(x) \Big| \, dx \qquad (3\text{-}65)$$

and for the second independent rotor mode

$$W_2 = \int_0^R MS_n(x) \cdot A_2(x) - MS_n(x) \cdot A_4(x) \, dx \qquad (3\text{-}66)$$

and the two independent modal equations (one for each mode) would be

$$\ddot{\epsilon}_1 + 2\zeta\omega_n\dot{\epsilon}_1 + \omega_n^2\epsilon_1 = \frac{W_1}{2I_n} = \frac{\int_0^R MS(x) \cdot A_1(x) - MS(x) \cdot A_3(x)\ dx}{2I_n} \quad (3\text{-}67)$$

and

$$\ddot{\epsilon}_2 + 2\zeta\omega_n\dot{\epsilon}_2 + \omega_n^2\epsilon_2 = \frac{W_2}{2I_n} = \frac{\int_0^R MS(x) \cdot A_2(x) - MS(x) \cdot A_4(x)\ dx}{2I_n} \quad (3\text{-}68)$$

If ϵ_1 and ϵ_2 are independent generalized coordinates, the δ_1, δ_2, δ_3, δ_4 are localized dependent blade coordinates such that

$$\begin{aligned}
\delta_1 &= \epsilon_1 & \delta_3 &= -\epsilon_1 & \delta_2 &= \epsilon_2 & \delta_4 &= -\epsilon_2 \\
\dot{\delta}_1 &= \dot{\epsilon}_1 & \dot{\delta}_3 &= -\dot{\epsilon}_1 & \dot{\delta}_2 &= \dot{\epsilon}_2 & \dot{\delta}_4 &= -\dot{\epsilon}_2 \\
\ddot{\delta}_1 &= \ddot{\epsilon}_1 & \ddot{\delta}_3 &= -\ddot{\epsilon}_1 & \ddot{\delta}_2 &= \ddot{\epsilon}_2 & \ddot{\delta}_4 &= -\ddot{\epsilon}_2
\end{aligned} \quad (3\text{-}69)$$

It then becomes possible to write four dependent equations of

$$\ddot{\delta}_j + 2\zeta\omega_n\dot{\delta}_j + \omega_n^2\delta_j = F_j \qquad j = 1, 4 \quad (3\text{-}70)$$

where F_j is written as

$$\begin{Bmatrix} F_1 \\ F_2 \\ F_3 \\ F_4 \end{Bmatrix} = \frac{1}{2I_n} \begin{bmatrix} 1 & 0 & -1 & 0 \\ 0 & 1 & 0 & -1 \\ -1 & 0 & 1 & 0 \\ 0 & -1 & 0 & 1 \end{bmatrix} \times \begin{bmatrix} W_1 \\ W_2 \\ W_3 \\ W_4 \end{bmatrix} \quad (3\text{-}71)$$

where W_i is the work done by the air loads on blade i, acting through the input blade mode shape.

For a cyclic blade mode shape for a three-bladed rotor, Equation (3-71) would have the following form for a gimbaled rotor:

$$\begin{Bmatrix} F_1 \\ F_2 \\ F_3 \end{Bmatrix} = \frac{2}{3I_n} \begin{bmatrix} 1 & -\frac{1}{2} & -\frac{1}{2} \\ -\frac{1}{2} & 1 & -\frac{1}{2} \\ -\frac{1}{2} & -\frac{1}{2} & 1 \end{bmatrix} \times \begin{bmatrix} W_1 \\ W_2 \\ W_3 \end{bmatrix} \tag{3-72}$$

and for a teetering hub the cyclic blade mode would be described

$$\begin{bmatrix} F_1 \\ F_2 \end{bmatrix} = \frac{1}{2I_n} \begin{bmatrix} 1 & -1 \\ -1 & 1 \end{bmatrix} \times \begin{bmatrix} W_1 \\ W_2 \end{bmatrix} \tag{3-73}$$

For any cyclic mode for any number of blades,

$$HTC(i,j) = \cos [\Psi(i) - \Psi(j)] \tag{3-74}$$

which gives the effect of blade i on blade j.

The second case will be the collective mode for a four-bladed gimbaled rotor. The one independent mode would be

Mode No.	Blade 1	Blade 2	Blade 3	Blade 4
1	MS(x)	MS(x)	MS(x)	MS(x)

The forcing function for the independent equation would be

$$F_1 = \int_0^R MS(x) \cdot A_1(x) + MS(x) \cdot A_2(x) + MS(x) \cdot A_3(x) + MS(x) \cdot A_4(x) \quad dx \tag{3-75}$$

and the equation of motion would be

$$\epsilon_1 + 2\zeta\omega_n\epsilon_1 + \omega_n^2\epsilon_1 + \omega_n^2\epsilon_1 = \frac{F_1}{4I_n} \tag{3-76}$$

Since $\zeta_1 = \zeta_2 = \zeta_3 = \zeta_4 = \epsilon_1$, it becomes possible to write four dependent equations as

$$\ddot{\zeta}_j + 2\omega_n\zeta\dot{\zeta}_j + \omega_n^2\zeta_j = F_j \tag{3-77}$$

where

$$\begin{Bmatrix} F_1 \\ F_2 \\ F_3 \\ F_4 \end{Bmatrix} = \frac{1}{4I_n} \begin{bmatrix} 1 & 1 & 1 & 1 \\ 1 & 1 & 1 & 1 \\ 1 & 1 & 1 & 1 \\ 1 & 1 & 1 & 1 \end{bmatrix} \times \begin{bmatrix} W_1 \\ W_2 \\ W_3 \\ W_4 \end{bmatrix} \tag{3-78}$$

Thus, for a collective mode for a gimbaled rotor,

$$HTC(i,j) = \cos[NB(\psi(i) - \psi(j))] \tag{3-79}$$

where NB is the number of blades.

The third case is that of a scissor mode for a four-bladed gimbaled rotor. The rotor mode for a scissor mode would be

Mode No.	Blade 1	Blade 2	Blade 3	Blade 4
1	MS(x)	-MS(x)	MS(x)	-MS(x)

and the forcing function for the independent rotor modal equation would be

$$F_1 = \int_0^R \Big[MS(x) \cdot A_1(x) - MS(x) \cdot A_2(x) - MS(x) \cdot A_3(x) \quad MS(x) \cdot A_4(x) \Big] dx \tag{3-80}$$

The localized blade coordinate would be

$$\delta_1 = \delta_3 = \epsilon \qquad \delta_2 = \delta_4 = -\epsilon \tag{3-81}$$

The four dependent equations could be written

$$\ddot{\delta}_j + 2\zeta\omega_n\dot{\delta}_j + \omega_n^2\delta_j = \frac{F}{4I_n} \tag{3-82}$$

where

$$\begin{bmatrix} F_1 \\ F_2 \\ F_3 \\ F_4 \end{bmatrix} = \frac{1}{4I_n} \begin{bmatrix} 1 & -1 & 1 & -1 \\ -1 & 1 & -1 & 1 \\ 1 & -1 & 1 & -1 \\ -1 & 1 & -1 & 1 \end{bmatrix} \times \begin{bmatrix} W_1 \\ W_2 \\ W_3 \\ W_4 \end{bmatrix} \tag{3-83}$$

which leads to the conclusion

$$HTC(i,j) = \cos \left| 2 \left(\psi(i) - \psi(j) \right) \right| \tag{3-84}$$

The only hub type remaining is that where there is no moment carry-over at the hub, i.e., rigid or articulated. For this type rotor, the response of blade i is not related dynamically to the loads on blade j. Therefore, the Hub Transfer Coefficient matrix would have the following form:

$$HTC(i,j) = \begin{cases} 1 & \text{for } i = j \\ 0 & \text{for } i \neq j \end{cases} \tag{3-85}$$

Equations (3-74), (3-79), (3-84), and (3-85) can be brought together in the following form:

$$HTC(i,j) = \begin{cases} \cos \; \psi(i) - \psi(j) & \text{cyclic} \\ \cos \; 2\left(\psi(i) - \psi(j)\right) & \text{scissor} \end{cases} \Bigg\} \text{Teetering}$$
$$\left.\begin{cases} \cos \; NB\left(\psi(i) - \psi(j)\right) & \text{collective} \end{cases}\right\} \text{Gimbaled} \qquad (3\text{-}86)$$
$$\left\{ 1 \text{ or } 0 \qquad \text{articulated or hingeless} \right.$$

which defines the dynamic effects of blade i on blade j for each mode type. The actual program has been written to consider up to six mode shapes and up to seven blades. The HTC matrix is therefore 7 x 7 x 6.

3.2.12 Cyclic Detuning

The rotor blade natural frequencies and mode shapes are a function of the rotor speed and hub geometric pitch. Previous versions of the digital program have been structured to accept as input the mode shapes and natural frequencies at one combination of rotor speed and hub geometric pitch. This limiting assumption is modified by including the effects of cyclic detuning in the following manner: The blade natural frequencies and mode shapes are calculated at three values of collective pitch (low, mid, high) and three values of rotor speed (low, mid, high). The mode shapes at the mid collective pitch and mid rotor speed are assumed to represent the mode shape at all combinations of pitch and rotor speed.

Four values of the natural frequencies for mode shape are input data. The four values of ω_n are obtained from the extreme combinations of rotor speed and collective pitch (low rotor speed in combination with low collective pitch and high collective pitch, etc.). The increments on rotor speed and collective pitch used in calculating the mode shapes and natural frequencies are also required input data.

The previous section (Hub Transfer Coefficient Matrix) has shown that for each blade, for each input mode shape there is an equation of the form

$$\ddot{\delta}_j + 2\delta\omega_n\dot{\delta}_j + \omega_n^2\delta_j = F_j \qquad (3\text{-}87)$$

For each blade an instantaneous value of rotor speed and hub geometric pitch (collective plus cyclic pitch) is known which permits bivariant interpolation to calculate an instantaneous value of the natural frequency from the input data.

3.3 AERODYNAMICS

3.3.1 General

The detailed representation of rotor dynamics can be most effective when used with a similarly refined analysis of aerodynamic effects. Previous versions of C81 dealt mainly with steady-state aerodynamics. Tip vortex

effects, lift variation time lag, and radial flow were also included. AGAJ73 includes the aerodynamic features described in Reference 2, and in addition, two procedures for evaluating the first-order effects of unsteady aerodynamics. These features allow the interaction of the blade rigid body and elastic motions and the aerodynamic forces acting thereon, which is essential for the study of aeroelastic response phenomena.

The steady, as well as unsteady, aerodynamic model is also improved by accounting for the effect of the angle between the resultant wind velocity and the blade leading edge. This angle can be modified by a sweep angle built into the blade tip.

Figure 3-15 shows the organization of the rotor aerodynamic analysis and the possible computational paths.

The rotor aerodynamic analysis is basically the same as discussed in Reference 2. The relative wind velocity at a point P on the blade, considered as rigid, is given in Reference 2 as

$$\vec{v}_p = \vec{v}_i - \vec{v}_h + \left(\vec{\omega}_b \times \vec{r}_p \right) \tag{3-88}$$

where

$\vec{v}_i$ is the induced velocity at the point P on the blade x-axis

$\vec{v}_h$ is the linear velocity of the hub

$\vec{\omega}_b$ is the angular velocity of the rotating shaft reference system relative to an inertial reference system (see Equation (3-6) in Section 3.2.3)

$\vec{r}_p$ is the distance vector from the hub to point P on the blade x-axis, i.e., the rigid body part of x in Equation (3-5) for $\vec{\rho}$.

Note that the acceleration $\vec{a}_p$ in Equation (3-15), Section 3.2.5, is the time derivative of the bracketed expression in Equation (3-88).

3.3.2 Induced Velocity Analysis

The analysis which determines the magnitude and direction of $\vec{v}_i$ assumes that the vector is always parallel to the centerline of the rotor shaft. Hence, in the following discussion, the vector notation is dropped and the quantity v_i is the value of the local induced velocity. This quantity is defined as

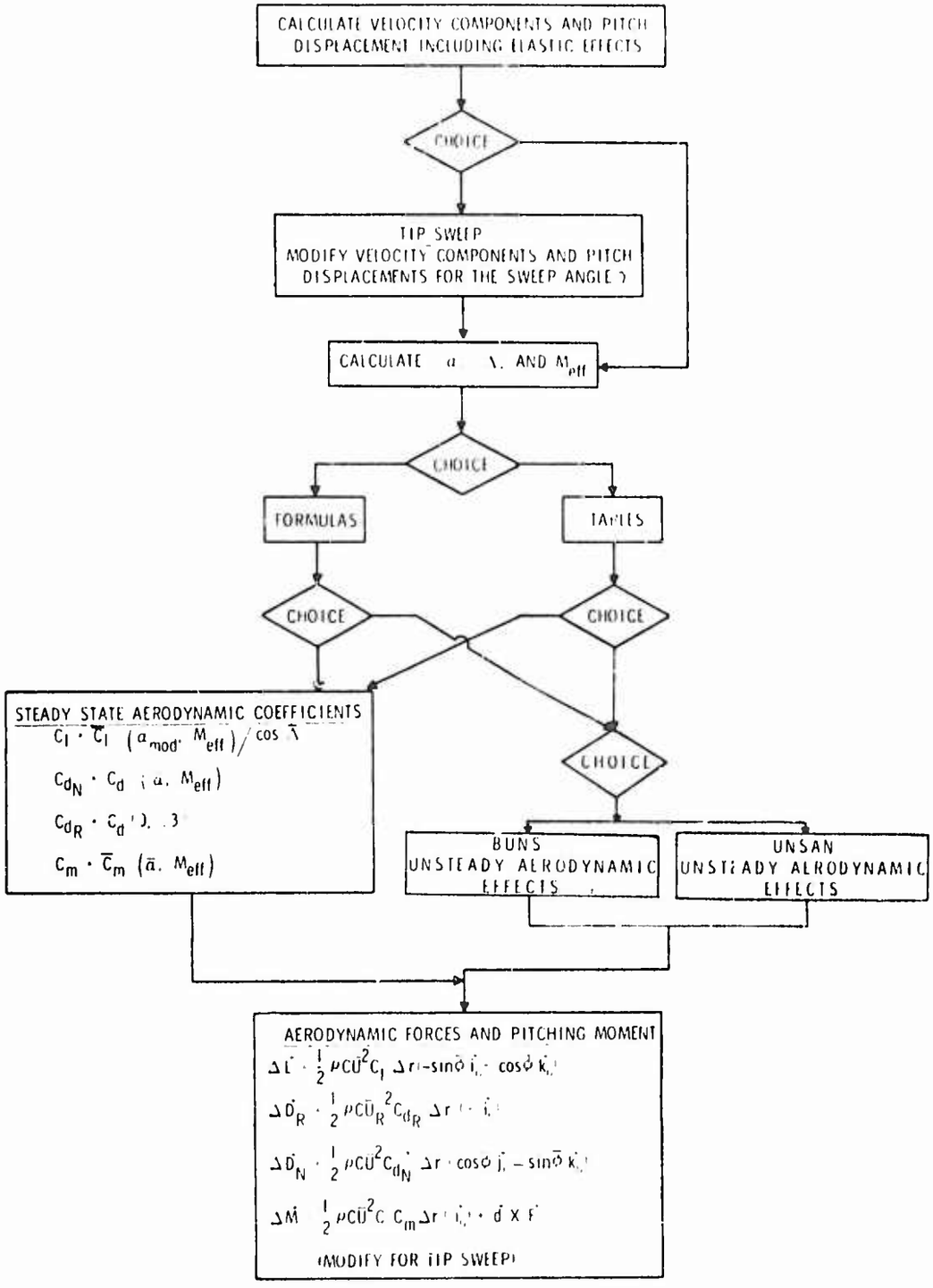

Figure 3-15. Flow Chart for Rotor Aerodynamic Logic.

$$v_i = \bar{V}_i \, F_N \tag{3-89}$$

where

$\bar{V}_i$ = the average value of v_i across the rotor disc as determined from momentum theory

F_N = a function for the value of v_i normalized by $\bar{V}_i$; defined in Section 3.26.2 of Volume II

For the computer program, the function F_N can be defined by either an equation or a data table. Both the equation and the table are functions of advance ratio, μ; radial station, x; and blade azimuth, ψ. In addition, the table is a function of inflow ratio, λ. The equation and the table used to generate the function are discussed in Section 3 of Volume II.

The equation for the momentum theory value of induced velocity, $\bar{V}_i$, is based on the analysis and experimental work presented in References 8 and 9. After converting to the nomenclature and sign conventions of this report, the following definitions are made for the average advance ratio, $\bar{\mu}$, average induced inflow ratio, $\bar{\lambda}_i$, and average inflow ratio, $\bar{\lambda}$,

$$\bar{\mu} = V_h/\Omega R \tag{3-90}$$

$$\bar{\lambda}_i = \bar{V}_i/\Omega R \tag{3-91}$$

$$\bar{\lambda} = \left(V_z - \bar{V}_i\right)/\Omega R \tag{3-92}$$

$$= V_z/\Omega R - \bar{\lambda}_i$$

where

V_h is the component of the free-stream velocity at the hub in the plane perpendicular to the rotor shaft (always positive)

V_z is the component of the free-stream velocity along the centerline of the rotor shaft (positive up).

Note that the square root of the sum of the squares of V_h and V_z is equal to the magnitude of $\vec{v}_h$ in Equation (3-88).

The expression for $\bar{V}_i$ is then

$$\bar{V}_i = \bar{\lambda}_i(\Omega R)$$

$$= \frac{C_B(\Omega R)}{\sqrt{0.866\bar{\lambda}^2 + \bar{\mu}^2} + \frac{0.6|C_B|^{1.5}\left(|C_B| + 8\bar{\lambda}|\bar{\lambda}|/3\right)}{\left(C_B + 8\bar{\lambda}^2\right)\left(C_B + 8\bar{\mu}^2\right)}} \qquad (3\text{-}93)$$

The factor C_B is the thrust coefficient corrected for tip loss and hub extent:

$$C_B = C_T / \left(B^2 - X_h^2\right)$$

$$= T / \rho\pi R^2(\Omega R)^2\left(B^2 - X_h^2\right) \qquad (3\text{-}94)$$

where

- T is thrust
- ρ is air density
- R is rotor radius
- X_h is the hub extent divided by the rotor radius

The tip loss factor is defined as

$$B = 1 - \frac{2\sqrt{C_T}}{b} \qquad (3\text{-}95)$$

where b is the number of rotor blades.

Since $\bar{\lambda}$ is a function of $\bar{V}_i$, as defined in Equation (3-92), Equation (3-93) is not a closed form solution for $\bar{V}_i$. Hence, the equation is solved by iteration.

When the center of gravity of the rotorcraft is between one-fourth and one rotor diameter above the ground and the airspeed is less than 30 feet per second, $\bar{V}_i$ is corrected for ground effect.

$$\bar{V}_i = \left(\bar{V}_i\right)_{OGE} \left[1 + (G - 1) \left| (V - 30)/30 \right|^2 \right] \qquad (3\text{-}96)$$

where

$\left(\bar{V}_i\right)_{OGE}$ is the value of $\bar{V}_i$ from iterative solution of Equation (3-93), i.e., out-of-ground effect

G is 0.25 plus the altitude of the cg divided by the rotor diameter, and

V is the flight path velocity in feet per second.

If the value of G drops below 0.25 the rotorcraft is assumed to have contacted the ground. The VIND subroutine in C81 performs the above iterative procedure and ground effect correction. The flow chart of the subroutine is shown in Figure 3-16. The equation for VIR corresponds to Equation (3-92) except that the numerator and denominator have both been multiplied by ΩR so that the units of all the terms in the equation are in powers of feet per second rather than being nondimensional.

3.3.3 Blade Reference Velocities

The reference axis system for blade aerodynamics is obtained from the reference system described in Section 3.2.3 (Figure 3-1) by a rotation through the blade flapping angle β about the y-axis. The relative wind can be expressed in the blade reference as

$$\vec{v}_p = U_R \vec{i}_b + U_T \vec{j}_b - U_P \vec{k}_b \qquad (3\text{-}97)$$

The axis systems and wind velocity components are shown in Figure 3-17. In the determination of angle of attack and dynamic pressure $\dot{Z}\cos\beta$ and $\ddot{Z}\cos\beta$ are assumed equal to $\dot{Z}$ and $\ddot{Z}$. The angle from the blade xy-plane to the section reference line is θ_p, and the angle from the blade xy-plane to $(U_T\vec{j}_b - U_P\vec{k}_b)$ is ϕ. Let $U^2 = U_T^2 + U_P^2$. In Reference 1, the dynamic pressure is

$$q = 1/2\ \rho U^2 \qquad (3\text{-}98)$$

The inflow angle is

$$\phi = \tan^{-1} \frac{U_P}{U_T} \qquad (3\text{-}99)$$

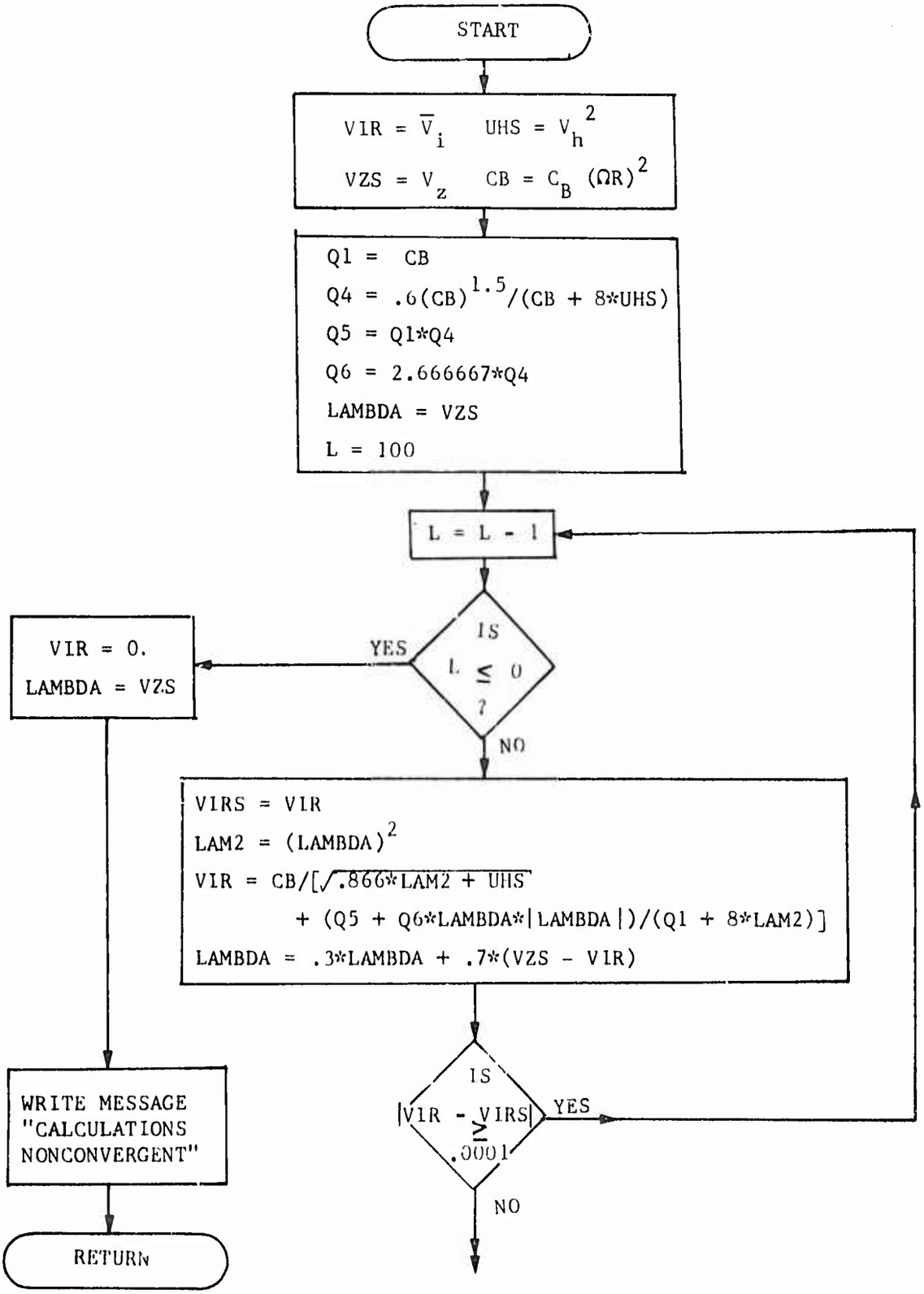

Figure 3-16. Flow Chart of Induced Velocity Calculations.

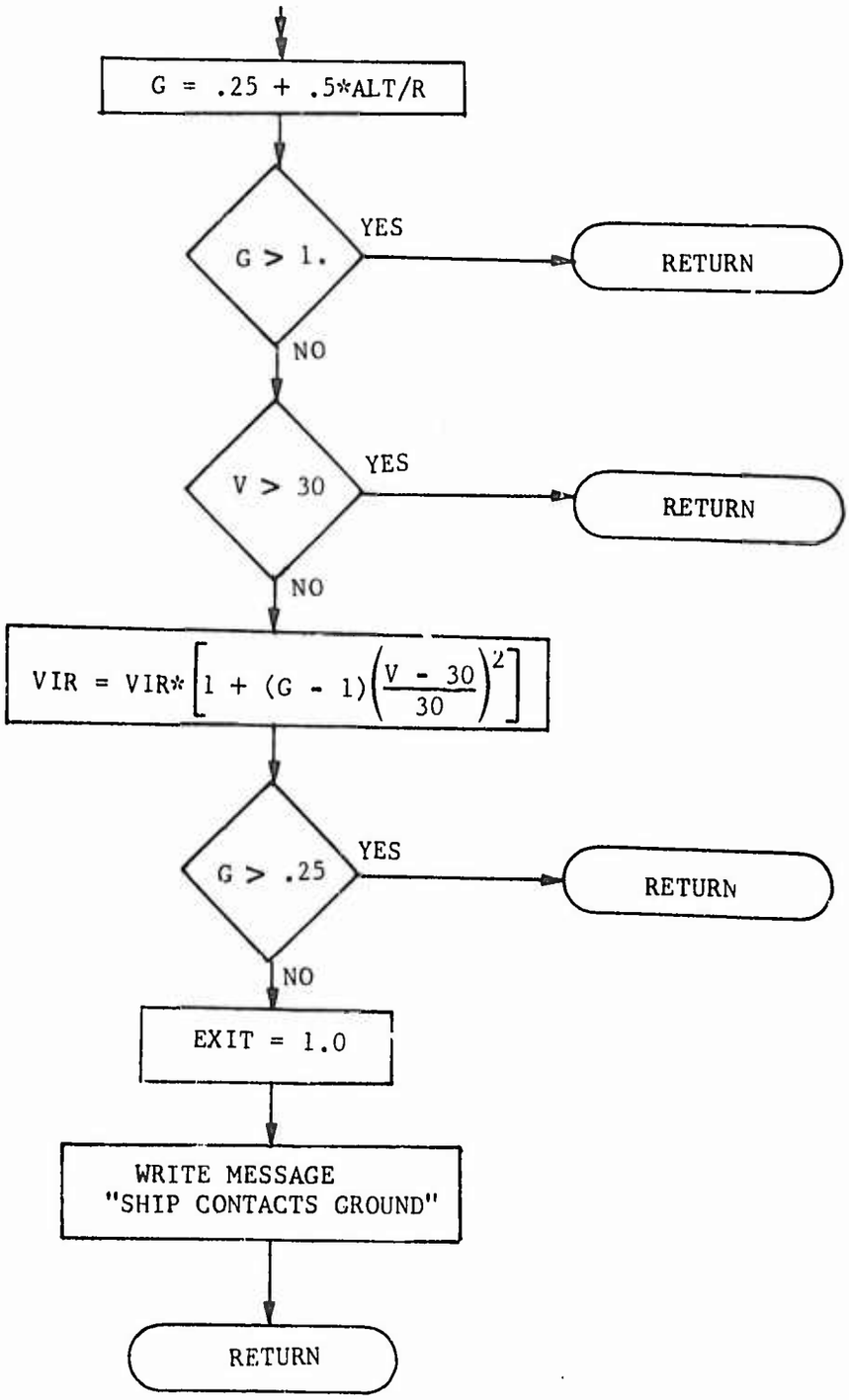

Figure 3-16. Concluded.

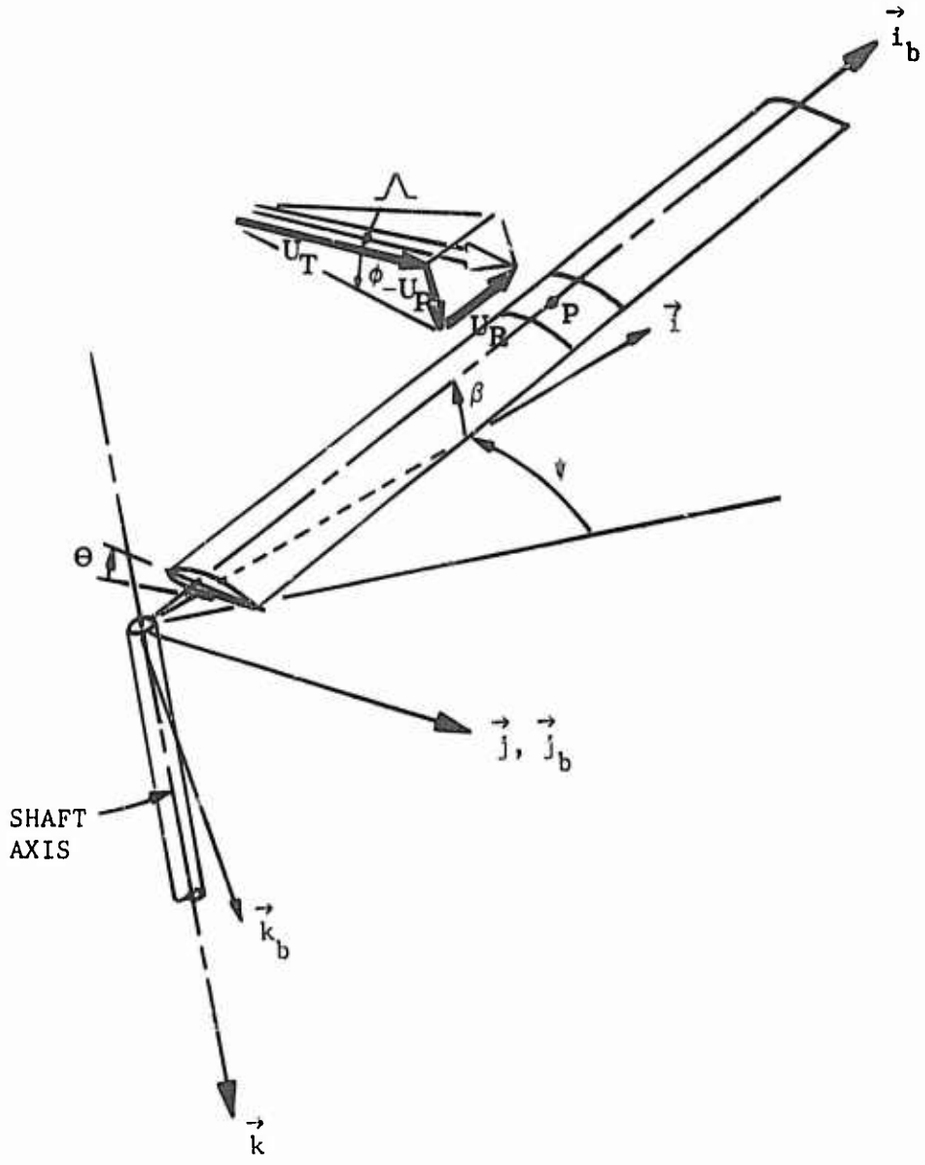

Figure 3-17. Reference Axis System for Blade Aerodynamics.

and the angle of attack is

$$\alpha = \theta_p + \phi \tag{3-100}$$

The new rotor aeroelastic analysis includes blade bending and pitching displacements and velocities as developed in Section 3.2.4. The velocity due to both rigid and elastic motion is included in v_p. Hub motion and mast windup (Section 3.2.9) are included in the elastic velocity components. Both the rigid body feathering motion and the elastic torsion are used to compute the blade pitching velocity and acceleration and the rate of change of angle of attack. Thus,

$$\bar{U}_T = U_T - \dot{Y} + l_F \dot{a}_F \sin\psi + l_L \dot{a}_L \cos\psi + r\dot{\psi}_T \tag{3-101}$$

Since $\dot{Z}$ (Equation 3-13) includes rigid-body flapping,

$$\bar{U}_P = U_P + X\dot{\beta} - \dot{Z} \tag{3-102}$$

$$\bar{U}_R = U_R \tag{3-103}$$

$$\bar{\phi} = \tan^{-1}\left(\frac{\bar{U}_P}{\bar{U}_T}\right) \tag{3-104}$$

$$\bar{\theta} = \theta + \theta_p \tag{3-105}$$

$$\dot{\bar{\theta}} = \dot{\theta} + \dot{\theta}_p \tag{3-106}$$

$$\ddot{\bar{\theta}} = \ddot{\theta} + \ddot{\theta}_p \tag{3-107}$$

$$\bar{\alpha} = \bar{\theta} + \bar{\phi} \tag{3-108}$$

$$\dot{\bar{\alpha}} = \dot{\bar{\theta}} + \dot{\bar{\phi}} \tag{3-109}$$

$$\bar{U} = \sqrt{\bar{U}_T^2 + \bar{U}_P^2} \tag{3-110}$$

$$\bar{q} = \frac{1}{2} \rho \bar{U}^2 \tag{3-111}$$

The symbols θ, $\dot{\theta}$, and $\ddot{\theta}$ are defined in Equations (3-7), (3-13), and (3-14), respectively. The effects of blade pitching velocity and acceleration are discussed in the section on nonsteady aerodynamics.

3.3.4 Steady-State Aerodynamic Coefficients

3.3.4.1 Lift and Drag Coefficients

The methods for calculating C_l and C_d for steady-state assumptions are discussed in Reference 2. Formulas or tables can be used for these evaluations. Aerodynamic data tables for C_l, C_d and C_m may be supplied by the user, or a set of NACA 0012 airfoil data tables is available as compiled data. Since the publication of Reference 2, pitching moment coefficients in the tables and the formulas have been added and are discussed in this section of the report.

Usually the blade aerodynamics are defined in a plane perpendicular to the leading edge. However, investigators have found that the angle in the xy-plane between the wind vector and the leading edge of the blade, the yawed flow angle, Λ, influences the aerodynamic forces generated. From Figure 3-17,

$$\Lambda = \tan^{-1}\left(\frac{\bar{U}_R}{\bar{U}_T}\right) \tag{3-112}$$

Harris's development (Reference 10) suggests that the influence of yawed flow be included in all aspects of the steady-state lift determination. Hoerner, in Reference 11, emphasizes the need for varying the effective Mach number with Λ to improve correlation with test data. A modified angle of attack and a three-dimensional effective Mach number are calculated as follows for $|\bar{\alpha}| < 30^\circ$:

$$\bar{\Lambda} = \text{sign}(\Lambda) \cdot \min\left\{\frac{|\Lambda|}{60^\circ}\right\} \tag{3-113}$$

$$\alpha_{mod} = \bar{\alpha} \cos \bar{\Lambda} \tag{3-114}$$

$$M_{eff} = \frac{\sqrt{\bar{U}_R^2 + \bar{U}_T^2 + \bar{U}_P^2}}{v_{sound}} \left(\cos q_1 \bar{\Lambda}\right)^{q_2} \tag{3-115}$$

Hoerner's results can be closely approximated by taking $q_1 = 0.2$, $q_2 = 1$ or $q_1 = 1$, $q_2 = 0.5$; both q_1 and q_2 are inputs to the program. The steady-state lift coefficient is

$$C_{l_S} = C_l\left(\alpha_{mod}, M_{eff}\right) \Big/ \cos \Lambda, \tag{3-116}$$

whether formulas or tables are used. For $|\bar{\alpha}|$ below stall, Λ is effective only to the extent of lowering the Mach number. When $|\bar{\alpha}|$ is above stall, the yawed flow consideration can delay loss of lift as illustrated in Figure 3-18.

The steady-state drag calculation has been modified only by the inclusion of radial flow and the use of M_{eff}. According to Harris (Reference 10),

> "skin friction drag force should be calculated in the direction of the resultant velocity."

This is accomplished by computing, in addition to the conventional drag normal to the blade axis, a frictional drag along the blade based on $\bar{U}_R$. The drag coefficient appropriate for this effect is the steady-state value

$$C_{d_R} = C_d(\bar{\alpha} = 0,\ M = .3) \tag{3-117}$$

Harris's requirement that "Pressure drag force is then calculated only in the blade element plane normal to the blade span axis" is also satisfied by using

$$C_{d_N} = C_d\left(\bar{\alpha},\ M_{eff}\right) \tag{3-118}$$

3.3.4.2 Pitching Moment Coefficient

The method of calculating pitching moment coefficient is indicated in Figure 3-19. The C_m coefficient depends on the angle of attack, $\bar{\alpha}$, the effective Mach number, M_{eff}, and input constants. The inputs A_1, A_2, and A_3 are coefficients for a quadratic function of $|\bar{\alpha}|$ determining the corresponding value of Mach number at which the C_m curve breaks sharply away from an input constant value, A_4. For $|\bar{\alpha}| < 90^\circ$, the first series of calculations and tests is to determine the relative size of $\bar{\alpha}$; the angle of attack, α_B, corresponding to M_{eff} on the "break" curve; and A_5, a critical value of angle of attack which is independent of Mach number (Figure 3-20, (a) and (b)). The evaluation of C_m is different for $|\bar{\alpha}| \leq \alpha_B$, $\alpha_B < |\bar{\alpha}| \leq A_5$ and $A_5 < |\bar{\alpha}|$.

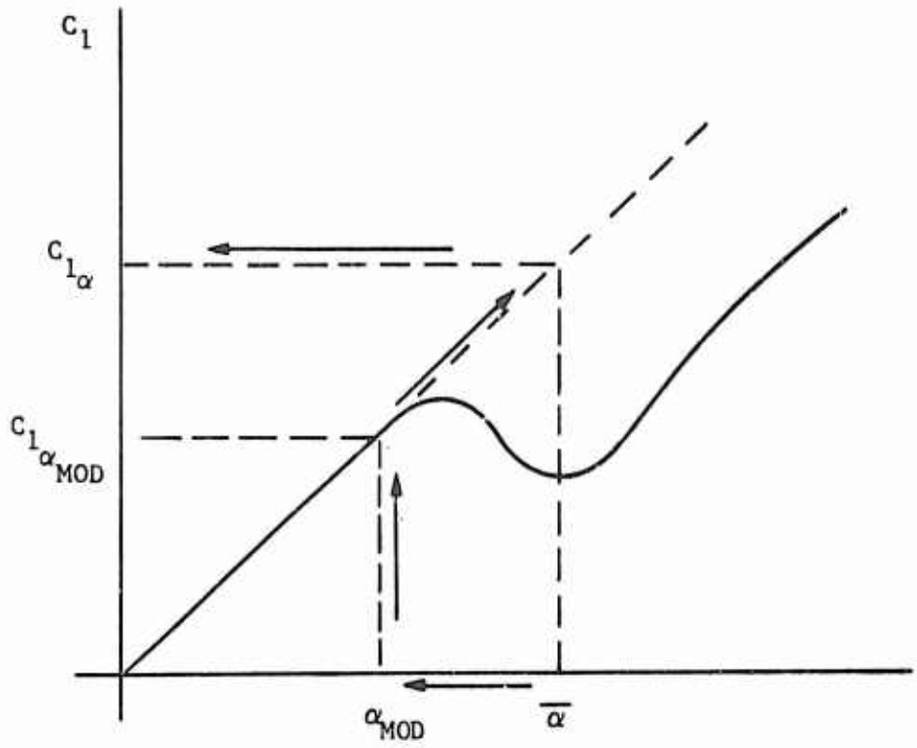

Figure 3-18. Effect of Yawed Flow on Lift Coefficient.

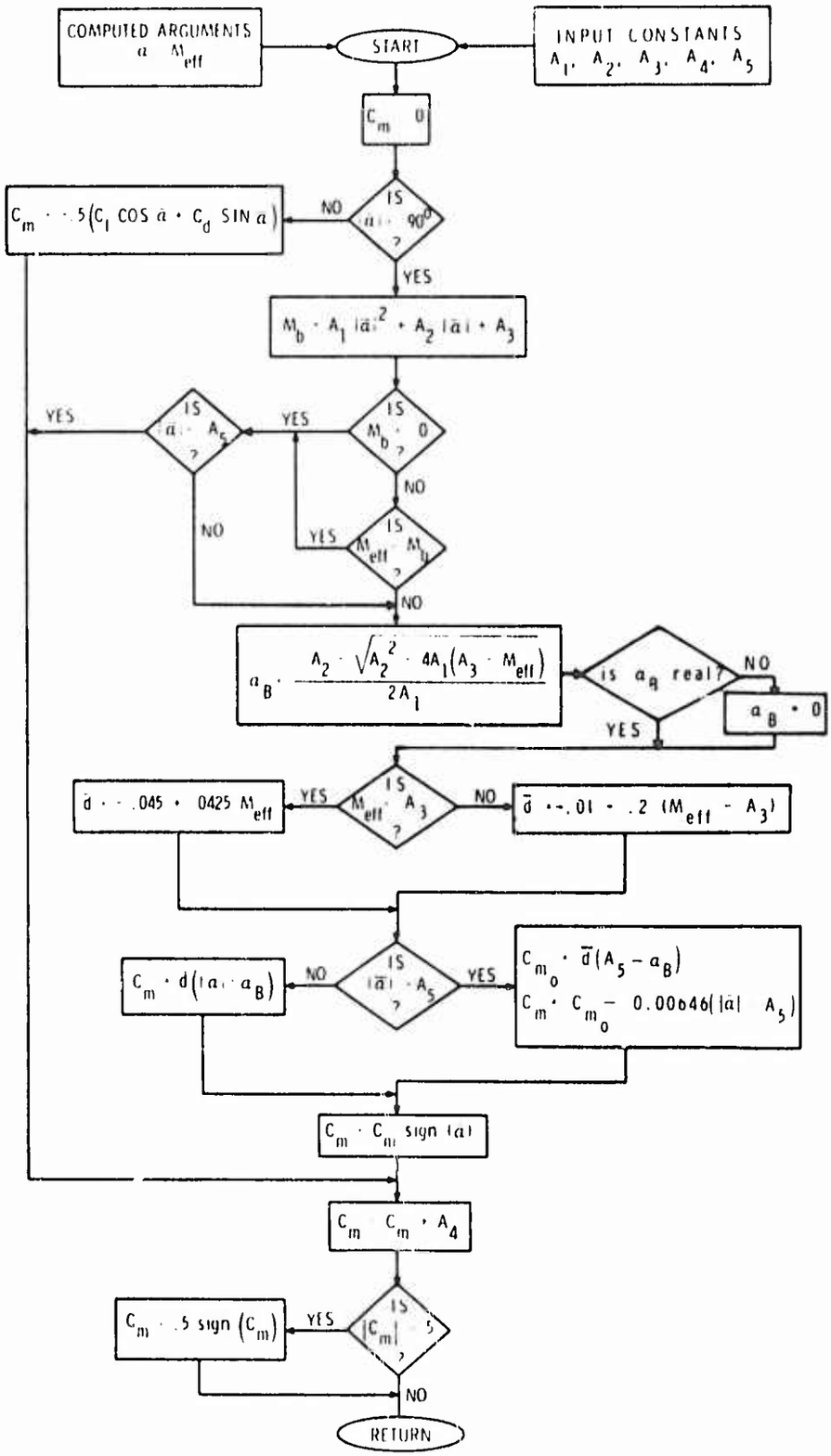

Figure 3-19. Flow Chart for Steady-State Pitching Moment Calculation.

(a) If $|\bar{\alpha}| < 90°$, determine α_B and A_5 from equation for M_b and value of M_{eff}; otherwise go to (d) to determine normal force (C_N).

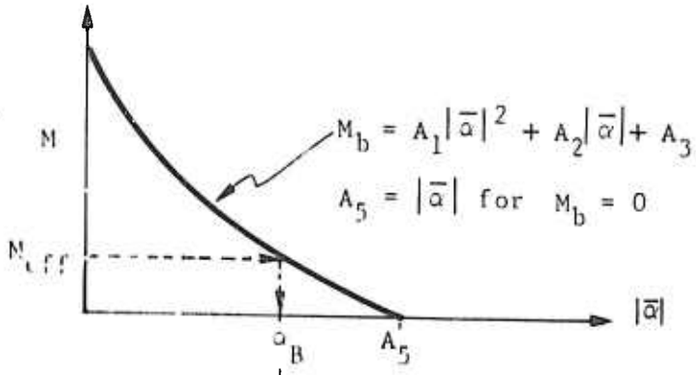

(b) If $|\bar{\alpha}| \leq \alpha_B$, set $C_m = A_4$; otherwise go to (c) to determine the value of $\bar{d}$.

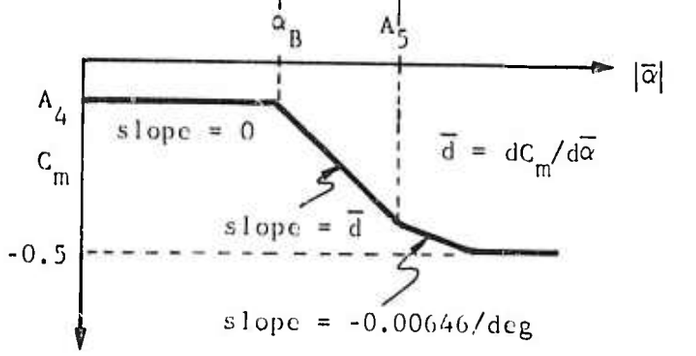

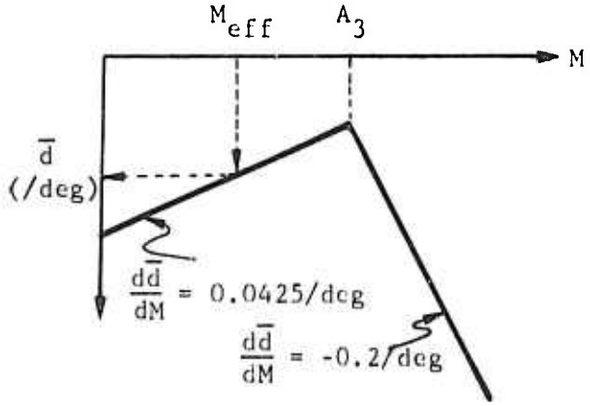

(c) Determine value of $\bar{d}$ as a function of M_{eff}; note that $\bar{d}$ is a slope and $d\bar{d}/dM$ is the rate of change of a slope.

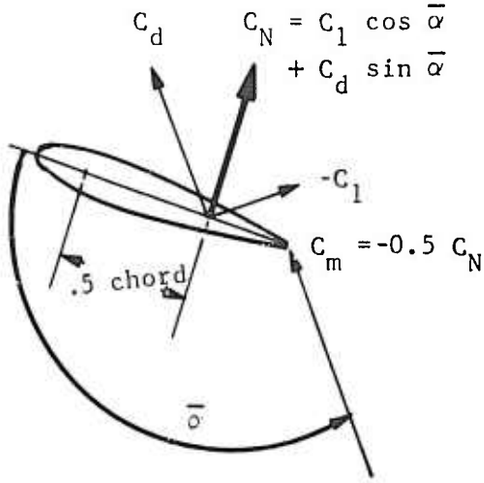

(d) If $|\bar{\alpha}| \geq 90°$, lift and drag act at 75% chord, and hence contribute to pitching moment.

Figure 3-20. Determination of Steady-State Pitching Moment Coefficient.

For $|\bar{\alpha}|$ less than α_B,

$$C_m = A_4 \tag{3-119}$$

For $|\bar{\alpha}|$ between α_B and A_5, a slope, $\bar{d}$, is computed for the C_m line between α_B and A_5. This slope depends on M_{eff} and an input critical value, A_3, as shown in Figure 3-20(c). The pitching moment coefficient is calculated from

$$C_m = \bar{d}\left(|\bar{\alpha}| - \alpha_B \right)(\text{sign } \bar{\alpha}) + A_4 \tag{3-120}$$

If $|\bar{\alpha}|$ is greater than A_5, a second slope, included in the program, is used. In this case,

$$C_m = \left[\bar{d}\left(A_5 - \alpha_B\right) - .00646\left(|\bar{\alpha}| - A_5\right)\right](\text{sign } \bar{\alpha}) + A_4 \tag{3-121}$$

For $|\bar{\alpha}| > 90^\circ$, the aerodynamic center is assumed to be located at the .75 chord rather than at the .25 chord. The pitching moment about the blade neutral axis (assumed to be at the .25 chord) is in this case mainly due to lift and drag forces.

Hence,

$$C_m = -.5\left(C_l \cos \bar{\alpha} + C_d \sin \bar{\alpha} \right) + A_4 \tag{3-122}$$

The relationships of the blade profile and the aerodynamic vectors are shown in Figure 3-20 (d). As shown in the flow diagram (Figure 3-19), the magnitude of C_m is limited to 0.5 in any case.

3.3.4.3 Tip Sweep Effect

Tip sweep affects the aerodynamic forces on the top segment of the blade. For a sweep angle γ (Figure 3-21), velocities and angle-of-attack components are modified as follows:

$$\bar{\bar{U}}_R = \bar{U}_R \cos \gamma + \bar{U}_T \sin \gamma \tag{3-123}$$

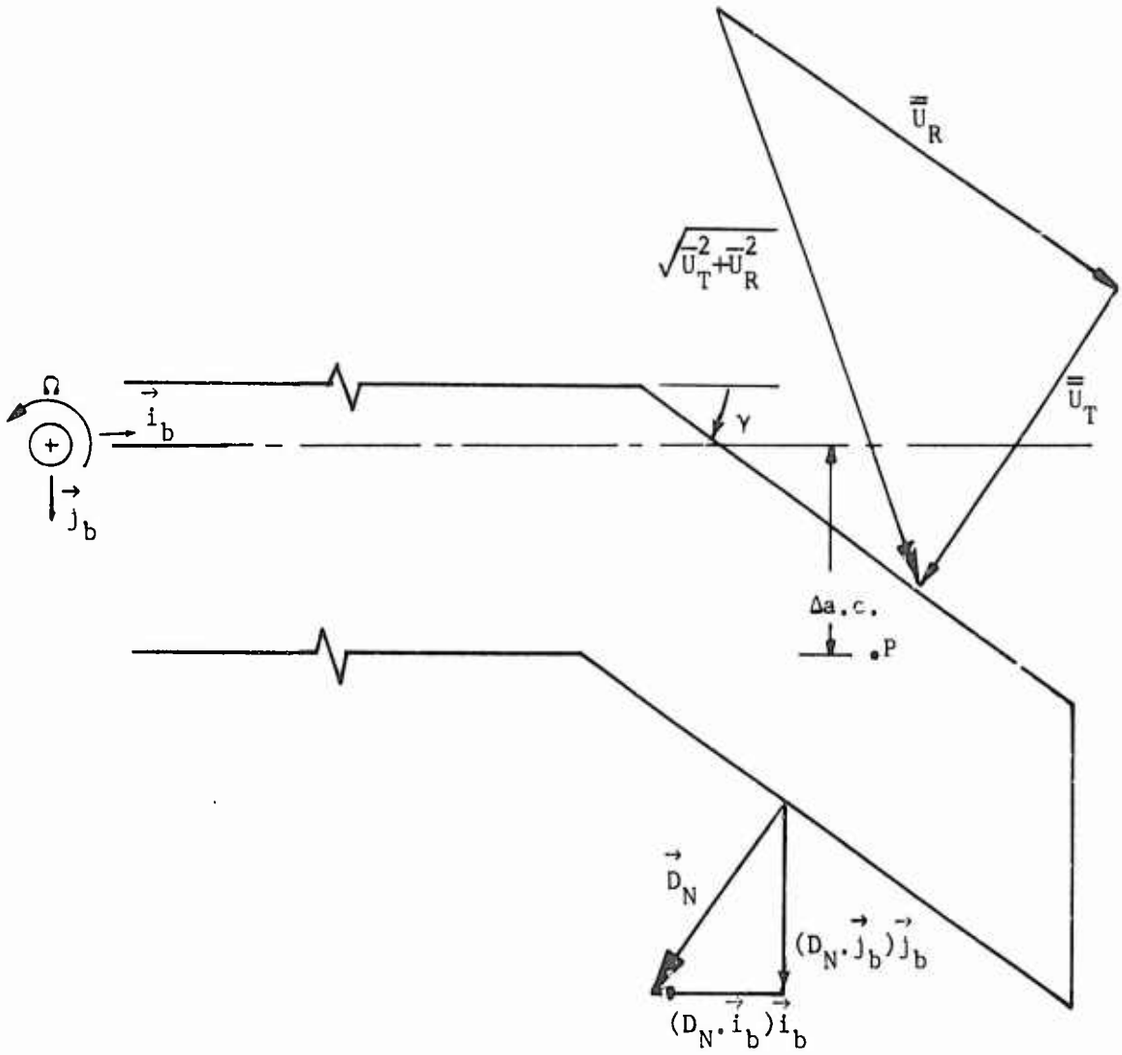

Figure 3-21. Effect of Tip Sweep.

$$\bar{\bar{U}}_T = \bar{U}_T \cos\gamma - \bar{U}_R \sin\gamma \tag{3-124}$$

$$\bar{\bar{U}} = \sqrt{\bar{\bar{U}}_T^{\,2} + \bar{U}_P^{\,2}} \tag{3-125}$$

$$\bar{\bar{q}} = \frac{1}{2}\rho\,\bar{\bar{U}}^2 \tag{3-126}$$

Then the revised inflow angle and angle of attack are

$$\bar{\bar{\phi}} = \tan^{-1}\frac{U_P}{\bar{\bar{U}}_T} \tag{3-127}$$

$$\bar{\bar{\theta}} = \bar{\theta}\cos\gamma \tag{3-128}$$

$$\bar{\bar{\alpha}} = \bar{\bar{\theta}} + \bar{\bar{\phi}} \tag{3-129}$$

and

$$\bar{\bar{\Lambda}} = \tan^{-1}\frac{\bar{\bar{U}}_R}{\bar{\bar{U}}_T} \tag{3-130}$$

3.3.4.4 Aerodynamic Forces and Moments

Aerodynamic forces and moments at a representative blade segment are then

Lift:

$$\Delta\vec{L} = \frac{1}{2}\rho c\bar{U}^2 C_l\,\Delta r\left(-\sin\bar{\phi}\,\vec{j}_b - \cos\bar{\phi}\,\vec{k}_b\right) \tag{3-131}$$

Radial Component of Drag:

$$\Delta\vec{D}_R = \frac{1}{2}\rho c\bar{U}^2 C_{d_R}\,\Delta r\,(-\vec{i}_b) \tag{3-132}$$

Normal Component of Drag:

$$\Delta\vec{D}_N = \frac{1}{2}\rho c\bar{U}^2 C_{d_N} \Delta r \left(\cos \bar{\phi}\, \vec{j}_b - \sin \phi\, \vec{k}_b \right) \tag{3-133}$$

Pitching Moment:

$$\Delta\vec{M} = \left(\frac{1}{2}\rho c\bar{U}^2 (c\, C_m)\, \Delta r\right)\vec{i}_b + \vec{d} \times \Delta\vec{F} \tag{3-134}$$

where
$$d = Y\vec{j}_b - Z\vec{k}_b \tag{3-135}$$

and
$$\Delta\vec{F} = \Delta\vec{L} + \Delta\vec{D}_N \tag{3-136}$$

At the blade tip, $\bar{\bar{U}}$ and $\bar{\bar{\phi}}$ replace U and ϕ in the calculations. Also, the normal component of drag $\vec{D}_N$ has components in the blade axis system defined by

$$\Delta\vec{D}_{N_{tip}} = \frac{1}{2}\rho c\bar{\bar{U}}^2 C_d \Delta r \left(- \sin\gamma \cos \bar{\bar{\phi}}\, \vec{i}_b + \cos\gamma \cos \bar{\bar{\phi}}\, \vec{j}_b + \sin \bar{\bar{\phi}}\, \vec{k}_b \right) \tag{3-137}$$

Due to the offset Δa.c., the lift force at the tip will produce an additional pitching moment given by the following equation:

$$\Delta\vec{M}_{tip} = - (\Delta a.c.)(\Delta L_{TIP})\vec{i}_b \tag{3-138}$$

This increment is added to the value from Equation (3-134) for the unswept tip.

The radial component of drag at the tip is taken in the same direction as for the rest of the blade.

The applied aerodynamic forces and moments are the source of the rotor rigid body and elastic deflections, velocities, and accelerations; and the resulting response, in shaft reference, allows calculation of H-force, Y-force, thrust, and rotor torque required.

In the shaft reference coordinate system, the aerodynamic forces and moments for a blade segment with center at a radial distance x from the origin are

$$\vec{A} = A_x\vec{i} + A_y\vec{j} + A_z\vec{k} \tag{3-139}$$

and

$$\vec{M}_A = A_\theta\vec{i} + M_y\vec{j} + M_z\vec{k} \tag{3-140}$$

where

$$A_x = (\Delta\vec{L} + \Delta\vec{D}_N) \cdot \vec{k}_b \sin\beta - \Delta\vec{D}_R \cdot \vec{i}_b \cos\beta \tag{3-141}$$

$$A_y = (\Delta\vec{L} + \Delta\vec{D}_N) \cdot \vec{j}_b \tag{3-142}$$

$$A_z = -(\Delta\vec{L} + \Delta\vec{D}_N) \cdot \vec{k}_b \cos\beta + \Delta\vec{D}_R \cdot \vec{i}_b \sin\beta \tag{3-143}$$

$$A_\theta = \Delta\vec{M} \cdot \vec{i}_b \cos\beta \tag{3-144}$$

M_y, M_z } neglected

Note that $\vec{M}_A$ is actually the <u>total</u> moment vector with components A_θ, M_y, and M_z, while $\Delta\vec{M}$ is specifically <u>pitching</u> moment. However, since M_y and M_z are neglected, $\vec{M}_A$ in effect becomes exclusively a pitching moment vector also.

The term A_x is used in the rotor aerodynamic H-force and Y-force calculations, while A_y, A_z and A_θ are in Equation (3-12) to compute the time-variant aeroelastic rotor response.

3.3.5 <u>Unsteady Aerodynamics</u>

The following two sections are discussions of the BUNS and UNSAN unsteady aerodynamic options. The two mathematical models were developed under separate contracts with the Eustis Directorate of USAAMRDL.

3.3.5.1 BUNS Unsteady Aerodynamic Model

As previously mentioned, the additional velocities due to flexible blade dynamics can be included in computing the angle of attack, Mach number, and dynamic pressure at a point on the blade. The major modification to the aerodynamic simulation of Reference 2, done as a part of Contract DAAJ02-70-C-0063, was the consideration of unsteady effects.

Several investigators have discussed the importance of unsteady aerodynamics on rotary-wing aircraft. Loewy and also Timman and Van de Vooren (References 12 and 13) have shown that special circulatory terms are significant in hover flight, but conservative results are obtained by neglecting them (Drees, Reference 14). On the other hand, according to Carta (Reference 15) and Harris (Reference 10), the nonsteady air loads can assume a major role in blade aeroelastic response and can produce stall flutter.

One of the major difficulties in implementing these aerodynamic refinements is the lack of meaningful measured values over the full range of angles of attack and yaw angles that are applicable for the rotating blade. In particular, the wind tunnel data are presented in terms of angle-of-attack rates due to rotation about the pitch-change axis ($\dot{\theta}$, $\ddot{\theta}$). Rotation about the shaft also results in inflow angle rates $\dot{\phi}$, $\ddot{\phi}$; however, the damping and inertial effects from these rates are not the same as from pitch change rates. Simplification of the problem is unavoidable due to the lack of data. It is therefore appropriate in the calculation of unsteady aerodynamics to use $\dot{\theta}$ and $\ddot{\theta}$ in terms related to blade motion only, and $\dot{\alpha}$ in terms pertaining to stall hysteresis. The variables $\dot{\bar{\theta}}$ and $\ddot{\bar{\theta}}$ include changing geometric pitch due to cyclic variations, control motions, and elastic blade torsion.

The remaining consideration is the blade section linear acceleration. The principal effect is due to the component normal to the blade xy-plane (the heaving acceleration) and is represented as the sum of the rigid body and elastic accelerations ($\ddot{Z}$). The linear accelerations in the xy-plane are not considered in the aerodynamics.

The computer program allows the user the option of including or omitting the unsteady aerodynamic effects. The flow diagram in Figure 3-15 indicates optional paths of calculation. The application of the unsteady effects to the calculation of incremental aerodynamic coefficients in stalled or unstalled flow is discussed in the following sections.

3.3.5.1.1 Pitching Moment

The aerodynamic pitching moment for steady-state assumptions has first been obtained from data tables or from formulas. Unsteady effects which include pitching velocity and acceleration of the section, both elastic

and rigid body, can now be determined. The technique developed by Carta et al (References 15 and 16) is based on data for a two-dimensional airfoil executing forced, sinusoidal motion.

The analytical background for the theory of unsteady aerodynamics used by Carta is found in Bisplinghoff (Reference 17), and a similar discussion is given by Scanlan and Rosenbaum (Reference 4). The basic development is referred to a point aft of the quarter chord, so that equations for both the normal force and the pitching moment are usually presented and, subsequently, the reference is shifted to the quarter chord. Carta's work is unique in the development of tables based on measured data and theoretical considerations.

It is assumed in Carta's method that "the sinusoidal data could be generalized, through crossplots, to functions of instantaneous angle of attack, angular velocity parameter A, and angular acceleration parameter B for a given Mach number." In the considerations which follow, the parameters A and B are defined as

$$A = \left(\frac{c}{2U}\right)\dot{\alpha} \tag{3-145}$$

$$B = \left(\frac{c}{2\bar{U}}\right)^2 \ddot{\theta} \tag{3-146}$$

where c is the chord length and $\bar{U}$ is the net wind velocity perpendicular to the airfoil leading edge. The actual A-B tables are listed in Reference 16, and are based on data from a differential pressure transducer mounted on a 2-foot-chord NACA 0012 airfoil. The steady-state content in the tables is removed by requiring $\Delta C_m = 0$ when $A = B = 0$. Thus, at each α the original tabular value at $A = B = 0$ was subtracted from all entries for that α. The resulting adjusted Carta tables are included in the C81 program. The effect of Mach number on the stall point is discussed by Carta (Reference 16) and the variation represented for the NACA 0012 airfoil. This stall point variation is included by computing a shift in the angle-of-attack argument before entering the adjusted A-B tables, as follows:

$$\alpha_{Carta} = \left|\bar{\alpha}\right| \quad \text{for } M_{eff} \leq .2 \tag{3-147}$$

$$\alpha_{Carta} = \left|\bar{\alpha}\right| \cdot \frac{13.5}{13.5 - 16.25\left(M_{eff} - .2\right)} \tag{3-148}$$

$$\text{for } .2 < M_{eff} < .6$$

$$\alpha_{Carta} = |\bar{\alpha}| \cdot 1.93 \text{ for } M_{eff} \geq .6 \tag{3-149}$$

A value $\Delta C_m (\alpha_{Carta})$ is computed by interpolation from the adjusted A-B tables. The effect of Mach number is again applied by dividing this value by N where

$$N = \sqrt{1 - M_{eff}^2} \text{ for } M_{eff} < .6 \tag{3-150}$$

$$N = .8 \text{ for } M_{eff} \geq .6 \tag{3-151}$$

Thus

$$\Delta C_m = (\text{sign } \bar{\alpha}) \, \Delta C_m \left(\alpha_{Carta}\right) \Big/ N \tag{3-152}$$

and

$$C_m = C_m \text{ (steady state)} + \Delta C_m \tag{3-153}$$

3.3.5.1.2 Lift Coefficient

The aerodynamic lift coefficient computed for steady-state can be augmented to represent unsteady effects. The effect of the unsteady terms on lift is defined separately for stalled and unstalled regions. In the derivation of the following equations, the slope of the lift curve is assumed to be 2π. The basic equation for unstalled, unsteady lift effects is, in the notation of Scanlan and Rosenbaum (Reference 4),

$$L' = \pi \rho b^3 \left\{ -\frac{\ddot{h}}{b} - \frac{2v}{b} C(k) \frac{\dot{h}}{b} + a\ddot{\alpha} + \left[2\left(a - \frac{1}{2}\right)C(k) - 1\right]\frac{v}{b}\dot{\alpha} - \frac{2v^2}{b^2} C(k)\,\alpha \right\} \tag{3-154}$$

where

L' is the lift per [illegible], positive down

$\underline{\alpha}$ is the angle of attack, excluding the effect of vertical velocity

b is the semichord

a is the distance from the midchord to the elastic axis, divided by the semichord

$C(k) = F(k) + iG(k)$ is the circulation function

$k = b\omega/v$, where ω is the frequency of oscillation

$\dot{h}$ and $\ddot{h}$ are respectively the vertical velocity and acceleration, positive down

v is the resultant wind velocity

In this analysis, circulation effects are curtailed by assuming that k is small; that is, $\omega \ll v/b$. The following approximations are then made:

$$F(k) = 1, \quad G(k) = 0 \tag{3-155}$$

Equation (3-154) may be rewritten with the sign convention for lift changed to positive up, $\dot{h}$ and $\ddot{h}$ replaced by $-\dot{Z}$ and $-\ddot{Z}$, v replaced by $\overline{U}$, and both sides divided by the product of the chord length and the dynamic pressure, thus:

$$\frac{\Delta L}{(2b)\,\frac{1}{2}\,\rho\,\overline{U}^2\,\Delta r} = 2\pi\left[-\frac{b\ddot{Z}}{2\overline{U}^2} - \frac{\dot{Z}}{\overline{U}} - \frac{ab^2}{2\overline{U}^2}\,\ddot{\underline{\alpha}} - \frac{b}{\overline{U}}\left(a - \frac{1}{2}\right)\dot{\underline{\alpha}} + \frac{b}{2\overline{U}}\cdot\dot{\underline{\alpha}} + \underline{\alpha}\right] \tag{3-156}$$

The first term on the right side of Equation (3-155) accounts for the inertia force generated by the vertical acceleration imparted to a cylindrical volume of air with the blade chord as a diameter. The sum of the second and last terms in the brackets

$$-\frac{\dot{Z}}{\overline{U}} + \underline{\alpha}$$

corresponds to the angle of attack used in the steady state aerodynamic evaluation. For the rigid body mode, $-\dot{Z}/(\bar{U})$ is the contribution to angle of attack from the flapping velocity.

The third term accounts for the effect of the inertia of the cylinder of air which moves when the blade pitches. This effect should include only the pitching acceleration $\ddot{\bar{\theta}}$. The fourth term is the effect of blade pitching velocity on the angle of attack and should include only the pitch rate $\dot{\bar{\theta}}$. The fifth term is interpreted as a damping term based on the total angle-of-attack change rate, $\dot{\bar{\alpha}}$.

Thus, the lift coefficient increment due to unsteady aerodynamics can be expressed in conventional helicopter notation:

$$\Delta C_l = 2\pi \left[- \frac{b\ddot{Z}}{2\bar{U}^2} - \frac{ab^2\ddot{\bar{\theta}}}{2\bar{U}^2} - \left(a - \frac{1}{2} \right) \frac{b\dot{\bar{\theta}}}{\bar{U}} + \frac{b\dot{\bar{\alpha}}}{2\bar{U}} \right] \tag{3-157}$$

If the pitch axis (or elastic axis) is assumed to be at the quarter chord, the value of a in Equation (3-157) is minus one-half.

Stall hysteresis due to variation in lift with blade pitch rate is discussed by Harris (Reference 10). This dynamic stall effect is included in the following manner.

For $\alpha_{mod} > (C_{l_{max}})/\underline{a}$, use Equation (5) of Reference 10 to obtain

$$\Delta\alpha = 61.5 \ln(.6/MM) \sqrt{|\dot{\bar{\alpha}} b/\bar{U}|} \tag{3-158}$$

where $\underline{a}$ is the lift curve slope, and

$$MM = \begin{cases} 0.3 \text{ for } M_{eff} \leq 0.3 \\ M_{eff} \text{ for } 0.3 < M_{eff} < 0.6 \\ 0.6 \text{ for } M_{eff} \geq 0.6 \end{cases}$$

Then

$$\alpha_{RL} = \alpha_{mod} - (\text{sign } \dot{\bar{\alpha}}) \text{ Min} \left\{ \begin{matrix} \Delta\alpha \\ |.2\ \alpha_{mod}| \end{matrix} \right\} \tag{3-159}$$

If $\alpha_{mod} \leq (C_{l_{max}})/\underline{a}$, $\alpha_{RL} = \alpha_{mod}$.

Then obtain a lift coefficient from the tables or formulas for steady state using α_{RL} and M_{eff} as arguments. Recalling that $\alpha_{mod} = \bar{\alpha} \cos \bar{\Lambda}$, the final value of lift coefficient is given by

$$C_{l_T} = C_l\left(\alpha_{RL}, M_{eff}\right) \cdot \frac{\bar{\alpha}}{\alpha_{RL}} + \Delta C_l \qquad (3\text{-}160)$$

3.3.5.1.3 Drag Coefficient

Unsteady effects on the aerodynamic drag coefficient are handled as suggested in Reference 10. Harris states, "To account for unsteady aerodynamic effect on pressure drag, the two-dimensional drag coefficient data was used, but at α_{ref}."

Therefore, for the drag coefficient determining drag force normal to the leading edge,

$$\alpha_{RD} = \bar{\alpha} - (\text{sign } \dot{\bar{\alpha}}) \text{ Min } \left\{ \begin{matrix} \Delta\alpha \\ .2\ddot{\bar{\alpha}} \end{matrix} \right\} \qquad (3\text{-}161)$$

and

$$C_{d_N} = C_d\left(\alpha_{RD}, M_{eff}\right) \qquad (3\text{-}162)$$

3.3.5.2 UNSAN Unsteady Aerodynamic Model

An alternate procedure for including unsteady aerodynamics is provided in AGAJ73. The analytical development was done under Contract DAAJ02-71-C-0045 and is presented in Reference 18.

The analysis for UNSAN may be considered to start with Equations (3) and (4) of Reference 18 which give the lift and moment, per unit span. The lift expression is similar to Equation (3-154), Section 3.3.5.1.2.

The terms in Equations (3) and (4) involving the Theodorsen function can be considered as the expression

$$E = C(k)\left[\theta_v + \frac{\dot{h}_v}{V} + d\,\frac{\dot{\theta}_v}{V}\right] \qquad (3\text{-}163)$$

where the subscript v indicates the vibratory part of the variable and

$$d = c(3/4 - PA) = 1/2\ c\ (1/2 - a) \tag{3-164}$$

where $PA = (a + 1)/2$

Assuming simple harmonic motion for θ_v and h_v (see Equations (9) and (10) of Reference 18), appropriate substitutions give

$$E = F(k)\left[\theta_v + \frac{\dot{h}_v}{V} + d\,\frac{\dot{\theta}_v}{V}\right] + iG(k)\left[-i\,\frac{\dot{\theta}_v}{\omega} - i\,\frac{\ddot{h}_v}{\omega V} + i\omega d\,\frac{\theta_v}{V}\right] \tag{3-165}$$

so that the imaginary unit is eliminated and

$$E = \left(F - \frac{\omega\, d}{V}\,G\right)\theta_v + \frac{F}{V}\,\dot{h}_v + \frac{G}{\omega V}\,\ddot{h}_v + \left(\frac{d}{V}\,F + \frac{G}{\omega}\right)\dot{\theta}_v \tag{3-166}$$

The contributions to blade pitch velocity and acceleration from coning and coning rate, $\Omega\beta$ and $\Omega\dot{\beta}$, are added, ω is replaced by Ω, and an equivalent angle of attack is given as

$$\begin{aligned}\alpha_{EQU} = {} & \theta_o + \left(F - c(3/4 - PA)\,\frac{G\,\Omega}{V}\right)\theta_V \\ & + \tan^{-1}\left\{\left[F\dot{h}_v + \dot{h}_o + \frac{G\ddot{h}_v}{\Omega} + c(3/4 - PA)\,\Omega\beta_o\right.\right. \\ & \left.\left. + \left(c\ (3/4 - PA)F + \frac{GV}{\Omega}\right)\left(\dot{\theta}_v + \Omega\beta_v\right)\right]/U_T\right\}\end{aligned} \tag{3-167}$$

Equation (3-167) is identical to Equation (31) in Reference 18.

The aerodynamic coefficients (C_l, C_d, and C_m) are obtained as functions of α_{EQU} and Mach number from formulas or tables as in the steady-state case. Other terms involving the vibratory variables are included separately and the expressions for aerodynamic lift, drag, and moment are given in Equation (32) of Reference 18.

In order to interface this procedure with the C81 calculations, some practical means of separating the vibratory part from the total $\dot{h}$, θ, and β was needed. One requirement was that the routine be operable in the maneuver section.

Since $\dot{h}$ as given by Equation (24) of Reference 18 is just U_p, Equation (26) of that reference can be expressed as

$$\dot{h}_o = V_{FLT} \sin \alpha_s - v_{Z_{(o)}} - \text{(rate of climb)} \tag{3-168}$$

where $\dot{h}_o$ is the "steady" part of $\dot{h}$ and is available in C81. The pitch angle, θ, and the coning angle, β, at a blade segment are computed in the maneuver section of C81 but are not separated into steady and vibratory parts. The following assumptions (not in Reference 18) are made to implement the C81 programming:

θ_o is the collective pitch at the segment (includes built-in twist)

β_o is the precone angle

These assumptions omit steady elastic pitch deflection and steady out-of plane bending but retain the principal contributions to θ_o and β_o.

Then

$$\dot{h}_v = \dot{h} - \dot{h}_o \tag{3-169}$$

$$\theta_v = \theta - \theta_o \tag{3-170}$$

$$\beta_v = \beta - \beta_o \tag{3-171}$$

The derivatives required are $\ddot{h}_v$, $\dot{\theta}_v$, $\ddot{\theta}_v$, and $\dot{\beta}$ for the basic unsteady coefficients and $\dot{\alpha}$ for stall hysteresis effects. Rather than attempt analytical derivatives, the rates are computed numerically using the formula

$$p_n^{(r)} = \frac{1}{\Delta t^r} \left(1 + \frac{1}{2} \nabla + \frac{1}{3} \nabla^2 + \ldots\right)^r \nabla^r p_n \tag{3-172}$$

from Reference 19.

A further modification to the analysis of Reference 18 was made by providing an input, Ω_k, for computing the reduced frequency as

$$k = \frac{c\,\Omega_k}{2V} \tag{3-173}$$

By this means the sensitivity of blade response to this part of the analysis can be investigated.

Stall hysteresis representation described in Reference 18 was retained without change. The starting equation, Equation (39) from Reference 18, corresponds to Equation (3-158) but UNSAN includes expanded procedures for determining the change in angle of attack for dynamic stall for C_l and for C_m (not necessarily the same).

Effects of radial flow in Reference 18 are also retained in UNSAN. These effects are similar to the radial flow considerations in BUNS. The equations for Λ are the same (Equation (53) in Reference 18 and Equation (3-112) in this report). A radial component of drag due to skin friction is included; see Equation (58) in Reference 18 and Equation (3-117). Compare Equation (75) in Reference 18 and Equation (3-116) in this report for the effect of Λ on the lift coefficient.

4. FUSELAGE MATHEMATICAL MODEL

4.1 INTRODUCTION

Over the past two decades, the maximum airspeeds of pure helicopters have increased twofold or more in all flight regimes (forward, rearward, lateral, and vertical). In addition, the maximum forward airspeed for composite or compound rotorcraft has increased to 300 knots or more. While the sophistication of the rotor simulation in C81 has kept pace with these expanding flight envelopes, the mathematical models for the airframe components have not. Consequently, one of the latest major revisions to the Rotorcraft Flight Simulation Program has been to improve the aerodynamic representation of the fuselage.

This section of the report documents the background and development of the fuselage mathematical model which is currently incorporated in C81. It also contains figures and tables which compare the current mathematical model to wind tunnel test data.

4.2 DEVELOPMENT OF THE FUSELAGE MATHEMATICAL MODEL

4.2.1 Background

The primary goals in the development of the current C81 representation of the fuselage aerodynamic forces and moments were to provide a mathematical model which would:

(1) Be valid at all orientations of the fuselage with respect to the wind, with particular emphasis on simulation of the forces and moments at the nominal forward flight aerodynamic angles and of the effects of aerodynamic coupling, i.e., variation of longitudinal forces and moments with sideslip, and lateral-directional forces and moments with angle of attack.

(2) Take maximum advantage of the availability of wind tunnel data without sacrificing or compromising the capability of inputting analytical estimates of such data.

Since the current version of the program has the capability of simulating the aerodynamic forces and moments on a wing, four stabilizing surfaces, four external stores or aerodynamic brakes, and two pylons, the fuselage representation was developed for simulating the basic fuselage only. The landing, or skid, gear was the only component other than the basic airframe which was considered part of the fuselage in the development of the model. This assumption eliminates the necessity of simulating in the fuselage representation the sharp stall characteristics associated with aerodynamic surfaces.

In the formulation of the current fuselage model, three separate approaches were considered for its general form:

(1) Equations only

(2) Data tables only

(3) A combination of equations and tables

It was concluded that equations were the best approach for the following reasons:

(1) Equations are better suited than data tables to configurations where little or no test data are available and analytical or empirical predictions of the aerodynamic characteristics must be made.

(2) Parametric studies of changes in fuselage aerodynamic characteristics can be made more easily by changing coefficients of an equation than by modifying entries in a data table.

(3) To provide adequate tabular representation at all aerodynamic angles, it was estimated that each of the six necessary tables should be permitted at least 500 and preferably up to 1000 or 1200 entries; this would be in addition to the more than 10,000 entries allocated for the rotor airfoil data tables.

(4) Using the method of least-squared errors, equations of order three or less can fit most test data with a root-mean-squared error per point which is well within the accuracy of the test data.

(5) Since test data are frequently not recorded as systematically as is required for the type of table and table interpolation routine in C81, data must be plotted and/or fitted to obtain all necessary entries for such tables. If a plot or fit step is required to construct the tables, little is gained by the use of tables.

(6) A table interpolation routine which could directly use the standard type of test data (sweeps of one angle with the other fixed) would increase run time and storage requirements for the fuselage representation.

The new representation of the fuselage is divided into two independent models and a third model which is dependent on the other two. The first model consists of six independent equations for the forces and moments where each equation is a function of both the aerodynamic pitch and yaw

angles. This model, referred to as the Nominal Angle Equation (NAE) model, is intended to simulate the forces and moments at aerodynamic angles less than approximately 15 to 25 degrees in magnitude, i.e., the angles where the majority of flight occurs and for which test data are most commonly available.

The second model also consists of six independent equations and is referred to as the High Angle Equation (HAE) model. This model cannot fit test data as accurately as the NAE model, but does provide more than adequate simulation of force and moment data throughout the range of aerodynamic angles, i.e., pitch between ±90 degrees and yaw between ±180 degrees. The intent of this model is to follow very closely the force and moment data trends at the large angles encountered in low speed flight (rearward, sideward, and vertical) and those which could occur after major system failures.

The third, or dependent, model provides a smooth transition between the NAE and HAE models. It in effect phases out one set of equations while phasing in the other set. The user may specify the angles where phasing starts and stops.

4.2.2 Choice of Reference Systems and Definitions of Angles

Choosing the equations-only approach for the general form of the current representation made it advisable to restrict the inputs to those from one specific reference system. Although it is desirable to permit the inputs to be in any conventional reference system (i.e., wind, stability, or body), doing so requires a separate representation for data from each reference system. The requirement of separate representations comes about because the generalized shapes of the force and moment curves at large angles are strongly affected by reference system. For example, in sideward flight, wind reference drag is large and side force is near zero; while for the same condition, body reference drag, or axial force, is near zero and side force equals the wind reference drag. Rather than programming three separate representations, when only one would be used at any one time, the representation for wind reference data was implemented for the following reasons:

(1) Wind reference data are consistent with previous versions of the program, which makes conversion to the current version easier.

(2) Wind reference data are readily available from the pyramidal-type balance systems used at most low speed wind tunnels, or it is a simple transformation from other reference systems.

(3) The trends of wind reference fuselage forces and moments relate easily to similar data for airfoils, making interpretation of wind reference inputs somewhat easier than those in other reference systems.

In the following discussion of definitions of angles and reference systems, Figures 4-1, 4-2, 4-3, and 4-4 will help visualize the relationships involved. The orientation, or aerodynamic, angles used in the fuselage representation were defined to be consistent with wind tunnel data. That is, the orientation of the body reference system with respect to the wind reference system is defined by two ordered rotations: yaw followed by pitch, where yaw angle (ψ_w) is defined to be between ± 180 degrees and pitch angle (θ_w) to be between ± 90 degrees. See Figure 4-1. However, this definition creates a problem in a simulation such as C81 where the wind and fuselage are each oriented with respect to the ground, and the orientation of the fuselage with respect to the wind is not explicitly defined. Specifically, in C81 the orientation of flight path (a vector) is defined by the vector sum of forward, lateral and vertical velocities (V_x, V_y, and V_z respectively) of the rotorcraft cg in ground reference. See Figure 4-2. On the other hand, the orientation of the fuselage (body reference system) is defined by three ordered rotations (Euler angles) from ground reference. Although the flight path (wind vector) corresponds to the X axis of the wind reference system, there are no parameters which directly define the orientation of the wind Y and Z axes about this X axis. Since the wind reference orientation is not completely defined, the body reference cannot be directly oriented with respect to it as in the wind tunnel.

The solution to this problem is to use the Euler angles (Ψ, Θ, and Φ) which orient the body reference system with respect to the ground to resolve the three ground reference velocities into body reference. See Figure 4-3. The results of the resolution are the body reference X, Y, and Z velocities (u, v, and w respectively). These body velocities can then be defined as the components of the flight path velocity (V) in a reference system which has been yawed ψ_w degrees, then pitched θ_w degrees with respect to the wind vector. See Figure 4-4. From this definition,

$$u = V \cos \psi_w \cos \theta_w \tag{4-1}$$

$$v = -V \sin \psi_w \tag{4-2}$$

$$w = V \cos \psi_w \sin \theta_w \tag{4-3}$$

Since the reference system of u, v, and w is the body, ordered rotations of $-\theta_w$ degrees pitch, then $-\psi_w$ degrees yaw define the orientation of the wind reference system with respect to the body. Therefore, the angles ψ_w and θ_w respectively are identical to the conventional wind tunnel yaw and pitch angles shown in Figure 4-1 and are termed the aerodynamic yaw and pitch angles.

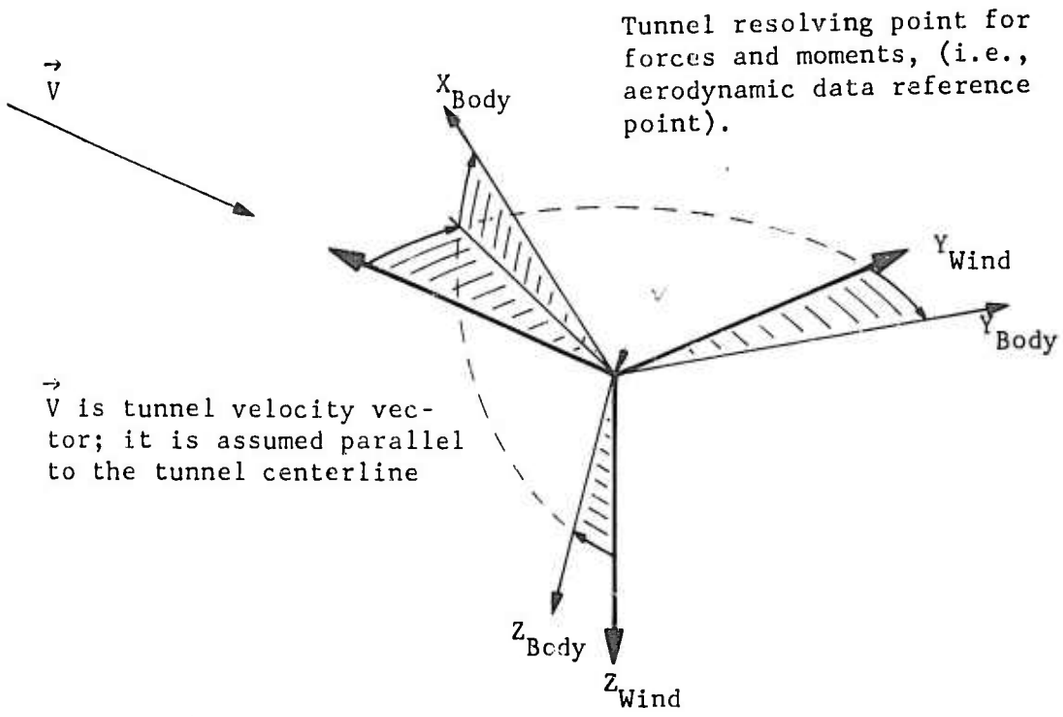

Figure 4-1. Definition of Aerodynamic Angles in a Wind Tunnel.

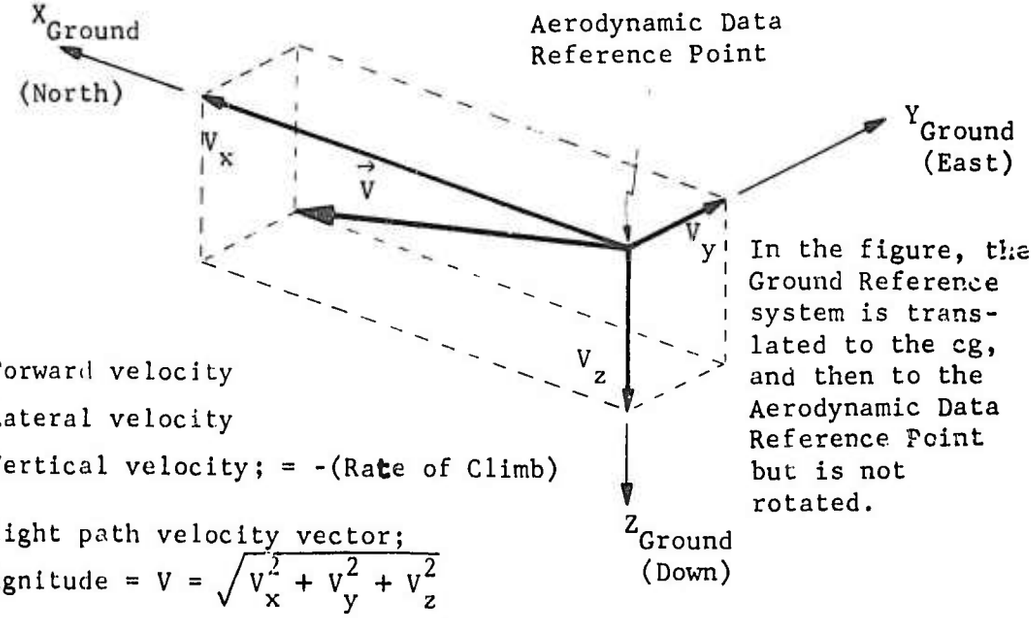

V_x = Forward velocity

V_y = Lateral velocity

V_z = Vertical velocity; = -(Rate of Climb)

$\vec{V}$ = Flight path velocity vector;

magnitude = $V = \sqrt{V_x^2 + V_y^2 + V_z^2}$

Figure 4-2. Orientation of Flight Path in Ground Reference.

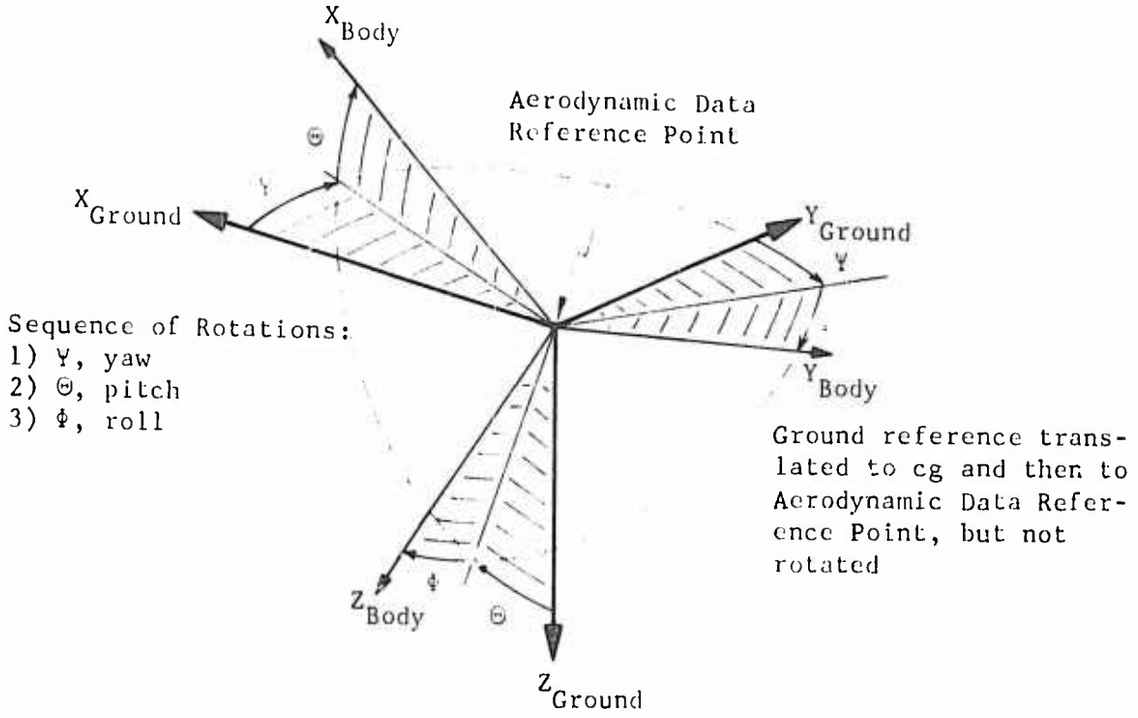

Figure 4-3. Euler Angles From Ground to Body Reference.

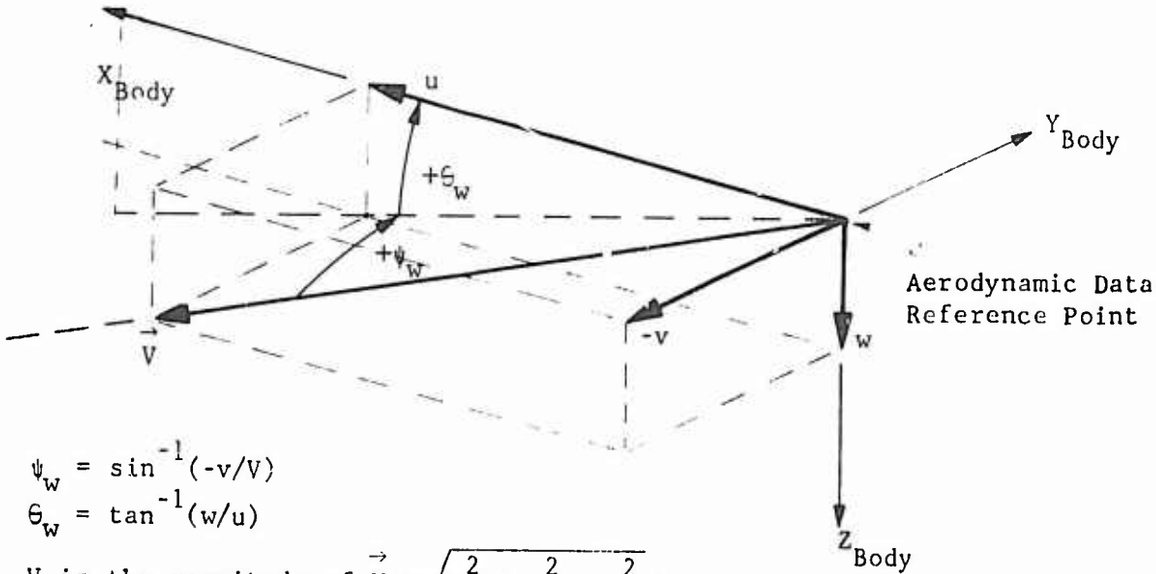

$\psi_w = \sin^{-1}(-v/V)$

$\theta_w = \tan^{-1}(w/u)$

V is the magnitude of $\vec{V}; = \sqrt{u^2 + v^2 + w^2} =$

$$\sqrt{V_x^2 + V_y^2 + V_z^2}$$

Figure 4-4. Aerodynamic Angles in Body Reference.

From Equations (4-1), (4-2), and (4-3), these aerodynamic angles can be defined as functions of the flight path velocity and its body reference components.

$$\psi_w = \sin^{-1}(-v/V) \tag{4-4}$$

$$\theta_w = \tan^{-1}(w/u) \tag{4-5}$$

These two angles are then the two independent variables in the wind reference equations for fuselage aerodynamic forces and moments. They also serve as the rotation angles for resolving the wind reference data into the body reference system, where C81 performs its final force and moment summations.

However, note that if V = 0, both ψ_w and θ_w are indeterminant. Similarly, if u = w = 0, θ_w is indeterminant. If V = 0, the indeterminancy is simply resolved by defining ψ_w and θ_w to be zero, since all aerodynamic forces and moments are zero at zero velocity.

If u = w = 0, while V ≠ 0 (i.e., ψ_w = ± 90 degrees), it may be physically possible to pitch the wind tunnel model, but the angle cannot be defined by Equation (4-5). However, considering how the parameter θ_w is used in C81, it can be defined to be zero regardless of the value in the tunnel. To understand this definition, consider the forces and moments acting on a wind tunnel model which is yawed 90 degrees but not pitched, as shown in Figure 4-5. If the model is subsequently pitched, the drag in wind reference (Y-force in body reference) remains constant, but the other wind reference forces and moments do not. However, in the body reference system, the forces and moments are not a function of θ_w. Therefore, by defining θ_w = 0 when ψ_w = ± 90 degrees, the wind reference data can be resolved to body reference with a single yaw rotation and used as body reference data independently of the wind tunnel pitch angle. Since the body reference is the system in which the data are needed for the final summation, this definition for θ_w provides the necessary results.

The interesting, if not obvious, implication of the above discussion is that aerodynamic forces and moments are dependent only on the orientation of the flight path with respect to the fuselage and independent of the orientation of the flight path with respect to the ground.

In its developed and programmed form, the equations of the representation of fuselage aerodynamics are actually functions of sines and cosines of ψ_w and θ_w rather than the angles themselves. Consequently, the sinusoids are defined by the velocity ratios implied by Equations (4-4) and (4-5) with the restriction that the inverses of sin θ_w and cos θ_w do not exceed ± 90 degrees and the inverses on sin ψ_w and cos ψ_w do not exceed ± 180 degrees.

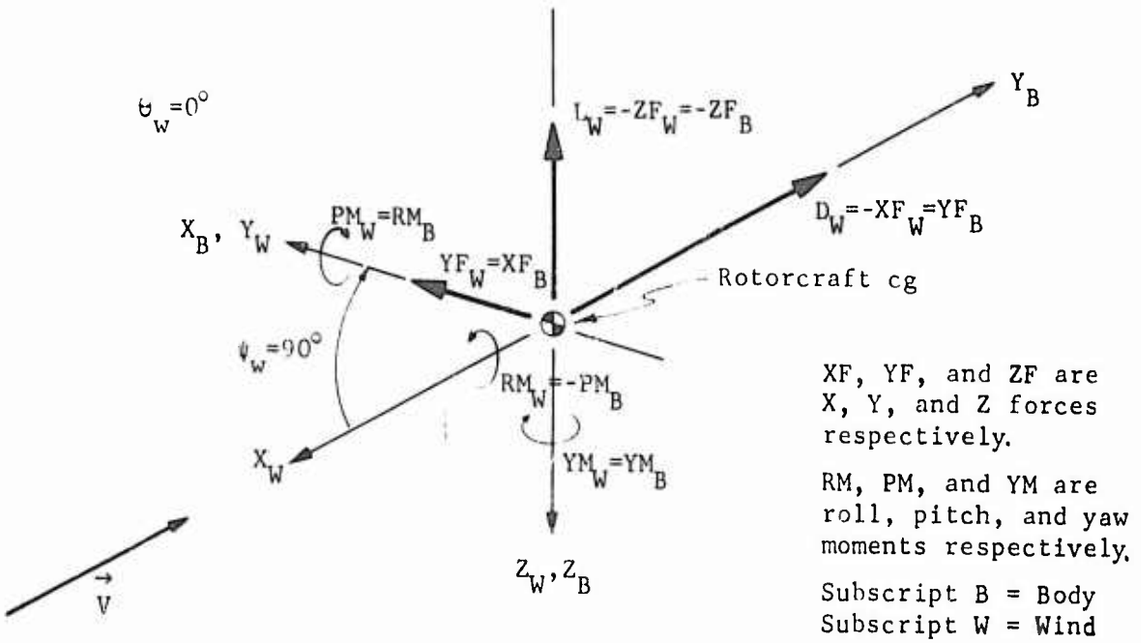

(a) Aerodynamic Pitch Angle Equal to Zero.

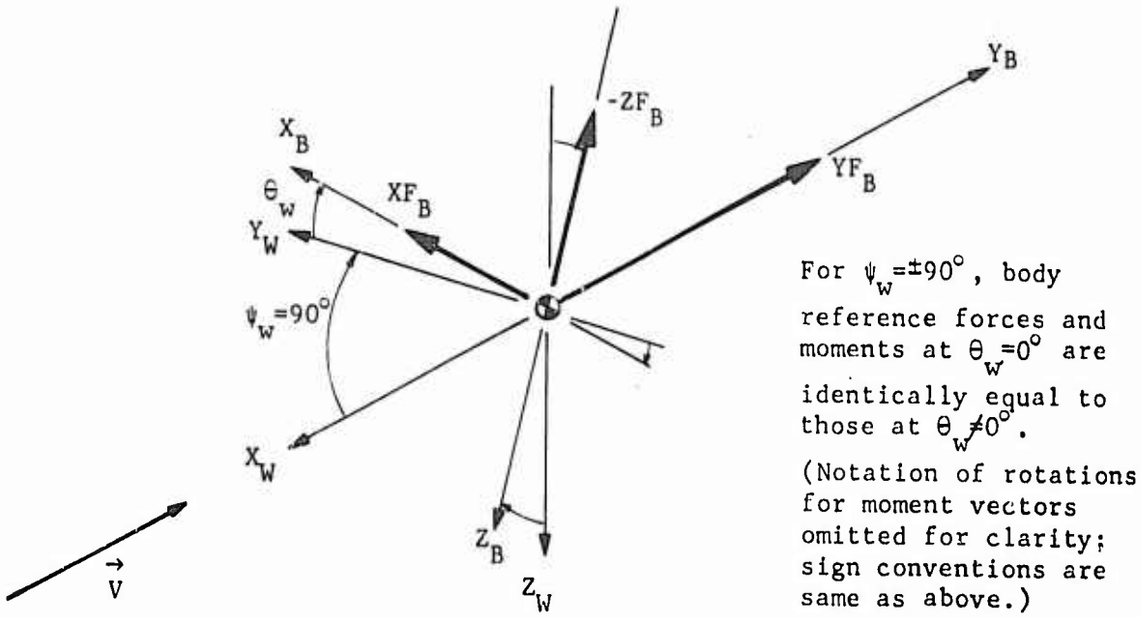

(b) Aerodynamic Pitch Angle Not Equal to Zero.

Figure 4-5. Aerodynamic Pitch Angle in Sideward Flight.

$$\sin \theta_w = w/\left(\text{sign}(u)\sqrt{u^2 + w^2}\right) \tag{4-6}$$

$$\cos \theta_w = |u|/\sqrt{u^2 + w^2} \tag{4-7}$$

$$\sin \psi_w = -v/V \tag{4-8}$$

$$\cos \psi_w = \left(\text{sign}(u)\sqrt{u^2 + w^2}\right)/V \tag{4-9}$$

It should be noted that ψ_w is not the traditional sideslip angle, β. Sideslip is defined as

$$\beta = \tan^{-1}(v/u), \tag{4-10}$$

and an alternate definition of ψ_w is

$$\psi_w = \tan^{-1}\left(-v/\left[\text{sign}(u)\sqrt{u^2 + w^2}\right]\right) \tag{4-11}$$

Equating v in the two equations yields

$$\tan\beta = -\tan \psi_w/\cos \theta_w \tag{4-12}$$

Hence for small pitch angles, $\cos \theta_w \approx 1$ and

$$\beta \approx -\psi_w, \tag{4-13}$$

but at large values of θ_w, the magnitudes of β and ψ_w are not interchangeable.

4.2.3 High Angle Equation Model; The Airfoil Analogy

Since one of the primary goals in the development of the new fuselage representation was a model which would be valid at all aerodynamic angles, the first efforts for the task were directed toward a single set of equations which would accomplish this goal as well as the others. A literature search uncovered no simple analytical methods for predicting the force and moment characteristics of generalized bodies at large aerodynamic angles. Methods which are available, such as using bound vortices, would be very time consuming if programmed, approximate even if the flow were potential, and prohibitively complex following separation or stall, all due primarily to the nonuniform shape of rotorcraft fuselages. Also, test data for bodies at large angles were very limited. Consequently, the mathematical model for large angles, the High Angle Equation (HAE) model, was derived by comparing fuselages and aerodynamic surfaces with what was termed the airfoil analogy, and then supporting the conclusions with the limited test data available.

The initial step in the airfoil analogy was to consider the fuselage as a special case of an aerodynamic surface. The geometry of conventional aerodynamic surfaces is described by parameters such as aspect ratio, taper ratio, sweep angle, thickness-chord ratio, twist, and airfoil sections. Of these parameters, aspect ratio and thickness-chord ratio have strong analogies when considering the fuselage shape. The conventional aspect ratio is defined as b^2/S (b = span, S = planform area), while the thickness-chord ratio is t/c (t = maximum thickness of airfoil, c = mean chord of airfoil). For a fuselage, the analogous parameters are not single valued. They depend on the orientation of the fuselage with respect to the wind. The fuselage parameters which can be related to the surface parameters of span, area, chord, and thickness are listed in Table 4-1 for forward, sideward and vertical flight. Based on the normal relationships of the fuselage parameters, the magnitude of the fuselage aspect and thickness-chord ratios can then be estimated as shown in Table 4-1. From this table, the following conclusions can be drawn:

(1) In forward or rearward flight, a fuselage is analogous to an aerodynamic surface with a relatively low aspect ratio, i.e., less than unity, and a moderate thickness-chord ratio, i.e., 0.1 to 0.3.

(2) In sideward or vertical flight, a fuselage is analogous to an aerodynamic surface with a very high thickness-chord ratio, i.e., unity or greater.

These conclusions imply a third:

(3) One type of model would be best for one of the flight regimes and a different one for the other.

A decision on whether to pursue this implication further was postponed until the HAE model was completed and could be compared to test data.

Using the above analogy and some limited aerodynamic surface test data, the shape of each fuselage force and moment curve was sketched for full-range yaw sweeps at constant pitch and full-range pitch sweeps at constant yaw.

The sets of sketches for each force or moment were then combined into a single three-dimensional sketch where the force or moment was plotted vertically (Z axis) as a function of the pitch and yaw angle (X and Y axes). Next, the lines of force or moment were faired together to form a surface above the X-Y plane. Figure 4-6 is an example of this technique for the drag of an arbitrary fuselage shape.

The dominant feature of Figure 4-6 and similar sketches is that vertical sections intersect the surface in lines which are periodic and very

TABLE 4-1. FUSELAGE/AERODYNAMIC SURFACE ANALOGY

AERODYNAMIC SURFACE PARAMETER	FUSELAGE PARAMETER WHICH IS ANALOGOUS TO THE AERODYNAMIC SURFACE PARAMETER				
	FLIGHT REGIME AND REFERENCE ORIENTATION				
	Forward/Rearward Flight ($\theta_w = 0, \psi_w = 0, \pm 180^c$)		Sideward* Flight ($\theta_w = 0, \psi_w = \pm 90^o$)	Vertical Flight ($\theta_w = \pm 90^o, \psi_w = 0^o$)	
	Pitch	Yaw	Yaw	Pitch	Yaw
Chord, c	Length	Length	Width	Height	Height
Thickness, t	Height	Width	Length	Length	Width
Span, b	Width	Height	Height	Width	Length
Plane of Reference Area, S**	X-Y Plane	X-Z Plane	Y-Z Plane	Y-Z Plane	X-Y Plane
Aspect Ratio, A ($=b^2/S$)	$\frac{(\text{Width})^2}{\text{X-Y Area}}$	$\frac{(\text{Height})^2}{\text{X-Z Area}}$	$\frac{(\text{Height})^2}{\text{Y-Z Area}}$	$\frac{(\text{Width})^2}{\text{Y-Z Area}}$	$\frac{(\text{Length})^2}{\text{X-Y Area}}$
Typical Value	$\lesssim 0.5$	$\lesssim 0.5$	~ 1	$\lesssim 2$	$\gtrsim 2$ and $\lesssim 10$
Thickness/Chord Ratio, t/c	$\frac{\text{Height}}{\text{Length}}$	$\frac{\text{Width}}{\text{Length}}$	$\frac{\text{Length}}{\text{Width}}$	$\frac{\text{Length}}{\text{Height}}$	$\frac{\text{Height}}{\text{Width}}$
Typical Value	$\gtrsim 0.1$ and $\lesssim 0.5$	$\gtrsim 0.1$ and $\lesssim 0.5$	$\gtrsim 2$ and $\lesssim 10$	$\gtrsim 2$ and $\lesssim 10$	~ 1

* In sideward flight ($\psi_w = \pm 90^c$), the equation for ϵ_w ($= \tan^{-1} w/u$) cannot define the angle. Hence, analogies with respect to the wind axis cannot be made. However, body axis forces and moments in sideward flight are independent of ϵ_w, and ϵ_w can be defined to be zero.

** The reference area of a surface is its planform. Reference area for a fuselage is the area projected on a body plane.

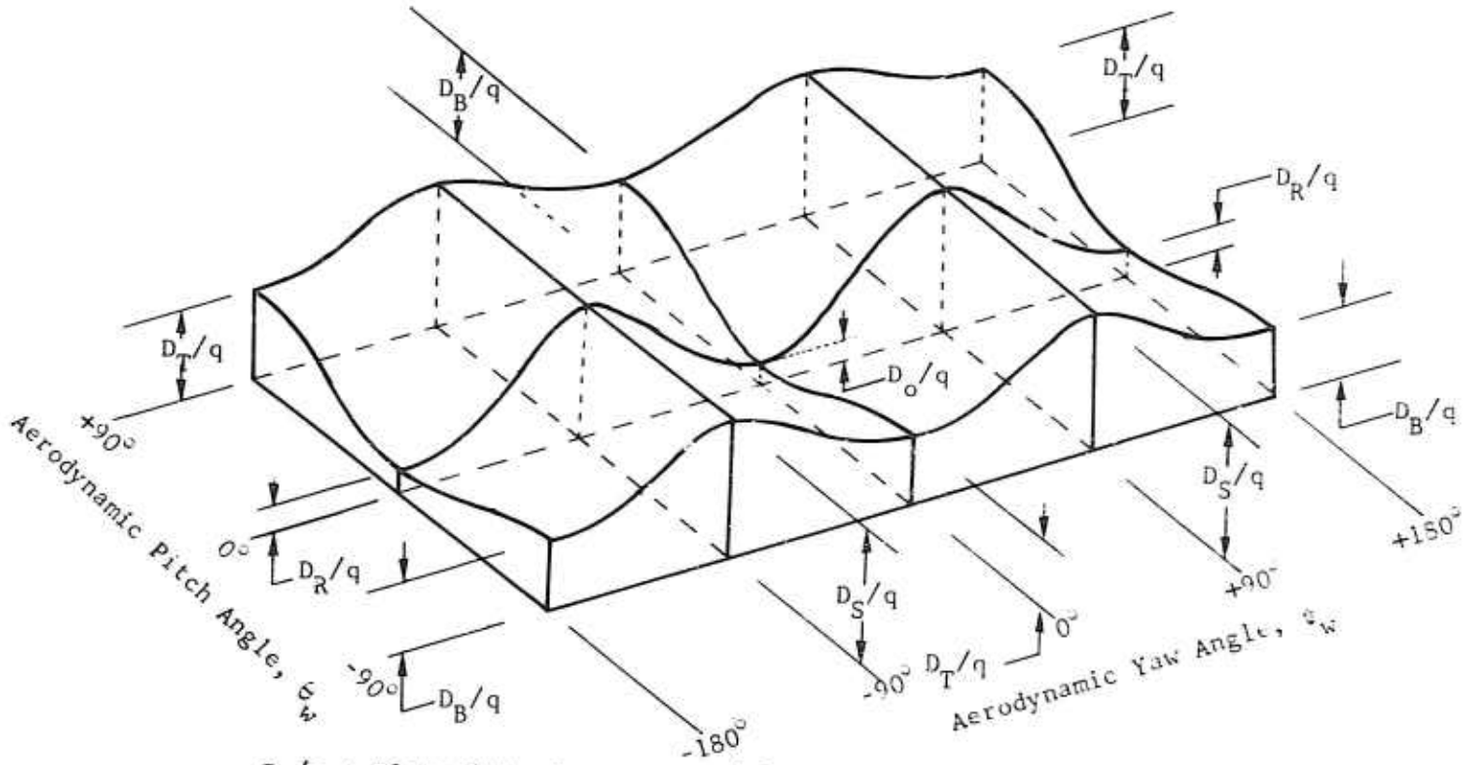

D_o/q = Flat plate drag area of front view

D_R/q = Flat plate drag area of rear view

D_S/q = Flat plate drag area of side view

D_T/q = Flat plate drag area of top view

D_B/q = Flat plate drag area of bottom view

Figure 4-6. Sketch of Fuselage Drag as a Function of ϵ_w and ψ_w.

sinusoidal in appearance. Based on the shapes of these intersections, equations were constructed as sinusoidal functions of integer multiples of θ_w and ψ_w to provide smooth transition between all combinations of θ_w and ψ_w. The periodic nature of the equations established the coefficients as the values of the forces or moments at integer multiples of 45 degrees.

Data from large angle wind tunnel tests of two different configurations were then used to check out the equations. Based on the results of this comparison, empirical modifications were made to the equations, which were then defined as the High Angle Equation model. These equations are listed in Table 4-2.

4.2.4 Nominal Angle Equations

The next step in the development of the new fuselage representation was to examine the accuracy and suitability of the High Angle Equation model in simulating the forces and moments at low, or nominal, aerodynamic pitch and yaw angles (both angles less than approximately ± 15 to ± 30 degrees). Data from force and moment wind tunnel tests of five different fuselages were examined:

(1) Bell Model 209 (AH-1G, or Huey Cobra) type fuselage: relatively high height-to-width ratio, low rectangular tail boom, very aerodynamically clean fuselage, smooth faired pylon, pointed nose.

(2) Bell Mode 205 (UH-1H, or Huey) type fuselage: much lower height-to-width ratio than Model 209; low rectangular tail boom; bulky, aerodynamically dirty fuselage; low, blunt nose.

(3) Bell Model 206 (OH-58A and JetRanger) type fuselage; height-to-width ratio between that of the 209 and 205; high, round tail boom; stylish, or aerodynamically clean, fuselage; low, pointed nose.

(4) A proposed advanced utility helicopter type fuselage: height-to-width ratio near unity; low, round tail boom; relatively clean aerodynamically compared to Model 205; low, pointed nose.

(5) A proposed advanced gunship type fuselage: similar to Model 209 but with twin engine pods, round tail boom, exposed tail rotor drive shaft, no pylon fairing.

The Model 205, 206, and 209 fuselages included skid gear, while the two other configurations included wheeled landing gear. In addition, data on the Model 206 with inflated pop-out float gear were examined.

Preliminary evaluation of the ability of the HAE model to simulate forces and moments in the nominal angle region showed that the HAE model could not simulate the data within the accuracy of the test data. In particular, the aerodynamic coupling was not represented as precisely as needed.

TABLE 4-2. HIGH ANGLE EQUATIONS FOR FUSELAGE AERODYNAMIC FORCES AND MOMENTS

$$\text{Lift} = L = L_1 * \cos^2\psi_w + L_2 * \sin^2\psi_w$$

where

$$L_1 = \begin{cases} L(0,0) + L_3 * \sin^2\theta_w + L_4 * \sin(2\theta_w) & \text{if } |\psi_w| \leq 90^\circ \\ L(180,0) - L_5 * \cos^2\theta_w - L_4 * \sin(2\theta_w) & \text{if } |\psi_w| > 90^\circ \end{cases}$$

$$L_2 = L(90,0) * \cos\theta_w + Y(90,0) * \sin\theta_w$$

$$L_3 = L(0,90) - L(0,0)$$

$$L_4 = [L(0,\theta_{wp}) - L(0,0) - L_3 * \sin^2(\theta_{wp})] / \sin(2 * \theta_{wp})$$

$$L_5 = L(0,90) - L(180,0)$$

$$\text{Drag} = D = D_1 * \cos^2\psi_w + D(90,0) * \sin^2\psi_w$$

where

$$D_1 = D_2 * \cos^2\theta_w + D_v * \sin^2\theta_w$$

$$D_2 = \begin{cases} D(0,0) & \text{if } |\psi_w| \leq 90^\circ \\ D(180,0) & \text{if } |\psi_w| > 90^\circ \end{cases}$$

$$D_v = \begin{cases} D(0,-90) & \text{if } \theta_w \leq 0 \\ D(0,+90) & \text{if } \theta_w > 0 \end{cases}$$

$$\text{Pitching Moment} = M = M_1 * \cos^2\psi + M_2 * \sin^2\psi$$

where

$$M_1 = \begin{cases} M(0,0) + M_3 * \sin^2\theta_w + M_4 * \sin^2\theta_w & \text{if } |\psi_w| \leq 90^\circ \\ M(0,90) - M_5 * \cos^2\theta_w - M_4 * \sin^2\theta_w & \text{if } |\psi_w| > 90^\circ \end{cases}$$

$$M_2 = N(90,0) * \sin\theta_w + M(90,0) * \cos^2\theta_w$$

$$M_3 = M(0,90) - M(0,0)$$

$$M_4 = [M(0,\theta_{wp}) - M(0,0) - M_2 * \sin^2(\theta_{wp},0)] / \sin(2 * \theta_{wp})$$

$$M_5 = M(0,90) - M(180,0)$$

TABLE 4-2. Continued.

Side Force = $Y = Y_1 * \cos^2\theta_w - L(90,0) * \sin^2\theta_w$

where

$$Y_1 = Y(90,0) * \sin\psi_w + Y_2 * \sin(2\psi_w)$$

$$Y_2 = [Y(\psi_{wp},0) - Y(90,0) * \sin(\psi_{wp})]/\sin(2 * \psi_{wp})$$

Rolling Moment = $l = l_1 * \cos^2\theta_w + l(90,0) * \sin^2\theta_w$

where

$$l_1 = l(90,0) * \sin\psi_w + l_2 * \sin(2\psi_w)$$

$$l_2 = l(\psi_{wp},0) - l(90,0) * \sin(\psi_{wp})]/\sin(2 * \psi_{wp})$$

Yawing Moment = $N = N_1 * \cos^2\theta_w - M(90,0) * \sin^2\theta_w$

where

$$N_1 = N(90,0) * \sin\psi_w + N_2 * \sin(2\psi_w)$$

$$N_2 = [N(\psi_{wp},0) - N(90,0) * \sin(\psi_{wp})]/\sin(2 * \psi_{wp})$$

The force or moment symbols with double subscripts in parentheses; e.g., D(0,-90), M(90,0), and N(90,0); indicate the orientation of the fuselage with respect to the wind for that particular force or moment. The first subscript is the aerodynamic yaw angle (ψ_w) and the second is the aerodynamic pitch angle (θ_w). For example, D(0,-90) is the drag at $\psi_w = 0^\circ$ and $\theta_w = -90^\circ$.

The subscript p on ψ_w and θ_w indicates peak values. For example, $M(0,\theta_{wp})$ is the maximum pitching moment for $\theta_w < 90^\circ$ at $\psi_w = 0^\circ$ and occurs at $\theta_w = \theta_{wp}$. The peak value and angle for each force and moment are independent of the peaks for any other force or moment.

Consequently, a study was performed to determine the set of equations which could best fit the referenced test data.

The general equation chosen for the study was

$$Z = C_0 + \sum_{i=1}^{N} C_i \, [f(x)]^{I_i} \, [f(y)]^{J_i} \qquad (4\text{-}14)$$

where

Z is the force or moment under consideration,

x and y are the aerodynamic angles,

I_i and J_i are the positive integer exponents for f(x) and f(y), and

C_i are constant coefficients.

The parameters varied in the study were then

(1) The functions of x and y, f(x) and f(y)

(2) The values of the exponents, I_i and J_i

(3) The number of terms, N

The functions of x and y chosen were the angles themselves and sine functions of the angles where the sine functions had the same period as the corresponding variations in the HAE model, i.e., $\sin(\theta_w)$ or $\sin(2\theta_w)$, and $\sin(\psi_w)$ or $\sin(2\psi_w)$, as appropriate.

Initially, the values of each exponent ranged from zero to five, and up to twenty-five terms were considered. Judgement of the quality of the curve fit was based on the summation of the absolute values of the difference between calculated and measured values divided by the number of data points in the data set and on the root-mean-squared error per point. These parameters were then compared to the accuracy of the wind tunnel data.

Based on preliminary analysis, the general equation was reduced to sixteen terms with exponents less than or equal to three because the higher order terms did not improve the fit enough to warrant their inclusion.

Hence, the baseline equation for the study was

$$Z = C_0 + C_1 f(x) + C_2 f^2(x) + C_3 f^3(x)$$
$$+ [C_4 + C_5 f(x) + C_6 f^2(x) + C_7 f^3(x)] f(y)$$
$$+ [C_8 + C_9 f(x) + C_{10} f^2(x) + C_{11} f^3(x)] f^2(y)$$
$$+ [C_{12} + C_{13} f(x) + C_{14} f^2(x) + C_{15} f^3(x)] f^3(y) \qquad (4\text{-}15)$$

For lift, drag, and pitching moment, x is the pitch angle and y is the yaw angle. To obtain a physical or analytical feel for this equation and how the coefficients relate to measurable quantities, consider yawing moment. In the wind tunnel, data are generally obtained by sweeping one angle with the other held constant. If the pitch angle is constant, then Equation (4-15) can be rewritten for yawing moment, N, as

$$N = q[(N_0/q) + (N_1/q) f(\psi_w) + (N_2/q) f^2(\psi_w) + (N_3/q) f^3(\psi_w)] \qquad (4\text{-}16)$$

where

$$N_0/q = C_0 + C_1 f(\theta_w) + C_2 f^2(\theta_w) + C_3 f^3(\theta_w) \qquad (4\text{-}17)$$

$$N_1/q = C_4 + C_5 f(\theta_w) + C_6 f^2(\theta_w) + C_7 f^3(\theta_w) \qquad (4\text{-}18)$$

$$N_2/q = C_8 + C_9 f(\theta_w) + C_{10} f^2(\theta_w) + C_{11} f^3(\theta_w) \qquad (4\text{-}19)$$

$$N_3/q = C_{12} + C_{13} f(\theta_w) + C_{14} f^2(\theta_w) + C_{15} f^3(\theta_w) \qquad (4\text{-}20)$$

N_0/q, N_1/q, N_2/q, and N_3/q are constant since pitch angle and hence $f(\theta_w)$ are constant. If N_2 and N_3 are small, and $f(\psi_w) = \sin \psi_w \approx \psi_w$, Equation (4-16) can then be approximated as

$$N/q \approx N_0/q + (N_1/q)\, \psi_w \qquad (4\text{-}21)$$

which is the familiar form of the small angle, linear approximation for calculating yawing moment. Hence, N_2/q and N_3/q are simply coefficients to provide a third-order fit to the wind tunnel yaw sweep data.

Now consider that most wind tunnel tests have yaw sweeps at more than one pitch angle and that the values of N_0/q, N_1/q, N_2/q, and N_3/q will generally be different at different pitch angles. In this case their values can be curve-fitted using the form of Equations (4-17) through (4-20). The resulting coefficients can then be substituted into Equation (4-16). Equation (4-16) will then simulate both the conventional variation of yawing moment with yaw angle and the generally neglected variation of yawing moment with pitch angle, i.e., aerodynamic cross-coupling.

From further analysis of the wind tunnel data and comparison of the quality of the curve fits and accuracies of the test data, it was concluded that the terms with the coefficients C_3, C_7, C_{10}, C_{11}, C_{13}, C_{14} and C_{15} could be deleted from Equation (4-15) for the lift, drag, and pitching moment equation and that the C_7, C_{10}, C_{11}, C_{14}, and C_{15} terms could be deleted from the side force, rolling moment, and yawing moment equations. The type of function used for $f(\theta_w)$ and $f(\psi_w)$ had a very small and random effect on the quality of the curve fit. For some data, the polynominal form, e.g., $f(\theta) = \theta_w$, provided the best fit; for other data, the sinusoidal forms, e.g., $f(\theta) = \sin(\theta_w)$, or $\sin(2\theta_w)$, provided the best fit. Hence, for maximum compatibility with the HAE model, the sinusoidal functions were used in the baseline equation. The resulting set of equations was termed the Nominal Angle Equations (NAE) model and is given in Tables 4-3 and 4-4.

Table 4-5 is a summary of the effect of deleting various combinations of coefficients from the baseline equation on the quality of the curve fit for the Model 206 data. Data for the other fuselages exhibited similar trends in quality of fit relative to the test data accuracy.

From the above study it was apparent that the HAE model was not sufficiently accurate to model the forces and moments in the nominal angle case. The HAE model is convenient and desirable in that the equations are continuous, give the proper data trends at all fuselage orientations, include some cross-coupling effects, and require relatively few inputs. However, only in isolated cases was their accuracy in the nominal angle case within the accuracy of the test data.

The possibility of using the NAE model for all fuselage orientations was then investigated. The conclusion was that it could not be used to replace the HAE model because of the cross-coupling terms in the NAE model. As is typical of most curve-fit techniques, extrapolation beyond the range of data fitted gives a very poor fit. Hence, it was decided that both the HAE and NAE models should be included in the revised mathematical model of the fuselage, since each model performs a function which the other cannot.

4.2.5 Logic for Phasing and Use of the High and Nominal Angle Equations

The transition from the HAE to the NAE model and vice versa should be continuous, smooth, and not cause any reversals or sharp changes in slope not actually in the data. Also, the transition should be dependent on both the pitch and yaw angle. The simplest parameter which can accomplish these objectives is the complex angle of attack, α_c.

$$\alpha_c = \cos^{-1} \frac{u}{V} \tag{4-22}$$

TABLE 4-3. NOMINAL ANGLE EQUATIONS FOR LONGITUDINAL AERODYNAMIC FORCES AND MOMENTS

$$FM = FM_0 + \frac{\partial FM}{\partial \sin\psi_w} \sin\psi_w + \frac{\partial FM}{\partial \sin^2\psi_w} \sin^2\psi_w$$

$$+ \left(\frac{\partial FM}{\partial \sin[ANG]} + \frac{\partial(\partial FM/\partial \sin[ANG])}{\partial \sin\psi_w} \sin\psi_w \right.$$

$$\left. + \frac{\partial(\partial FM/\partial \sin[ANG])}{\partial \sin^2\psi_w} \sin^2\psi_w \right) \sin[ANG]$$

$$+ \left(\frac{\partial FM}{\partial \sin^2[ANG]} + \frac{\partial(\partial FM/\partial \sin^2[ANG])}{\partial \sin\psi_w} \sin\psi_w \right) \sin^2[ANG]$$

$$+ \left(\frac{\partial FM}{\partial \sin^3[ANG]} \right) \sin^3[ANG]$$

The above equation represents the equations for lift (L), drag (D), and pitching moment (M). To obtain the complete equation for one of the forces or the moment, substitute its corresponding symbol for the representative variable FM. For lift and pitching moment, ANG = $2\theta_w$; for drag, ANG = θ_w.

FM_0 indicates the value of FM at $\theta_w = \psi_w = 0^\circ$.

TABLE 4-4. NOMINAL ANGLE EQUATIONS FOR LATERAL-DIRECTIONAL AERODYNAMIC FORCES AND MOMENTS

$$FM = FM_0 + \frac{\partial FM}{\partial \sin\theta_w} \sin\theta_w + \frac{\partial FM}{\partial \sin^2\theta_w} \sin^2\theta_w + \frac{\partial FM}{\partial \sin^3\theta_w} \sin^3\theta_w + \left(\frac{\partial FM}{\partial \sin[2\psi_w]} + \frac{\partial(\partial FM/\partial \sin[2\psi_w])}{\partial \sin\theta_w} \sin\theta_w + \frac{\partial(\partial FM/\partial \sin[2\psi_w])}{\partial \sin^2\theta_w} \sin^2\theta_w \right) \sin[2\psi_w] + \left(\frac{\partial FM}{\partial \sin^2[2\psi_w]} + \frac{\partial(\partial FM/\partial \sin^2[2\psi_w])}{\partial \sin\theta_w} \sin\theta_w \right) \sin^2[2\psi_w] + \left(\frac{\partial FM}{\partial \sin^3[2\psi_w]} + \frac{\partial(\partial FM/\partial \sin^3[2\psi_w])}{\partial \sin\theta_w} \sin\theta_w \right) \sin^3[2\psi_w]$$

The above equation is representative of the equations for side force (Y), rolling moment (l), and yawing moment (N). To obtain the complete equation for one of the moments or the force, substitute its corresponding symbol for the representative variable FM.

FM_0 indicates the value of FM at $\theta_w = \psi_w = 0^\circ$.

TABLE 4-5. EFFECT OF DELETING TERMS FROM BASELINE EQUATION ON ACCURACY OF CURVE FITS

Subscript of Coefficient of Terms Deleted from Baseline Equation	Summation of Absolute Value of Errors Divided by Number of Points Fitted					
	Lift-ft^2		Drag-ft^2		Pitching Moment-ft^3	
	Case 1	Case 2	Case 1	Case 2	Case 1	Case 2
None	.4342	.2576	.2268	.0916	1.6342	.8054
15	.4362	.2579	.2267	.0940	1.6345	.8034
14, 15	.5093	.2703	.2382	.0939	2.1877	1.0667
11, 14, 15	.5186	.2709	.2381	.0942	2.1897	1.0661
10, 11, 14, 15	.5455	.3543	.2601	.1276	2.1508	1.1992
7, 10, 11, 14, 15	.5520	.3545	.2637	.1299	2.1505	1.1991
7, 10, 11, 13→15	.5522	.3545	.2651	.1299	2.1555	1.1988
3, 7, 10, 11, 13→15 *	.5566	.3544	.2650	.1308	2.1619	1.1971
3, 6, 7, 10, 11, 13→15	1.2535	.4979	.2764	.1305	2.3987	2.1779
3, 6, 7, 10→15	1.2521	.6190	.2771	.1316	2.8462	2.7814
Accuracy of test data	± 0.7 ft^2		± 0.3 ft^2		± 2.0 ft^3	

TABLE 4-5. Continued.

Subscript of Coefficient of Terms Deleted from Baseline Equation	Summation of Absolute Value of Errors Divided by Number of Points Fitted					
	Side Force-ft^2		Rolling Moment-ft^3		Yawing Moment-ft^3	
	Case 1	Case 2	Case 1	Case 2	Case 1	Case 2
None	.4885	.2049	1.1296	.5673	2.4860	1.2110
15	.4860	.2070	1.2955	.5675	2.4623	1.3004
14, 15	.5052	.2146	1.2957	.5685	2.7781	1.4318
11, 14, 15	.5051	.2138	1.3221	.5730	2.8010	1.4279
10, 11, 14, 15	.5121	.2661	1.3293	.5949	2.8181	1.4301
7, 10, 11, 14, 15 *	.7057	.3734	2.0218	.6988	2.9320	1.7375
7, 10, 11, 13→15	.7180	.4532	2.0621	.7337	2.9065	1.9416
Accuracy of test data	± 0.5 ft^2		± 2.0 ft^3		± 3.4 ft^3	

Units of the errors are force or moment divided by dynamic pressure per point (ft^2/point or ft^3/point respectively). All data are for a 0.25 scale Bell Model 206 (JetRanger).

Case 1: Basic fuselage with skid gear; 136 data points fitted; $-12^\circ \leq \theta_w < 18^\circ$; $|\psi_w| \leq 16^\circ$ to 25°.

Case 2: Basic fuselage with inflated pop-out floats; 89 data points fitted; $-10^\circ \leq \theta_w < 18^\circ$; $\psi_w \leq 12^\circ$.

*Indicates the set of coefficients deleted from the baseline equation to form the programmed Nominal Angle Equation model. Baseline equation is Equation (4-15).

From Equation (4-22) and the orthogonality of the body axis velocities,

$$\sin \alpha_c = \frac{\sqrt{v^2 + w^2}}{V} \cdot \text{sign}(u) \qquad (4\text{-}23)$$

This parameter is the angle between the wind vector and the body X-axis. The locus of the body X-axis for a constant complex angle of attack is a conical surface of revolution about the wind vector (the positive wind X-axis).

If the angle is to be measured with respect to the positive wind Y-axis, the alternate definition of α_c is

$$\alpha_c = \cos^{-1}\left(\frac{-v}{V}\right) \qquad (4\text{-}24)$$

These separate definitions are made so that the Nominal Angle Equations can be centered about either the wind X-axis (for very precise simulation in forward and rearward flight) or the wind Y-axis (for sideward flight). The choice of which axis to use as the center of the cone for these equations has been made a user option.

Three inputs to the program (LGF, α_L, and α_H) control the use and phasing together of the Nominal Angle and High Angle Equations. LGF is a logic switch, while α_L and α_H are boundary angles:

LGF: = 0 for the region of use of the Nominal Angle Equations to be centered about the wind X-axis.

$\neq$ 0 for the region of use of the Nominal Angle Equations to be centered about the wind Y-axis.

α_L: The value of α_c at the boundary between the region where the Nominal Angle Equations are used and the region where the two sets of equations are phased together.

α_H: The value of α_c at the boundary between the region where the High Angle Equations are used and the phasing region.

The logical decisions made based on these three inputs are shown in Figure 4-7.

Within the phasing region, the value of individual forces and moments is calculated using the phasing angle, α_{ph},

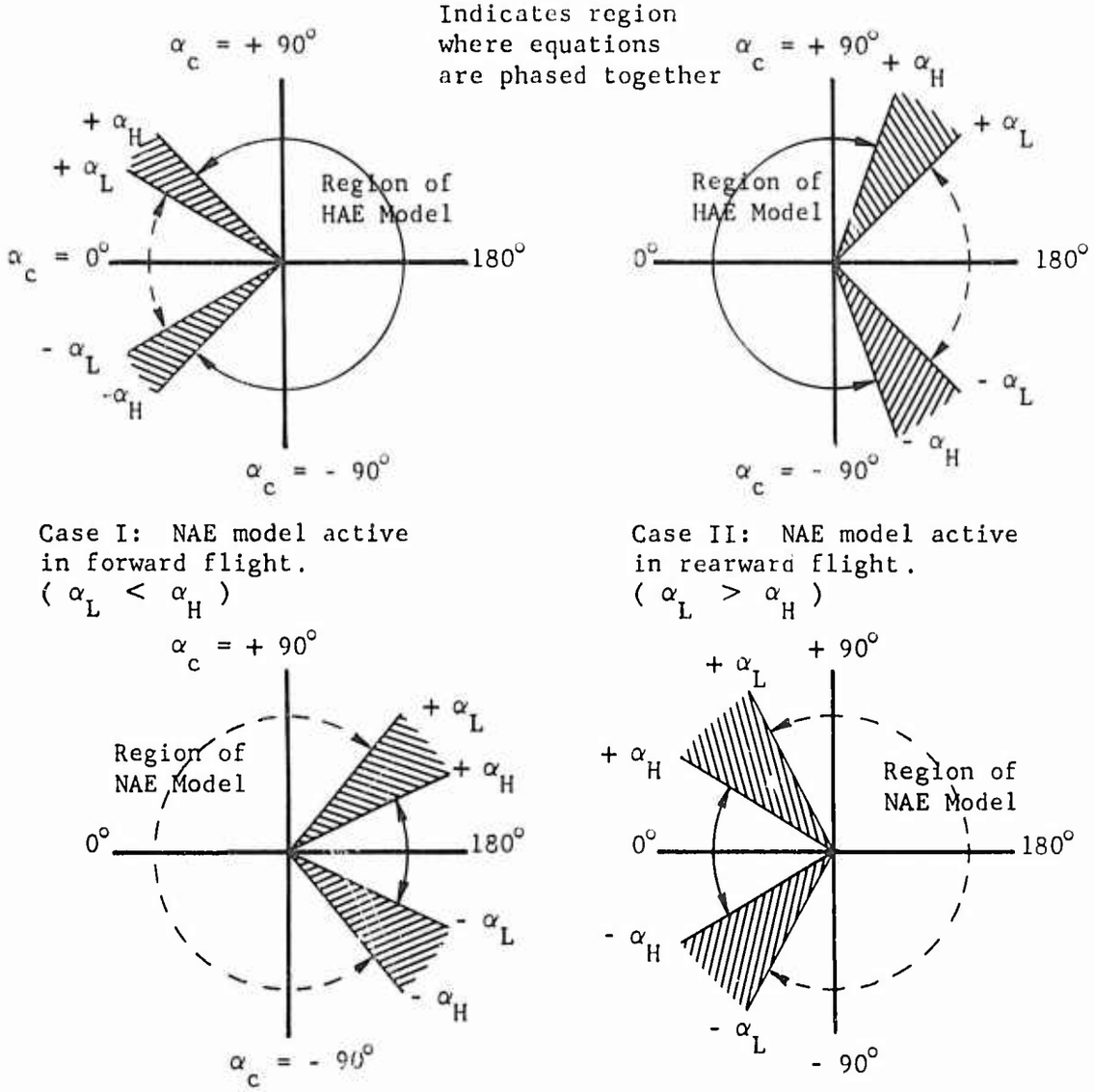

Case I: NAE model active in forward flight. ($\alpha_L < \alpha_H$)

Case II: NAE model active in rearward flight. ($\alpha_L > \alpha_H$)

Case III: Similar to Case I but region for NAE model much larger.

Case IV: Similar to Case II but region for NAE model much larger.

Cases I and II represent likely inputs. Although Cases III and IV are possible inputs, it is improbable that the NAE model will adequately simulate the data throughout such a large region.

Figure 4-7. Phasing of Fuselage NAE and HAE Models.

$$\alpha_{ph} = \left[\frac{\alpha_c - \alpha_L}{\alpha_H - \alpha_L}\right]\frac{\pi}{2} \qquad (4\text{-}25)$$

and the following relationship:

$$FM(\theta_w, \psi_w)_{wind} = FM(\theta_w, \psi_w)_{NAE} \cos^2\alpha_{ph} + FM(\theta_w, \psi_w)_{HAE} \sin^2\alpha_{ph} \qquad (4\text{-}26)$$

where

FM is a specific force or moment
wind indicates the final wind axis value
NAE indicates the value from the Nominal Angle Equation
HAE indicates the value from the High Angle Equation

4.3 EXAMPLES OF THE FUSELAGE REPRESENTATION

Figure 4-8 is an example of the High Angle Equation model for a medium utility helicopter. Data for drag and yawing moment are shown. Other data exhibited similar correlation. Table 4-6 is an example of the Nominal Angle Equation model for a light commercial helicopter. The data presented are a sample of the output of computer program AS812A discussed in the next section and consist of the coefficients of the curve fit and a comparison of the input and calculated force or moment. The quality of the curve fit can be judged by referring to the columns labeled "DELTA" (input minus calculated value) and "REL-DEL" (DELTA divided by input value) and to the two parameters at the end of the calculations labeled "SUM OF ABS(ERRORS)/ POINTS" (the summation of the absolute values of DELTA divided by the number of data points) and "RMS ERROR/POINTS" (the square root of the summation of DELTA-squared, divided by the number of points). These data and parameters indicate that the NAE model can fit the input data so closely that separate plots of the input and calculated data (e.g., contour or carpet plots) would virtually overlie each other.

4.4 AIDS TO DETERMINING THE INPUTS FOR FUSELAGE REPRESENTATION

Included with the Rotorcraft Flight Simulation Program is a separate computer program designed to aid the user in determining the inputs to the fuselage representation. This program, designated AS812A, curve-fits force and moment test data to the Nominal Angle Equations of C81. The output of the program is the set of coefficients of each equation, a comparison of the test and calculated data, and parameters for estimating the quality of the fit. At the user's option the coefficients are punched on cards. The format of the punched output is precisely that required for input to C81. See Section 3.26.3 of Volume II for additional information regarding this program.

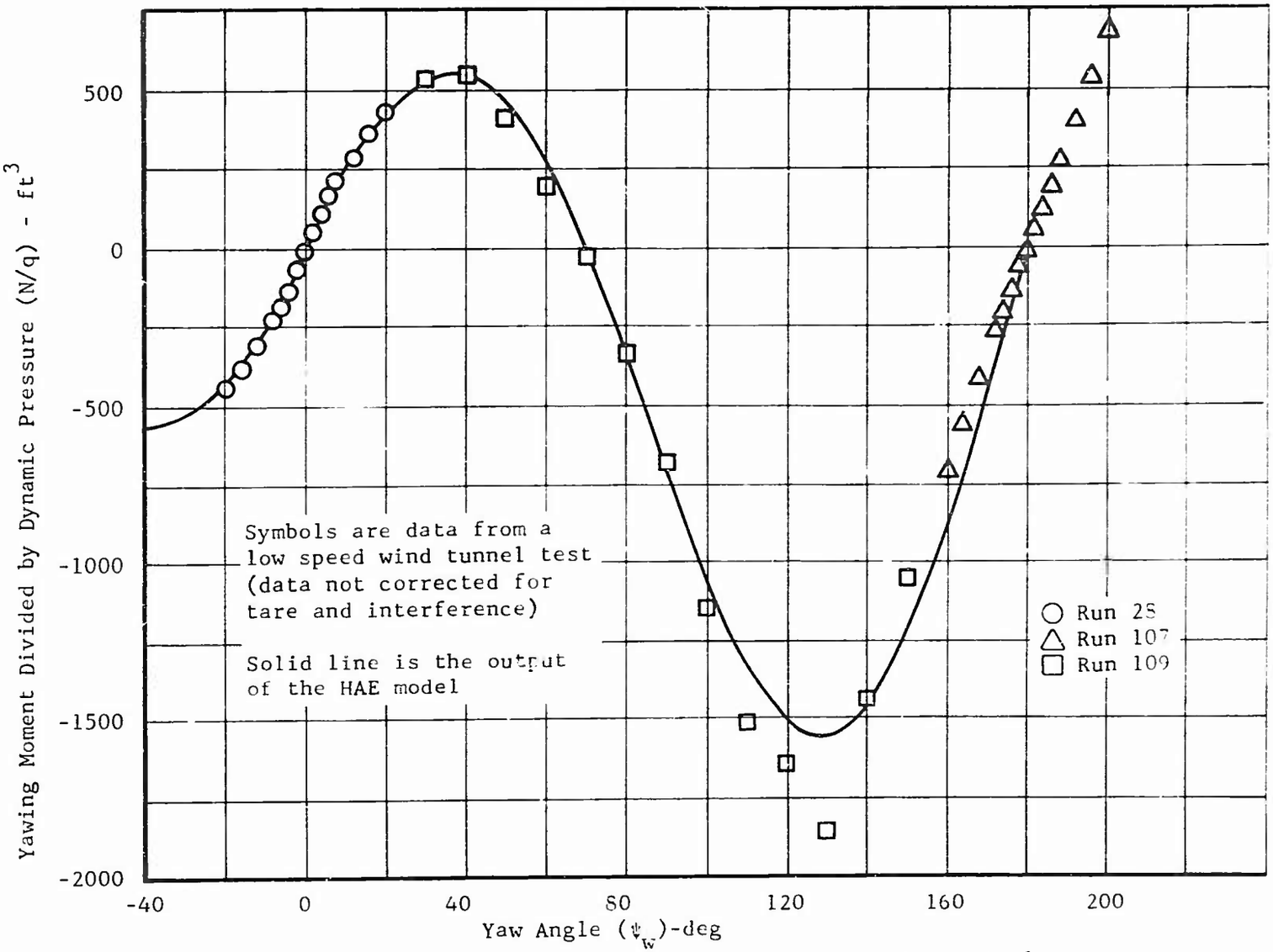

Figure 4-8. Examples of Fuselage Aerodynamic Representation at Large Angles for a Medium Utility Helicopter.

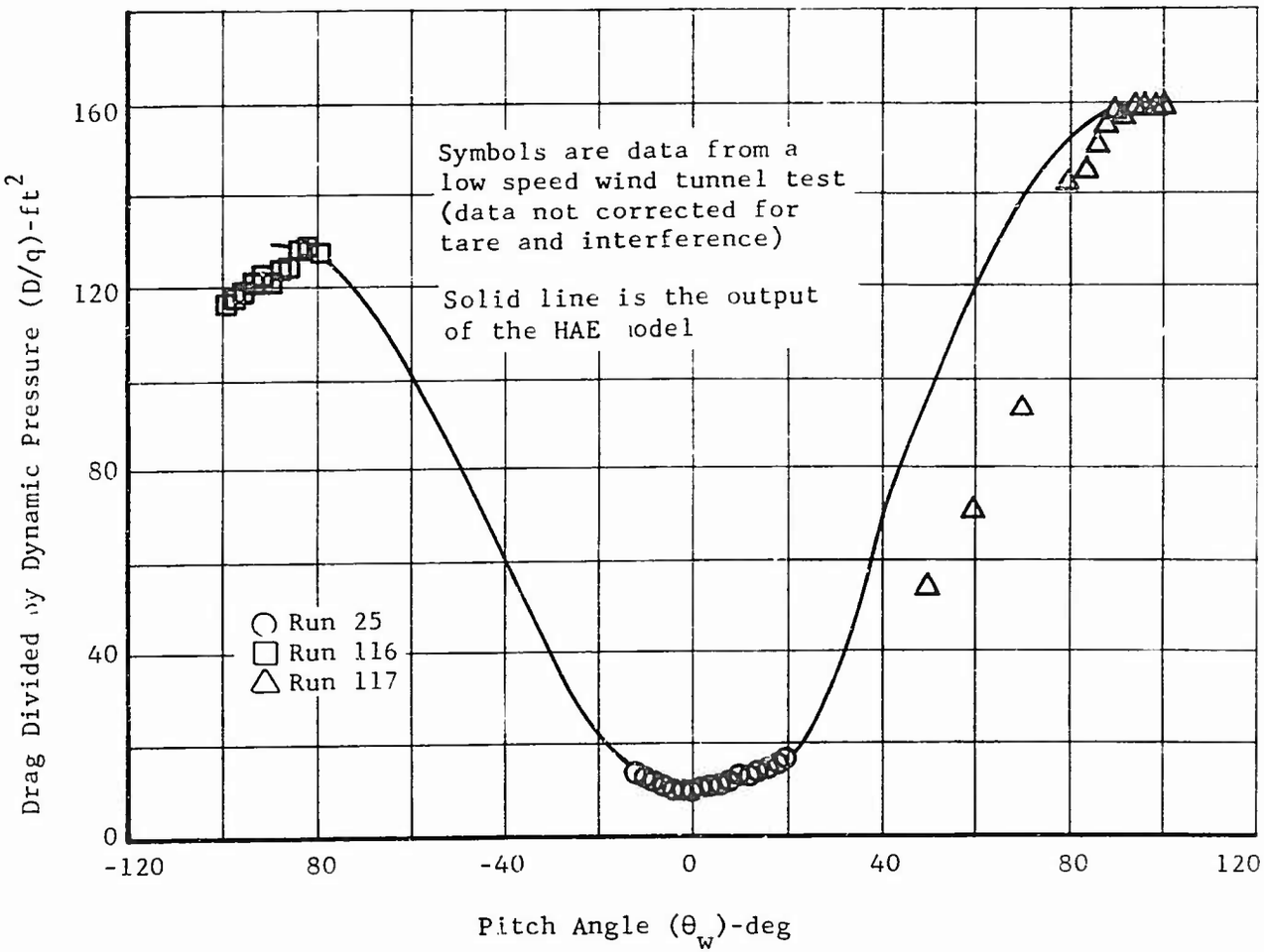

Figure 4-8. Concluded.

TABLE 4-6. EXAMPLES OF FUSELAGE AERODYNAMIC REPRESENTATION AT SMALL ANGLES FOR A LIGHT COMMERCIAL HELICOPTER

DRAG DATA

COEFFICIENTS OF EQUATION

SUB-SCRIPT	NON-DIMENSIONAL	DIMENSIONAL	AGAU73 INPUT
00	2.10 FT**2	2.099379 FT**2/DEG**0	XFS(29)
10	-0.66 FT**2	-0.011553 FT**2/DEG**1	XFS(35)
20	67.67 FT**2	0.020613 FT**2/DEG**2	XFS(36)
01	-2.92 FT**2	-0.050906 FT**2/DEG**1	XFS(37)
11	2.32 FT**2	0.000615 FT**2/DEG**2	XFS(38)
21	0.84 FT**2	0.000004 FT**2/DEG**3	XFS(39)
02	29.90 FT**2	0.009108 FT**2/DEG**2	XFS(40)
12	-1.95 FT**2	-0.000010 FT**2/DEG**3	XFS(41)
03	-10.99 FT**2	-0.000058 FT**2/DEG**3	XFS(42)

INPUT DATA AND CALCULATIONS

RUN/PT		PITCH	YAW	INPUT	CALCULATION	DELTA	REL-DEL
210	1	-11.76	0.00	3.8100	4.0269	-0.219	-0.05746
210	2	-10.46	-16.01	9.3000	9.1174	0.183	0.01964
210	3	-10.53	-12.01	6.6600	6.6494	-0.189	-0.02844
210	4	-10.45	-8.01	4.9300	5.1406	-0.211	-0.04278
210	5	-10.69	-4.01	4.5200	4.5950	-0.075	-0.01660
210	6	-10.76	-4.00	4.2600	4.1833	0.117	0.02726
210	7	-11.62	-1.99	4.0600	4.1110	-0.051	-0.01256
210	8	-11.65	-0.01	3.8100	4.0404	-0.230	-0.06046
210	9	-11.65	1.99	3.8800	4.0507	-0.171	-0.04399
210	10	-11.46	3.99	4.1800	4.1766	0.003	0.00081
210	11	-10.81	6.02	4.5600	4.3969	0.163	0.03577
210	12	-10.71	8.02	5.0300	4.9046	0.125	0.02495
210	13	-10.57	10.01	5.6300	5.5573	0.073	0.01291
210	14	-10.56	12.01	6.3800	6.4056	-0.026	-0.00401
210	15	-10.47	14.02	7.3500	7.3803	-0.030	-0.00412
210	16	-10.46	15.99	8.7900	8.5024	0.286	0.03272
210	17	-11.81	0.00	3.8300	4.0430	-0.213	-0.05562
211	1	-6.98	0.00	3.1300	2.9151	0.215	0.06866
211	2	-5.78	-16.00	8.2000	8.0828	0.117	0.01429
211	3	-5.78	-13.99	6.8200	6.8680	-0.048	-0.00704
211	4	-5.75	-11.99	5.5700	5.5630	-0.233	-0.04184
211	5	-5.82	-10.01	4.9100	4.9101	-0.000	-0.00002
211	6	-5.92	-8.01	4.1500	4.1467	-0.017	-0.00403
211	7	-6.05	-6.01	3.6900	3.5865	0.104	0.02865
211	8	-6.48	-4.00	3.3500	3.2178	0.132	0.03947
211	9	-6.66	-2.02	3.3400	2.9770	0.363	0.10867
211	10	-6.96	-0.01	3.1300	2.9116	0.218	0.06976
211	11	-6.97	1.99	3.1900	2.9622	0.228	0.07140
211	12	-6.99	3.99	3.4100	3.1789	0.231	0.06777
211	13	-6.85	5.99	3.6000	3.5299	0.070	0.01946
211	14	-6.31	7.99	4.1800	3.9752	0.205	0.04899
211	15	-5.86	9.99	4.6500	4.6002	0.050	0.01076
211	16	-5.76	11.99	5.4000	5.4373	-0.037	-0.00691
211	17	-5.72	13.99	6.3100	6.4345	-0.124	-0.01975
211	18	-5.81	15.99	7.5200	7.5673	-0.047	-0.00629
211	19	-6.98	0.01	3.1800	2.9149	0.265	0.08335
212	1	-1.99	-0.01	2.4800	2.2373	0.243	0.09786
212	2	-1.94	-25.00	15.5300	14.6232	0.907	0.05839
212	3	-1.95	-24.00	14.1900	13.7217	0.468	0.03301
212	4	-1.96	-22.00	11.9600	12.0010	-0.041	-0.00343
212	5	-2.00	-20.01	10.0100	10.4093	-0.399	-0.03984
212	6	-1.95	-18.01	8.3900	8.9262	-0.536	-0.06391
212	7	-2.00	-16.01	7.0600	7.5755	-0.519	-0.07358
212	8	-1.96	-14.01	5.8800	6.3763	-0.496	-0.08440
212	9	-1.87	-12.01	4.9000	5.3074	-0.407	-0.08314
212	10	-1.90	-10.01	4.1700	4.4601	-0.290	-0.05517
212	11	-1.84	-8.01	3.4600	3.6392	-0.179	-0.05178
212	12	-1.79	-6.00	3.0500	3.0350	0.015	0.00496
212	13	-1.97	-4.01	2.7900	2.6175	0.172	0.06183
212	14	-2.00	-2.00	2.6100	2.3461	0.264	0.10112
212	15	-1.94	-0.01	2.4400	2.2329	0.207	0.08486

TABLE 4-6. Continued.

212	16	-1.75	1.99	2.3100	2.2763	0.034	0.01458
212	17	-2.00	3.99	2.8400	2.5144	0.326	0.11465
212	18	-1.99	6.01	3.0900	2.9018	0.188	0.06092
212	19	-1.97	8.01	3.6000	3.4465	0.153	0.04263
212	20	-1.97	9.99	4.0400	4.1437	-0.104	-0.02566
212	21	-2.00	11.99	4.6600	5.0044	-0.344	-0.07391
212	22	-1.98	13.99	5.6000	6.0119	-0.412	-0.07356
212	23	-1.97	15.99	6.5800	7.1371	-0.557	-0.08466
212	24	-1.96	18.01	7.9100	8.4415	-0.532	-0.06720
212	25	-1.93	19.99	9.3600	9.8590	-0.499	-0.05331
212	26	-1.72	21.99	11.1100	11.4270	-0.317	-0.02853
212	27	-1.64	23.99	13.2300	13.0962	0.134	0.01012
212	28	-1.74	24.99	14.3900	13.9818	0.408	0.02837
212	29	-1.97	0.00	2.4100	2.2354	0.175	0.07244
213	1	8.04	-0.01	2.5800	2.2463	0.334	0.12932
213	2	8.22	-25.01	15.2400	14.5526	0.687	0.04511
213	3	8.32	-24.00	14.0500	13.6519	0.398	0.02834
213	4	8.50	-22.00	11.8900	11.9514	-0.061	-0.00517
213	5	8.73	-20.00	9.9900	10.3746	-0.385	-0.03856
213	6	8.81	-18.01	8.3700	8.9187	-0.549	-0.06556
213	7	8.79	-16.01	7.0400	7.5759	-0.490	-0.06909
213	8	8.83	-14.01	5.9400	6.3862	-0.446	-0.07513
213	9	8.86	-12.00	4.9200	5.3095	-0.390	-0.07917
213	10	8.96	-10.00	4.3100	4.3505	-0.041	-0.01008
213	11	8.95	-8.02	3.6700	3.6911	-0.021	-0.01992
213	12	8.96	-6.02	3.0900	3.0405	0.050	0.01602
213	13	8.97	-4.01	2.8700	2.6094	0.261	0.09080
213	14	8.97	-2.00	2.6900	2.3459	0.344	0.12793
213	15	8.94	0.00	2.6000	2.2463	0.354	0.13605
213	16	8.95	1.99	2.6400	2.3143	0.326	0.12338
213	17	8.97	3.99	2.8000	2.5479	0.252	0.10911
213	18	8.98	5.99	3.1000	2.9443	0.156	0.05023
213	19	8.99	8.00	3.5100	3.5118	-0.002	-0.00052
213	20	9.11	10.00	4.0000	4.2318	-0.232	-0.05796
213	21	9.11	12.01	4.7700	5.1006	-0.331	-0.06931
213	22	9.19	14.01	5.8700	6.1316	-0.262	-0.04456
213	23	9.44	15.99	7.0100	7.3126	-0.303	-0.04316
213	24	9.79	18.01	8.2600	8.6702	-0.410	-0.04960
213	25	9.83	20.02	9.8100	10.1261	-0.316	-0.03222
213	26	9.81	22.01	11.8300	11.8873	0.143	0.01206
213	27	9.71	24.01	13.9100	13.3752	0.535	0.03845
213	28	9.66	25.02	15.1100	14.2571	0.843	0.05582
213	29	9.01	-0.01	2.6400	2.2439	0.396	0.15005
214	1	18.77	0.00	4.0800	3.8904	0.170	0.04177
214	2	18.98	-20.02	12.1100	11.7792	0.331	0.02731
214	3	18.95	-18.01	10.1800	10.3020	-0.122	-0.01198
214	4	18.85	-16.01	8.7300	8.9682	-0.238	-0.02726
214	5	18.88	-14.01	7.5400	7.7807	-0.241	-0.03193
214	6	18.83	-11.99	6.6800	6.7749	-0.095	-0.01420
214	7	18.49	-10.00	5.9600	5.9174	0.043	0.00715
214	8	18.80	-8.01	5.2300	5.2036	0.026	0.00505
214	9	18.69	-6.01	4.6800	4.6407	0.039	0.00840
214	10	18.73	-4.01	4.3200	4.2292	0.091	0.02103
214	11	18.75	-2.01	4.1100	3.9773	0.133	0.03230
214	12	18.76	0.00	4.0600	3.8883	0.172	0.04229
214	13	18.76	1.99	4.1500	3.9628	0.187	0.04512
214	14	18.75	4.01	4.3000	4.2034	0.097	0.02247
214	15	18.75	5.99	4.5300	4.6036	-0.074	-0.01625
214	16	18.75	8.01	5.0700	5.1754	-0.105	-0.02079
214	17	18.87	10.01	5.7500	5.6842	-0.134	-0.02335
214	18	18.49	12.01	6.5300	6.7271	-0.197	-0.03019
214	19	18.35	13.99	7.6000	7.7187	-0.119	-0.01562
214	20	18.19	15.99	8.7100	8.8619	-0.152	-0.01744
214	21	18.05	17.99	9.9700	10.1497	-0.180	-0.01803
214	22	18.06	20.02	11.6700	11.6261	0.044	0.00376
214	23	18.78	-0.01	4.0600	3.8926	0.167	0.04123

SUM OF ABS(ERRORS)/POINTS= 0.2304
RMS ERROR/POINTS= 0.0267
STANDARD DEVIATION= 0.2899

INPUTS FOR AGAJ73

2.0994 -0.011553 CARD 25

0.020613 -0.0505Ce 0.000615 0.000004 0.009108 -0.000010 -0.000058 CARD 26

TABLE 4-6. Continued.

YAWING MOMENT DATA

COEFFICIENTS OF EQUATION

SUB-SCRIPT	NON-DIMENSIONAL	DIMENSIONAL	AGAJ73 INPUT
00	-3.72 FT**3	-3.724587 FT**3/DEG**0	XFS(88)
10	0.45 FT**3	0.007865 FT**3/DEG**1	XFS(89)
20	-8.02 FT**3	-0.002444 FT**3/DEG**2	XFS(90)
30	-48.75 FT**3	-0.000259 FT**3/DEG**3	XFS(91)
01	143.71 FT**3	5.016450 FT**3/DEG**1	XFS(92)
11	84.34 FT**3	0.051384 FT**3/DEG**2	XFS(93)
21	-226.82 FT**3	-0.002412 FT**3/DEG**3	XFS(94)
02	3.29 FT**3	0.004004 FT**3/DEG**2	XFS(95)
12	-21.21 FT**3	-0.000451 FT**3/DEG**3	XFS(96)
03	-74.97 FT**3	-0.003189 FT**3/DEG**3	XFS(97)
13	95.09 FT**3	0.000071 FT**3/DEG**4	XFS(98)

INPUT DATA AND CALCULATIONS

RUN/PT		PITCH	YAW	INPUT	CALCULATION	DELTA	REL-DEL
210	1	-11.76	0.00	-5.0400	-3.7366	-1.303	0.25860
210	2	-10.46	-12.01	-52.1100	-52.1386	0.029	-0.00055
210	3	-10.53	-12.01	-45.0700	-45.5020	0.432	-0.00959
210	4	-10.45	-8.01	-39.9800	-34.6767	-5.303	0.13265
210	5	-10.69	-6.01	-34.7300	-27.6679	-7.062	0.20334
210	6	-10.76	-4.00	-26.2100	-20.0894	-6.121	0.23352
210	7	-11.02	-1.99	-15.6600	-11.6311	-3.829	0.24456
210	8	-11.80	-0.01	-5.6500	-3.7758	-1.874	0.33171
210	9	-11.69	1.99	8.6100	4.4079	4.202	0.48805
210	10	-11.40	3.99	16.4700	12.5493	3.921	0.23805
210	11	-10.61	6.02	24.3300	20.7175	3.612	0.14848
210	12	-10.71	8.02	36.5500	28.0383	8.512	0.23288
210	13	-10.57	10.01	41.4800	34.6465	6.834	0.16474
210	14	-10.58	12.01	41.1700	40.2616	0.908	0.02207
210	15	-10.47	14.02	44.8500	45.0465	-0.196	-0.00438
210	16	-10.46	15.99	49.7900	48.5635	1.227	0.02463
210	17	-11.81	0.00	-4.7700	-3.7346	-1.035	0.21706
211	1	-6.98	0.00	-4.5100	-3.8103	-0.700	0.15515
211	2	-5.76	-16.00	-58.8700	-60.1626	1.293	-0.02196
211	3	-5.76	-13.99	-55.6100	-56.2619	0.652	-0.01172
211	4	-5.75	-11.99	-50.9200	-51.2818	0.362	-0.00711
211	5	-5.82	-10.01	-42.5000	-45.2422	2.742	-0.06452
211	6	-5.92	-8.01	-30.4400	-38.1976	7.758	-0.25485
211	7	-6.05	-6.01	-24.0300	-30.3491	6.319	-0.26297
211	8	-6.48	-4.00	-24.4500	-21.7403	-2.710	0.11083
211	9	-6.68	-2.02	-15.8200	-12.9675	-2.852	0.18031
211	10	-6.96	-0.01	-5.2600	-3.8556	-1.404	0.26699
211	11	-6.97	1.99	6.5000	5.2216	1.278	0.19668
211	12	-6.99	3.99	15.2700	14.1309	1.139	0.07460
211	13	-6.85	5.99	21.2500	22.7412	-1.491	-0.07017
211	14	-6.31	7.99	23.3900	31.0945	-7.705	-0.32939
211	15	-5.86	9.99	29.8600	38.8104	-8.950	-0.29975
211	16	-5.76	11.99	41.3500	45.4572	-4.107	-0.09933
211	17	-5.72	13.99	51.0200	51.0853	-0.069	-0.00136
211	18	-5.61	15.99	58.0100	55.7823	2.228	0.03840
211	19	-6.48	0.01	-4.3700	-3.7648	-0.605	0.13848
212	1	-1.99	-0.01	-2.2600	-3.7969	1.537	-0.68005
212	2	-1.94	-25.00	-73.5800	-73.9496	0.370	-0.00502
212	3	-1.95	-24.00	-74.3300	-73.9058	-0.424	0.00571
212	4	-1.96	-22.00	-74.4200	-73.2315	-1.189	0.01597
212	5	-2.00	-20.01	-71.8400	-71.6073	-0.233	0.00324
212	6	-1.95	-18.01	-67.7600	-69.1255	1.366	-0.02015
212	7	-2.00	-16.00	-62.9100	-65.4156	2.506	-0.03983
212	8	-1.96	-14.01	-57.9200	-60.7845	2.864	-0.04946
212	9	-1.87	-12.01	-51.9300	-55.1005	3.171	-0.06105
212	10	-1.90	-10.01	-46.1100	-48.3006	2.191	-0.04751
212	11	-1.84	-8.01	-42.6900	-40.6519	-2.038	0.04774
212	12	-1.79	-6.00	-29.4400	-32.1591	2.719	-0.09236
212	13	-1.97	-4.01	-20.4400	-23.0653	2.625	-0.12844
212	14	-2.00	-2.00	-10.0400	-13.5020	3.462	-0.34482
212	15	-1.94	-0.01	-0.6100	-3.7962	3.186	-5.22330

TABLE 4-6. Concluded.

212	16	-1.79	1.99	7.1800	6.0244	1.156	C.16094
212	17	-2.00	3.99	13.8900	15.6241	-1.734	-C.12484
212	18	-1.99	6.01	21.1700	24.9809	-3.811	-C.18001
212	19	-1.97	8.01	29.3200	33.6997	-4.380	-C.14938
212	20	-1.97	9.99	38.1700	41.6223	-3.452	-C.09045
212	21	-2.00	11.99	46.2500	48.7592	-2.509	-0.05425
212	22	-1.98	13.99	53.1400	54.9846	-1.845	-0.03471
212	23	-1.57	15.99	58.8000	60.6161	-1.816	-C.03089
212	24	-1.50	18.01	63.2500	64.9557	-1.706	-0.02697
212	25	-1.53	19.99	64.6200	68.0746	-3.455	-C.05346
212	26	-1.72	21.99	71.3900	69.9811	1.409	C.01974
212	27	-1.64	23.99	72.8400	71.3816	1.458	C.02002
212	28	-1.74	24.99	72.5700	71.5252	1.045	C.01440
212	29	-1.97	0.00	-1.3800	-3.7476	2.368	-1.71563
213	1	8.04	-C.01	-4.2400	-4.0047	-0.235	C.05549
213	2	8.22	-25.01	-92.8300	-92.0107	-0.819	C.00883
213	3	8.32	-24.00	-91.6200	-91.0708	-0.549	C.00599
213	4	8.50	-22.00	-89.2500	-88.5453	-0.705	C.00790
213	5	8.73	-20.00	-85.9100	-85.1507	-0.759	C.00884
213	6	8.81	-18.01	-82.9100	-80.7000	-2.210	C.02666
213	7	8.79	-16.01	-78.4600	-75.2181	-3.242	0.04132
213	8	8.83	-14.01	-72.4500	-68.8383	-3.612	0.04985
213	9	8.60	-12.00	-65.1800	-61.4120	-3.768	C.05781
213	10	8.38	-10.00	-57.2900	-53.2207	-4.069	C.07103
213	11	8.25	-8.02	-46.3400	-44.4190	-1.921	C.04145
213	12	8.10	-6.02	-38.6000	-34.9018	-3.698	C.09581
213	13	8.07	-4.01	-28.2600	-24.8596	-3.400	C.12033
213	14	8.07	-2.00	-13.3500	-14.4708	1.121	-C.08396
213	15	8.04	0.00	-4.2700	-3.9520	-0.318	C.07448
213	16	8.05	1.99	9.1200	6.5139	2.606	C.28576
213	17	8.07	3.99	20.6300	16.8608	3.769	C.18271
213	18	8.08	5.99	30.6700	26.8675	3.803	C.12398
213	19	8.09	8.02	39.0200	36.5144	2.506	C.06421
213	20	8.11	10.02	49.5400	45.3763	4.164	C.08405
213	21	8.11	12.01	58.2900	53.4430	4.847	C.08315
213	22	8.19	14.01	63.5600	60.7198	2.840	0.04469
213	23	8.44	15.99	70.2400	67.0791	3.161	C.04500
213	24	8.75	18.01	74.8400	72.6823	2.158	C.02883
213	25	8.83	20.02	73.6800	77.2591	-3.579	-C.04858
213	26	8.81	22.01	81.4600	80.8724	0.588	C.00648
213	27	8.71	24.02	82.7900	83.6186	-0.829	-C.01001
213	28	8.66	25.02	83.4200	84.6799	-1.260	-C.01510
213	29	8.01	-0.01	-3.3300	-4.0023	0.672	-C.20189
214	1	18.77	C.00	-6.4500	-6.0355	-0.414	C.06426
214	2	18.06	-26.02	-88.9300	-90.3076	1.378	-C.01549
214	3	18.05	-18.01	-83.0000	-84.7615	1.762	-C.02122
214	4	18.05	-16.01	-77.1400	-78.4544	1.314	-0.01704
214	5	18.08	-14.01	-69.5600	-71.3759	1.816	-C.02611
214	6	18.33	-11.99	-60.3100	-63.4967	3.187	-C.05284
214	7	18.49	-10.00	-52.0000	-55.0519	3.052	-C.05869
214	8	18.60	-8.01	-44.3500	-46.0228	1.673	-C.03772
214	9	18.65	-6.01	-37.8700	-36.4658	-1.404	C.03708
214	10	18.73	-4.01	-29.6800	-26.5362	-3.144	C.10592
214	11	18.75	-2.01	-18.4900	-16.3634	-2.127	C.11501
214	12	18.76	C.00	-7.4600	-6.0323	-1.428	C.19139
214	13	18.76	1.99	3.1000	4.1649	-1.065	-C.34352
214	14	18.75	4.01	15.0600	14.3447	0.655	C.04369
214	15	18.75	5.99	25.1900	24.0145	1.176	C.04667
214	16	18.75	8.01	31.8400	33.4429	-1.603	-C.05034
214	17	18.67	10.01	38.9700	42.2844	-3.314	-C.08505
214	18	18.49	12.01	48.8800	50.5623	-1.682	-C.03442
214	19	18.35	13.99	57.5000	58.0364	-0.536	-C.00933
214	20	18.19	15.99	65.2700	64.8367	0.433	C.00664
214	21	18.05	17.99	72.4600	70.8208	1.639	C.02262
214	22	18.06	20.02	76.0900	75.9655	0.125	0.00164
214	23	18.78	-0.01	-5.7500	-6.0903	0.340	-C.05918

SUM OF ABS(ERRORS)/PCINTS= 2.3521
RMS ERROR/PCINTS= 0.2769
STANDARD DEVIATION= 3.0079

INPUTS FOR AGAJ73

-3.724587 0.007865 -0.002444 -0.000259 CARD 2D
5.016450 C.051384 -0.002412 0.004004 -0.000451 -0.003189 0.000071 CARD 2E

The inputs to the High Angle Equations are stated in terms of the value of forces or moments divided by dynamic pressure at specific aerodynamic angles. Provided sufficient test data are available, these inputs can be read directly from plots of the data. If test data are insufficient or not available, the inputs can be estimated by analytically determining the forces (particularly drag force or equivalent flat plate area) and the location of the fuselage center of pressure at the appropriate orientations.

Jorgensen's work (References 20 and 21) was published shortly after the development of the current fuselage representation. The engineering-type methods which are presented in the referenced reports are in general agreement with the HAE model. However, no attempts were made to incorporate Jorgensen's methods directly into C31 because of the large amount of geometric data on the body required, the high Mach number range for which the methods were derived, and the uncertainty of the validity limits of the methods. Regardless, the methods may be helpful and should be considered when estimating the inputs to the HAE.

5. AERODYNAMIC SURFACE MATHEMATICAL MODEL

5.1 INTRODUCTION

In the course of developing C81, mathematical models have been incorporated for aerodynamic surfaces. The earliest versions of the program contained very simple models for a wing and a horizontal stabilizer. When lateral-directional degrees of freedom were added, a vertical stabilizing surface was added. Although minor improvements were subsequently made to each of the three models, each model remained distinct and applicable only to a specific surface. The most serious shortcoming of these models was that they were restricted to simulating surfaces which were parallel to either the horizontal or vertical planes of the fuselage. Specifically, the wing and horizontal stabilizer had to be in the body X-Y plane and the vertical stabilizer in the body X-Z plane. In accordance with these restrictions, the models were referred to as the wing-elevator-fin models.

The current model for aerodynamic surfaces was developed to remove the restrictions inherent to the previous collection of models. The primary goal in the development of the current model was to provide a single model which could be used for any surface at any orientation with respect to the body. Other desirable features were:

(1) A better representation for the flow field at each surface and the effect of surface geometry on the aerodynamic characteristics

(2) The inclusion of aerodynamic pitching moment characteristics for each surface

(3) The capability of simulating flaps or control surfaces on each aerodynamic surface

(4) The capability of simulating a wing and four stabilizing surfaces

5.2 DEVELOPMENT OF THE MATHEMATICAL MODELS

The complete aerodynamic surface mathematical model was broken into four submodels for development purposes: the flow field model, the chord line orientation model, the aerodynamic angles model, and the surface aerodynamic model. The flow field and chord line models were defined to be completely independent of each other with their output being combined to define the aerodynamic angles in the third model. These three models completely replaced the comparable models which were part of the previous wing-elevator-fin models.

The current mathematical model for computing the aerodynamic force and

moment coefficients is a minor update and expansion of the previous representation. The major differences include:

(1) Changes to specific equations to improve the simulation of the effects of surface geometry

(2) The addition of pitching moment coefficient to the model

(3) A method for modifying the coefficients computed for flap, or control surface, deflection

5.2.1 Flow Field Model

In the development of its mathematical model, the flow field at each aerodynamic surface was considered to be dependent on the aerodynamic angles of the fuselage, the location of the surfaces with respect to the fuselage, and velocity component induced at the surface by the rotor(s). In addition, the flow field at each stabilizing surface was considered to be dependent on the wing lift coefficient and location of the surface with respect to the wing.

Although C81 has been developed exclusively for subsonic, incompressible aerodynamics of the airframe components, the incompressible flow interactions of aerodynamic surfaces on the flow fields of each other and the wing have been neglected. These interactions were neglected primarily because of the iterative procedure which would be required if each surface could affect the flow field at every other surface. Since most stabilizing surfaces are located well aft of wings, it is reasonable and justifiable to neglect the effect of the surfaces on the flow field at the wing. Neglecting the interactions between individual stabilizers was also considered justified because most stabilizing surfaces fall into one of the three following categories where mutual interference is minimal:

(1) They are at approximately right angles to other surfaces.

(2) If parallel, the planes of the surfaces are generally separated by distances greater than the span of either surface, or

(3) They are separated (end plated) by major structure such as the fuselage or tail boom.

In the unusual case of two surfaces in approximately the same plane and only a few chord lengths apart, the input data used in the aerodynamic coefficient computations can be modified to yield a reasonable simulation of the situation, e.g., reduce the lift curve slope by the ratio of downwash to angle of attack ($d\epsilon/d\alpha$).

The flow field model computes in the following order the effects of the fuselage, the wing (for stabilizers only), rotor wash, fuselage angular velocities, and gusts on the local flow field.

Figure 5-1 is a flow chart of the model as currently programmed. Most of the actual equations used are given in the User's Manual (Volume II, Sections 3.8 and 3.9). The basic inputs to the model are the body-axis components of the flight path velocity, and the outputs are the body-axis components of the local velocity. The equations were empirically derived from several rotorcraft wind tunnel tests. It was felt that none of the analytical methods were general enough to provide the necessary simulation. The first step in the model is to compute the downwash and sidewash angles due to the fuselage (ϵ_f and σ_f, respectively) at the surface center of pressure from program input data and the fuselage aerodynamic angles. The three body-axis components of velocity are then reduced to account for dynamic pressure loss and assumed to be acting in an axis system which is oriented by Euler rotations of σ_f degrees of yaw and ϵ_f degrees of pitch with respect to the body axis. Next, the velocities are resolved back to body-axis. For stabilizers, these recomputed velocities are then reduced for dynamic pressure loss due to the wing and assumed to be acting in an axis system which is pitched ϵ_{wing} degrees with respect to the body, where ϵ_{wing} is the downwash angle at the stabilizer due to the wing. Next, the velocities are resolved back to body axis and are termed the basic local velocities.

Finally, the body-axis components of linear velocity at the appropriate surface due to rotor wash, angular velocities of the surface center of pressure about the aircraft center of gravity, and those due to gusts are superimposed on the basic local velocities to yield the total local flow components in body axis: u_{SB}, v_{SB}, w_{SB} for the X, Y, and Z components, respectively. These components are then used in the aerodynamic angles model as discussed in Section 5.2.3.

5.2.2 Chord Line Orientation Model

Previous versions of the program required that the axis of incidence change of the wing and horizontal stabilizer (elevator) lie in the body X-Y plane while that the axis for the vertical stabilizer (fin) lie in the body X-Z plane. The current surface model removes these restrictions with a method for specifying the orientation of the axis of incidence change and the chord line of each surface with respect to the aircraft. The initial step in the development of the chordline orientation model was to define a new reference system. This system, referred to as the Aerodynamic Surface Reference System, was defined to be a right-handed coordinate system with its origin at the center of pressure of a surface and the reference airfoil section in the X-Z plane of the system. Each of the four stabilizing surfaces was assigned its own independent system while the right and left panels of the wing were assigned systems which were dependent on each other, but independent of the stabilizing surfaces. The orientation of each system was then defined with respect to the body reference system by two ordered rotations:

(1) Γ: a positive rotation about the body X axis; a dihedral angle rotation, and

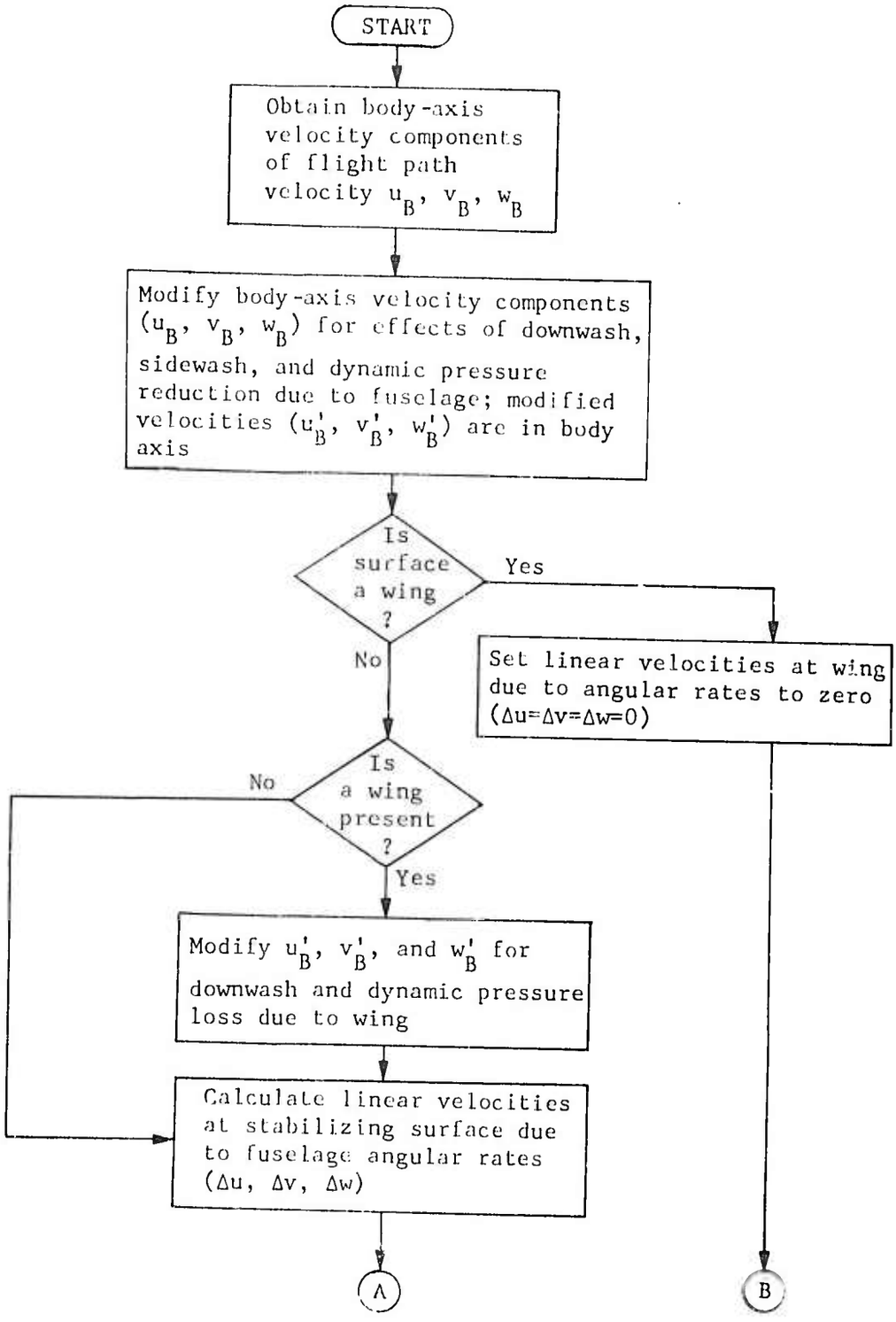

Figure 5-1. Flow Chart for Flow Field Model.

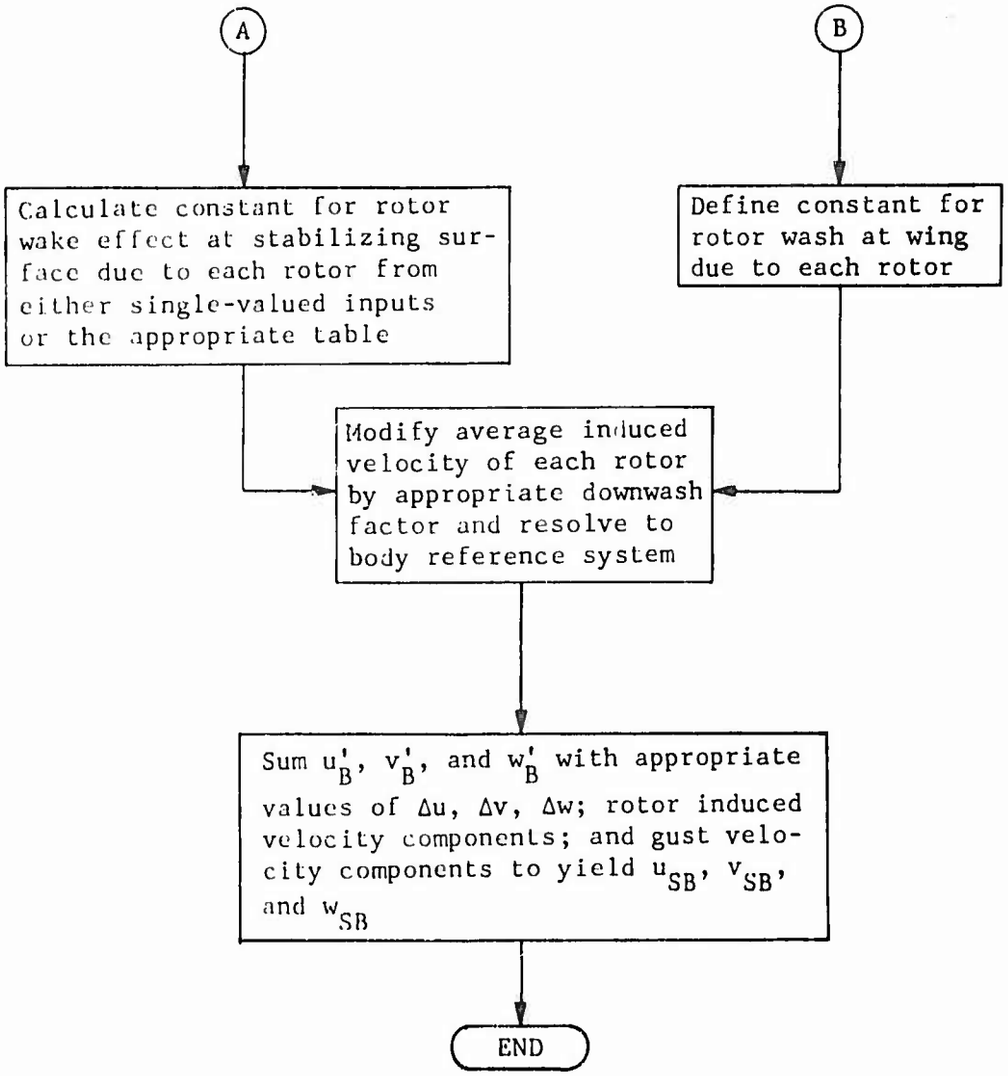

Figure 5-1. Concluded.

(2) i: a positive rotation about the Y axis which has been rotated through Γ previously; an incidence rotation.

Within the model, it was most convenient to define both positive Γ and i as right-handed rotations. However, this definition would say that a surface on the right side of an airframe with its outboard tip down would have a positive dihedral angle. This definition would not be compatible with a designer's normal definition: dihedral angle is positive for the outboard tip up, whether a surface is on the right or left side of the airframe. In addition, confusion results when trying to define the dihedral angle of a vertical or ventral fin.

After considering several different conventions, it was decided to use the positive right-handed rotation within the program, but to define another convention for input purposes, i.e., a user-oriented convention. The input convention is keyed to the buttline location of the center of pressure (cp) of the surface. If the cp is at or to the left of the centerline of the airframe (Buttline ≤ 0.0), positive Γ is a right-handed rotation about the body X axis. If the cp is to the right of the centerline (Buttline > 0.0), positive dihedral is a left-handed rotation about the body X axis. Hence, to the user, positive dihedral is simply outboard tip up.

With this convention, a vertical fin with sweepback, its cp at Buttline 0.0, and its incidence defined to be positive for leading edge right would have a dihedral angle of +90 degrees. Similarly, a swept-back ventral fin with its cp at Buttline 0.0 would have a dihedral angle of -90 degrees and positive incidence would be leading edge left. This convention for input data is illustrated in Figure 5-2.

5.2.3 Aerodynamic Angles Model

The aerodynamic angles of attack and sideslip, respectively, used to compute the aerodynamic coefficients are measured with respect to the aerodynamic surface reference system discussed in the preceding section. The first step in defining these angles is to transform the body-axis components of the total local flow velocity determined by the flow field model into the surface reference system. These surface reference components of the total local flow are then used to define the two aerodynamic angles in the conventional manner.

$$\alpha_s = \tan^{-1} (w_s/u_s) \tag{5-1}$$

$$\beta_s = \tan^{-1} (v_s/V_{AS}) \tag{5-2}$$

where u_s, v_s, and w_s are the X, Y, and Z velocity components, respectively, in the surface reference system, and

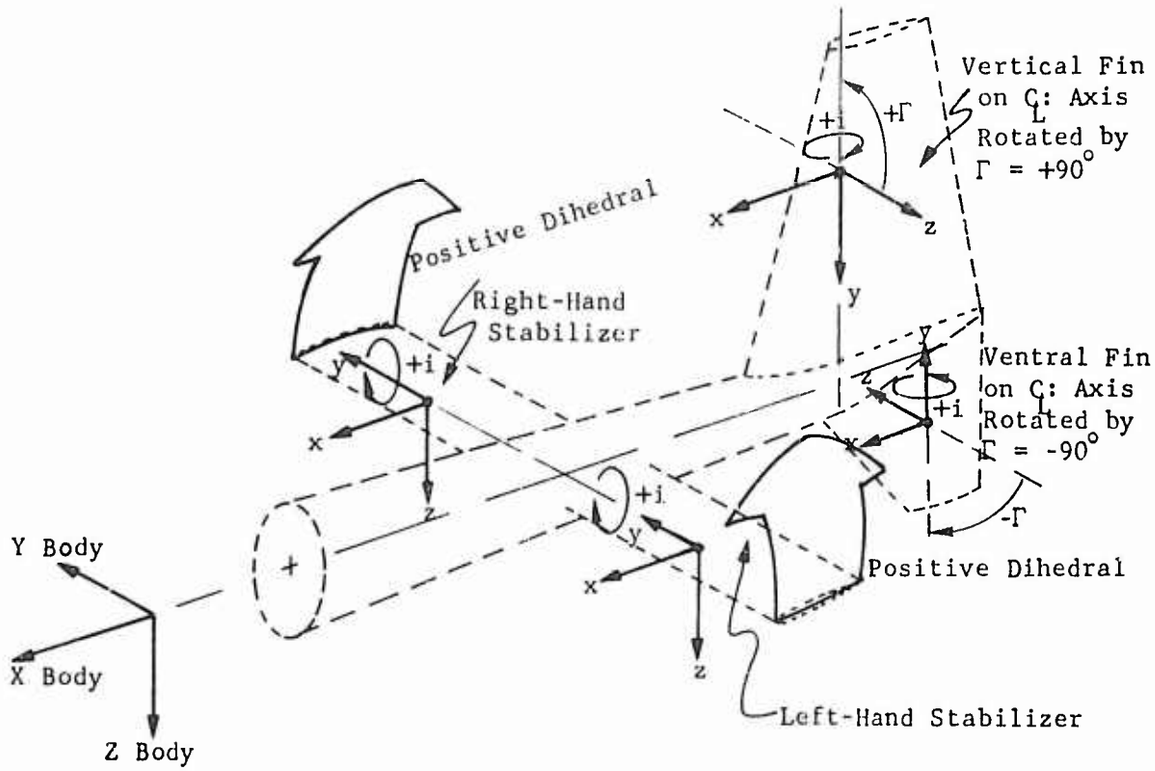

SURFACE	WING AND HORIZONTAL STABILIZERS		VERTICAL AND VENTRAL FINS	
C.P. Location	Dihedral: Γ	Incidence	Dihedral: Γ	Incidence
Buttline > 0 (Rt of C_L)	< + 90 > - 90	+ L.E. UP + L.E. UP	+90 -90	+ L.E. Left + L.E. Right
Buttline ≤ 0 (ON or LT of C_L)	< + 90 > - 90	+ L.E. UP + L.E. UP	+90 -90	+ L.E. Right + L.E. Left

L. E. = Leading Edge

Figure 5-2. Relationship of Body and Aerodynamic Surface Reference Systems.

$$V_{AS} = \sqrt{u_s^2 + v_s^2 + w_s^2}$$

$$= \sqrt{u_{SB}^2 + v_{SB}^2 + w_{SB}^2} \tag{5-3}$$

The Mach number at the aerodynamic surface is then

$$M_{AS} = V_{AS}/V_S \tag{5-4}$$

where V_S is the speed of sound.

5.2.4 Surface Aerodynamic Model

The C81 user has the option of computing the C_L, C_D, and C_M aerodynamic coefficients of a surface from sets of data tables or from equations. Each set of data tables consists of a table for each of the three coefficients where each table is a function of the surface angle of attack and Mach number.

Although the rotor blade aerodynamics and aerodynamic surface representations have access to the same group of five sets of data tables, these sets must not be used interchangeably. Tables used for rotor aerodynamics must represent the airfoil section, or two-dimensional characteristics, while tables used for aerodynamic surfaces must represent the surface, or three-dimensional characteristics.

The mathematical model for determining the coefficients from equations is described in detail in Section 3.1.2 of Volume II of this report. The major change to the model documented in References 1 and 2 is the introduction of the concept of effective aspect ratio and effective sweep angle. Based on the work in Reference 22, the effective sweep angle is

$$\Lambda^* = \Lambda_{1/2} + \begin{cases} \beta \text{ for the trailing panel of a swept surface} \\ -\beta \text{ for the leading panel of a swept surface} \end{cases} \tag{5-5}$$

where $\Lambda_{1/2}$ is the sweepback of the half-chord line, and β is the sideslip angle. This effective sweep angle also impacts on the aspect ratio to yield an effective ratio

$$\Lambda^* = eA \cos^2(\Lambda^*)/\cos^2(\Lambda_{1/2}) \tag{5-6}$$

where A is the geometric aspect ratio, and e is the spanwise efficiency factor. The factor of one-half which is included in the equation for A^*

in Reference 23 is replaced here by the spanwise efficiency factor since this analysis was developed for a total surface, not a single panel (half of a surface). Also in Equation (5-5), the concepts of leading and trailing panels are reference to the surface rather than a panel. Hence

$$\Lambda^* = \Lambda_{1/2} - \text{sign}(\bar{y}) * \beta_s \tag{5-7}$$

where $\bar{y}$ is the buttline of the surface cp.

The development of the equation for three-dimensional lift curve slope of an aerodynamic surface in Reference 22 was compared to the equivalent equation in Reference 23. Converting the nomenclature of these two references to that of this report, and introducing the effective sweep and aspect ratio parameters, yielded the identical equation for three-dimensional lift curve slope:

$$C_{L_\alpha} = (2\pi A^*) \Big/ \left[2 + \sqrt{(2\pi A^*/a_0)^2 \left[1 + \{ \tan^2 \Lambda^*/(1-M^2) \} \right] + 4} \right] \tag{5-8}$$

where a_0 is the experimental two-dimensional lift curve slope, and M is Mach number. Equation (5-8) was then evaluated over a wide range of aspect ratios and sweep angles. These results were compared to the charts in Reference 24 and showed very good agreement.

The model for the effect of control surface deflection on the aerodynamic coefficients of a surface was taken from the charts of Reference 25. Equations were empirically derived to fit the type of data presented in the referenced report. The equations compute increments which are added to the coefficients computed for zero deflection. This approach, rather than a detailed analytical model of the effects of deflection, was chosen so that test data could more easily be input to the program and so that the model would be well suited to parametric analysis.

5.3 EXAMPLES OF THE REPRESENTATION

An example of the current mathematical model for aerodynamic surfaces is shown in Figure 5-3. This figure is a plot of a set of level-flight trim conditions from 100 to 260 knots for the Bell Model 533 High Performance Helicopter (HPH). Several versions of this compound research helicopter were flight tested under contract to USAAMRDL. The configuration selected for simulation was the one flown in 1968 and 1969. The significant configuration parameters were as follows:

(1) Two-bladed, teetering, low-twist main rotor (44 ft diameter)

(2) A 78.4 ft^2 wing with flaps, ailerons, and spoilers

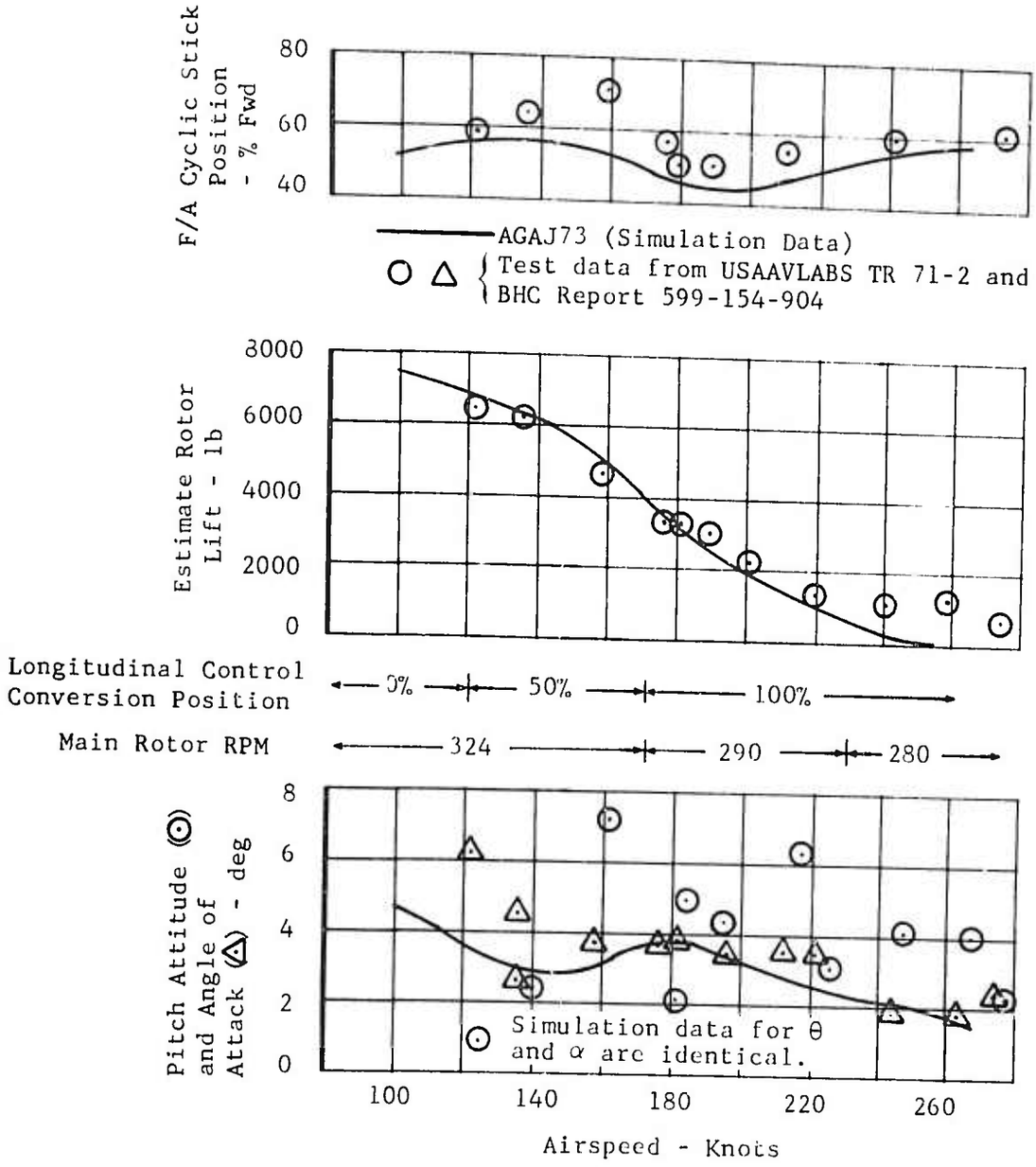

Figure 5-3. Comparison of Test and Simulation Data for the Bell Model 533.

(3) Two JT12A-3 jet engines, one mounted on each wing tip

(4) A 35.0 ft^2 controllable stabilator mounted on the tail boom

(5) A 5.86 ft^2, fixed incidence stabilizer mounted at the top of the vertical fin

(6) A 19.95 ft^2 vertical fin with a sealed rudder (no ventral fin)

(7) A convertible control system which allowed control of the aircraft using either standard rotor controls or fixed-wing type control surfaces, or a combination of both

At the time of the HPH flight tests, the version of the Rotorcraft Flight Simulation Computer Program then in use was considerably less sophisticated than the current version. Consequently, many of the data now needed or desirable for a complete AGAJ73 input data deck were never developed in the course of flight and wind-tunnel tests and analyses of the aircraft. Regardless, the AGAJ73 simulation data shown in Figure 5-3 follows the trends and magnitudes of the available test data quite well.

In level flight, the pitch attitude and angle of attack should be equal. The scatter in these data shown in Figures 5-3 indicates that either the test data are slightly inaccurate or the flight condition was actually a mild climb or descent rather than level flight as indicated in the flight test reports, or a combination of both. All simulation data were computed as level-flight cases, and the two angles were equal. Also, the test reports emphasize that the rotor thrust data are estimates based on blade bending, not direct thrust measurements.

In the course of gathering the data for the AGAJ73 input deck from previous C81 decks and test reports, several inconsistencies were noted in the rigging definitions for rotor controls, aerodynamic surface incidences, and the convertible control system. Average values were used as input data when such conflicts were apparent.

Consequently, in view of the absence of current data on the HPH, the fact that it is no longer on flight status (which precludes new rigging checks), and the nature of the test data, the correlation of the simulation and the test data is considered excellent. This situation indicates the validity of the current mathematical model for aerodynamic surfaces, as well as the accuracy of the program as a whole.

6. EXTERNAL STORES/AERODYNAMIC BRAKES MATHEMATICAL MODEL

6.1 GENERAL

The current version of C81 includes the capability of simulating the effects of external stores and aerodynamic brakes. The input group for the store/brake model consists of four subgroups where each subgroup is independent of all other subgroups and may represent either a store or a brake. The mathematical models for the stores and brakes were developed concurrently, and each requires essentially the same inputs.

The features which are common to both models are simulation of

(1) aerodynamic lift, drag, and side force, and
(2) the influence of dynamic pressure loss and local flow orientation on the aerodynamic forces.

In addition to the common features, the aerodynamic brake model provides for changing the brake deployment (i.e., the magnitude of the aerodynamic forces) during maneuvers, while the store model can simulate store drops or jettisons during maneuvers.

Development of the two models began by reviewing the store/brake configurations and maneuvers which had previously been simulated with artificial inputs to the jet, weapons, and other groups. Next, program users were questioned as to what features they felt were mandatory, desirable, and convenient for the store/brake models. Also, recent flying qualities design and test specifications were reviewed to assure that the models would be able to simulate the demonstrations required by them. From these discussions and investigations, the features noted above were chosen for the models.

6.2 DEVELOPMENT OF THE MATHEMATICAL MODELS

The model for the aerodynamic forces for both stores and brakes was taken directly from the High Angle Equation (HAE) model developed for the fuselage group (see Section 4.2.3 and Table 4-2). The HAE model equations for the aerodynamic moments of store/brakes about their own center of gravity were not included because of their small magnitude for most stores and brakes. However, inputs are provided for locating the store/brake aerodynamic center at a stationline different from its center of gravity and to move the aerodynamic center as a function of angle of attack. This feature is most applicable to large stores. It is intended that analytical inputs be used to approximate the aerodynamic moments about the store center of gravity, since test data for stores are generally limited.

Each model also includes simple approximations for the influence of nearby structure and rotor downwash on the flow field at the store/brake. The

influence of nearby structure is represented by reducing the magnitude of the free-stream velocity vector at the fuselage. This reduction factor has the form of

$$\eta_V = \sqrt{1-\Delta\eta_q}$$

where $\Delta\eta_q$ is the input for dynamic pressure loss, and η_V is then the scalar by which the velocity vector is multiplied. The value of η_V is independent of all aerodynamic angles.

The effect of rotor downwash on the local flow field is accounted for in the same manner as it is for the aerodynamic surfaces. That is, the average induced velocity at the rotor disc is multiplied by an input constant, assumed to be acting parallel to the rotor mast, and then added vectorially to the local velocity which was reduced for dynamic pressure loss. The constant which multiplies the induced velocity is independent of all aerodynamic angles. Representation of downwash and sidewash due to the fuselage and a more sophisticated model of dynamic pressure loss are not included because of the general lack of good test data or means of analytical prediction. In view of the interactions of the rotor downwash with other parts of the airframe prior to affecting the flow field at the store, the simple model of a constant times the induced velocity is considered adequate for the store/brake model. As the sophistication of the rotor wake analysis is enhanced in future versions of C81, it is anticipated that the representation of the effects of rotor downwash on such airframe components as stores and brakes will also be improved.

The above discussion summarizes the common features of the store and brake mathematical models. The features unique to each model are discussed below. To determine whether a subgroup represents a store or a brake, the model checks the value of the input for weight. If the weight is greater than zero, the subgroup is treated as a store; if less than zero as a brake; and if equal to zero, the subgroup is ignored.

6.2.1 Aerodynamic Brake Model

The primary purpose of the aerodynamic brake model is to simulate an aerodynamic force whose magnitude is a function of not only the local aerodynamic angles and dynamic pressure, but also of the position of an appropriate control in the cockpit. The model incorporates a brake deployment control to accomplish this task.

The control position is input to the model as a percentage of full deployment, where full deployment of the brake results in the aerodynamic forces as calculated from the force equations using the local aerodynamic angles and dynamic pressure. The full deployment forces are then multiplied by the fraction of full control displacement, resolved to body axis, and included in the force and moment summary.

During the TRIM procedure, the control position is fixed at its input value. Then, in the maneuver section of the program, the position can be changed to simulate the deployment or retraction of the aerodynamic brake. The model does not restrict the control to being between 0 and 100 percent, nor the drag to being positive. Hence, if the need arises, negative control positions or negative drag areas (not both simultaneously) can be input to simulate propulsive forces which are proportioned to dynamic pressure and act parallel to the local flow.

6.2.2 External Store Model

The purpose of the external store model is to simulate the aerodynamic forces acting on external stores; the contribution of stores to weight, center of gravity location, and inertia of the total rotorcraft; and the reaction force caused by store jettison. The aerodynamic forces are represented in the same manner as are the forces on the aerodynamic brake except that the calculated forces are not affected by the input, or commanded, value of deployment control position.

The first version of the store model required that the store weight and inertias be reflected in the weight, center of gravity, and inertial inputs to the fuselage group. This requirement proved very cumbersome in that the user had to locate, or in most cases, calculate, these mass properties for each store configuration of interest. Hence, the model was changed to require that mass properties input to the fuselage group must exclude the contributions of any and all stores. Consequently, during reading and initialization of the input data and prior to commencing the TRIM procedure, the mass properties of the total rotorcraft are recalculated using the inputs to the fuselage and each store subgroup. No recalculation is made if the subgroup is an aerodynamic brake, i.e., weight input less than or equal to zero.

The equations for recalculation of weight, center of gravity, and inertia were developed from conventional weight and balance equations in the following manner.

Consider that the rotorcraft is composed of K discrete parts, each with weight (W_j), mass ($m_j = W_j/g$), location (x_j, y_j, z_j), and inertia about its own cg ($(I_{xx})_j$, $(I_{yy})_j$, $(I_{zz})_j$, $(I_{xz})_j$). With K parts, the rotorcraft includes the store of interest and is termed in the new, or N, configuration. With K-1 parts, it excludes the specific store and is termed in the original, or 0, configuration. Hence, the Kth part is the store with weight (W_s), mass ($m_s = W_s/g$), location (x_s, y_s, z_s), and inertia ($(I_{xx})_s$). Then, the new stationline of the cg, x_N, can be determined from the known quantities.

$$W_N = W_0 + W_s \tag{6-1}$$

$$W_N x_N = \sum_{j=1}^{K} \left[W_j x_j \right]$$

$$= \sum_{j=1}^{K-1} \left[W_j x_j \right] + W_s x_s$$

$$= W_0 x_0 + W_s x_s \qquad (6\text{-}2)$$

Substituting Equation (6-1) into (6-2) yields

$$x_N = (W_0 x_0 + W_s x_s)/(W_0 + W_s) \qquad (6\text{-}3)$$

Similarly, for the buttline, y_N, and waterline, z_N,

$$y_N = (W_0 y_0 + W_s y_s)/(W_0 + W_s) \qquad (6\text{-}4)$$

$$z_N = (W_0 z_0 + W_s z_s)/(W_0 + W_s) \qquad (6\text{-}5)$$

The new rolling moment of inertia, $(I_{xx})_N$, is then determined:

$$(I_{xx})_N = \sum_{j=1}^{K} m_j (y_j^2 + z_j^2) - \left(\sum_{j=1}^{K} m_j\right)(y_N^2 + z_N^2) + \sum_{j=1}^{K} (I_{xx})_j \qquad (6\text{-}6)$$

The first term of Equation (6-6) can be broken down as follows:

$$\sum_{j=1}^{K} m_j (y_j^2 + z_j^2) = \sum_{j=1}^{K-1} \left[m_j (y_j^2 + z_j^2) \right] + m_s (y_s^2 + z_s^2) \qquad (6\text{-}7)$$

where the first term of Equation (6-7) can be expressed as

$$\sum_{j=1}^{K-1} m_j (y_j^2 + z_j^2) = (I_{xx})_0 + m_0 (y_0^2 + z_0^2) - \sum_{j=1}^{K-1} (I_{xx})_j \qquad (6\text{-}8)$$

The summation factor in the second term of Equation (6-6) can be restated as

$$\sum_{j=1}^{K} m_j = \sum_{j=1}^{K-1} \left[m_j\right] + m_s$$

$$= m_0 + m_s \tag{6-9}$$

and the third term as

$$\sum_{j=1}^{K} (I_{xx})_j = \sum_{j=1}^{K-1} \left[(I_{xx})_j\right] + (I_{xx})_s \tag{6-10}$$

Substituting Equation (6-8) into (6-7) and Equations (6-7), (6-8), and (6-9) into (6-6) yields

$$(I_{xx})_N = (I_{xx})_0 + (I_{xx})_s + m_0 (y_0^2 - y_N^2 + z_0^2 - z_N^2)$$

$$+ m_s(y_s^2 - y_N^2 + z_s^2 - z_N^2) \tag{6-11}$$

Similarly, for the pitching moment of inertia, $(I_{yy})_N$, and yawing moment of inertia, $(I_{zz})_N$,

$$(I_{yy})_N = (I_{yy})_0 + (I_{yy})_s + m_0 (x_0^2 - x_N^2 + z_0^2 - z_N^2) \tag{6-12}$$

$$+ m_s (x_s^2 - x_N^2 + z_s^2 - z_N^2)$$

$$(I_{zz})_N = (I_{zz})_0 + (I_{zz})_s + m_0 (x_0^2 - x_N^2 + y_0^2 - y_N^2) \tag{6-13}$$

$$+ m_s (x_s^2 - x_N^2 + y_s^2 - y_N^2)$$

For the cross product of inertia, $(I_{xz})_N$,

$$(I_{xz})_N = \sum_{j=1}^{K} \left[m_j \, x_j \, z_j \right] - \left(\sum_{j=1}^{K} m_j \right) x_N \, z_N + \sum_{j=1}^{K} (I_x)_j \qquad (6\text{-}14)$$

The first term of Equation (6-14) can then be written as

$$\sum_{j=1}^{K} m_j \, x_j \, z_j = \sum_{j=1}^{K-1} \left[m_j \, x_j \, z_j \right] + m_s \, x_s \, z_s \qquad (6\text{-}15)$$

where the first term of Equation (6-15) can be expanded as follows:

$$\sum_{j=1}^{K-1} \left[m_j \, x_j \, z_j \right] = (I_{xz})_{} + m_0 \, x_0 \, z_0 - \sum_{j=1}^{K-1} \left[m_j \, x_j \, z_j \right] \qquad (6\text{-}16)$$

The third term of Equation (6-14) expands to the following:

$$\sum_{j=1}^{K} (I_{xz})_j = \sum_{j=1}^{K-1} \left[(I_{xz})_j \right] + (I_{xz})_s \qquad (6\text{-}17)$$

Substituting Equation (6-16) into (6-15) and Equations (6-9), (6-15), and (6-16) into (6-14) yields

$$(I_{xz})_N = (I_{xz})_0 + (I_{xz})_s + m_0 \, (x_0 \, z_0 - x_N \, z_N) \qquad (6\text{-}18)$$

$$+ m_s \, (x_s \, z_s - x_N \, z_N)$$

These equations for recalculating mass properties to reflect weight added to the configuration are summarized in Table 6-1.

The recalculated mass properties are printed out for each recalculation prior to printout of the first trim iteration. When using the parameter sweep option (NPART = 10), the baseline mass properties input to fuselage group are used as the initial properties for each subsequent case. The recalculated values are not carried forward. The recalculations are then performed independently for each case in the sweep. This procedure prevents cumulative changes in mass properties and permits the user to change either the fuselage or store properties with NAMELIST input before starting each case.

TABLE 6-1. EQUATIONS FOR RECALCULATION OF WEIGHT, CENTER OF GRAVITY, AND INERTIAS

$$W_N = W_0 + k_s W_s$$

$$x_N = (W_0 x_0 + k_s W_s x_s)/W_N$$

$$y_N = (W_0 y_0 + k_s W_s z_s)/W_N$$

$$z_N = (W_0 z_0 + k_s W_s z_s)W_N$$

$$(I_{xx})_N = (I_{xx})_0 + k_s (I_{xx})_s + m_0 (y_0^2 - y_N^2 + z_0^2 - z_N^2)/144 + k_s m_s (y_s^2 - y_N^2 + z_s^2 - z_N^2)/144 \quad \text{Roll}$$

$$(I_{yy})_N = (I_{yy})_0 + k_s (I_{yy})_s + m_0(x_0^2 - x_N^2 + z_0^2 - z_N^2)/144 + k_s m_s (x_s^2 - x_N^2 + z_s^2 - z_N^2)/144 \quad \text{Pitch}$$

$$(I_{zz})_N = (I_{zz})_0 + k_s (I_{zz})_s + m_0 (x_0^2 - x_y^2 + y_0^2 - y_N^2)/144 + k_s m_s (x_s^2 - x_N^2 + y_s^2 - y_N^2)/144 \quad \text{Yaw}$$

$$(I_{xz})_N = (I_{xz})_0 + k_s (I_{xz})_s + m_0 (x_0 z_0 - x_N z_N)/144 + k_s m_s (x_s z_s - x_N z_N)/144 \quad \text{Cross-product}$$

$$k_s = \begin{cases} +1.0 \text{ for adding store a baseline configuration} \\ -1.0 \text{ for dropping store from a baseline configuration} \end{cases}$$

x = Stationline of cg, in.
y = Buttline of cg, in.
z = Waterline of cg, in.

W = weight, lb
m = mass, slugs
I = inertia, slug-ft^2

0 = baseline configuration
s = store parameters
N = configuration resulting from addition or drop of store

In the maneuver section of the program, the mathematical model can simulate store jettison. Each store may be jettisoned independently of any and all other stores. The user specifies the time for jettison and the store to be jettisoned. At the instant of jettison, the aerodynamic forces of that store are set to zero for the remainder of the maneuver, and the rotorcraft weight, cg, and inertias are recalculated to reflect the loss of the store weight. Also, the moment arms of all rotorcraft components (e.g., fuselage data reference point, rotor, and aerodynamic surfaces) are recalculated using the new cg location. The equations for recalculating the mass properties to reflect weight lost from a configuration were developed in the same manner as those equations for weight added and are also summarized in Table 6-1. The equations are identical except for the signs on terms associated with the store.

Consideration was given to a model of the jettison reaction forces which could accurately simulate the forces caused by typical jettison mechanisms. One common mechanism is a gas-powered piston where force exerted by the piston is primarily a function of piston displacement, and piston velocity and displacement are functions of the mass being jettisoned. Since C81 requires models which are specifically functions of time, a new set of nonlinear differential equations of motion would be required to simulate such a mechanism. The added complexity of including such a model when store jettison is just one of many features of the program was not considered practical.

6.3 EXAMPLES OF THE STORE/BRAKE REPRESENTATION

To demonstrate the capabilities of the aerodynamic brake and external store representation, two cases are presented:

(1) Application of dive brakes on the Bell Model 309 (KingCobra)

(2) Asymmetric release of stores from an AH-1G (HueyCobra) with the Stability and Control Augmentation System off and on

6.3.1 Dive Brakes on a KingCobra

Figure 6-1 shows the time history of symmetrical deployment of two wing-mounted dive brakes on the KingCobra. The trim condition prior to brake application is a 3000-foot-per-minute dive at 170 KTAS. In the simulation, each brake travels from zero to full deployment in 1 second (starting at t = 0.05 second), and the flat plate drag area of each brake is 5.0 square feet. Since no dive brakes have been designed for the KingCobra, the inputs for the brake configuration are only meant to demonstrate the capability of the program and should not be interpreted as an optimum dive brake for any rotorcraft. In fact, during initial trial runs of the simulation it was found that with controls locked the wing location for the brakes caused a mild, but undesirable, nose-down pitching moment. To correct this situation, a control gearing was added which caused one degree of nose-down incidence to each horizontal stabilizer panel as the brakes

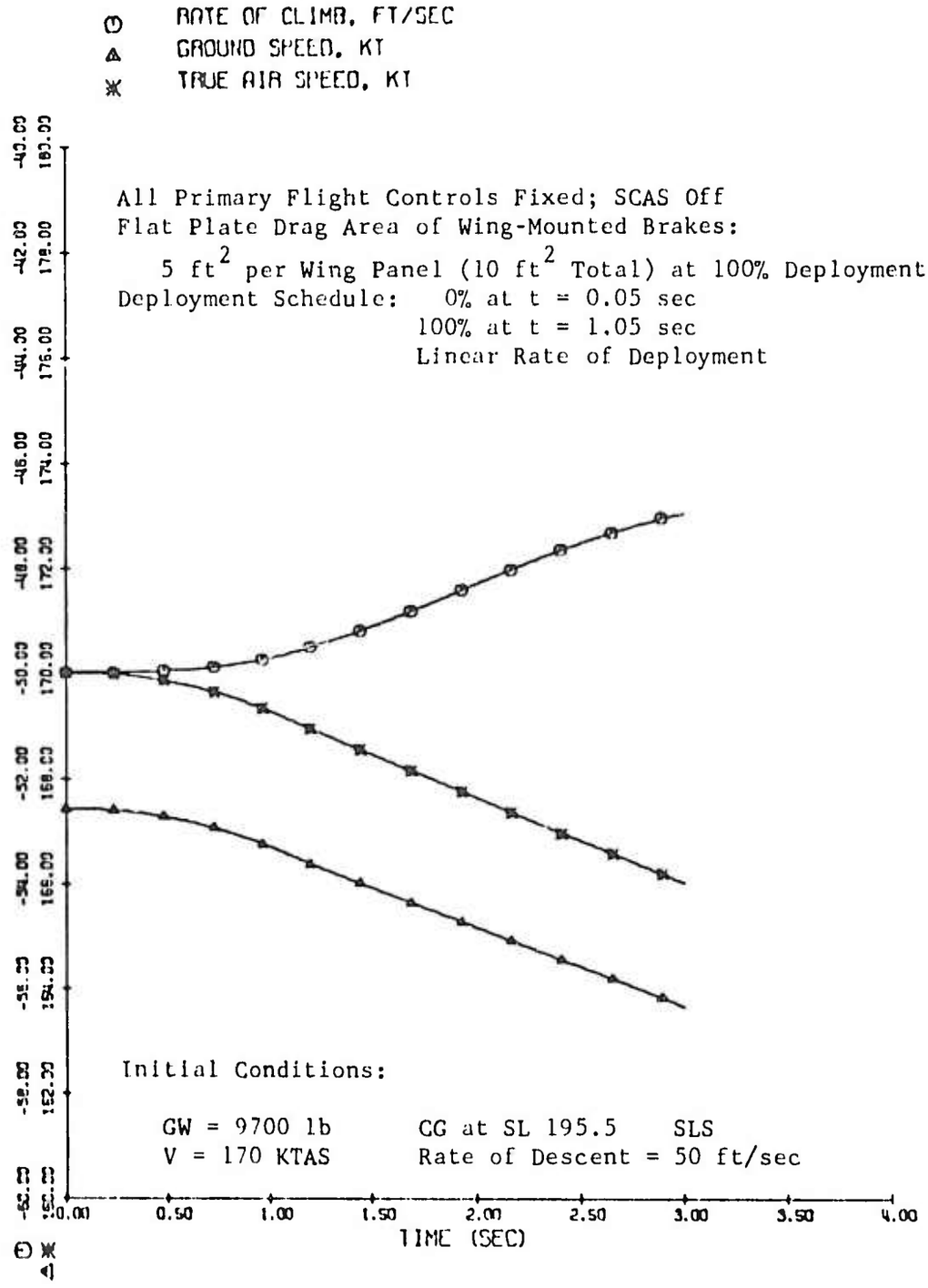

Figure 6-1. Time History of Dive Brake Application on a Bell Model 309.

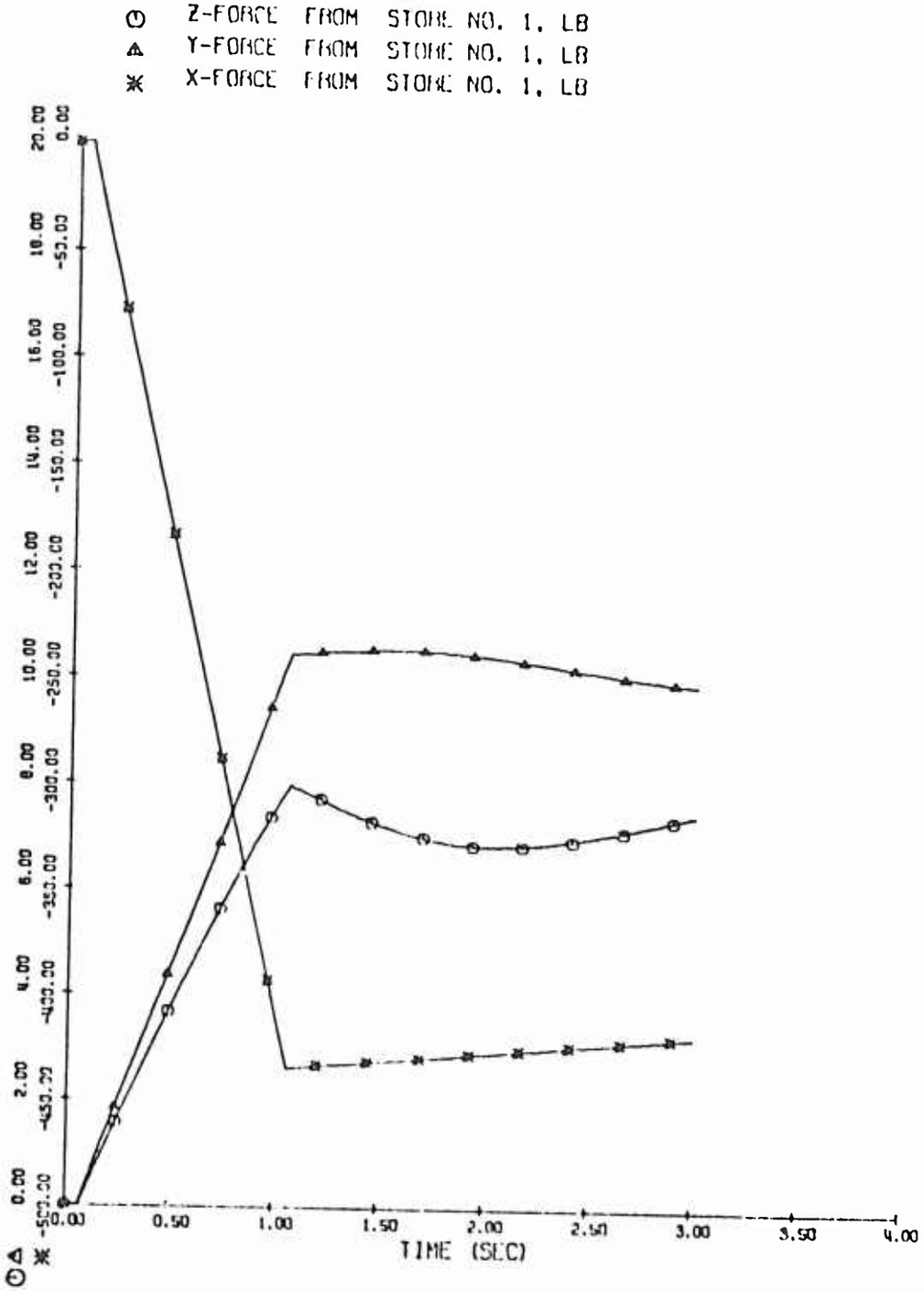

Figure 6-1. Continued.

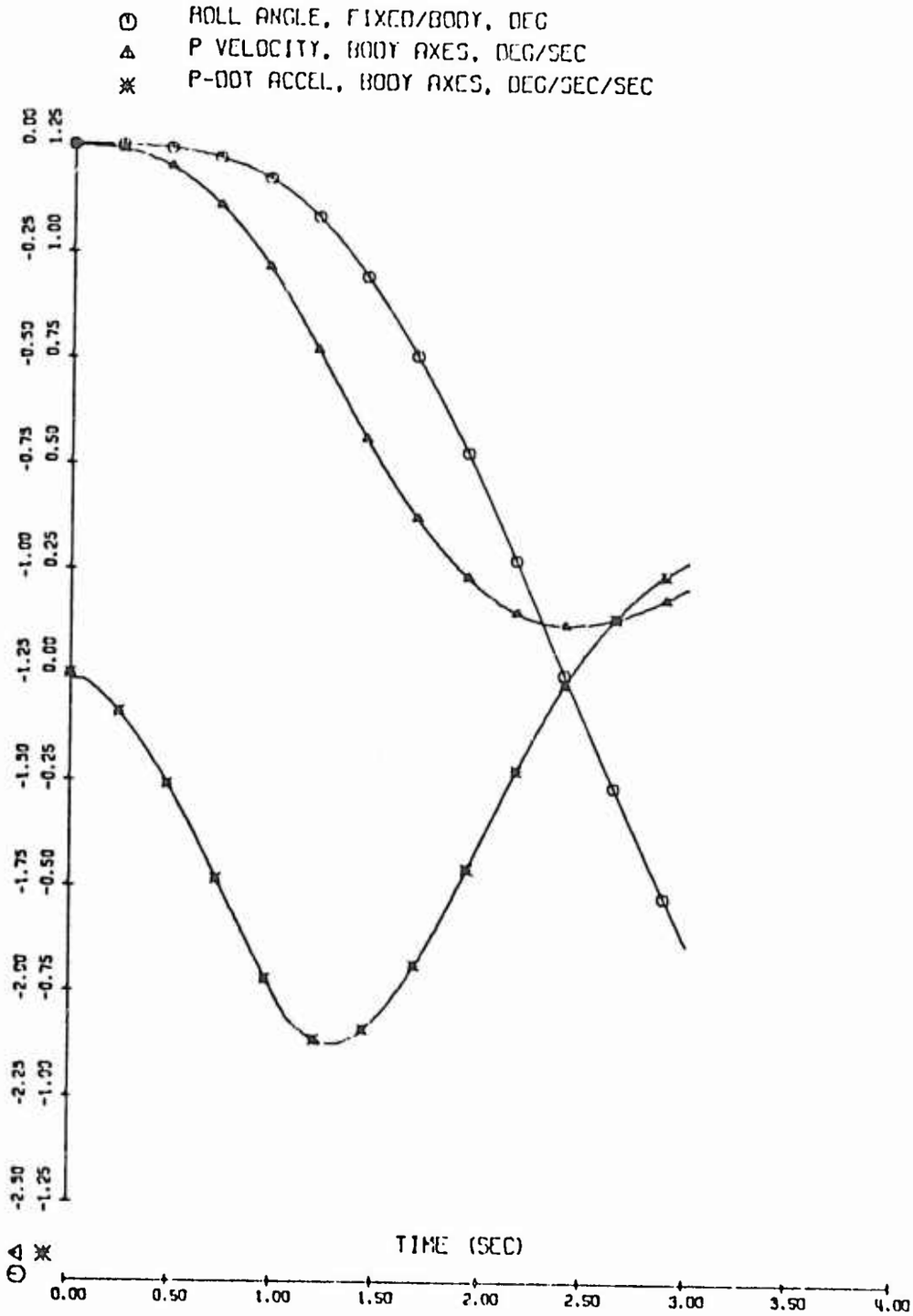

Figure 6-1. Continued.

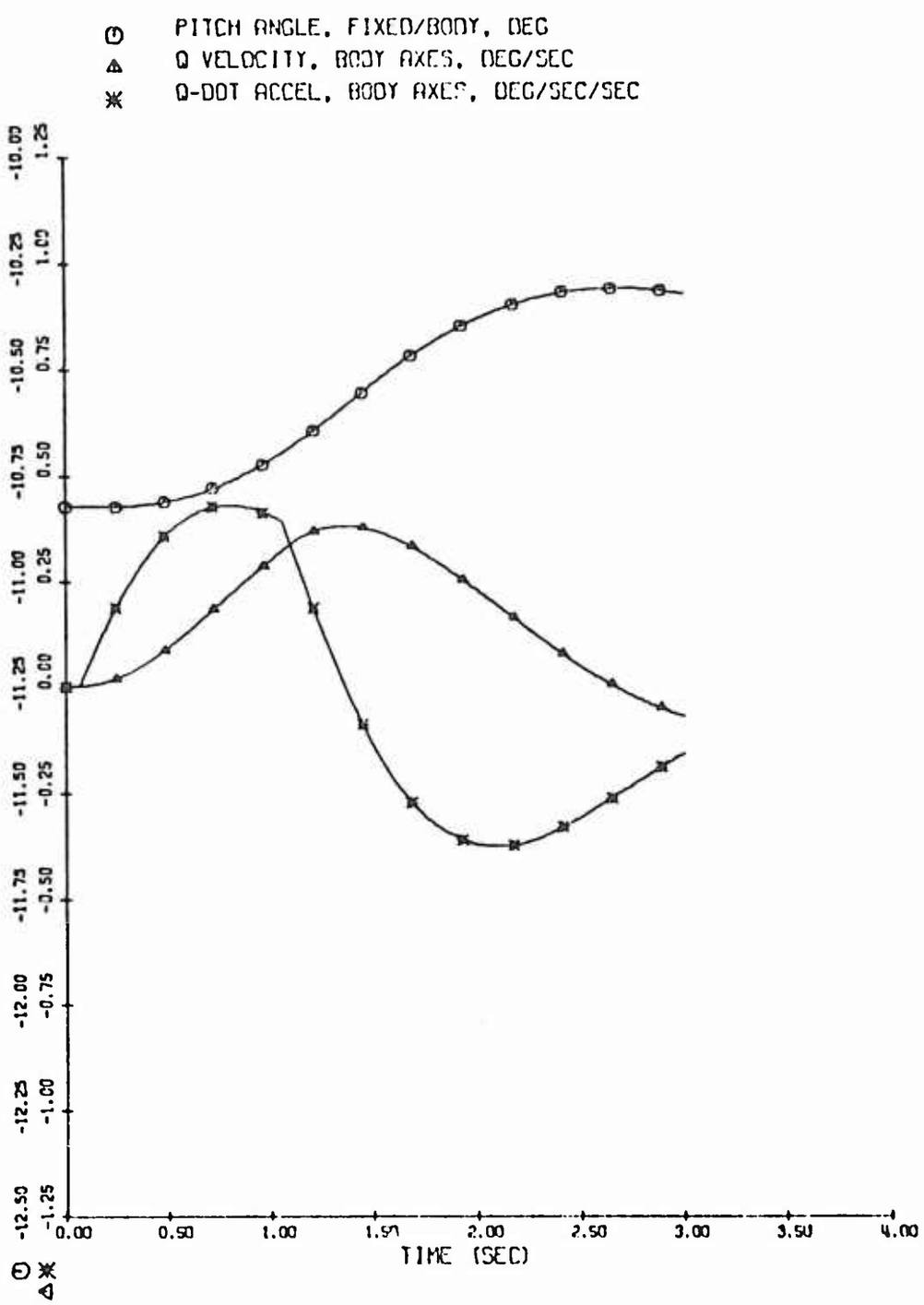

Figure 6-1. Concluded.

went from zero to full deployment. As a result of this gearing, the helicopter pitched up less than 3/4 degree (instead of 3 degrees nose down) in the 3 seconds following the start of the brake deployment. During the same period of time, changes in roll and yaw attitudes were less than 2 degrees and the airspeed decreased slightly more than 4 KTAS. The combination of these effects indicated that the aerodynamic brake model functions in the desired manner.

6.3.2 Store Drops From an AH-1G

Figures 6-2 and 6-3 show time histories for store drops from an AH-1G. The initial conditions and helicopter configurations are identical for the two examples: level flight at 100 KTAS in sea level standard atmosphere and each store location loaded to within 20 to 50 pounds of its maximum permissible loading. In both examples, the right outboard store (533 pounds) was dropped at t = 0.05 second maneuver time, at which time the lateral cg shifted 3.6 inches to the left. Also, the roll channel of the Automatic Pilot Simulator (see Section 8.2.2) was activated at t = 2.05 seconds in both cases. The only difference between the two cases is that for the simulation shown in Figure 6-2 the SCAS is off, while for that in Figure 6-3 it is on. Note that both cases used the identical autopilot gains and time constants. In particular, the rate for stick motion was limited to 25 percent per second, and desired times to achieve zero rate and zero attitude were 0.75 and 2.0 seconds respectively. This rate and these times are quite slow and long compared to pilot capability. Even though the lateral SCAS actuator saturates at 12.5 percent of lateral cyclic range within about 0.3 second, the simulation shows that SCAS can make a potentially dangerous asymmetric store drop into a relatively mild maneuver.

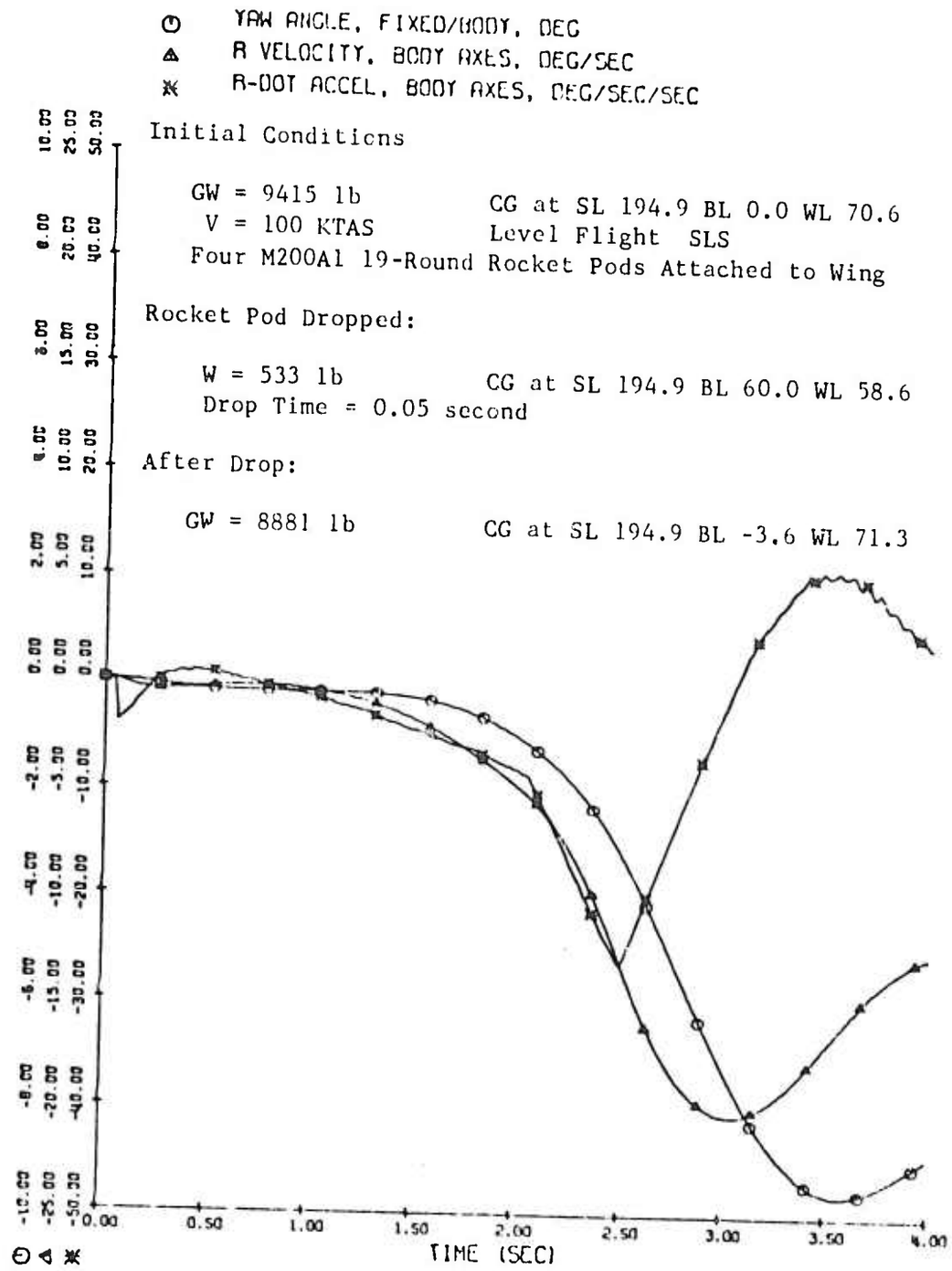

F/A cyclic, collective, and pedal position fixed for entire maneuver. Lateral cyclic position fixed until t = 2.05 sec; controlled by Automatic Pilot Simulator for the remainder of the maneuver.

Figure 6-2. Time History of an External Store Drop From a Bell Model 209 (SCAS Off).

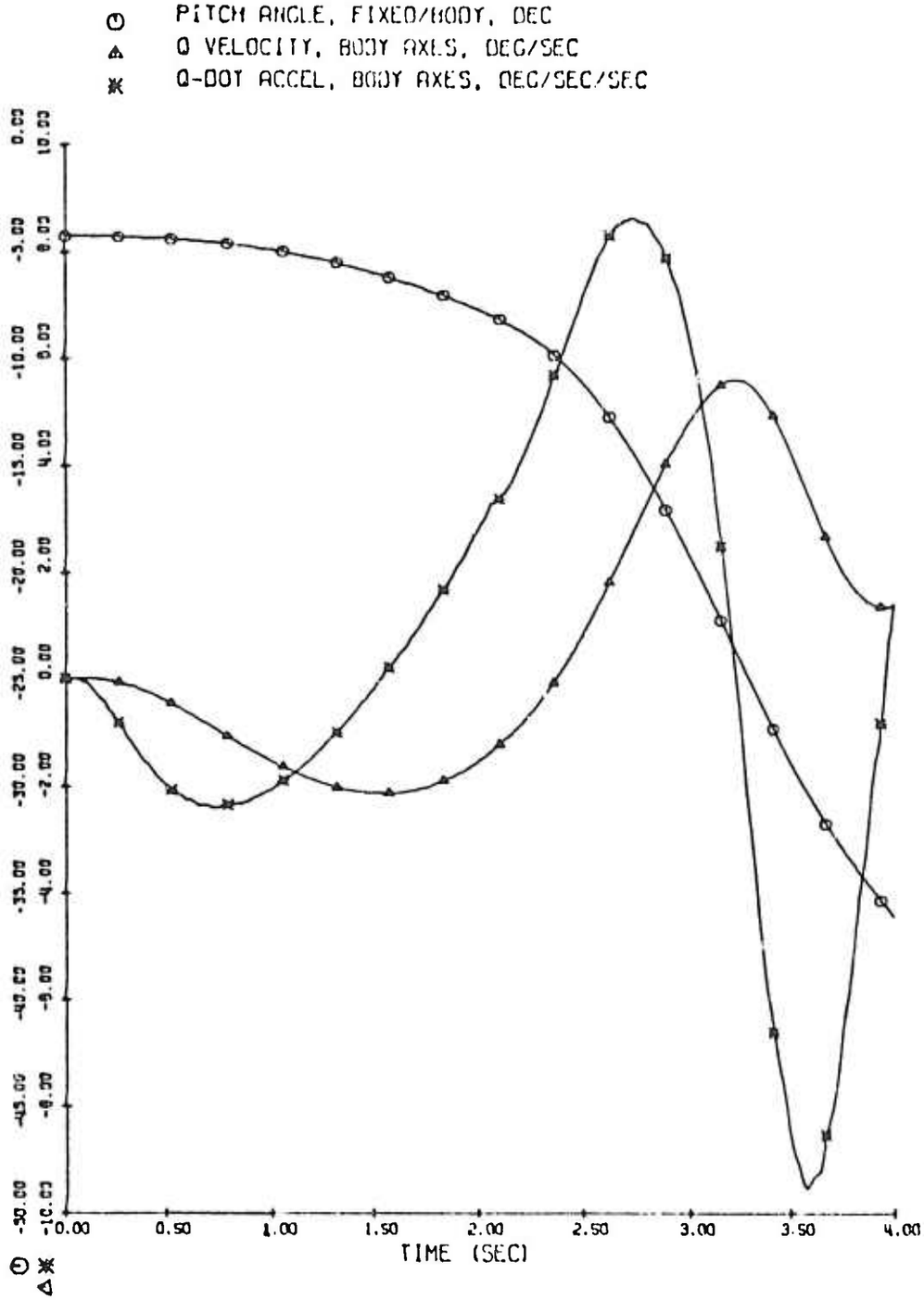

Figure 6-2. Continued.

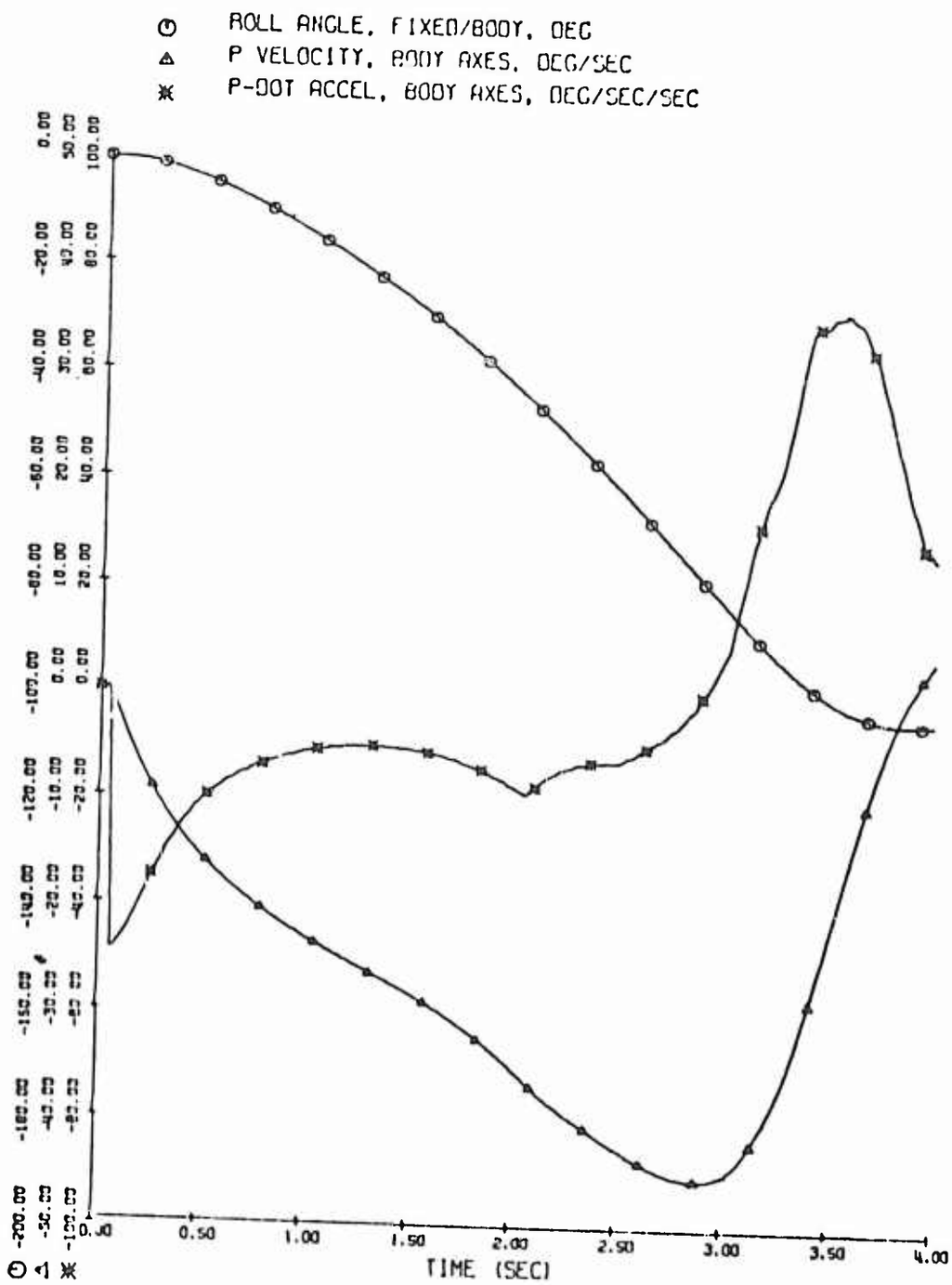

Figure 6-2. Concluded.

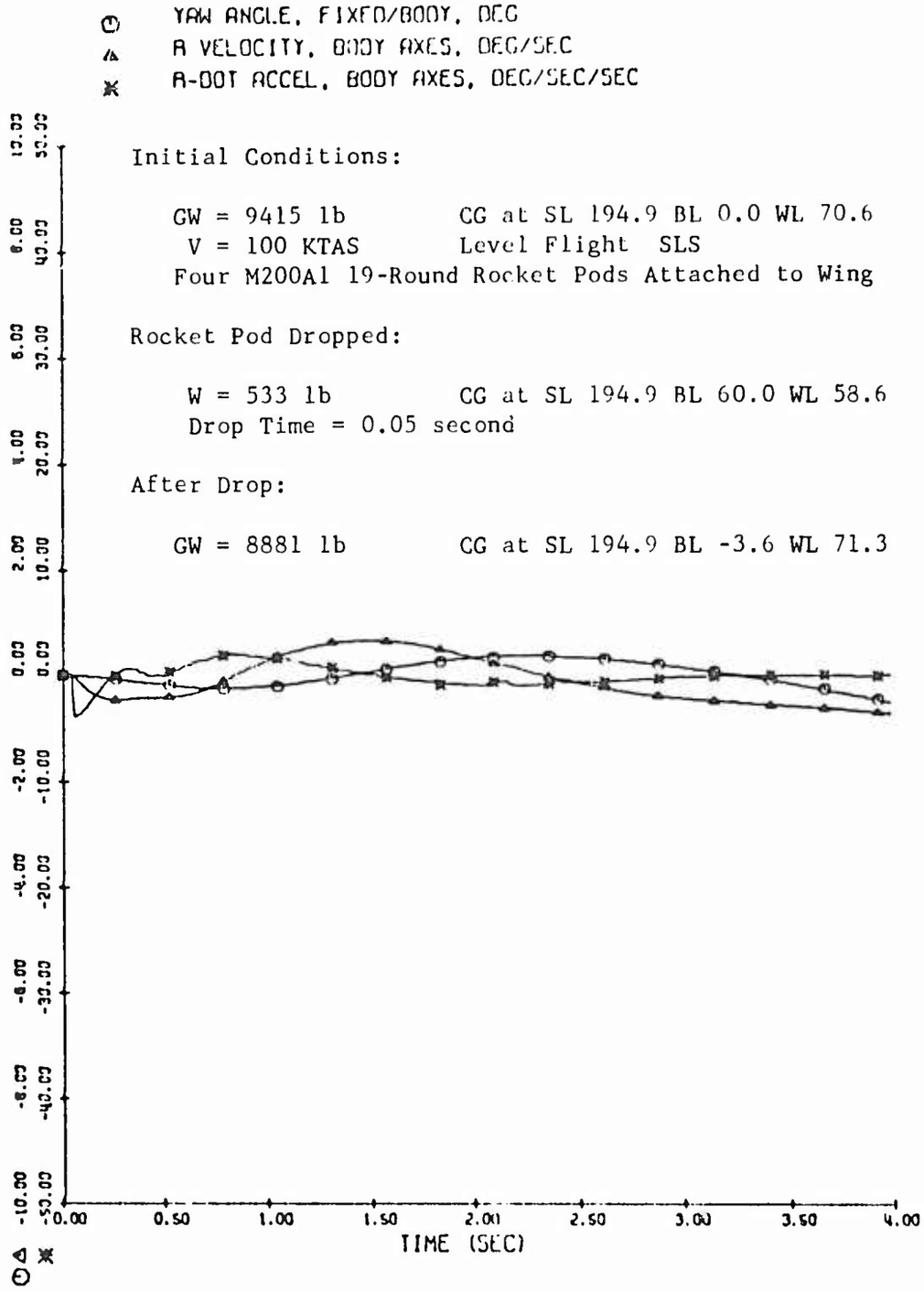

F/A cyclic, collective, and pedal position fixed for entire maneuver. Lateral cyclic position fixed until t = 2.05 sec; controlled by Automatic Pilot Simulator for the remainder of the maneuver.

Figure 6-3. Time History of an External Store Drop From a Bell Model 209 (SCAS On).

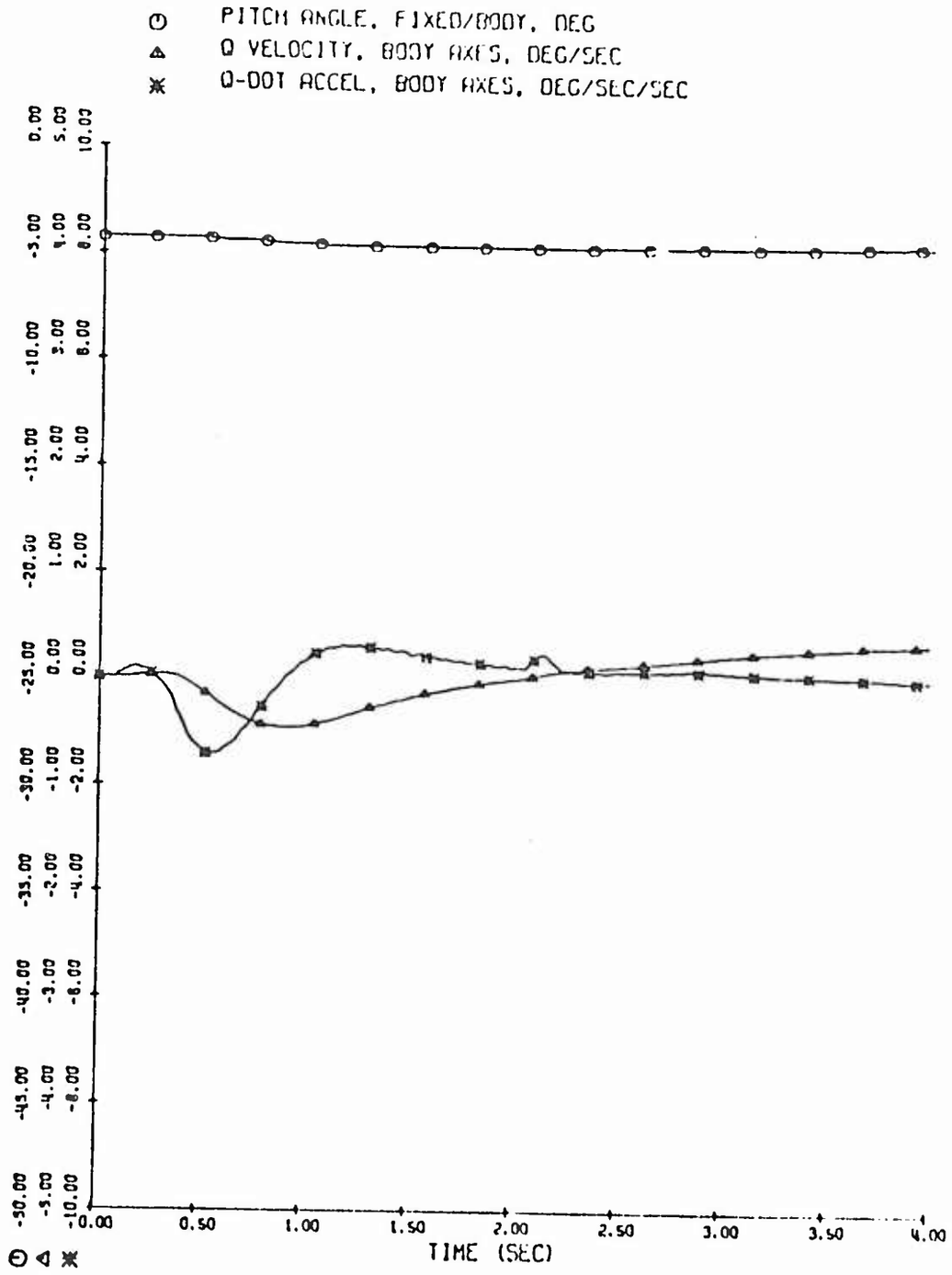

Figure 6-3. Continued.

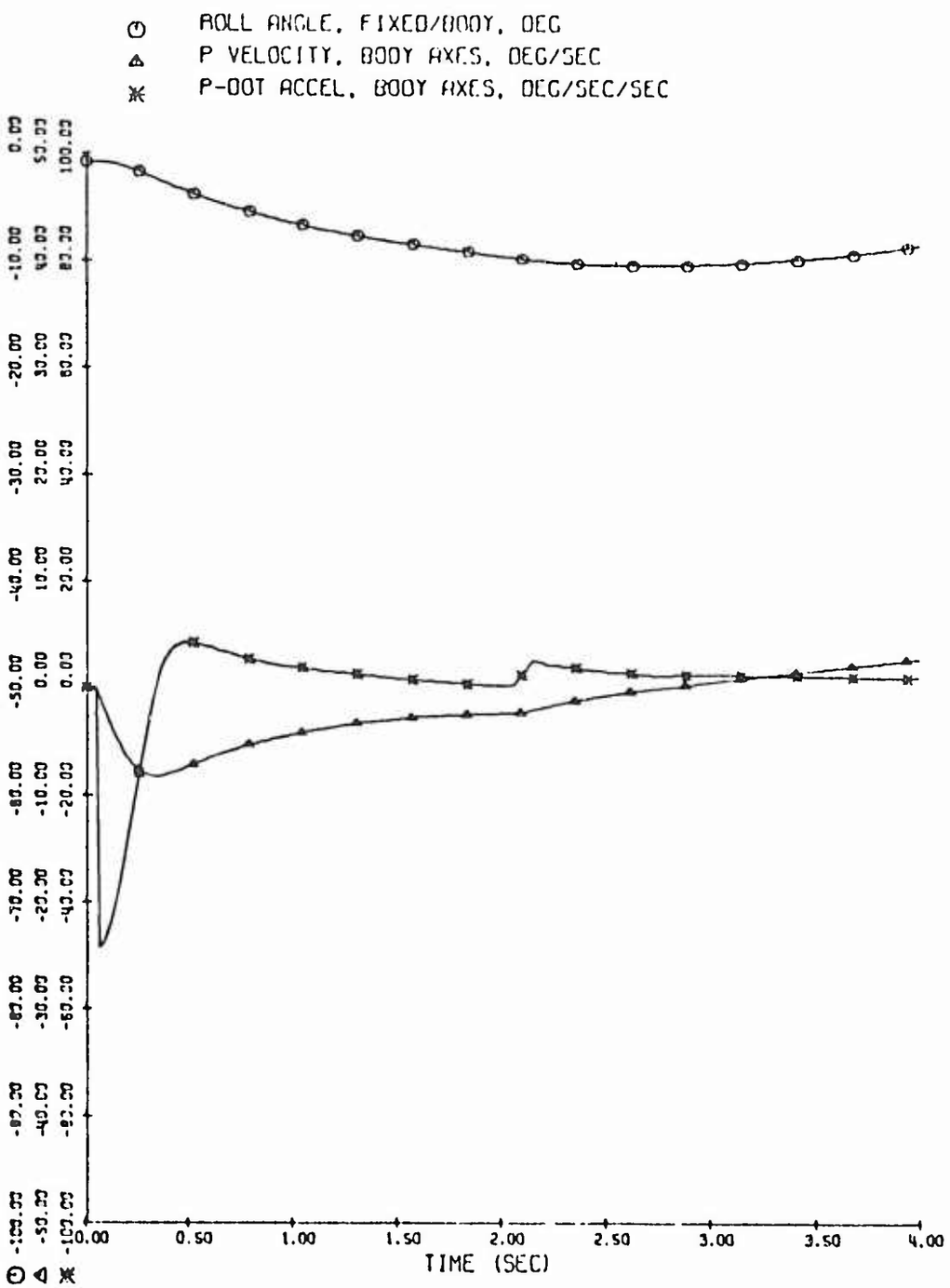

Figure 6-3. Continued.

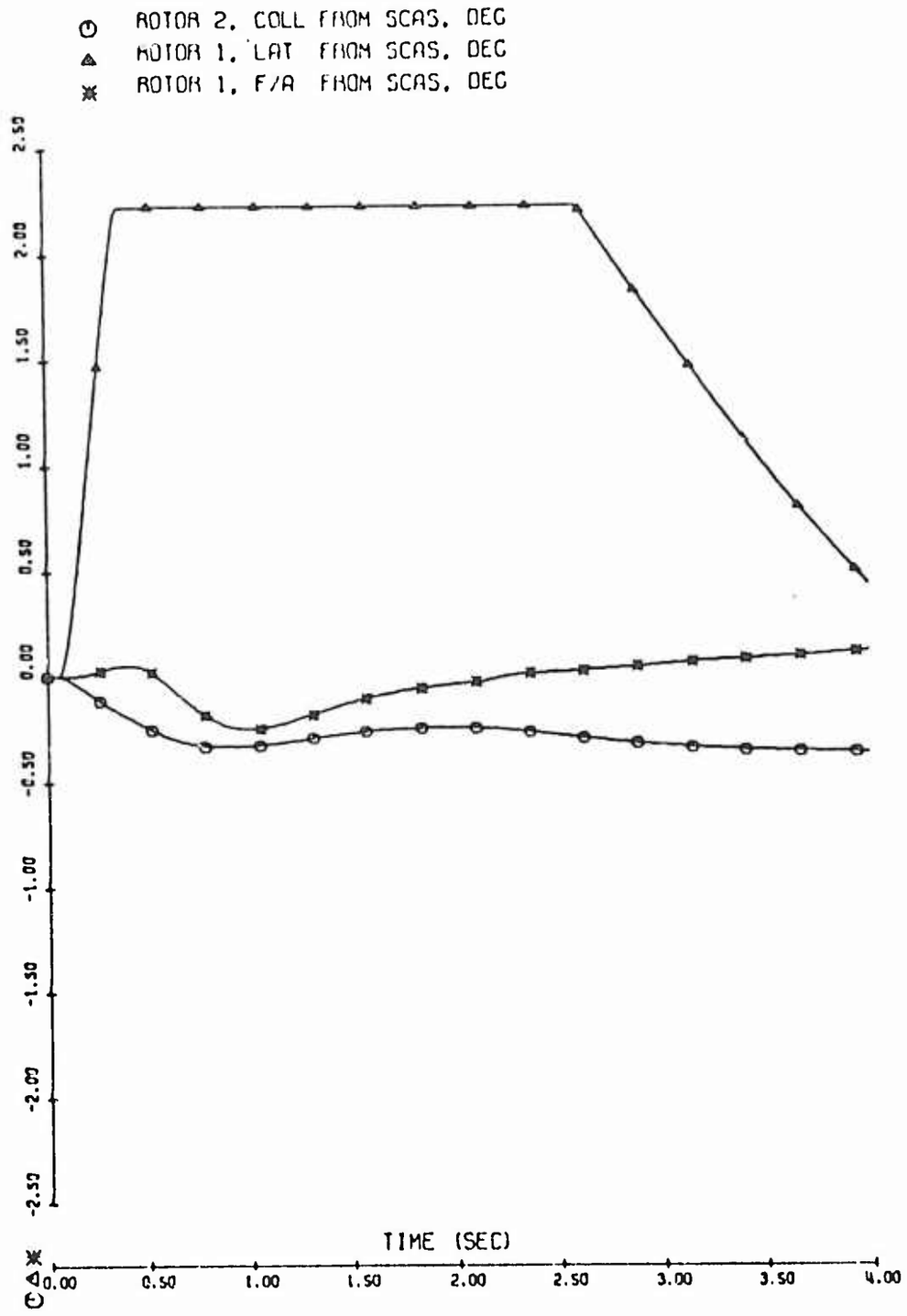

Figure 6-3. Concluded.

7. AUXILIARY PROPULSION (JETS) MATHEMATICAL MODEL

It is frequently desirable to simulate a force acting in a specific direction and at a specific point with respect to the airframe. To this end, C81 includes a very simple model for auxiliary propulsion in what is referred to as the Jet, or Jet Thrust, Group. The model is strictly a force vector acting at a point and is not in any way a mathematical model of a turbojet engine. At this time, use of turbojets for propulsion is limited to a very few research aircraft and configurations in preliminary design. Hence, the complexity of including a complete engine model for the very few cases where it is needed is not considered justifiable.

The Jet Group model currently incorporated into C81 provides for one or two jet thrusts, or, more precisely, force vectors. Inputs to the model include the point of application of the first jet; the Euler angle rotations from body axis to that vector; the magnitudes of the first and the second jets; and a logic switch to specify which jets can and cannot be controlled by the control linkages between the flight controls and jet thrust.

In the User's Guide, the first jet is defined as the right jet and the second as the left jet. However, this distinction of left and right is for input/output convenience only. The definitions define the two jets to be symmetrical in position and orientation with respect to the body X-Z plane passing through buttline zero, regardless of the signs of buttline and yaw angle of the first jet.

Jet thrust is controllable in TRIM and MANEUVER with the linkages discussed in Section 8. If the number of controlled jets equals one, only the first, or right, thrust vector is controlled and the second, or left, jet remains locked at its input value. If the number of controlled jets equals two, both the first and second jets are controlled. In maneuver, jet thrusts may be changed independently of the control linkages.

When both Euler angle rotations from body axis to the thrust vector are zero, the jet thrust is a positive X-force in body axis (i.e., a propulsive force). The jet thrust can be used to simulate a drag force by inputting a negative jet thrust with zero rotation angles or by inputting 180 degrees for one of the rotations (zero for the other) and a positive jet thrust.

8. CONTROL SYSTEM MATHEMATICAL MODEL

8.1 PRIMARY FLIGHT CONTROL SYSTEM REPRESENTATION

The mathematical model of the primary flight control system was developed to provide for simulation of all major rotor configurations: single main rotor, tandem, coaxial, and side-by-side (or tilt rotor). Considering the generality of the model and options within it, quite complex control systems can be represented when the model is applied to a specific configuration.

(1) Nonlinear linkages between the primary flight controls and the swashplate angles

(2) Coupling of the swashplate angles to control angles and mast tilt

(3) Coupling of main rotor collective pitch to load factor (g-level), i.e., a collective bobweight

(4) Coupling of swashplate angles to pylon position

(5) Pitch-flap coupling (δ_3 angles) and control phasing in the linkages between the swashplate and the blades

(6) Nonlinear linkages between any or all primary flight controls and the incidence or control surface deflection of any or all aerodynamic surfaces

(7) Linkages between the primary flight controls and jet thrust

The basic independent variables, or controlling elements, in the model are:

(1) Collective stick position

(2) F/A cyclic stick position

(3) Lateral cyclic stick position

(4) Pedal position

(5) F/A mast tilt angle of the main rotor (Rotor 1)

In addition to the control riggings, the model also uses the following configuration-dependent inputs:

(1) Stability and Control Augmentation System (SCAS) inputs

(2) F/A and lateral pylon deflection angles of each rotor

(3) Increment to collective pitch due to the collective bobweight (g-level)

(4) Swashplate phasing angle and pitch-flap coupling

(5) Blade flapping as a function of blade azimuth

The dependent variables, or controlled elements, are then

(1) Blade pitch angle at the theoretical root of each rotor as a function of blade azimuth

(2) Change in incidence or control surface deflection angle of the wing and each of the four stabilizing surfaces

(3) Change in magnitude of the jet thrust vector

The blade pitch angles at the root computed by the control system model represent the geometric angles for a rigid blade at the centerline of the mast.

The local blade pitch angle, i.e., the angle at the outboard end of each of the twenty blade segments, is the sum of the root angle and the angle of blade twist between the root and the blade radial station of interest. This angle of blade twist is the sum of the twist built into the blade plus the change in twist resulting from blade flexibility when the aeroelastic rotor option is used. The local inflow angle is subtracted from the local blade pitch angle to give the local angle of attack used in the rotor aerodynamic computations.

The change in aerodynamic surface angle is added to the input value of incidence or control surface deflection angle of the corresponding surface. The change in the magnitude of the jet thrust vector is added to its input magnitude.

Figures 8-1 and 8-2 are schematic diagrams of the mathematical models of the Primary Flight Control System. With appropriate inputs to the programmed model, the various features of the model can be bypassed or locked out. For example, consider a single-main-rotor helicopter with no nonlinear rigging, no mast tilt coupling, no rotor control coupling, no collective bobweight, no SCAS, no jet thrust, no pitch-flap coupling or swashplate phasing, a rigid pylon, rigid blades, and fixed aerodynamic surfaces. Then, the control system can be represented by the simple schematic in Figure 8-3. In this example, the collective stick is then linked only to the collective pitch of the main rotor, the F/A cyclic stick only to the main rotor F/A cyclic pitch, the lateral cyclic stick only to the main rotor lateral cyclic pitch, and the pedals only to the

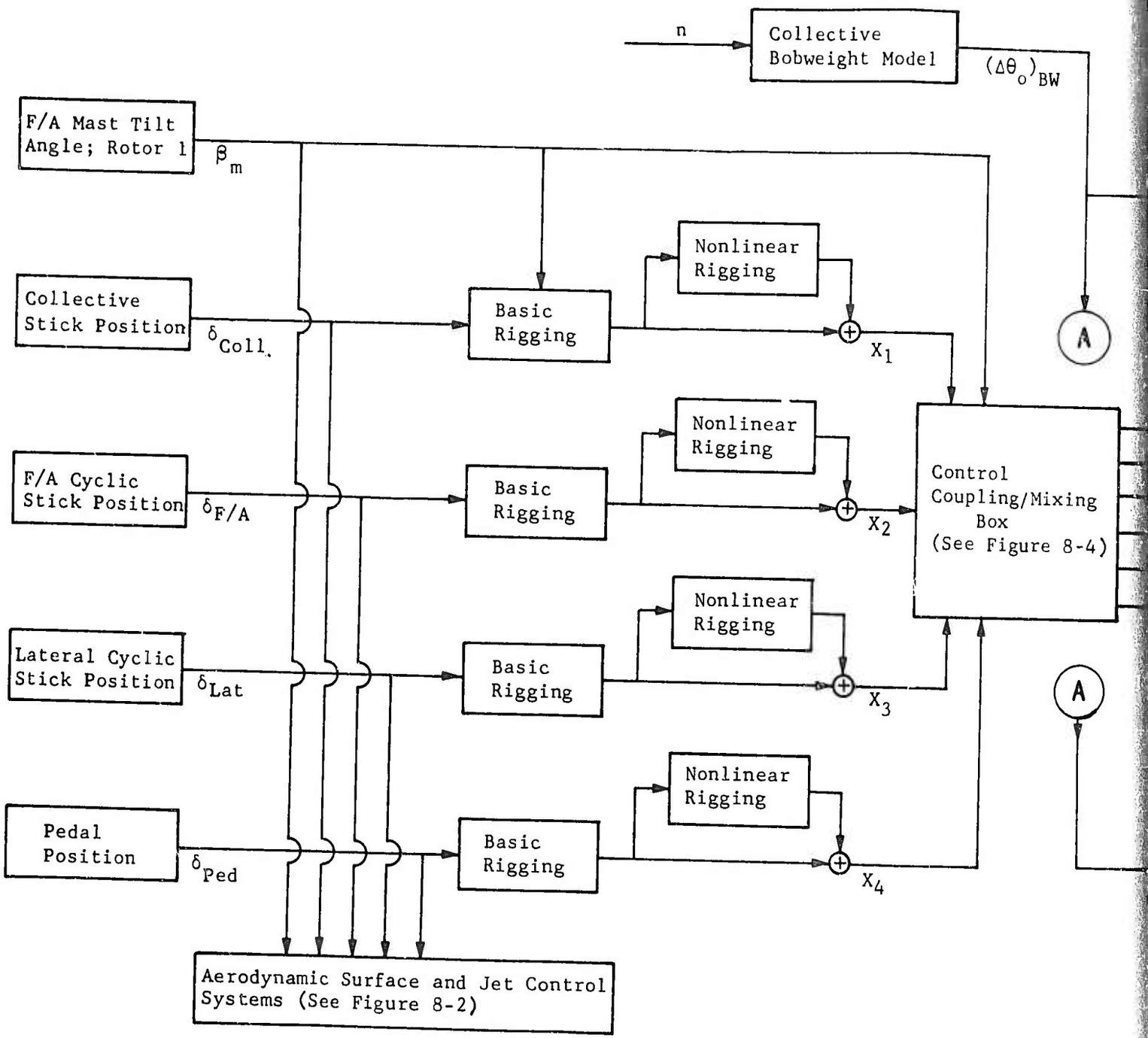

Figure 8-1. Schematic of Rotor Control System.

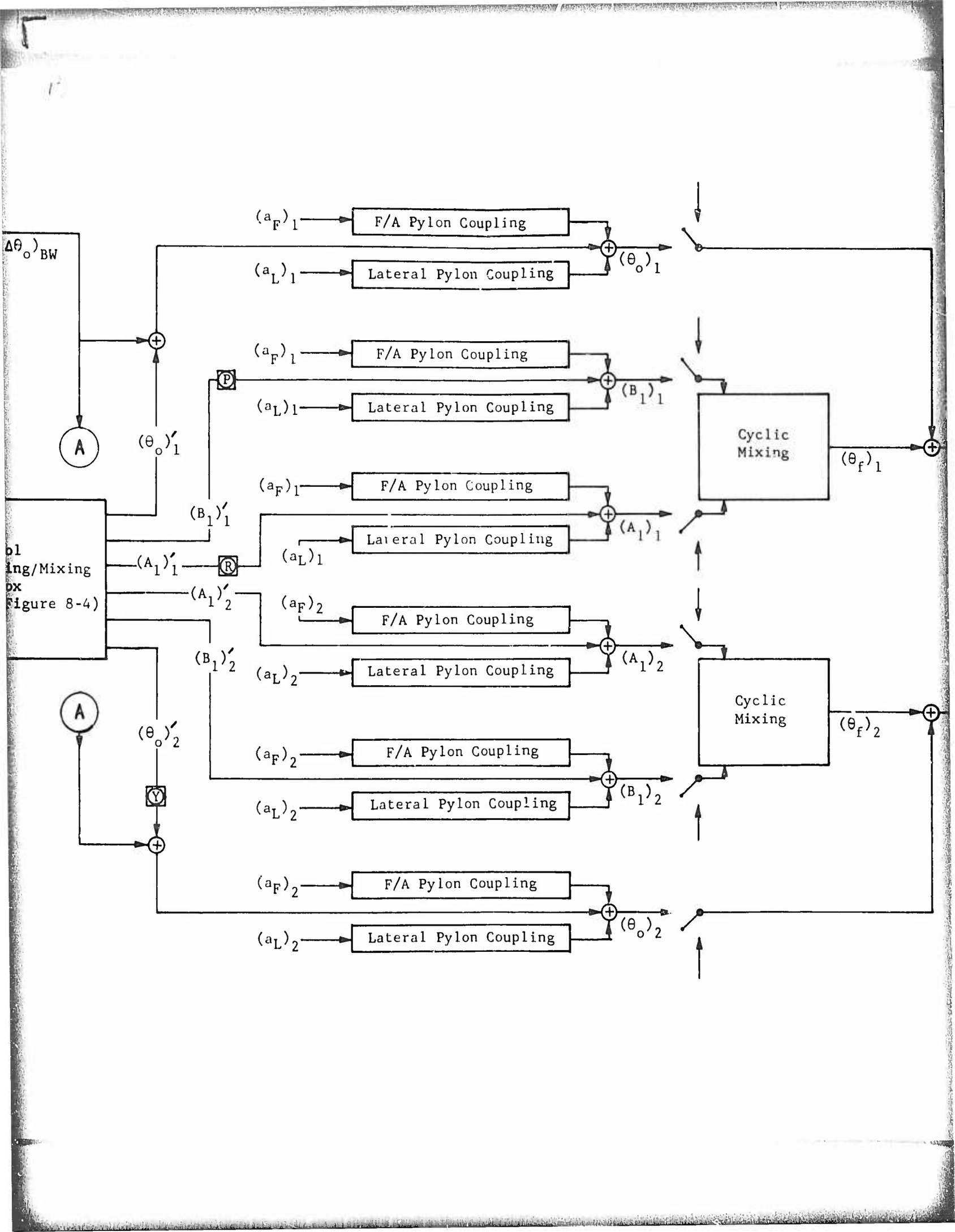
$(a_F)_1$
F/A Pylon Coupling
$(a_L)_1$
Lateral Pylon Coupling
$(\theta_o)_1$
$\Delta\theta_o)_{BW}$
A
$(\theta_o)'_1$
P
$(B_1)_1$
Cyclic Mixing
$(\theta_f)_1$
$(B_1)'_1$
$(A_1)_1$
$(A_1)'_1$
R
$(a_L)_1$
ol
ing/Mixing
ox
igure 8-4)
$(A_1)'_2$
$(a_F)_2$
F/A Pylon Coupling
$(A_1)_2$
$(B_1)'_2$
$(a_L)_2$
Lateral Pylon Coupling
A
Cyclic Mixing
$(\theta_f)_2$
$(\theta_o)'_2$
$(a_F)_2$
F/A Pylon Coupling
Y
$(B_1)_2$
$(a_L)_2$
Lateral Pylon Coupling
$(a_F)_2$
F/A Pylon Coupling
$(\theta_o)_2$
$(a_L)_2$
Lateral Pylon Coupling

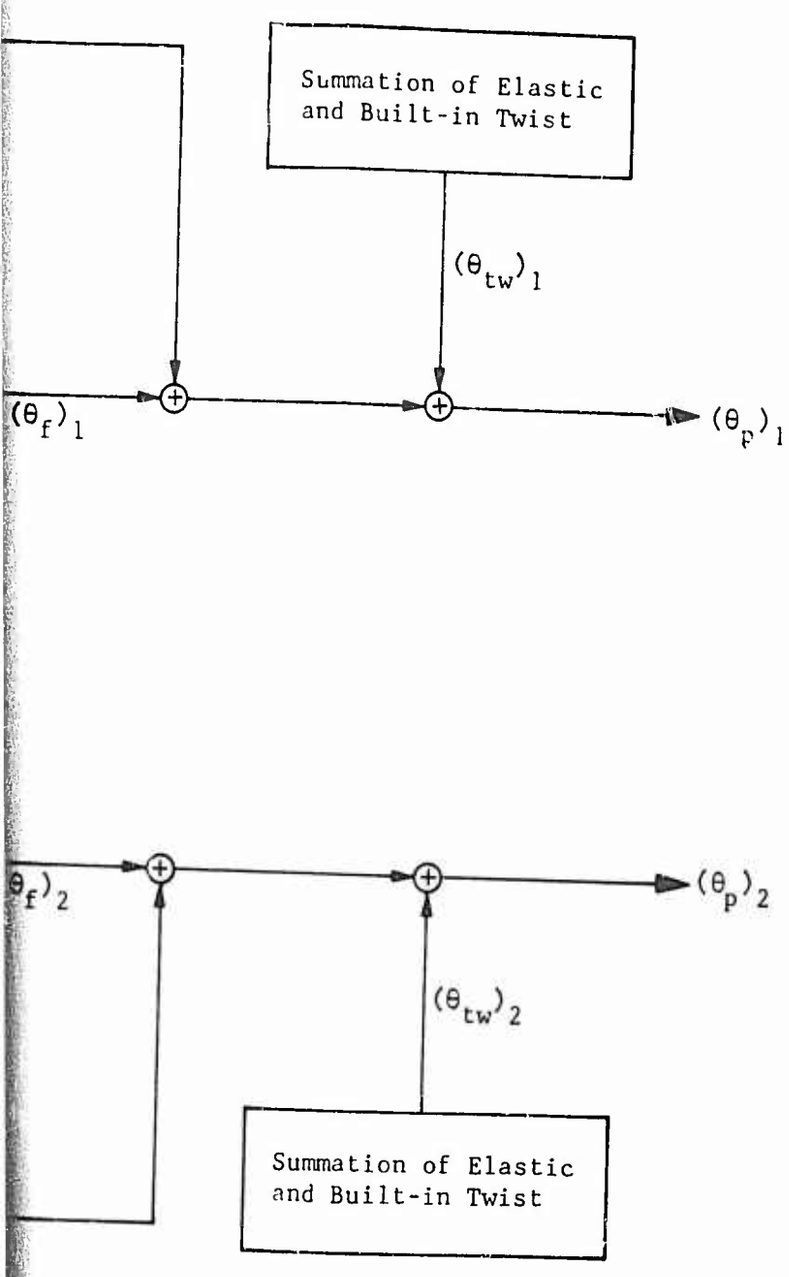

Rotor 1 (Main, Right, or Forward Rotor)

Rotor 2 (Tail, Left, or Aft Rotor)

Nomencla

X_1, X_2, X_3, and X_4 are respecti collective, F/A, lateral and pe

Stability and Control Augme points. P = Pitch SCAS; R = Ro

$(a_F)_i$ and $(a_L)_i$ are the angular the F/A and lateral pylon respec rotor (i = 1 or 2).

$(\theta_o)_i$ is the root collective pit rotating system) for the i^{th} rot

$(B_1)_i$ and $(A_1)_i$ are respectively swashplate angles (nonrotating s rotor.

The switches (⟵ ⟍⟝) near the Cy indicate the point at which cont defined directly rather than by

$(\theta_f)_i$ is the feathering angle (i of the blade root as a function the i^{th} rotor.

$(\theta_{tw})_i$ is the twist angle (in th the blade root to the appropriat azimuth for the i^{th} rotor.

$(\theta_p)_i = (\theta_o)_i + (\theta_f)_i + (\theta_{tw})_i$ a angle at the appropriate blade st i^{th} rotor.

The primes (′) on the collective angles indicate the output of the Mixing Box (i.e., the angles befo and pylon inputs are included).

Nomenclature

X_1, X_2, X_3, and X_4 are respectively the intermediate collective, F/A, lateral and pedal control angles.

Rotor 1 (Main, Right, or Forward Rotor)

$(\theta_p)_1$

⊠ Stability and Control Augmentation System input points. P = Pitch SCAS; R = Roll SCAS; Y = Yaw SCAS.

$(a_F)_i$ and $(a_L)_i$ are the angular displacements of the F/A and lateral pylon respectively of the i^{th} rotor (i = 1 or 2).

$(\theta_o)_i$ is the root collective pitch angle (in the rotating system) for the i^{th} rotor.

$(B_1)_i$ and $(A_1)_i$ are respectively the F/A and lateral swashplate angles (nonrotating system) for the i^{th} rotor.

The switches (⊸ ↘) near the Cyclic Mixing Block indicate the point at which control angles may be defined directly rather than by the control system.

Rotor 2 (Tail, Left, or Aft Rotor)

$(\theta_p)_2$

$(\theta_f)_i$ is the feathering angle (in the rotating system) of the blade root as a function of blade azimuth for the i^{th} rotor.

$(\theta_{tw})_i$ is the twist angle (in the rotating system) from the blade root to the appropriate blade station and azimuth for the i^{th} rotor.

$(\theta_p)_i = (\theta_o)_i + (\theta_f)_i + (\theta_{tw})_i$ and is the total pitch angle at the appropriate blade station azimuth for the i^{th} rotor.

The primes (′) on the collective pitch and swashplate angles indicate the output of the Control Coupling/ Mixing Box (i.e., the angles before SCAS, bobweight, and pylon inputs are included).

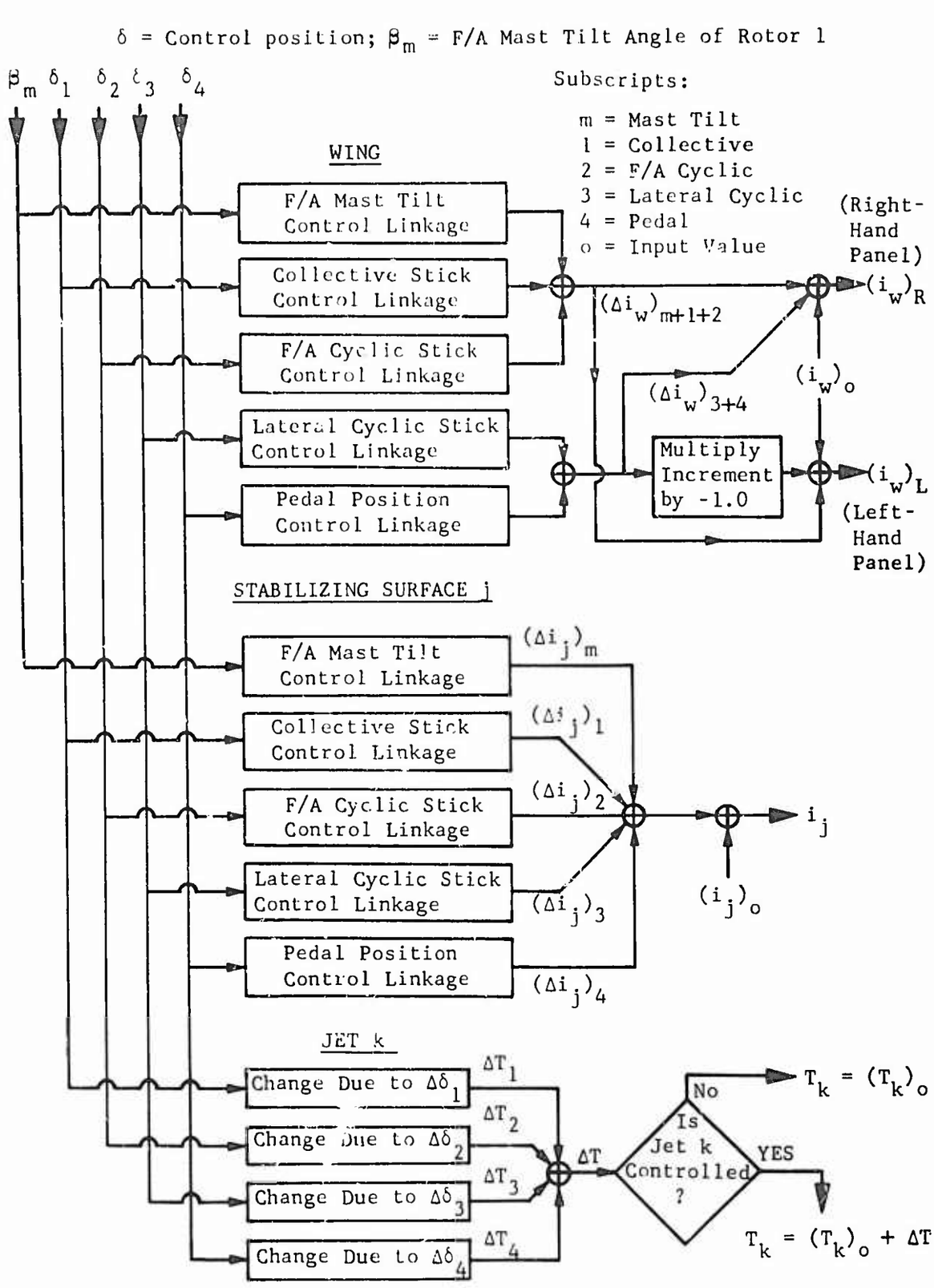

Figure 8-2. Schematic Diagram of Aerodynamic Surface and Jet Control Systems.

Preceding page blank

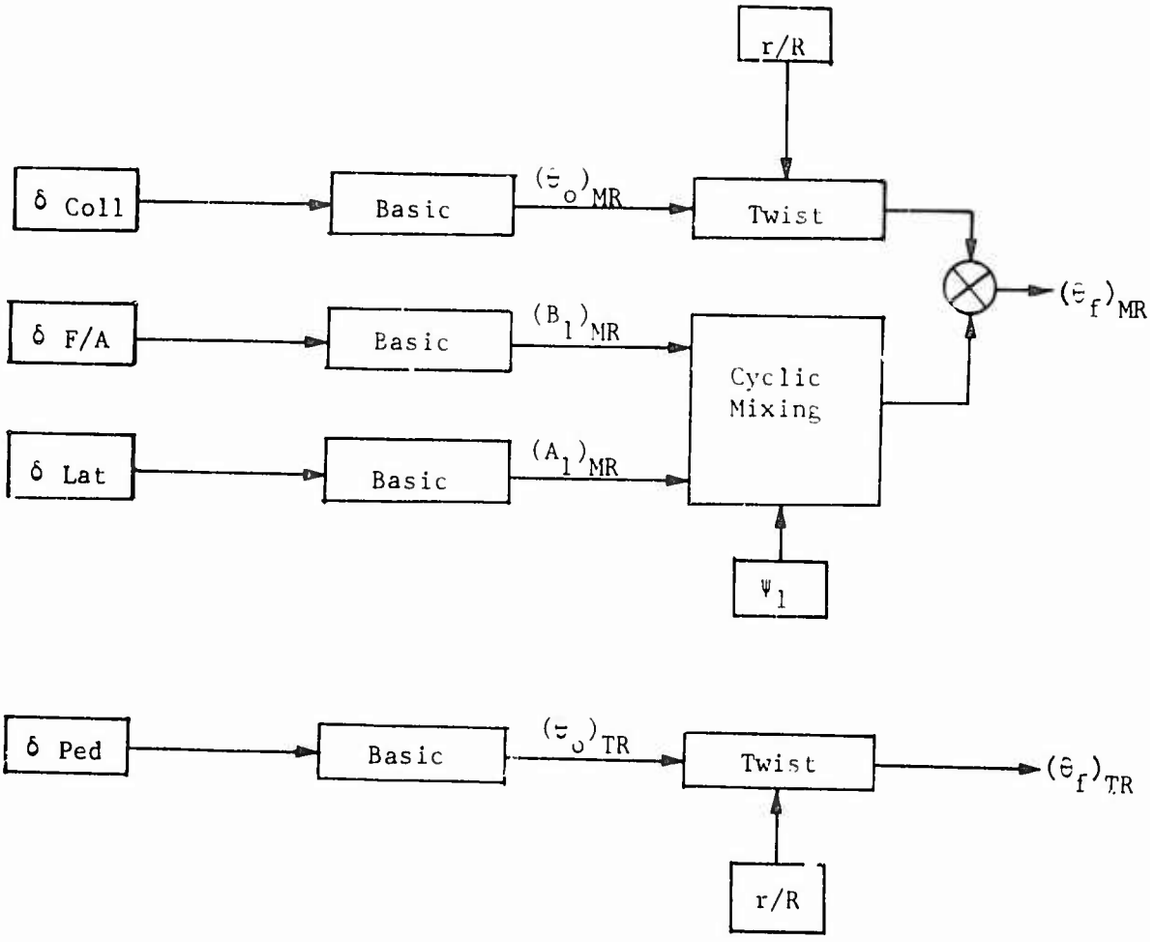

Figure 8-3. Control System Schematic for Simple Single-Main-Rotor Helicopter.

tail rotor collective pitch. This simple control system is typical of the system definitions which are available in the very early preliminary design stage of a helicopter. As a new configuration becomes better defined, inputs for other features of the mathematical model can be added as required.

The current control system representation assumes that the system and the airframe are rigid between the pilot controls and the rotor pylon. Hence, uncommanded control inputs which result from flexing of the airframe are neglected. Recommended future improvements to CSL include development of models for an aeroelastic fuselage and elastic control system. The following two sections discuss the development of the rotor and nonrotor subsystems of the Flight Control System.

8.1.1 Rotor Controls Subsystem

The rotor controls subsystem uses the position of the collective and cyclic sticks, pedals, and the F/A mast tilt of the main rotor to compute the root geometric blade angle of each rotor in its respective rotating system. In the rotating system, the collective and cyclic pitch angles of a nonrotating system reduce to a single blade angle at the root which is a function of control system geometry and blade azimuth.

Positive motions of the flight controls are defined as up collective, forward F/A cyclic, right lateral cyclic, and left pedal. In flight test, a standard definition of positive control motions is the motion required to execute a climbing right-hand turn, i.e., up collective, aft F/A stick, right lateral stick, and right pedal. Hence, the CSL and flight test definitions of positive F/A stick and pedal are opposite. The C81 sign convention has not been changed to correspond to the flight test convention since the flight test convention for F/A stick is not universal and the compatibility of control motion and angular definitions can aid the programmer and user of CSL in assuring that the programmed control linkages produce the desired system characteristics.

The rotor control subsystem was originally developed for a linear, uncoupled, single-main-rotor helicopter. In this early model, the collective stick controlled only the main rotor collective pitch, the F/A cyclic stick only the main rotor F/A cyclic, the lateral cyclic stick only the main rotor lateral cyclic, and the pedals only the tail rotor collective pitch. The linkages were defined by the value of an angle with its appropriate control at zero percent and the range of the angle as the control was moved from zero to 100 percent.

Subsequently, the representation was expanded to model rotor control systems of all major rotorcraft configurations. The linkages discussed above were then redefined to first compute intermediate control angles rather than collective pitch and swashplate angles specifically. Provisions were added so that these intermediate control angles could be modeled as parabolic or cubic functions of the control positions in order that the nonlinearities associated with control-tube bellcrank systems could be simulated. Also, the range and minimum value of the intermediate

collective control angles were made functions of the F/A mast tilt angle of Rotor 1 to simulate the change in collective rigging needed for tilt-rotor configurations during conversion.

The intermediate control angles are input to a mathematical model of a control coupling, or mixing, box. This mixing box provides for linearly linking each control angle to one, or more, of the three nonrotating control angles of each rotor as indicated in Figure 8-1 and detailed in Figure 8-4. The output of the coupling model is then six angles: the root collective pitch and the F/A and lateral cyclic swashplate angles for each rotor.

These values of collective pitch are then incremented by the output of the collective bobweight model. The bobweight is a simple spring-mass-damper system and is assumed to be mounted parallel to the body vertical, or Z, axis so that the body axis load factor (g-level) acts as the forcing function of the bobweight. The model includes a preload feature which sets the forcing function to zero at g-levels less than the value of preload. At g-levels above the preload, the forcing function equals the bobweight mass times the current g-level minus the preload. The increment added to the preliminary value of collective pitch is then proportional to the bobweight displacement. If the bobweight model is used, the increment is always added to the main rotor collective pitch; however, it is added to the collective pitch of the other rotor only if the lateral mast tilt angle of Rotor 2 is less than 45 degrees.

The six control angles, with collective modified by the bobweight input, are then modified further by the coupling of these angles to pylon angular displacements. Each rotor pylon is independent of the other pylon, and the F/A and lateral displacements of each pylon are also mutually independent. Hence, increments to each of the six preliminary angles are computed for each degree of freedom of their respective rotor. The increments due to F/A displacement and the increment due to lateral displacement are added to the appropriate angle, with the resulting six angles being the conventional collective pitch and cyclic swashplate angles.

The next step in the model is to compute the blade angle in the rotating system for each rotor from the swashplate angles and collective pitch angle. The collective pitch angle output from the pylon model is the pitch angle of the blade at its theoretical root (shaft centerline). The angle is measured with respect to the plane perpendicular to the shaft and assumes that both F/A and lateral cyclic pitch angles are zero. In the rotating system this root collective pitch angle becomes the mean value of blade root pitch angle and is independent of blade azimuth angle. This means blade angle is then corrected at each blade radial station for the geometric and elastic twist of the blade.

A relatively simple model, which includes several small angle assumptions, is used to compute the blade feathering angle in the rotating system as a function of the swashplate tilt angles in the nonrotating system. The

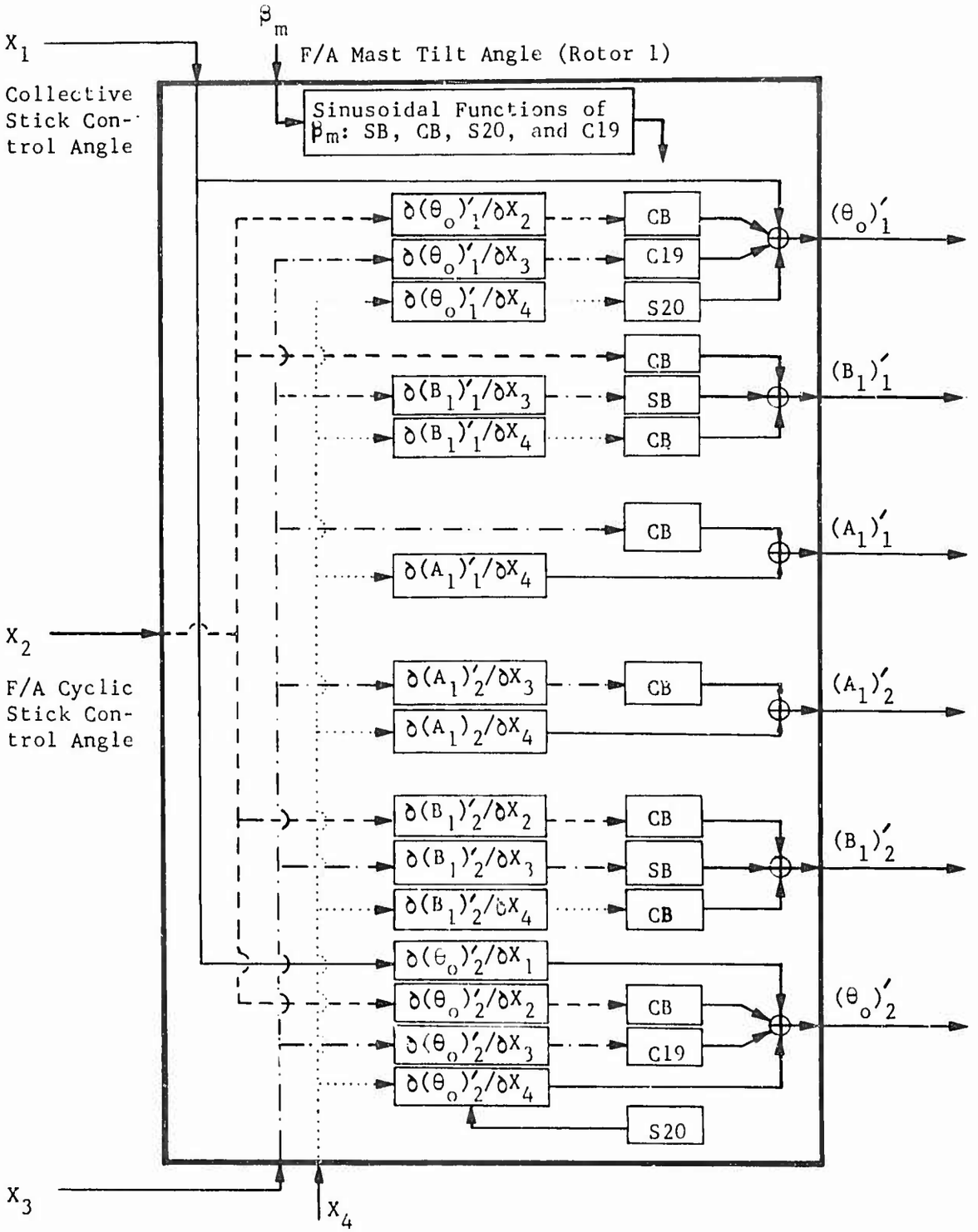

Figure 8-4. Schematic Diagram of Control Coupling/Mixing Box.

design and construction of most swashplate systems cause many inherent nonlinearities. These nonlinearities result primarily from the motion of the pivot points or attach points used to convert linear motion to angular motion or vice versa. To model these nonlinearities would require a very detailed geometric description of the swashplate and feathering systems. Some of the necessary parameters would be location of the pitch link attach point on the swashplate, length of the pitch link, description of any walking beams used in the system, location of the pitch link attach point on the pitch horn (blade), displacement of the pitch link attach point due to blade aeroelasticity, etc. To date, the inclusion of such a sophisticated and complex model has not been warranted because of certain small angle and rigid body assumptions in other related parts of the program and the variety of systems which are in use. However, as these assumptions are removed, the development of improved swashplate/feathering models becomes increasingly important. The development of such models is included with the future improvements recommended for C81.

In the current swashplate/feathering system model, the first step is to determine the angle in the rotating system between an arbitary point on the swashplate and the plane perpendicular to the mast based on the swashplate tilt angles in the nonrotating system. Figure 8-5 is a sketch of the swashplate model and geometry used to develop the relationship. It is assumed in the model that F/A cyclic tilt, B_1, is a rotation about the Y-axis and lateral cyclic tilt, A_1, is about the X-axis; i.e., the axes of swashplate tilt are 90 degrees apart and parallel to the X and Y axes of the rotor shaft.

Since triangle BOA in Figure 8-5 is a 45-degree right triangle,

$$a + b = \sqrt{2}\ R \tag{8-1}$$

From the law of sines,

$$\frac{a}{\sin \psi} = \frac{R}{\sin(135 - \psi)} \tag{8-2}$$

and

$$\frac{r}{\sin(45^\circ)} = \frac{a}{\sin \psi} \tag{8-3}$$

Hence,

$$a = \sqrt{2}\ R \sin\psi / (\sin \psi + \cos \psi) \tag{8-4}$$

$$b = \sqrt{2}\ R \cos\psi / (\sin \psi + \cos \psi) \tag{8-5}$$

$$r = R/(\sin \psi + \cos \psi) \tag{8-6}$$

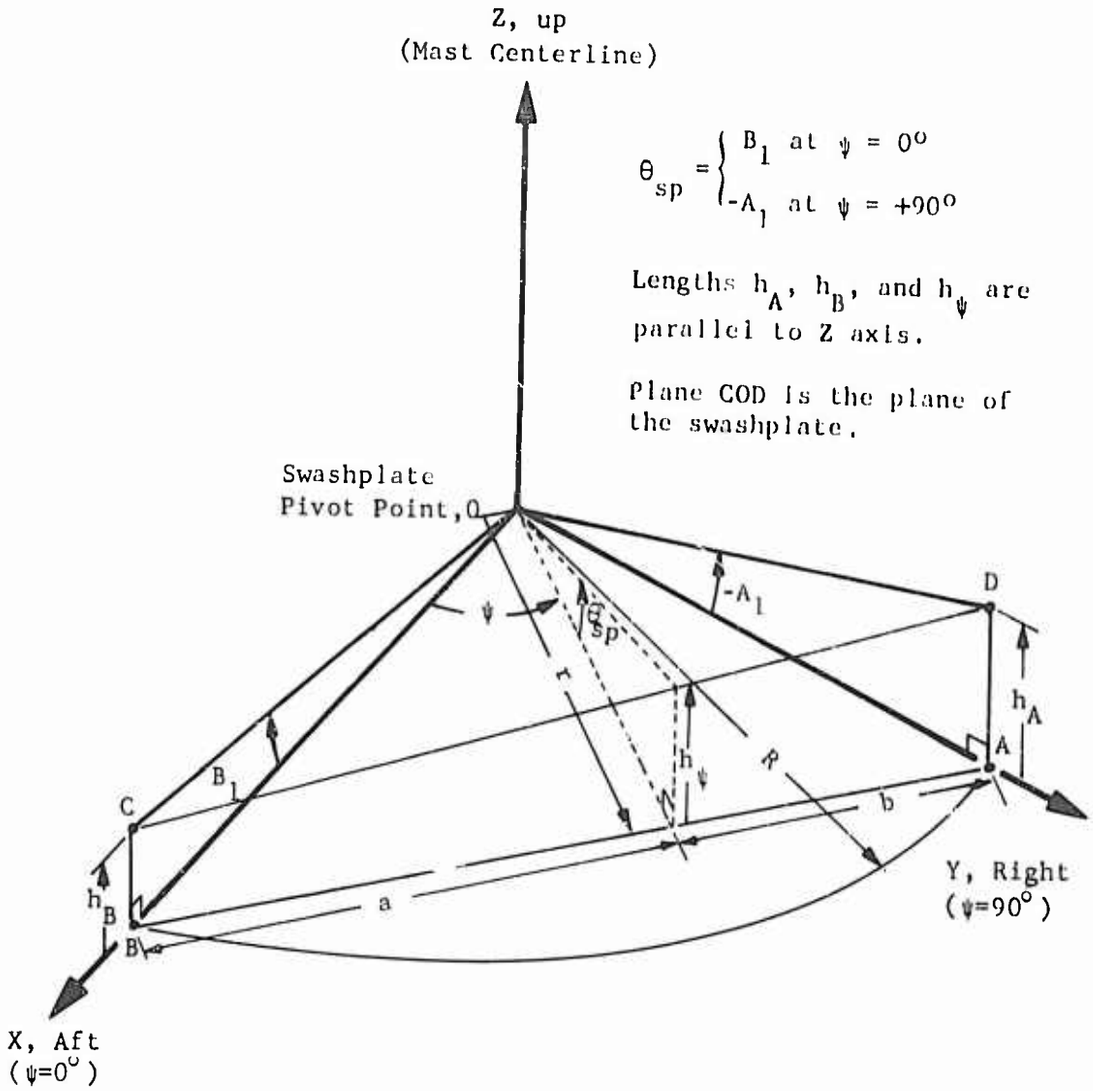

Figure 8-5. Model for Swashplate in the Nonrotating System.

The vertical distance from the X-Y plane to the line CD in the ABCD plane is then

$$h_\psi = \left[(h_A - h_B)/(\sqrt{2}\ R)\right]a + h_B \tag{8-7}$$

Noting that

$$h_A = R \tan(-A_1) \tag{8-8}$$

$$h_B = R \tan(B_1) \tag{8-9}$$

and then substituting Equations (8-4), (8-8) and (8-9) into (8-7) yields

$$h_\psi = R\left[\tan(-A_1) \sin\psi + \tan(B_1) \cos\psi\right]/(\sin\psi + \cos\psi) \tag{8-10}$$

and from Figure 8-5

$$\tan\theta_{sp} = h_\psi/r$$

$$= \tan(-A_1) \sin\psi + \tan(B_1) \cos\psi \tag{8-11}$$

where θ_{sp} is the angle in the rotating system between the X-Y plane and a line passing through point 0 and an arbitrary point on the rotating part of the swashplate.

Next, the swashplate angle in the rotating system, θ_{sp}, is used to determine the cyclic blade feathering angle, θ_f, as a function of blade azimuth. Figure 8-6 shows a top and side view of a typical swashplate to rotor blade linkage. The following assumptions are made for the model:

(1) The feathering angle is computed at the theoretical blade root (mast centerline).

(2) The radii to points P and S are equal, the pitch link is very long with respect to the radii, and the control phasing angle, γ, is a small angle; i.e., the pitch link is parallel to the mast for all swashplate and feathering angles.

(3) The flapping hinge axis is perpendicular to the feathering axis and both axes pass through the mast centerline.

(4) The swashplate pivots about a point on the mast centerline.

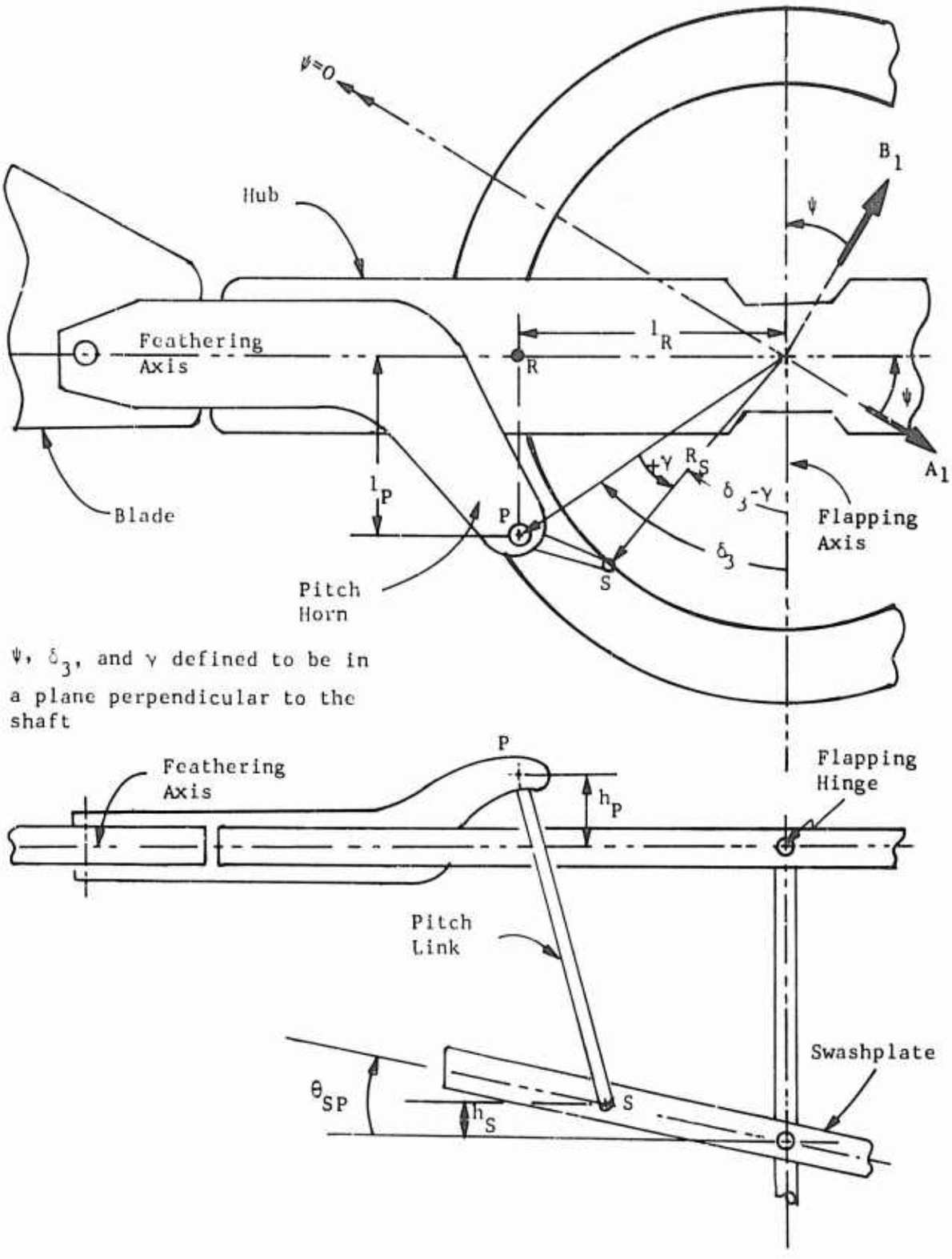

Figure 8-6. Rotating Control Linkages.

(5) The swashplate, pitch links, and pitch horns are rigid.

(6) The angles ψ, δ_3, and γ in Figure 8-6 are all measured in a plane perpendicular to the mast.

From the above assumptions and the geometry shown in Figures 8-6 and 8-7, the equation for the feathering angle is derived as follows:

$$\tan \delta_3 = l_R/l_P \tag{8-12}$$

$$\sin \beta = h_R/l_R \tag{8-13}$$

and

$$\sin \theta_f = -(h_R - h_P)/l_P \tag{8-14}$$

From Equations (8-12) and (8-13), the vertical displacement of Point R in Figures 8-6 and 8-7 is then

$$h_R = \tan \delta_3 \sin \beta \, l_P \tag{8-15}$$

and from Equations (8-14) and (8-15), the feathering angle is then

$$\sin \theta_f = -\tan \delta_3 \sin \beta + h_P/l_P \tag{8-16}$$

Based on the assumptions, the vertical displacement of point P, h_P, is equal to that of point S, h_S. However, h_P, and hence θ_f, are referenced to the azimuth angle of the feathering axis while h_P is referenced to the azimuth angle of point S. Therefore, from the geometry, when feathering axis is at an azimuth angle of ψ, point S is at an azimuth angle of $\psi + 90-(\delta_3 - \gamma)$.

$$h_P(\psi) = h_S(\psi') \tag{8-17}$$

where

$$\psi' = \psi + 90 - (\delta_3 - \gamma) \tag{8-18}$$

Then from Figure 8-6,

$$h_S(\psi') = R_S \sin [\theta_{sp}(\psi')] \tag{8-19}$$

TPP indicates the tip path plane of a rigid blade.

Point P is the attachment point of the pitch link to the pitch horn

NFP indicates the no feathering plane for a rotor without precone.

β is the flapping angle.

δ_3 is the pitch-flap coupling angle.

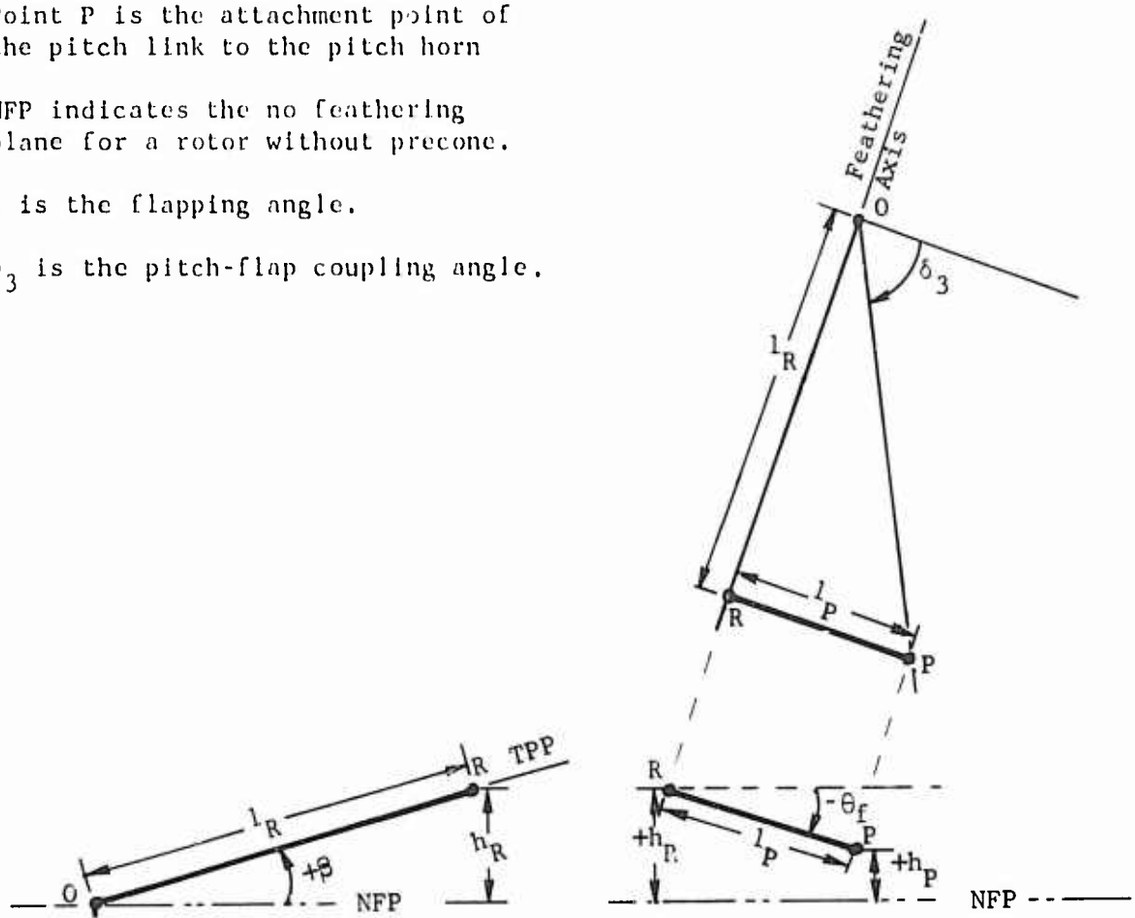

$$\sin \beta = h_R/l_R$$

$$\tan \delta_3 = l_R/l_P$$

$$h_R = l_R \sin \beta = l_P \tan \delta_3$$

$$\sin \theta_f = -(h_R - h_P)/l_P$$

$$= -\tan \delta_3 \sin \beta + (h_P/l_P)$$

Figure 8-7. Blade Feathering Angle.

Substitution, using Equations (8-11), (8-17), and (8-19), yields

$$h_p(\psi) = R_s \sin[\theta_{sp}(\psi')]$$

$$= R_s \sin\left[\tan^{-1}\{\tan(-A_1)\sin(\psi') + \tan(B_1)\cos(\psi')\}\right] \quad (8\text{-}20)$$

From the assumptions of the analysis and Figure 8-6, the ratio R_s/l_p can be replaced by $1/\cos(\delta_3 - \gamma)$. Using Equations (8-16), (8-18), (8-19), and the R_s/l_p substitution, the blade feathering angle is then

$$\theta_f(\psi) = \sin^{-1}\Big(-\tan\delta_3 \sin\beta$$

$$- \sin\Big[\tan^{-1}\{[\tan B_1 \cos(\delta_3-\gamma) + \tan A_1 \sin(\delta_3-\gamma)]\sin\psi$$

$$+[\tan A_1 \cos(\delta_3-\gamma) - \tan B_1 \sin(\delta_3-\gamma)]\cos\psi\}\Big]/\cos(\delta_3-\gamma)\Big) \quad (8\text{-}21)$$

Equation (8-21) can then be simplified by making small angle assumptions to the following form:

$$\theta_f = -\beta\tan\delta_3 - \tan^{-1}\{[\tan(B_1) + \tan(A_1)*\tan(\delta_3-\gamma)]*\sin\psi$$

$$+ [\tan(A_1) - \tan(B_1)*\tan(\delta_3-\gamma)]*\cos\psi\} \quad (8\text{-}22)$$

Equation (8-22) is currently used in AGAJ73. If, in addition, A_1 and B_1 are assumed to be small angles while δ_3 and γ are zero, the above equation can be reduced to the familiar form of

$$\theta_f(\psi) \approx -B_1 \sin\psi - A_1 \cos\psi \quad (8\text{-}23)$$

Although the equation for θ_f was developed for leading edge pitch horns, it is equally valid for trailing edge pitch horns as long as δ_3 and γ remain referenced to the same lines and their sign conventions are unchanged. For example, with a trailing edge pitch horn, δ_3 would normally be between 135 and 180 degrees, and positive γ would rotate point S back toward the feathering axis. Alternately, 180 degrees may be subtracted from values of δ_3 which are greater than 90 degrees, with the resulting angle yielding identical results from Equations (8-21) and (8-22).

8.1.2 Nonrotating Controls Subsystems

8.1.2.1 Aerodynamic Surface Control Subsystems

Earlier versions of C81 contained very simple and limited linkages between the flight controls and the aerodynamic surfaces (a wing plus one horizontal and one vertical stabilizer). In the earlier model, only the zero lift line incidence was controlled (i.e., the surfaces all moveable), the linkages were defined to be linear, and the surfaces were assumed to have symmetrical airfoil sections. The collective stick could control only wing incidence; the F/A cyclic stick only horizontal stabilizer incidence; the lateral cyclic stick only differential wing panel incidence; and the pedals only the vertical stabilizer incidence.

When the representation of the aerodynamic surfaces was expanded to five surfaces, the subsystem for the surface controls was also expanded. As discussed in the section on aerodynamic surfaces, the expansion from three to five surfaces included removing the restriction that the axes of incidence change for the surfaces must lie in a horizontal or vertical plane and adding a representation for control surface (flap) deflection. Hence, in the expanded control subsystem, the capability of linking flight controls to either zero lift line incidence or flap angle was added.

In view of the infrequency of configurations where both the incidence and flap angle of one surface are variable, the current model restricts a single surface to having either incidence or flap angle controlled by any or all flight controls. Both angles cannot be linked simultaneously to the flight controls. However, each surface is independent of all others and one surface may have variable incidence while another has variable flap angle, e.g., an all-moveable horizontal stabilizer (no elevator) and a fixed vertical stabilizer with a rudder. With the generality of the current aerodynamic surface model, the capability of linking any flight control, plus mast tilt angle for tilt-rotor configurations, to any aerodynamic surface became necessary and was added to the model. The revised linkages between the flight controls and the surfaces were then defined to be linear or parabolic, and provisions for nonlinearities were incorporated as discussed below. In view of the limited use to which mast tilt to surface linkages are put, these linkages were defined to be linear.

Although the incidence and flap angles of one surface cannot be controlled simultaneously by the flight controls, each angle is an input and, during maneuver, each can be changed regardless of which angle, if either, is linked to the flight controls. This model is capable of simulating the aerodynamic surface control systems of virtually any type of rotorcraft.

As noted above, the current model provides for linking each and every flight control to each and every surface. For the wing, a restriction is included so that lateral cyclic stick and pedal motions can cause

only differential deflection of the appropriate angle. A control system where lateral and/or pedal inputs result in symmetrical angle changes to the left and right wing panels was considered too remote a possibility for inclusion.

Each linkage between a flight control and an aerodynamic surface includes a breakpoint option. This option was incorporated to help model nonlinear linkages. To use this option, a nonzero value is input for the breakpoint control position. The difference between the actual control position and the absolute value of the breakpoint input is computed. If the signs of this difference and the breakpoint input are the same, an increment to the appropriate angle of the surface is computed using the difference. If the signs are opposite, the increment is defined to be zero. That is, for a positive breakpoint input, the control linkage is only active for control positions greater than the breakpoint; while for a negative breakpoint, the linkage is only active for control positions less than the magnitude of the breakpoint. If the breakpoint input is zero, the 50 percent control position is used to compute the difference, and the linkage is active throughout the entire range of the control. Figure 8-8 shows examples of the types of control linkages which may be simulated with this breakpoint option.

8.1.2.2 Auxiliary Propulsion, or Jet, Control Subsystem

Linkages are provided between each flight control and the magnitude of the left and/or right jet thrust vectors. The difference between each control position and the respective input control position is multiplied by the appropriate pounds per inch linkage, and the four values are summed and added to the input thrust values to yield the total jet thrust. See the discussion of the Jet Group mathematical model for additional information.

8.2 AUTOMATIC FLIGHT CONTROLS

The Generalized Automatic Control Stability Package is divided into two major headings: Stability and Control Augmentation System (SCAS), and Automatic Pilot Simulator (APS). The SCAS simulation is based on the transfer functions used to design the actual system. In the maneuver portion of the program a series of differential equations is integrated numerically to define the effects of the SCAS. The APS is an algebraic technique used to simulate the pilot's response to nonstandard flight conditions.

8.2.1 Stability and Control Augmentation System

The SCAS can best be described in terms of the block diagram shown in Figure 8-9. In the diagram, the following definitions are applicable:

B = Pilot control input

B_G = SCAS feedforward added to pilot input to offset feedback

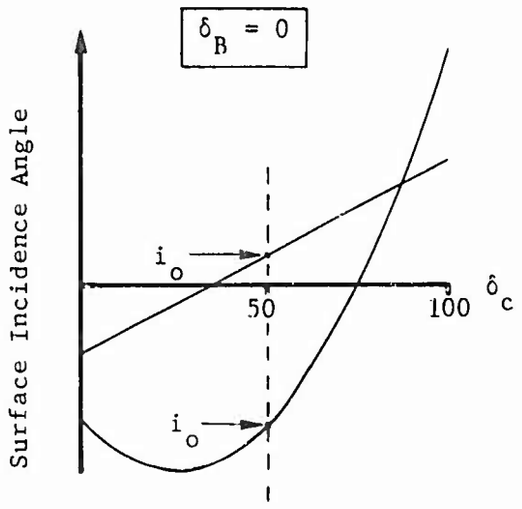

(a) Linear and parabolic linkages, no breakpoint.

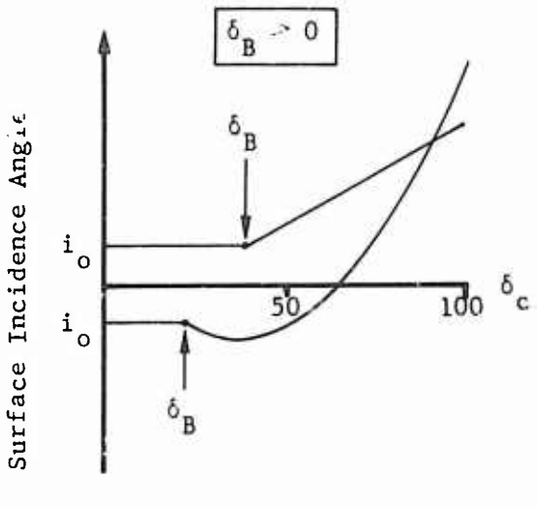

(b) Linear and parabolic linkages, positive breakpoint.

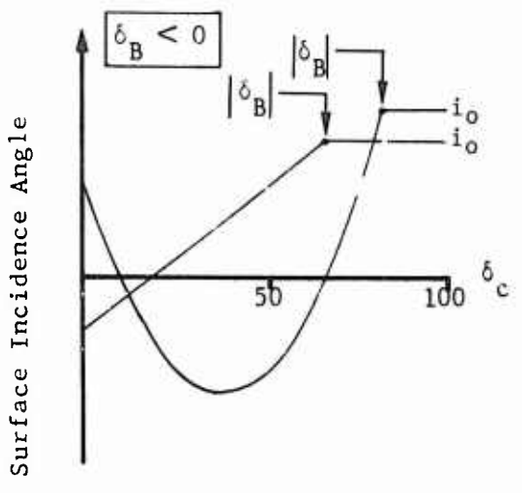

(c) Linear and parabolic linkages, negative breakpoint.

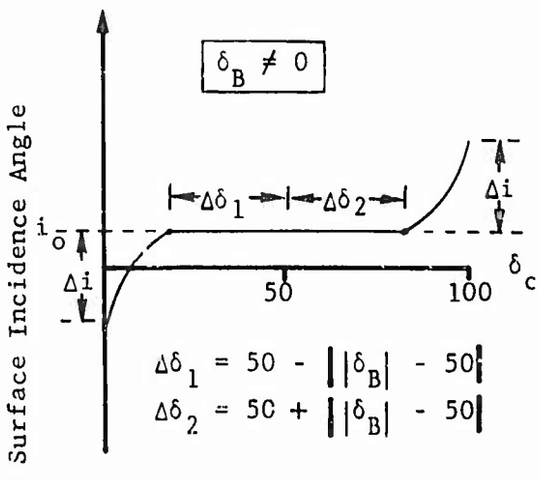

(d) Parabolic linkages from pedals or lateral cyclic to wing, nonzero breakpoint.

δ_c = Control position, percent of full throw

δ_B = Control position for breakpoint, percent

i_o = Basic (input) incidence angle for surface, degrees

Figure 8-8. Aerodynamic Surface Control Linkages.

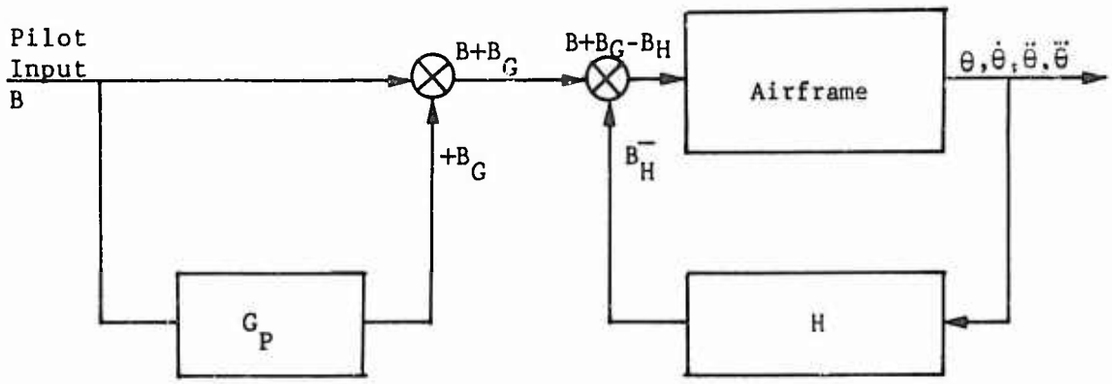

Figure 8-9. Schematic Diagram of SCAS.

B_H = SCAS feedback dependent on ship's response

SM = $B + B_G - B_H$, total input to the swashplate

G_P = Feedforward transfer function

H = Feedback transfer function

Three independent systems (roll, pitch, and yaw) are simulated in the maneuver. Only the pitch system is described below, but the other channels are based on the same principle. The symbol s is the Laplace transform variable and the τ terms are the time constants associated with the SCAS. All time constants must have nonzero values because of programming considerations.

The feedback transfer function has the form

$$H = \frac{K_H s(\tau_1 s + 1)(\tau_2 s + 1)}{(\tau_3 s + 1)(\tau_4 s + 1)(\tau_5 s + 1)} = \frac{B_H}{\theta} \tag{8-24}$$

The feedforward transfer function has the following form

$$G_P = \frac{K_G s}{(\tau_3 s + 1)(\tau_4 s + 1)(\tau_5 s + 1)} = \frac{B_G}{B} \tag{8-25}$$

where K_H and K_G are the gains associated with the feedback and feedforward transfer functions, respectively.

In the digital program, Equation (8-24) is written

$$C_1\dddot{B}_H + C_2\ddot{B}_H + C_3\dot{B}_H + B_H = C_4\dddot{\theta} + C_5\ddot{\theta} + K_H\dot{\theta} \tag{8-26}$$

and Equation (8-25) is written as

$$C_1\dddot{B}_G + C_2\ddot{B}_G + C_3\dot{B}_G + B_G = K_G\dot{B} \tag{8-27}$$

where

$$C_1 = \tau_3\tau_4\tau_5 \tag{8-28}$$

$$C_2 = \tau_3\tau_4 + \tau_4\tau_5 + \tau_3\tau_5 \tag{8-29}$$

$$C_3 = \tau_3 + \tau_4 + \tau_5 \tag{8-30}$$

$$C_4 = \tau_1 \tau_2 K_H \tag{8-31}$$

$$C_5 = (\tau_1 + \tau_2) K_H \tag{8-32}$$

In Equations (8-26) and (8-27), all independent variables are known except the third derivative of the angular displacement with respect to time ($\dddot{\theta}$). In the program, $\dddot{\theta}$ is obtained by numerically differentiating $\ddot{\theta}$ with respect to time. The maneuver portion of the program has calculated θ, $\dot{\theta}$, $\ddot{\theta}$, and the stick rates $\dot{B}$. Using those already calculated values, Equations (8-26) and (8-27) are numerically integrated in conjunction with the other differential equations which describe the motion of the rigid fuselage and the elastic rotor.

The basic feedback function, Equation (8-26), is written with the pitch attitude and its derivatives as the independent variables. Any other variable, and its associated derivatives which are calculated in the maneuver portion of the program, could be substituted as the independent variable with only minor changes to the program.

The maximum authority of the SCAS (in percent of full range) is an input quantity. The third time derivative of the angular displacements is obtained from the numeric differentiation of the angular acceleration terms. This numeric differentiation can introduce "noise" into the equations of motion. The program is structured so that the product of the derivative of angular acceleration times the appropriate fuselage inertia is set to zero if it is less than the input dead band (ft-lb/sec).

8.2.2 Automatic Pilot Simulator

The second major item in the Generalized Automatic Control Stability Package is the Automatic Pilot Simulator (APS). The APS is an algebraic simulation of the pilot response to minimize any deviation from the desired flight condition. The user-supplied inputs to the APS include: (1) the time to eliminate any deviation of a given angular rate, and (2) the maximum rate at which the controls can be moved. The flow chart of the APS is shown in Figure 8-10.

The primary objective of the APS is to move the pilot's control so that the fuselage Z force balance and all fuselage moments are held to the trim point values. The secondary objective is to eliminate any fuselage angular rates, unless that rate is returning the attitude to the trim position. The final objective is to maintain the maximum fuselage angular displacement from trim to less than .02 radian.

The control partial derivatives computed for the trimmed flight condition are used throughout the maneuver as a measure of the effectiveness of each of the pilot's controls (collective, fore and aft cyclic, lateral cyclic, and pedal) on the fuselage Z force and fuselage moments. At each time

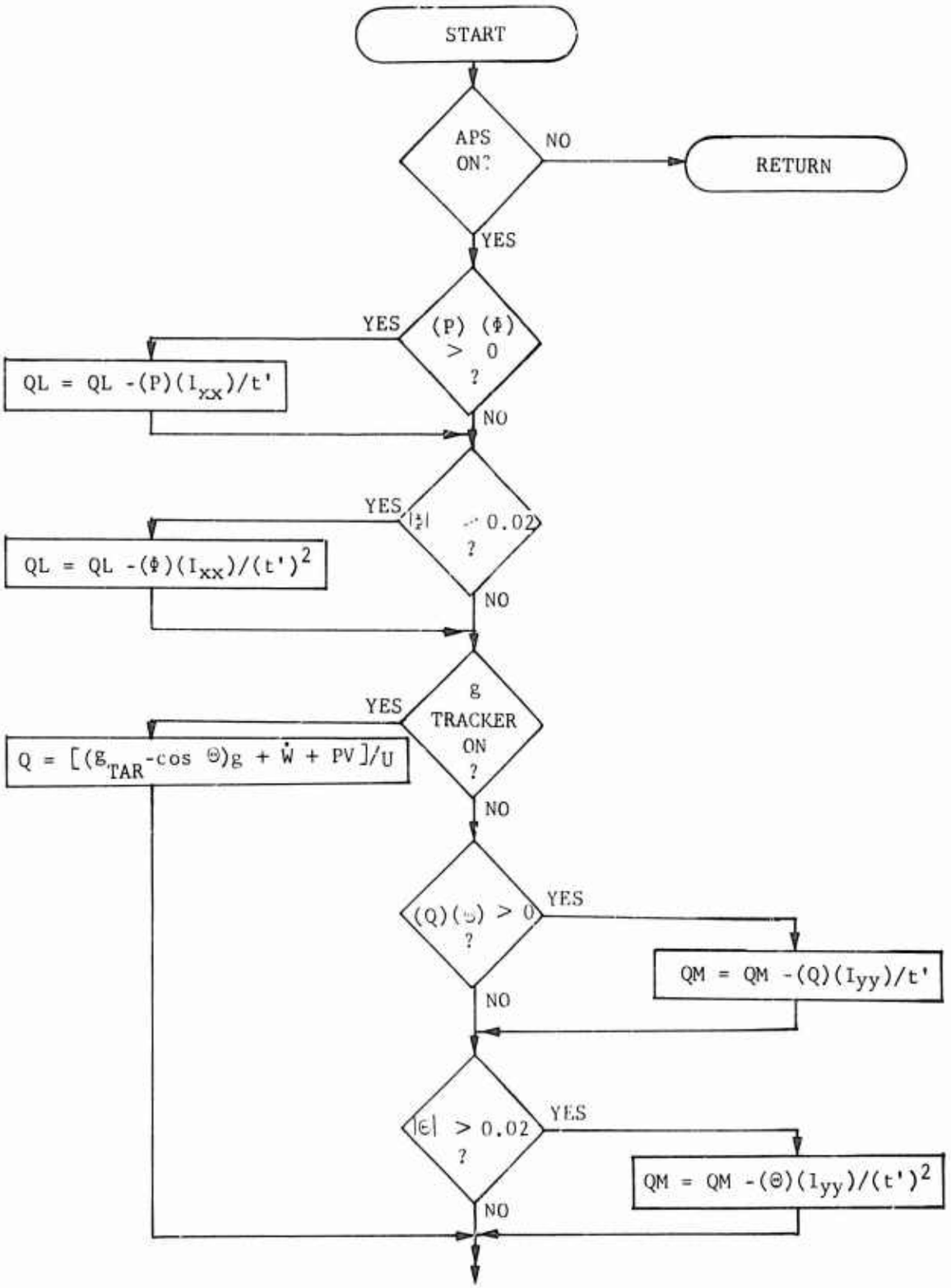

Figure 8-10. Automatic Pilot Simulation Flow Chart.

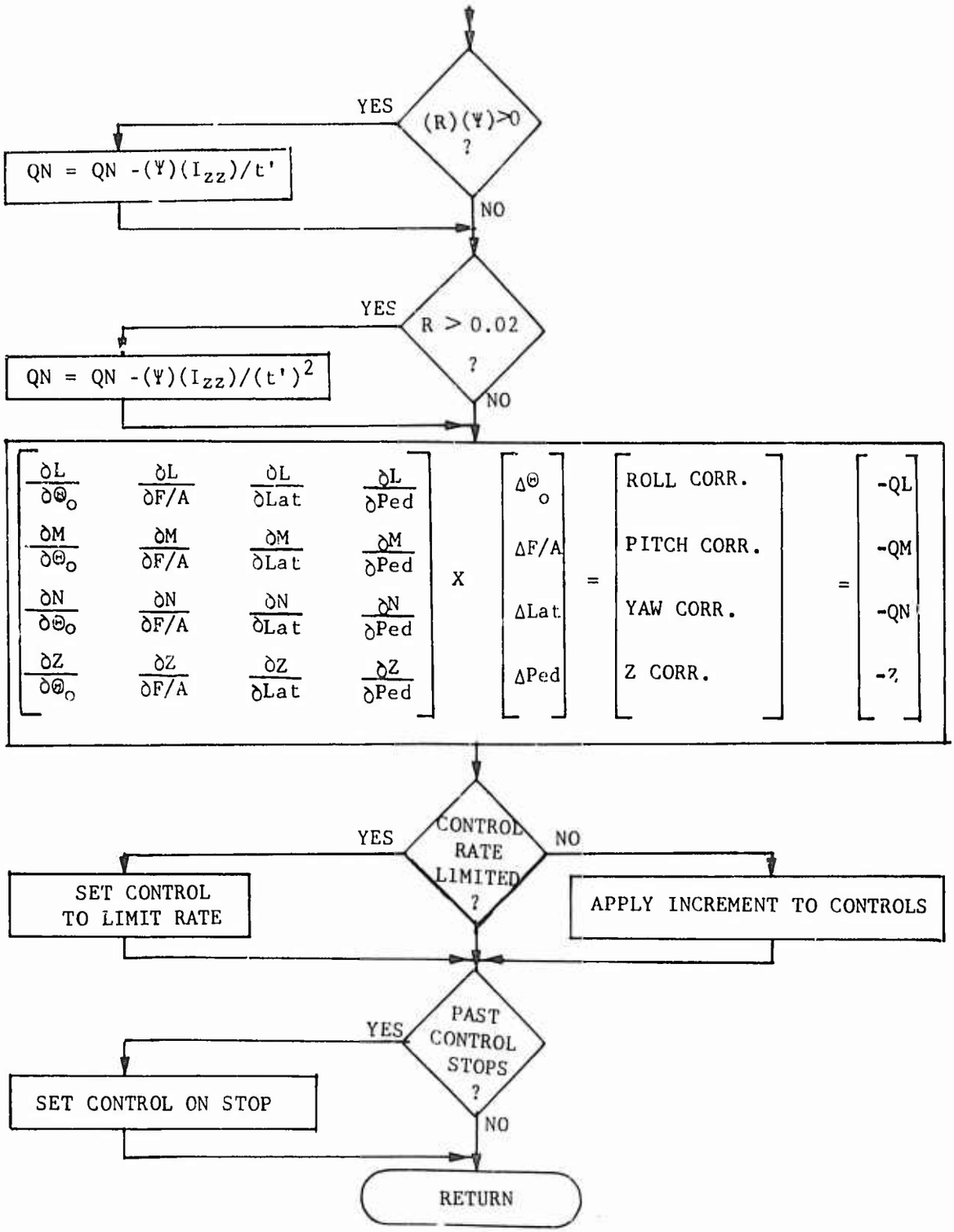

Figure 8-10. Concluded.

point in the maneuver, the Z force, roll, pitch, and yaw moments are known.

Knowing the control effectiveness and the appropriate fuselage forces and moments, four linear algebraic equations can be written where the dependent variables would be the control increments necessary to eliminate the force and moment unbalance. This technique has the capability to eliminate accelerations, but cannot deal directly with rates and displacements. Any fuselage rate can be expressed as a moment by the following expression:

$$\text{Moment} = \left[\frac{\text{Angular Rate}}{t'}\right]\left[\text{Inertia}\right] \tag{8-33}$$

where t' is the user input time to arrest a given angular rate. The moment term given by Equation (8-33) is added to computed force and moment summaries so that extra control inputs are generated whenever unfavorable angular rates are present. Equation (8-33) is used only when the product of angular rate times angular displacement is positive, i.e., when the rate tends to make the deviation larger.

Thus far, the effect of accelerations and rates has been considered. Fuselage angular displacements are represented as a moment increment

$$\text{Moment} = \left[\frac{\text{Angular Displacement}}{[t']^2}\right]\left[\text{Inertia}\right] \tag{8-34}$$

which is added to the previously defined moment term. In this manner, extra control inputs are generated due to angular displacements. Equation (8-34) is used only when the absolute value of an angular displacement is greater than .02 radians.

The four linear algebraic equations, as shown in Figure 8-10, are solved to define increments to be applied to the pilot's controls. The program moves the pilot controls to the new position unless the rate required is greater than an input maximum rate of control motion. If the required control increment is greater than the maximum input would permit in a given time increment, then the control increment is set to the maximum allowable.

The APS can also be used to simulate the closed-loop response of the pilot to perform a symmetric pull-up. The fuselage pitch rate, Q, associated with the required g level, g_{TAR}, can be written in the notation of Reference 24 as

$$Q = [(g_{TAR} - \cos\theta)g + \dot{W} + PV]/U \tag{8-35}$$

This pitch rate can be used as the required pitch rate deviation that the APS must achieve.

9. TRIM PROCEDURE

9.1 GENERAL

An essential part of any flight simulation program is its ability to define the trim attitude of the aircraft throughout the flight envelope, including accelerated as well as unaccelerated flight. AGAJ73 includes three types of trim procedure which can accomplish this task. The names given to these procedures are:

(1) Quasi-static (QS) trim

(2) Quasi-static followed by time-variant rotor (QS-TV) trim

(3) Fully time-variant (FTV) trim

The terms quasi-static and time-variant refer to the primary rotor analysis (see Section 2.2) which is used in the procedure. Both analyses can include the effects of blade elasticity (mode shapes other than the rigid-body mode shape), but only the time-variant analysis can include the interaction of the aerodynamic loads and blade elasticity, i.e., aeroelasticity. In the QS trim procedure, the quasi-static rotor analysis is used for both rotor systems. In the QS-TV trim procedure, the standard QS trim is performed first. The rotor modal equations of motion are then numerically integrated for 5 rotor revolutions using the time-variant rotor analysis with the control positions and fuselage orientation held fixed at the positions determined by the QS trim. It is assumed that after five revolutions, the aeroelastic effects included in the time-variant analysis will have caused the rotor either to stabilize or to diverge, depending on the basic stability of the rotor system. The user may elect that such time-variant trims be computed for either or both rotors. If both rotors are selected, the two time-variant trims are computed independently of each other. In the FTV trim procedure, the user specifies the rotor or rotors which use the time-variant analysis. In doing so, any reference to the QS trim procedure is deleted for the specified rotor(s). (A rotor which does not use the time-variant analysis uses the quasi-static analysis.)

The basic program flow, which is the same for all three types of trim, is shown in Figure 9-1. The iterative technique represented by this figure is discussed in Section 9.3.1. The three basic blocks in the figure are the computation of the partial derivative matrix (shown in Figure 9-2 and discussed in Section 9.3.2), the time-variant portion of the QS-TV trim (shown in Figure 9-3), and the rotor force and moment computations (shown in Figure 9-4 and discussed in Section 9.3.3). Some of the considerations used in programming the trim procedure are discussed in Section 9.3.4.

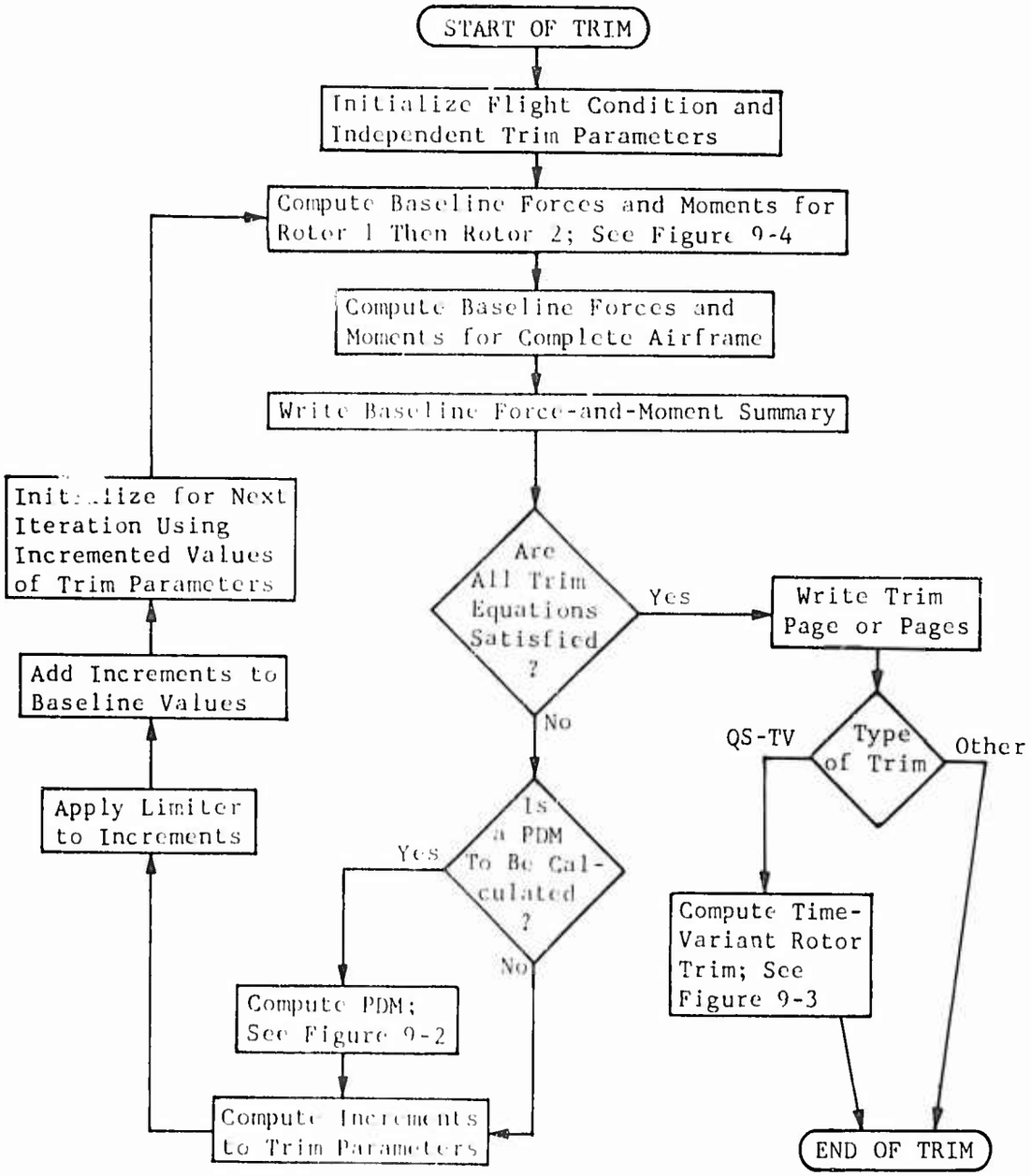

PDM = Partial Derivative Matrix
QS-TV = Quasi-Static Trim Followed by Time-Variant Rotor Trim

Figure 9-1. Flow Chart of Trim Procedure.

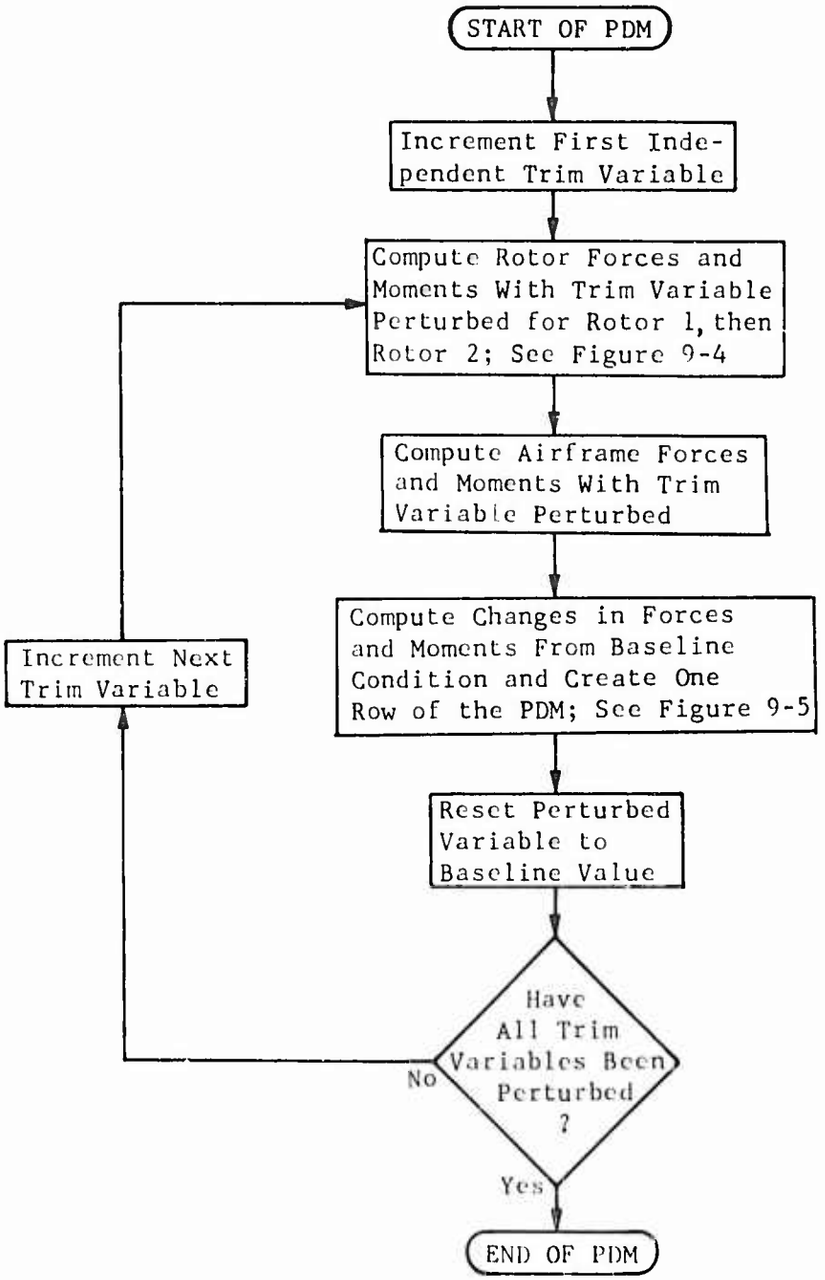

PDM = Partial Derivative Matrix

Figure 9-2. Flow Chart of Partial Derivative Matrix Computation.

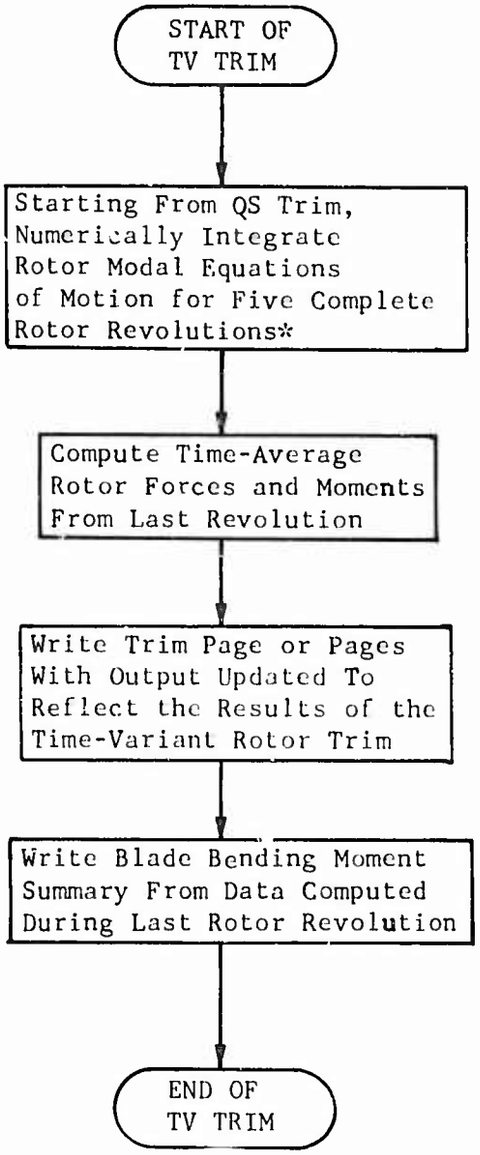

*Control positions and fuselage degrees of freedom held fixed at the final values computed during the QS trim.

Figure 9-3. Flow Chart of Time-Variant Rotor Trim.

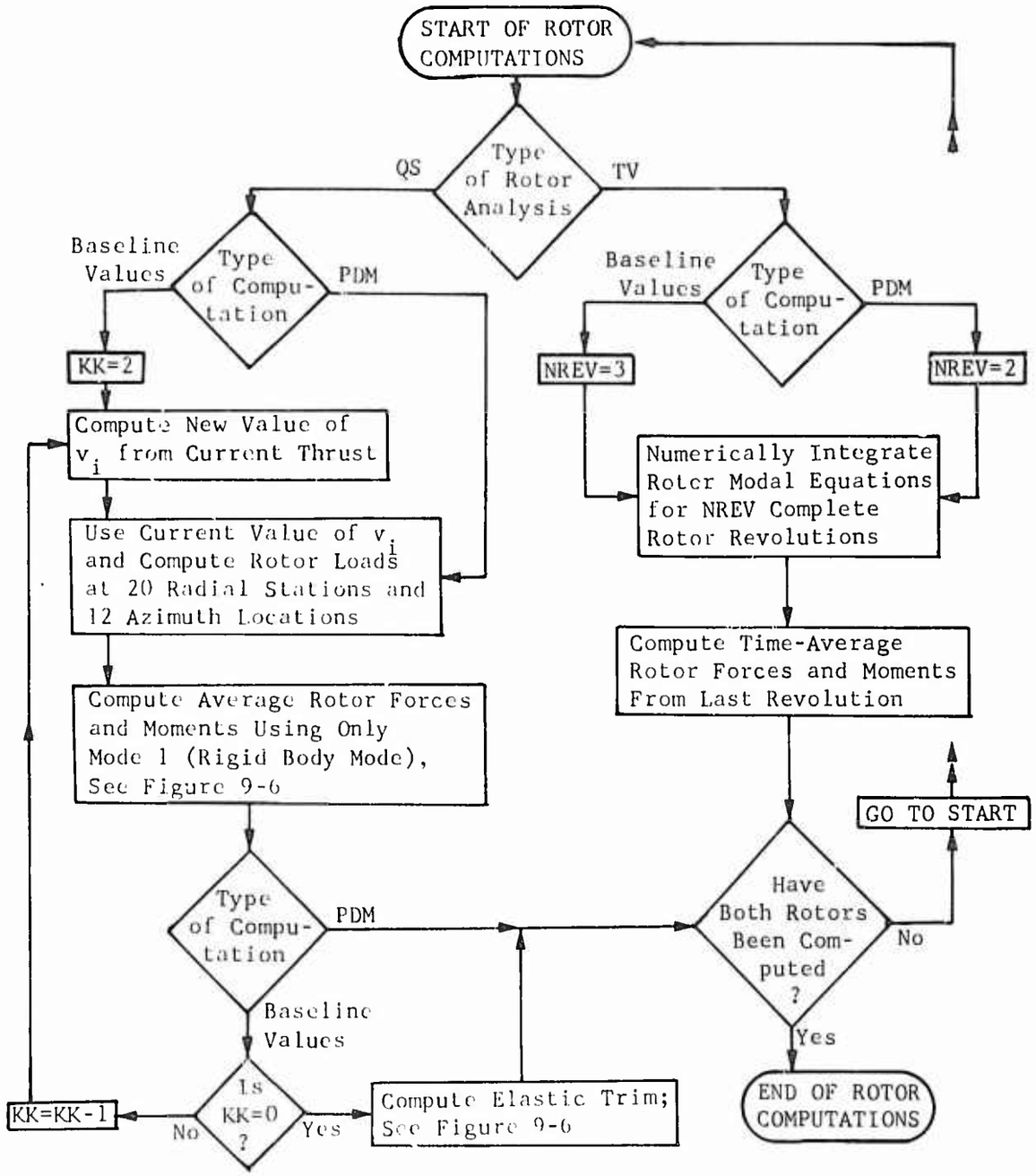

v_i = Rotor-Induced Velocity
PDM = Partial Derivative Matrix
KK = Thrust/v_i Looping Variable

QS = Quasi-Static Rotor Analysis
TV = Time-Variant Rotor Analysis
NREV = Number of Rotor Revolutions in TV Analysis

Figure 9-4. Flow Chart of Rotor Force and Moment Computations During Trim Procedures.

9.2 DEFINITION OF TRIMMED FLIGHT CONDITION

The inputs to all three trim procedures are identical: rotorcraft configuration and control positions, flight path orientation, atmospheric conditions, g-level, and type of flight (pull-up, turn, or unaccelerated). Trim is defined as that combination of appropriate independent trim parameters for which the summations of all external forces and moments (aerodynamic, gravitational, and inertial) about the center of gravity of the rotorcraft (due to both the rotor and the airframe) are less than a preassigned set of limits. For convenience, the body axis has been chosen as the reference system for the force and moment summation, and the summation actually consists of six independent summations: the X, Y, and Z forces and the pitch, roll, and yaw moments.

For each rotor which uses the quasi-static rotor analysis, there are two additional requirements for trim: the summations of F/A and lateral rotor moments acting at the hub (due to aerodynamic, dynamic, and gravitational forces and moments which have been averaged over the rotor disk) must also be less than a preassigned limit. These requirements are referred to, somewhat loosely, as the flapping-moment balance criteria, or equations. For a teetering or gimbaled rotor, this name implies that, for trim, the one-per-rev components of the flapping moment must be zero (or must balance any moment due to flapping restraint if such is present); i.e., the tip-path plane is not accelerating with respect to the rotor shaft. However, for rigid or articulated rotor configurations, the term flapping-moment balance is something of a misnomer; the condition actually being satisfied is that the tip-path is not accelerating with respect to the rotor shaft. These moment balance equations are discussed more fully in Section 9.3.3.

Hence, the mathematical definition of trim consists of three force and three moment summation equations for all external forces and moments acting on the rotorcraft plus two rotor-moment balance equations for each rotor which uses the quasi-static analysis, i.e., 6 to 10 equations. Since the tip-path plane is not a meaningful concept in the time-variant rotor analysis, rotor-moment balance equations for a rotor which uses that analysis are not included in the trim procedure as such. Rather, the moment balances are performed by numerically integrating the modal equations of motion of the rotor for an appropriate number of rotor revolutions. All ten possible trim equations are summarized in Table 9-1.

The independent trim variables which are used in all three trim procedures are the three Euler angles (which orient the body axis with respect to the fixed, or ground, reference system) and the positions of the four primary flight controls (collective, F/A cyclic, lateral cyclic, and pedals). When the quasi-static rotor analysis is used, the F/A and lateral flapping angles of the rotor which uses that analysis are also included as independent trim variables. As explained in Section 2.2.2, tip-path plane flapping angles are not independent variables in the time-variant rotor analysis; i.e., these angles cannot be included as independent trim variables for any rotor which uses this analysis. Hence, in the QS trim

TABLE 9-1. DEFINITION OF TRIM CONDITION

Definition	Description
$\lvert\Sigma L\rvert \leq \epsilon_1$	Total rolling moment about cg
$\lvert\Sigma M\rvert \leq \epsilon_2$	Total pitching moment about cg
$\lvert\Sigma N\rvert \leq \epsilon_2$	Total yawing moment about cg
$\lvert\Sigma F_x\rvert \leq \epsilon_3$	Total X-force at cg
$\lvert\Sigma F_y\rvert \leq \epsilon_4$	Total Y-force at cg
$\lvert\Sigma F_z\rvert \leq \epsilon_5$	Total Z-force at cg
$(M_{F/A})_1 \leq \epsilon_6$	F/A moment acting on Rotor 1 at its hub
$(M_{LAT})_1 \leq \epsilon_6$	Lateral moment acting on Rotor 1 at its hub
$(M_{F/A})_2 \leq \epsilon_7$	F/A moment acting on Rotor 2 at its hub
$(M_{LAT})_2 \leq \epsilon_7$	Lateral moment acting on Rotor 2 at its hub

L, M, N, F_x, F_y, and F_z are in the Body Reference System; $(M_{F/A})_i$ and $(M_{LAT})_i$ are in the Shaft Reference System of the ith rotor ϵ_j; j=1,2 ..., 7 represent the seven allowable errors input to the program

TABLE 9-2. INDEPENDENT TRIM VARIABLES

Symbol	Description
Ψ	Fuselage Euler Yaw Angle
Θ	Fuselage Euler Pitch Angle
Φ	Fuselage Euler Roll Angle
δ_{COLL}	Pilot's Collective Stick Position
$\delta_{F/A}$	Pilot's F/A Cyclic Stick Position
δ_{LAT}	Pilot's Lateral Cyclic Stick Position
δ_{PED}	Pilot's Pedal Position
$(a_1)_1$	F/A Flapping Angle of TPP for Rotor 1
$(b_1)_1$	Lateral Flapping Angle of TPP for Rotor 2
$(a_1)_2$	F/A Flapping Angle of TPP for Rotor 2
$(b_1)_2$	Lateral Flapping Angle TPP for Rotor 2

The flapping angles are with respect to the Rotor Shaft Reference System. For elastic blades they are based on Mode 1. TPP means tip-path plane.

(or QS portion of a QS-TV trim), there are 11 independent trim variables; while in the FTV trim, there will be 9 if only one rotor uses the time-variant analysis or 7 if both rotors use the time-variant analysis. These independent trim variables are summarized in Table 9-2.

9.3 METHODOLOGY OF THE TRIM PROCEDURE

9.3.1 Iterative Technique and Trim Parameters

A modification of the Newton-Raphson iterative technique is used to compute the desired trim condition. This technique, which is shown in the flow chart of Figure 9-1, consists of the following steps:

(1) Compute the forces and moments acting on the rotorcraft using the input (or current) values of the independent trim variables.

(2) If all force and moment summations (imbalances) are less than the input allowable errors (ϵ_i in Table 9-1), the rotorcraft is considered trimmed and the trim procedure ends; otherwise, compute a partial derivative matrix.

(3) Use the matrix and the imbalances to compute increments to the values of the independent trim variables.

(4) Add the increments to the previous values of the trim parameters, go back to Step (1), and continue the iterative process until the rotorcraft is trimmed or the maximum number of iterations is exceeded.

The key feature of this technique is the computation of the partial derivative matrix (see Figure 9-3). The computation of this matrix requires that the mathematical model of trim consist of an equal number of trim equations and independent trim variables. However, in the definition of trim given in the previous section and in Tables 9-1 and 9-2, the number of trim variables is always one more than the number of trim equations. Specifically, there are $7 + 2n$ variables and $6 + 2n$ equations, where n is the number of rotors which use the quasi-static analysis. Consequently, one of the independent trim variables must be eliminated (held constant) if the matrix is to be used to compute increments to the variables.

Since the flapping angles are not always included in the list of trim variables and all flight controls must normally be free to move, the choice of variables which can be held constant is limited to the Euler angles. Of these three angles, a pilot will normally be concerned with only the yaw (heading) or roll (bank) angles when trimming the rotorcraft (i.e., pitch attitude is a consequence of the desired flight condition, not a commanded condition itself). Since the mathematical procedure for computing the corrections to the trim variables is independent of the nature of the variables, the choice of which of these two angles is held constant has been made a user option. The user should consider the flight condition being simulated when specifying the angle to be held constant.

For example, pilots normally fly rotorcraft at constant heading, particularly at low airspeeds. However, at high airspeeds the pilot may be more apt to command a particular roll angle, such as zero in unaccelerated flight (or in a pull-up or pushover) or the bank angle associated with a desired g-level in a turn. In practice, a fixed yaw angle trim works well and is basically representative of actual flight at all airspeeds, while a fixed roll angle trim is only really suitable for flight above the speed for minimum power.

9.3.2 Computation of the Partial Derivative Matrix and Increments

The procedure for computing a partial derivative matrix (PDM) is shown in Figure 9-2 and can be described as follows:

(1) Perturb one of the independent trim variables from its baseline value.

(2) Compute the imbalance in each of the trim equations.

(3) Subtract the imbalances in the baseline condition from those in the perturbed condition.

(4) Divide each of the differences by the perturbation.

The complete PDM is generated by performing the above procedure for each independent trim variable.

The complete PDM is then used in conjunction with the force and moment imbalances of the baseline condition to compute increments to the independent trim variables. Each increment is compared to a maximum allowable change. The initial limit is an input; however, the limit is reduced as the imbalances get closer to the allowable errors. If any increment is larger than the limit, all increments are ratioed by the same factor, with the result being that the largest increment is equal to the limit. The increments are subsequently added to their corresponding value at the baseline condition.

If the system of equations in C81 were linear, the new values of the variables would trim the rotorcraft, i.e., reduce the imbalance to zero. However, the equations in C81 are not linear, and the program generally must repeat the above operations several times to reduce the imbalances to less than allowable errors.

The algebraic formulation of this trim procedure is shown in Figure 9-5 for the QS trim, i.e., 10 equations and 10 trim variables. However, the method of computation is the same for the 8 by 8, or the 6 by 6, system of equations used in the FTV trim. The formulation can be expressed by the following matrix equation:

$$\left[PDM_{ij}\right] \times \left[\Delta y_j\right] = \left[-(x_i)_B\right] \qquad (9\text{-}1)$$

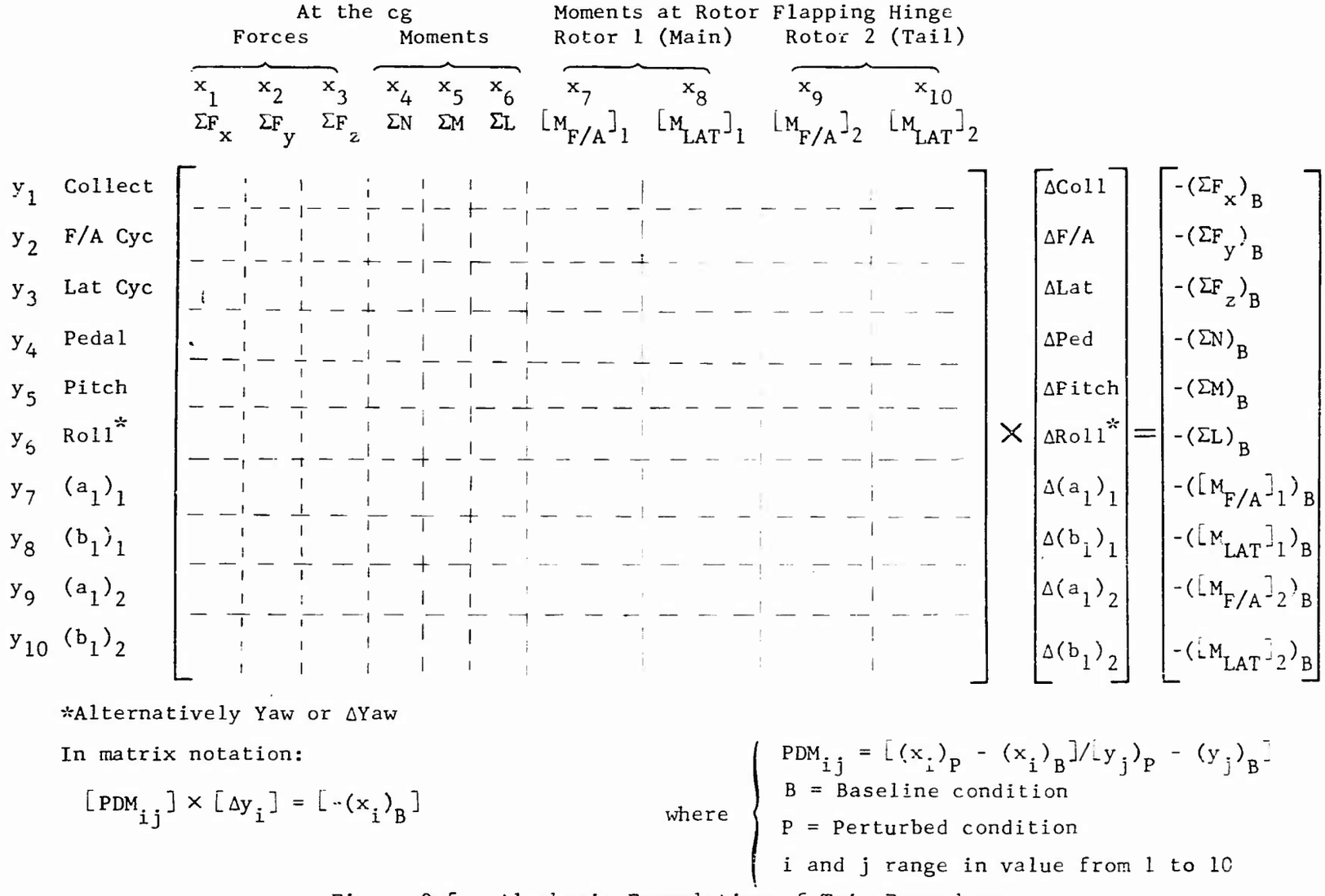

*Alternatively Yaw or ΔYaw

In matrix notation:

$$[PDM_{ij}] \times [\Delta y_i] = [-(x_i)_B]$$

where

$PDM_{ij} = [(x_i)_P - (x_i)_B]/[(y_j)_P - (y_j)_B]$

B = Baseline condition

P = Perturbed condition

i and j range in value from 1 to 10

Figure 9-5. Algebraic Formulation of Trim Procedure.

where PDM_{ij} is the square partial derivative matrix (a 10 by 10 matrix for the QS trim),

$[\Delta y_j]$ is the matrix of increments to the independent trim variables, y_j (a 10 by 1 matrix for the QS trim), and

$[-(x_i)_B]$ is the matrix of the negatives of the force and moment imbalances, x_i, at the baseline flight condition (a 10 by 1 matrix for the QS trim).

The value of each element in PDM_{ij} is computed as follows:

$$PDM_{ij} = \left[(x_i)_P - (x_i)_B\right] \Big/ \left[(y_j)_P - (y_j)_B\right] \tag{9-2}$$

where the subscript B indicates the baseline condition and P the perturbed condition. Hence, each time one of the values of y_j is perturbed, the resulting calculations generate one row of the partial derivative matrix. If the perturbations are small and the equations are nearly linear over the range of the perturbation, then

$$PDM_{ij} \approx \partial x_i / \partial y_i \tag{9-3}$$

The ten equations in ten unknowns represented by Equation (9-1) are then solved for the values of Δy_j by Gauss reduction (Reference 19, Chapter 10.3). Subject to the limiting technique discussed earlier, the values of Δy_j are then added to the previous values of the trim variables to obtain a better approximation of the final trim condition to be used for the next trim iteration. The iterative process is continued until all trim requirements are satisfied

9.3.3 Rotor Force and Moment Computations

The flow charts in both Figures 9-1 and 9-2 include a block for computing the rotor forces and moments. Details of the computations within this block are shown in Figure 9-4. The primary factor affecting the path of the program through the rotor computations is the type of rotor analysis which is to be used. For the QS trim (and QS portion of a QS-TV trim), the QS path in Figure 9-4 is followed for both rotors. For the FTV trim, the TV path is followed only if the rotor in question is to use the time-variant rotor analysis. When only one rotor is to be time-variant in the FTV trim, the other rotor follows the QS path.

Regardless of the path chosen, the next decision is whether the forces and moments to be computed are for the baseline values of an iteration or for a PDM. In the QS path this decision determines whether or not the thrust/induced-velocity iteration loop and the elastic trim routine are

to be used. (They are used for baseline values; they are not used for the PDM). In the TV path the decision determines the number of rotor revolutions to be made in the numerical integration of the modal equations. (Computation of baseline values uses 3 revolutions; computation of a PDM uses 2).

A flow chart of the elastic trim technique is shown in Figure 9-6. This technique is used to include the steady and one-per-rev components of blade elasticicty in the quasi-static analysis. The procedure consists of performing a harmonic analysis of the virtual work done by the airloads on the mode shapes. The virtual work for the i^{th} mode shape is defined as

$$VW_i(\psi) = \int_0^R F(x,\psi)\ \delta_i\ dx/I_i \qquad (9\text{-}4)$$

where $F(x, \psi)$ is the summation of the aerodynamic, dynamic, and gravitational forces,

x is the blade station,

ψ is the blade azimuth location,

δ_i is the participation factor of the i^{th} mode, and

I_i is the generalized inertia of the i^{th} mode.

From the harmonic analysis of the virtual work parameters, only the steady one-per-rev components are retained, such that

$$VW_i(\psi) = A_{o_i} + A_{lc_i} \cos\psi + A_{ls_i} \sin\psi \qquad (9\text{-}5)$$

where A_{o_i}, A_{lc_i}, and A_{ls_i} are the coefficients generated by the analysis.

The modal participation factor is then truncated to a first harmonic series:

$$\delta_i(\psi) = \delta_{o_i} + \delta_{lc_i} \cos\psi + \delta_{ls_i} \sin\psi \qquad (9\text{-}6)$$

Substituting Equations (9-5) and (9-6) into the modal equations of motion,

$$\delta_i + 2\zeta\omega_{n_i}\delta_i + \omega_{n_i}^2\delta_i = VW_i \qquad (9\text{-}7)$$

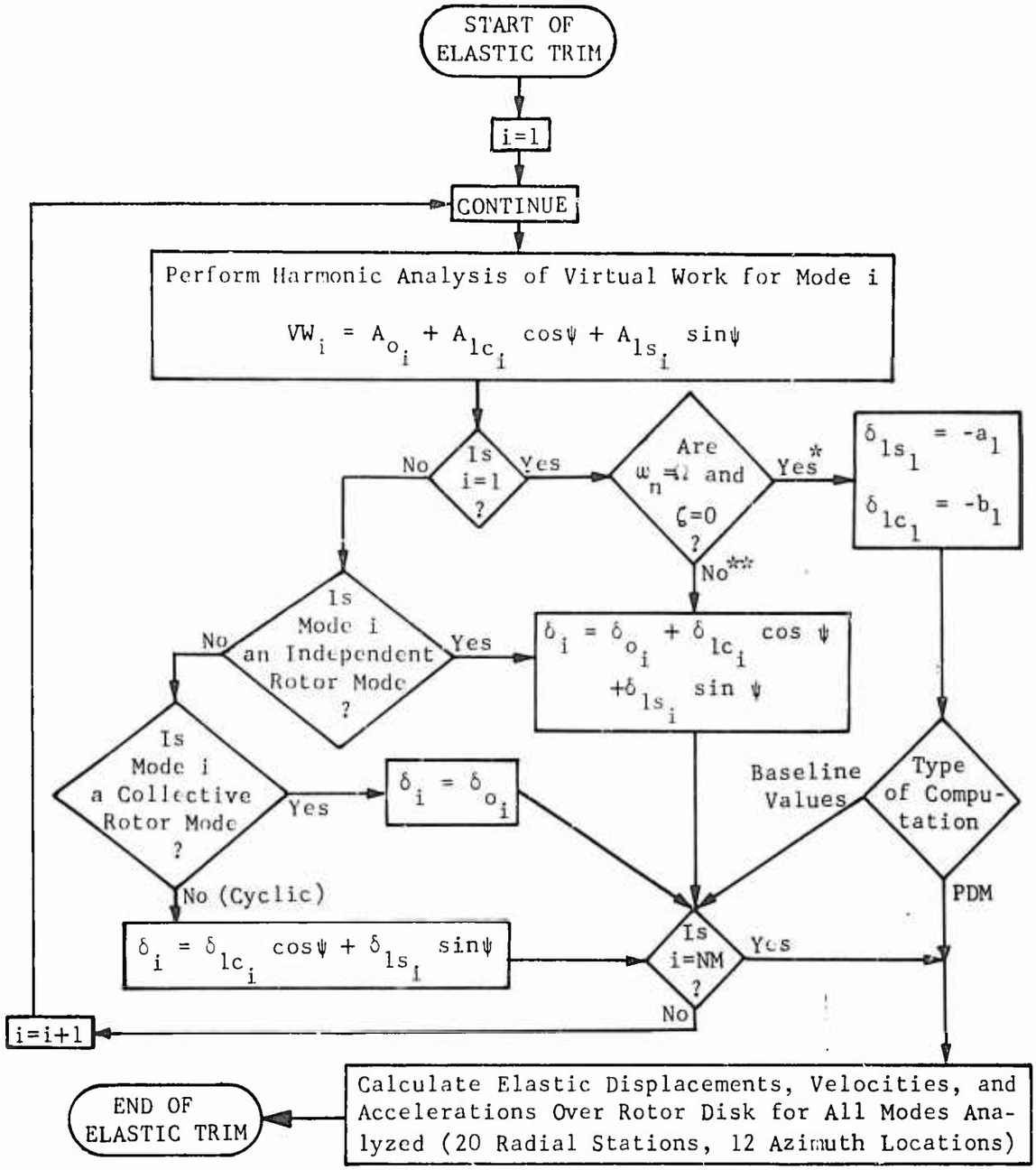

*Gimbaled Rotor **Rigid or Articulated Rotor

NM = Number of Modes
ζ = Damping Ratio
ω_n = Natural Frequency
PDM = Partial Derivative Matrix
a_1 = F/A Flapping Angle
b_1 = Lateral Flapping Angle

δ_{o_i}, δ_{lc_i}, δ_{ls_i}: See Equations (9-8), (9-9), and (9-10), respectively.

Figure 9-6. Elastic Trim Technique.

yields the following:

$$\delta_{o_i} = A_{o_i} / \omega_{n_i}^2 \tag{9-8}$$

$$\delta_{lc_i} = \left[A_{lc_i} (\omega_{n_i}^2 - \Omega^2) - A_{ls_i} (2 \zeta \omega_{n_i} \Omega) \right] \Big/ \text{Denom} \tag{9-9}$$

$$\delta_{ls_i} = \left[A_{ls_i} (\omega_{n_i}^2 - \Omega^2) + A_{lc_i} (2 \zeta \omega_{n_i} \Omega) \right] \Big/ \text{Denom} \tag{9-10}$$

$$\text{Denom} = (\omega_{n_i}^2 - \Omega^2)^2 + (2 \zeta \omega_{n_i} \Omega)^2 \tag{9-11}$$

where ω_{n_i} is the natural frequency of the i^{th} mode (rad/sec),

Ω is the rotor speed (rad/sec), and

ζ is the nondimensional damping ratio of the mode.

Finally, the elastic displacements, velocities, and accelerations over the rotor disk due to these participation factors are computed and used. This routine provides reasonable starting values for all modal participation factors when a time-variant rotor trim (the TV portion of a QS-TV trim) or a time-variant maneuver follows a QS trim. Without the elastic trim routine these participation factors would have to be assumed to be zero, which would increase the magnitude of the transient rotor motion which occurs when the program switches from the quasi-static to the time-variant rotor analysis.

The participation factors output from the elastic trim routine are also used in the computation of the rotor moments which must be balanced as part of the QS trim procedure (see Section 9.2). The rotor moments computed at each of the 12 azimuth locations of the quasi-static rotor analysis are subjected to a harmonic analysis like that performed on the virtual work in the elastic trim routine. Discarding the higher harmonics, the moment is expressed as

$$M(\psi) = M_o + M_{lc} \cos\psi + M_{ls} \sin\psi \tag{9-12}$$

Equating like harmonics then yields the following expressions for the F/A and lateral rotor moments about the hub:

$$M_{F/A} = M_{lc} - \sum_{i=1}^{NM} (BBMC_i \, \delta_{lc_i}) - (M_H)_{F/A} \tag{9-13}$$

$$M_{LAT} = M_{1s} - \sum_{i=1}^{NM} (BBMC_i \, \zeta_{1s_i}) - (M_H)_{LAT} \qquad (9\text{-}14)$$

where $BBMC_i$ is the blade bending moment coefficient at the hub for the i^{th} mode,

NM is the number of modes, and

M_H is the moment (F/A and lateral) at the hub due to flapping restraint and/or stops.

In the QS trim procedure, it is these two moments which must be less than the input limits (ϵ_6 or ϵ_7 in Table 9-1) for the rotor to be considered trimmed.

For a teetering or gimbaled rotor without flapping restraint (hub spring), there is no moment transfer from the hub to the rotor shaft. Hence, BBMC is zero, and $M_{F/A}$ and M_{LAT} can properly be termed flapping moments. For a rigid or articulated rotor, BBMC is normally nonzero and the restraint at the hub is included in the mode shapes, not as a hub spring (i.e., $(M_H)_{F/A}$ and $(M_H)_{LAT}$ both equal zero).

One of the implications of Equations (9-13) and (9-14) is that with appropriate inputs to the QS trim, a rigid or articulated rotor can be modeled as a gimbaled rotor with rigid blades and a hub spring that simulates the rotor mode shapes. Obviously, this approximation is not suitable for dynamic analyses where blade loads, etc., are required; however, it can be useful in performance and stability analyses when complete mode shape data are not available.

9.3.4 Programming and Running Considerations

The overall trim procedure has been developed to iterate to a trimmed flight condition in a minimum amount of computer time. Since the rotor calculations are the most time consuming operation of the procedure, the number of times that these calculations must be performed is held to a minimum. For example, in a QS trim, the computation of the PDM does not include the thrust/induced-velocity iteration loop or the elastic trim routine used in the computation of the baseline forces and moments of the rotor. Although their inclusion would create a more accurate PDM, the increased accuracy does not necessarily reduce the number of iterations required to trim and generally increases rather than decreases overall run time. Similarly, the number of rotor revolutions used with the time-variant rotor analysis is 5 in the TV portion of the QS-TV trim, but only 3 in the computation of the baseline values, and only 2 in the computation of the PDM in the FTV trim because the increased number of revolutions does not shorten the run time in the FTV trim.

In terms of computer time required to achieve trim, the QS trim is always the fastest procedure. Since the TV portion of a QS-TV trim is essentially a post-processor to a QS trim, a QS-TV trim will obviously take longer than a QS trim. The FTV trim will take the longest of all. Because of the marked differences in the QS and FTV trim procedures and the many rotorcraft configuration variables, it is impossible to estimate the relative run times of the two procedures, even for the same configuration starting at the same point. However, it is strongly recommended that all the inputs for the trim variables in FTV trims be obtained from previously computed QS or QS-TV trims for the identical flight condition and rotorcraft configuration.

Although past use of the program has shown that the trim procedure can generally iterate to a trimmed flight condition from most any reasonable combination of guessed inputs, the user should choose inputs that are as close to the trim condition as possible to insure a successful trim and to minimize the computer time required to trim. One of the more common reasons for failure of the program to trim is starting with too high a collective stick position, i.e., with the rotor in a stalled condition. If the rotor is stalled, the partial derivative matrix is likely to indicate that up collective will reduce rotor thrust (which it could well do in a stalled condition) while also increasing rotor torque. The result of this apparent control reversal may be a fictitious trim at a very high power level (somewhat equivalent to trimming on the backside of the power curve) or, more likely, no trim at all. Hence, while the trim procedure is basically forgiving, it can run into problems when gross nonlinearities are encountered.

9.4 ROTOR-ONLY TRIM PROCEDURE

It is not mandatory that C81 simulate an entire rotorcraft system. Frequently, it is desirable to simulate an isolated rotor, e.g., a wind tunnel simulation. A special path has been included in the general trim procedure to provide for such rotor-only simulations in conjunction with the quasi-static rotor analysis. For a rotor-only trim, all references to the fuselage force and moment balances are deleted. That is, the user sets ϵ_1 through ϵ_5 in Table 9-1 so large that the first six (total rotorcraft) trim equations are effectively deleted from the trim procedure. The allowable errors for the flapping moment imbalances (ϵ_6 for Rotor 1, ϵ_7 for Rotor 2) are kept at realistic values. Also, the two rotors are decoupled from each other, which in effect reduces the single 10 by 10 matrix in Figure 9-3 to a pair of 2 by 2 matrices. It is not necessary, or normal, that both rotors be included in a rotor-only trim. Assuming the second rotor is deleted, the 10 by 10 matrix then reduces to a single 2 by 2 matrix. The independent variables for reducing the flapping moments may then be either the fore-and-aft and lateral shaft-axis flapping angles or the fore-and-aft and lateral blade feathering angles. When the flapping angles are the independent variables, the

case is equivalent to letting the rotor seek a new equilibrium flapping condition for a prescribed set of blade feathering angles. When the feathering angles are the independent variables, the case is equivalent to letting the rotor control seek the values which will cause a prescribed set of flapping angles. The latter case is particularly useful in simulating wind tunnel tests where data are measured at specified flapping angles rather than control positions. The former case can also be useful during a total rotorcraft trim when difficulty is encountered in trimming the entire rotorcraft system with the 10 by 10 matrix. Either or both sets of rotor equations may be decoupled and allowed to trim within one conventional trim iteration.

It should be emphasized that the rotor-only procedure described here cannot be used for a time-variant rotor since the flapping angles and rotor moments on which it is based do not exist in the time-variant analysis. However, the equivalent of the trim at specified blade feathering angles can be performed with the QS-TV or FTV trim by using appropriate dummy inputs for the fuselage and aerodynamic surfaces. As another alternative, the allowable errors can be set very large so that the program will immediately "drop through" the trim procedure, and a time-variant maneuver with an appropriate number of rotor revolutions can be performed at fixed feathering angles.

A second (optional) trim page has been added to the program to present significant rotor performance data that are useful in analyzing wind tunnel simulations and are not printed as part of the standard trim page. The data are in both dimensional and nondimensional forms. A summary of the rotor and tunnel parameters, and the rotor bending moments are also printed. This optional page may be printed following either a total rotorcraft or rotor-only trim.

10. STABILITY ANALYSIS

10.1 INTRODUCTION

The principal objective of this section is to present a basis for evaluating each element in a 14-degree-of-freedom system characteristic determinant. The application of perturbation theory as presented herein follows the development given in Reference 24.

The first form of the stability analysis programmed as a subroutine in C81 was based on six rigid body degrees of freedom of the fuselage with rotor effects introduced as additional terms. The original analysis was performed assuming two decoupled systems of three equations each and then combining these six equations into a representation of a single coupled system. Later, eight more equations which are representative of rotor and pylon degrees of freedom were introduced. The system discussed herein consists of the six fuselage degrees of freedom and the additional rotor and pylon degrees of freedom: fore-and-aft and lateral pylon rotations relative to the fuselage for each of two pylons, and fore-and-aft and lateral rotor flapping motions relative to the pylon (shaft) for each of two rotors. The resulting set of 14 equations (see Table 10-1) of rigid body motion are presented herein, associated symbols are defined, and the procedure of analysis is delineated.

10.2 STABILITY ANALYSIS EQUATIONS

The basic stability analysis equations correspond to the equations of motion used in the calculations of maneuver time histories. However, it is convenient in the stability analysis to represent the rotors with two equations each, one for fore-and-aft flapping and one for lateral flapping.

The equations in Table 10-1 reduce to the usual equations of motion if

$$G_i = 0 \qquad i = 1,2, \ldots, 14 \tag{10-1}$$

except for the aerodynamic coefficients of $\dot{W}$ in the fuselage group.

For i = 1,2, ..., 6, 9, 10, 13, and 14, the equations are the same as given for the rigid body fuselage and the rotor flapping components developed in Reference 1, except as noted above. The fuselage equations are ordered so that the first three reduce to the traditional "longitudinal" equations when decoupled from the rest of the system. Similarly, the next three equations reduce to the "lateral" equations. For i=7, 8, 11, 12, the equations are the same as the pylon equations developed in Section 3.2.9.

The perturbation method requires representation of the partial derivatives of the G_i with respect to the fourteen base variables and their first and second derivatives. Some of these derivatives can be evaluated only by way of auxiliary equations relating the base variables to secondary variables. The weight components, W_x, W_y and W_z, are denoted explicitly

TABLE 10-1. STABILITY ANALYSIS EQUATIONS

FUSELAGE

$$G_1 = m(\dot{U} + QW - RV) - F_x - W_x$$

$$G_2 = m(\dot{W} + PV - QU) - F_z - W_z - Z_{\dot{w}}\dot{W}$$

$$G_3 = I_y\dot{Q} + RP(I_x - I_z) + I_{xz}(P^2 - R^2) - M - M_{\dot{w}}\dot{W}$$

$$G_4 = m(\dot{V} + RU - PW) - F_y - W_y - Y_{\dot{w}}\dot{W}$$

$$G_5 = I_x\dot{P} - I_{xz}\dot{R} + QR(I_z - I_y) - I_{xz}PQ - L - L_{\dot{w}}\dot{W}$$

$$G_6 = I_z\dot{R} - I_{xz}\dot{P} + PQ(I_y - I_z) + I_{xz}QR - N - N_{\dot{w}}\dot{W}$$

MAIN (FIRST) PYLON

$$G_7 = I_{FM}(\ddot{A}_{FM} - \dot{Q}_{SM}) + C_{FM}\dot{A}_{FM} + K_{FM}A_{FM} - M_{PM}$$

$$G_8 = I_{LM}(\ddot{A}_{LM} + \dot{P}_{SM}) + C_{LM}\dot{A}_{LM} + K_{LM}A_{LM} - L_{PM}$$

MAIN (FIRST) ROTOR

$$G_9 = I_{RM}(-\ddot{A}_{1M} - \dot{Q}_{SM}) - 2\Omega_M(\dot{B}_{1M} + P_{SM}) - M_{RM}$$

$$G_{10} = I_{RM}(-\ddot{B}_{1M} - \dot{P}_{SM}) + 2\Omega_M(\dot{A}_{1M} + Q_{SM}) - L_{RM}$$

TAIL (SECOND) PYLON

$$G_{11} = I_{FT}(\ddot{A}_{FT} - \dot{Q}_{ST}) + C_{FT}\dot{A}_{FT} + K_{FT}A_{FT} - M_{PT}$$

$$G_{12} = I_{LT}(\ddot{A}_{LT} + \dot{P}_{ST}) + C_{LT}\dot{A}_{LT} + K_{LT}A_{LT} - L_{PT}$$

TAIL (SECOND) ROTOR

$$G_{13} = I_{RT}(-\ddot{A}_{1T} - \dot{Q}_{ST}) - 2\Omega_T(\dot{B}_{1T} + P_{ST}) - M_{RT}$$

$$G_{14} = I_{RT}(-\ddot{B}_{1T} - \dot{P}_{SM}) + 2\Omega_T(\dot{A}_{1T} + Q_{ST}) - L_{RT}$$

so that their partial derivatives can be evaluated analytically. The effects of rate of change of angle of attack are also included explicitly as coefficients of $\dot{W}$ in G_2, G_3, G_4, G_5, and G_6. It is assumed that, except for these five terms, the aerodynamic forces and moments are not functions of the acceleration variables.

10.3 AUXILIARY EQUATIONS

Five reference systems involved in the stability analysis are

Ground, or Fixed
Body, or Fuselage
Main (First) Pylon Shaft
Tail (Second) Pylon Shaft
Wind (Section 10.6.3)

An ordered set of angular rotations (Ψ, Θ, Φ) relating the body reference system to the fixed reference as described in Reference 24 is called the "fuselage Euler angles." Note that in the following discussions, the names Body and Fuselage Reference are used synonymously. Similar sets are used to relate each pylon shaft reference system to the fuselage. The pylon angular deflections relative to the shaft reference (A_{FM}, A_{LM} for the main pylon and A_{FT}, A_{LT} for the tail pylon) are treated as rotations about the shaft x-axis and the shaft y-axis rather than as parts of an ordered set. The rotor tip-path plane flapping components (A_{1M}, B_{1M} for the main rotor and A_{1T}, B_{1T} for the tail rotor) are also represented as rotations about the shaft axes. The Euler angle velocities as functions of fuselage rotation velocity components (P, Q, R) and the transformations of components from one reference frame to another require the following group of auxiliary relationships.

10.3.1 Fuselage Euler Angle Velocities in Body Reference System

$$\dot{\Psi} = (Q \sin \Phi + R \cos \Phi) \sec \Theta \tag{10-2}$$

$$\dot{\Theta} = Q \cos \Phi - R \sin \Phi \tag{10-3}$$

$$\dot{\Phi} = P + (Q \sin \Phi + R \cos \Phi) \tan \Theta \tag{10-4}$$

10.3.2 Weight Components in Body Reference System

The fuselage Euler angle transformation matrix, T, given in Reference 1, is used to evaluate the components of the weight vector in the fuselage body reference system. Since $\Psi = 0$ in this case,

$$\left[T(0, \Theta, \Phi) \right] = \begin{bmatrix} \cos \Theta & \sin \Theta \sin \Phi & \sin \Theta \cos \Phi \\ 0 & \cos \Phi & -\sin \Phi \\ -\sin \Theta & \cos \Theta \sin \Phi & \cos \Theta \cos \Phi \end{bmatrix} \tag{10-5}$$

Then

$$[W_x \; W_y \; W_z] = [0 \; 0 \; mg][T(0, \Theta, \Phi)] \tag{10-6}$$

10.3.3 Body Angular Velocity and Acceleration Components in Pylon (Rotor) Shaft Reference Systems

Let Θ_M = the main rotor shaft tilt fore-and-aft, positive forward

Φ_M = the main rotor shaft tilt lateral, positive right

and similarly Θ_T and Φ_T for the tail rotor. Then

$$\left[P_{SM} \; Q_{SM} \; R_{SM}\right] = [P \; Q \; R] \; [T(0, -\Theta_M, \Phi_M)] \tag{10-7}$$

$$\left[\dot{P}_{SM} \; \dot{Q}_{SM} \; \dot{R}_{SM}\right] = [\dot{P} \; \dot{Q} \; \dot{R}] \; [T(0, -\Theta_M, \Phi_M)] \tag{10-8}$$

$$\left[P_{ST} \; Q_{ST} \; R_{ST}\right] = [P \; Q \; R] \; [T(0, -\Theta_T, -\Phi_T)] \tag{10-9}$$

$$\left[\dot{P}_{ST} \; \dot{Q}_{ST} \; \dot{R}_{ST}\right] = [\dot{P} \; \dot{Q} \; \dot{R}] \; [T(0, -\Theta_T, -\Phi_T)] \tag{10-10}$$

Elements of $T(0,-\Theta_M, \Phi_M)$ are denoted $T_{M_{ij}}$, so that, for example,

$$P_{SM} = PT_{M_{11}} + RT_{M_{31}} \tag{10-11}$$

10.4 INDEXED NOTATION

For convenience in developing the stability analysis, an indexed notation is introduced. Body displacement variables are supplied in the form of velocity integrals.

10.4.1 Basic Variables

$$\begin{aligned}
\bar{x}_1 &= \int U dt & \dot{\bar{x}}_1 &= U & \ddot{\bar{x}}_1 &= \dot{U} \\
\bar{x}_2 &= \int W dt & \dot{\bar{x}}_2 &= W & \ddot{\bar{x}}_2 &= \dot{W} \\
\bar{x}_3 &= \int Q dt & \dot{\bar{x}}_3 &= Q & \ddot{\bar{x}}_3 &= \dot{Q}
\end{aligned} \tag{10-12}$$

$$\bar{x}_4 = \int V dt \qquad \dot{\bar{x}}_4 = V \qquad \ddot{\bar{x}}_4 = \dot{V}$$

$$\bar{x}_5 = \int P dt \qquad \dot{\bar{x}}_5 = P \qquad \ddot{\bar{x}}_5 = \dot{P}$$

$$\bar{x}_6 = \int R dt \qquad \dot{\bar{x}}_6 = R \qquad \ddot{\bar{x}}_6 = \dot{R}$$

$$\bar{x}_7 = A_{FM} \qquad \dot{\bar{x}}_7 = \dot{A}_{FM} \qquad \ddot{\bar{x}}_7 = \ddot{A}_{FM}$$

$$\bar{x}_8 = A_{LM} \qquad \dot{\bar{x}}_8 = \dot{A}_{LM} \qquad \ddot{\bar{x}}_8 = \ddot{A}_{LM}$$

$$\bar{x}_9 = A_{lM} \qquad \dot{\bar{x}}_9 = \dot{A}_{lM} \qquad \ddot{\bar{x}}_9 = \ddot{A}_{lM} \qquad (10\text{-}12)$$

$$\bar{x}_{10} = B_{lM} \qquad \dot{\bar{x}}_{10} = \dot{B}_{lM} \qquad \ddot{\bar{x}}_{10} = \ddot{B}_{lM}$$

$$\bar{x}_{11} = A_{FT} \qquad \dot{\bar{x}}_{11} = \dot{A}_{FT} \qquad \ddot{\bar{x}}_{11} = \ddot{A}_{FT}$$

$$\bar{x}_{12} = A_{LT} \qquad \dot{\bar{x}}_{12} = \dot{A}_{LT} \qquad \ddot{\bar{x}}_{12} = \ddot{A}_{LT}$$

$$\bar{x}_{13} = A_{lT} \qquad \dot{\bar{x}}_{13} = \dot{A}_{lT} \qquad \ddot{\bar{x}}_{13} = \ddot{A}_{lT}$$

$$\bar{x}_{14} = B_{lT} \qquad \dot{\bar{x}}_{14} = \dot{B}_{lT} \qquad \ddot{\bar{x}}_{14} = \ddot{B}_{lT}$$

10.4.2 Auxiliary Variables

$$\bar{y}_1 = \Psi \qquad \dot{\bar{y}}_1 = \dot{\Psi} \qquad \dot{\bar{y}}_4 = P_{SM} \qquad \ddot{\bar{y}}_4 = \dot{P}_{SM}$$

$$\bar{y}_2 = \Theta \qquad \dot{\bar{y}}_2 = \dot{\Theta} \qquad \dot{\bar{y}}_5 = Q_{SM} \qquad \ddot{\bar{y}}_5 = \dot{Q}_{SM} \qquad (10\text{-}13)$$

$$\bar{y}_3 = \Phi \qquad \dot{\bar{y}}_3 = \dot{\Phi} \qquad \dot{\bar{y}}_6 = R_{SM} \qquad \ddot{\bar{y}}_6 = \dot{R}_{SM}$$

10.4.3 Applied Forces and Moments

$$F_1 = F_x \qquad F_5 = L \qquad F_9 = M_{RM} \qquad F_{13} = M_{RM}$$

$$F_2 = F_z \qquad F_6 = N \qquad F_{10} = L_{RM} \qquad F_{14} = L_{RM} \qquad (10\text{-}14)$$

$$F_3 = M \qquad F_7 = M_{PM} \qquad F_{11} = M_{PT}$$

$$F_4 = F_y \qquad F_8 = L_{PM} \qquad F_{12} = L_{PT}$$

10.4.4 The Perturbation Variables

Each base variable is represented as the sum of the initial value, $\bar{x}_{i_o}$, and an increment, $\Delta\bar{x}_i$. Denote $\bar{x}_{i_o}$ as x_{i_o} and $\Delta\bar{x}_i$ as x_i. Then

$$\bar{x}_i = x_{i_o} + x_i \; ; \; \dot{\bar{x}} = \dot{x}_{i_o} + \dot{x}_i \; ; \; \ddot{\bar{x}} = \ddot{x}_{i_o} + \ddot{x}_i \tag{10-15}$$

The x_i, $\dot{x}_i$, and $\ddot{x}_i$ are the basic perturbation variables. Similarly, for the auxiliary variables,

$$\bar{y}_i = y_{i_o} + y_i \; ; \; \dot{\bar{y}}_i = \dot{y}_{i_o} + \dot{y}_i \; ; \; \ddot{\bar{y}}_i = \ddot{y}_{i_o} + \ddot{y}_i \tag{10-16}$$

In the notation of Table 10-1, the uppercase symbols correspond to the $\bar{x}$'s and $\bar{y}$'s. Lowercase symbols are used elsewhere for the initial and incremental parts. Thus,

$$U = u_o + u \; , \quad V = v_o + v \; , \quad \text{etc.} \tag{10-17}$$

10.5 THE EIGENVALUE SOLUTION

The equations of motion are nonlinear in the basic variables and thus do not admit of a direct eigenvalue solution. They are linearized by considering a perturbation about an initial condition specified by the x_{j_o}, $\dot{x}_{j_o}$, and $\ddot{x}_{j_o}$. The equations of motion can be written

$$G_i\left(\bar{x}_j, \dot{\bar{x}}_j, \ddot{\bar{x}}_j, \bar{y}_k, \dot{\bar{y}}_k, \ddot{\bar{y}}_k\right) = 0, \tag{10-18}$$

where

$$i = 1, 2, \ldots, 14$$

$$j = 1, 2, \ldots, 14$$

$$k = 1, 2, \ldots, 6$$

or, since the $\bar{y}$ variables are functions of the $\bar{x}$ variables, the equations can be specified as

$$G_i\left(\bar{x}_j, \dot{\bar{x}}_j, \ddot{\bar{x}}_j\right) = 0 \tag{10-19}$$

The total differential of G_i can be expressed in terms of the base variables as

$$dG_i = \sum_j \frac{\partial G_i}{\partial x_j}\bigg|_o x_j + \sum_j \frac{\partial G_i}{\partial \dot{x}_j}\bigg|_o \dot{x}_j + \sum_j \frac{\partial G_i}{\partial \ddot{x}_j}\bigg|_o \ddot{x}_j = 0 \tag{10-20}$$

in which the partial derivatives are evaluated at the initial values, x_{j_o}.

Assume $x_j = x_{j_{oo}} e^{\lambda t}$. Then the equation represented by Equation (10-20) can be written as

$$\sum_j \left(\frac{\partial G_i}{\partial \ddot{x}_j} \bigg|_o \lambda^2 + \frac{\partial G_i}{\partial \dot{x}_j} \bigg|_o \lambda + \frac{\partial G_i}{\partial x_j} \bigg|_o \right) x_j = 0 \qquad (10\text{-}21)$$

The determinant of the coefficients is the characteristic determinant.

The solution procedure (Reference 25) used to compute eigenvalues and eigenvectors from the determinant of Equation (10-21) requires inputs specified as elements of the mass, damping, and stiffness matrices, respectively. These elements are

$$M_{ij} = \frac{\partial G_i}{\partial \ddot{x}_j} \bigg|_o \qquad (10\text{-}22)$$

$$C_{ij} = \frac{\partial G_i}{\partial \dot{x}_j} \bigg|_o \qquad (10\text{-}23)$$

$$K_{ij} = \frac{\partial G_i}{\partial x_j} \bigg|_o \qquad (10\text{-}24)$$

10.6 EVALUATION OF THE PARTIAL DERIVATIVES

The partial derivatives in Equation (10-21) are to be evaluated at the initial condition as indicated by the subscript o. There are

$$3 \times 14 \times 14 = 588$$

elements in the full set of partial derivatives. The discussion of their evaluation, which follows, is intended to be illustrative rather than exhaustive.

10.6.1 The Euler Angle Relationships

The relationships between the set of Euler angle perturbations, Ψ, Θ, and Φ, and the base perturbations, x_3, x_5, and x_6, are developed from Equations (10-2), (10-3), and (10-4).

In terms of the perturbation variables, the total differential of $\dot{\Theta}$ is, from Equation (10-3),

$$d\dot{\Theta} = \frac{\partial \dot{\Theta}}{\partial Q} dQ + \frac{\partial \dot{\Theta}}{\partial R} dR + \frac{\partial \dot{\Theta}}{\partial \Phi} d\Phi \tag{10-25}$$

or

$$d\dot{\Theta} = \cos \Phi \, dQ - \sin \Phi \, dR - (Q \sin \Phi + R \cos \Phi) d\Phi \tag{10-26}$$

In the perturbation notation,

$$\dot{\theta} = q \cos (\phi_o + \phi) - r \sin (\phi_o + \phi) - [(q_o + q) \sin (\phi_o + \phi) + (r_o + r) \cos (\phi_o + \phi)] \phi \tag{10-27}$$

The following approximations are used:

$$\cos (\phi_o + \phi) \approx \cos \phi_o - \phi \sin \phi_o$$
$$\sin (\phi_o + \phi) \approx \sin \phi_o + \phi \cos \phi_o \tag{10-28}$$

Omitting terms containing products of perturbation variables,

$$\dot{\theta} = q \cos \phi_o - r \sin \phi_o - (q_o \sin \phi_o + r_o \cos \phi_o)\phi \tag{10-29}$$

Whence

$$\theta = \cos \phi_o \int q \, dt - \sin \phi_o \int r \, dt - (q_o \sin \phi_o + r_o \sin \phi_o) \int \phi \, dt \tag{10-30}$$

Then

$$\frac{\partial \theta}{\partial x_3} = \cos \phi_o; \quad \frac{\partial \theta}{\partial x_6} = - \sin \phi_o \tag{10-31}$$

Similarly,

$$\frac{\partial \psi}{\partial x_3} = \sin \phi_o \sec \theta_o; \quad \frac{\partial \psi}{\partial x_6} = \cos \phi_o \sec \theta_o \tag{10-32}$$

$$\frac{\partial \phi}{\partial x_3} = \sin \phi_o \tan \theta_o; \quad \frac{\partial \phi}{\partial x_5} = 1; \quad \frac{\partial \phi}{\partial x_6} = \cos \phi_o \tan \theta_o \tag{10-33}$$

10.6.2 The Partial Derivatives of G_1

The partial derivatives of G_1 are developed in detail. The same procedure is applicable to the remaining G_i.

Consider the first fuselage rigid body equation.

$$G_1 = m\,(\dot{U} + QW - RV) - F_x - W_x \tag{10-34}$$

In the perturbation notation,

$$G_1 = m\left[\ddot{x}_{1_o} + \ddot{x}_1 + \left(\dot{x}_{3_o} + \dot{x}_3\right)\left(\dot{x}_{2_o} + \dot{x}_2\right) - \left(\dot{x}_{6_o} + \dot{x}_6\right)\left(\dot{x}_{4_o} + \dot{x}_4\right)\right] - F_x - W_x \tag{10-35}$$

or, dropping perturbation variable product terms,

$$G_1 = m\left(\ddot{x}_{1_o} + \dot{x}_{3_o}\dot{x}_{2_o} - \dot{x}_{6_o}\dot{x}_{4_o}\right) + m\left(\ddot{x}_1 + \dot{x}_{3_o}\dot{x}_2 + \dot{x}_{2_o}\dot{x}_3 - \dot{x}_{6_o}\dot{x}_4 - \dot{x}_{4_o}\dot{x}_6\right) - F_x - W_x \tag{10-36}$$

Then the M_{1j} are

$$\frac{\partial G_1}{\partial \ddot{x}_1} = m, \quad \frac{\partial G_1}{\partial \ddot{x}_j} = 0, \; j \neq 1 \tag{10-37}$$

Since from Equation (10-6)

$$\frac{\partial W_x}{\partial x_j} = \frac{\partial W_y}{\partial x_j} = \frac{\partial W_z}{\partial x_j} = 0 \tag{10-38}$$

and from Equation (10-36), the G_{1j} are

$$\left.\begin{aligned}
&\frac{\partial G_1}{\partial \dot{x}_1} = -\frac{\partial F_x}{\partial \dot{x}_1}; \quad \frac{\partial G_1}{\partial \dot{x}_2} = m\dot{x}_{3_o} - \frac{\partial F_x}{\partial \dot{x}_2} \\
&\frac{\partial G_1}{\partial \dot{x}_3} = m\dot{x}_{2_o} - \frac{\partial F_x}{\partial \dot{x}_3}; \quad \frac{\partial G_1}{\partial \dot{x}_4} = -m\dot{x}_{6_o} - \frac{\partial F_x}{\partial \dot{x}_4} \\
&\frac{\partial G_1}{\partial \dot{x}_5} = -\frac{\partial F_x}{\partial \dot{x}_5}; \quad \frac{\partial G_1}{\partial \dot{x}_6} = -m\dot{x}_{4_o} - \frac{\partial F_x}{\partial \dot{x}_6}
\end{aligned}\right\} \tag{10-39}$$

and

$$\frac{\partial G_1}{\partial \dot{x}_j} = - \frac{\partial F_x}{\partial \dot{x}_j}, \quad j = 7, 8, \ldots, 14 \tag{10-40}$$

Finally, the K_{1j} are derived from

$$\frac{\partial G_1}{\partial x_j} = - \frac{\partial F_x}{\partial x_j} - \frac{\partial W_x}{\partial x_j}, \quad j = 1, 2, \ldots, 14 \tag{10-41}$$

as follows.

By Equation (10-6)

$$W_x = - mg \sin (\theta_o + \theta) \tag{10-42}$$

Then

$$\frac{\partial W_x}{\partial x_j} = \frac{\partial W_x}{\partial \theta} \frac{\partial \theta}{\partial x_j} \tag{10-43}$$

From Equation (10-42)

$$\frac{\partial W_x}{\partial \theta} = - mg \cos \theta_o \tag{10-44}$$

According to Equation (10-30)

$$\frac{\partial \theta}{\partial x_j} = 0 \ , \ j = 1, 2, 4, 5, 7, 8, \ldots, 14 \tag{10-45}$$

and therefore

$$\frac{\partial W_x}{\partial x_j} = 0, \ j = 1, 2, 4, 5, 7, 8, \ldots, 14 \tag{10-46}$$

The nonzero partial derivatives of θ are given by Equation (10-31).

Thus

$$\frac{\partial W_x}{\partial x_3} = - mg \cos \theta_o \cos \phi_o \tag{10-47}$$

Since F_x is not a function of x_3,

$$\frac{\partial G_1}{\partial x_3} = mg \cos \theta_o \cos \phi_o \tag{10-48}$$

or, comparing with Equation (10-6),

$$\frac{\partial G_1}{\partial x_3} = W_z \tag{10-49}$$

Similarly,

$$\frac{\partial G_1}{\partial x_6} = - mg \cos \theta_o \sin \phi_o \tag{10-50}$$

or,

$$\frac{\partial G_1}{\partial x_6} = - W_y \tag{10-51}$$

For the remainder of the first row of the K-matrix,

$$\frac{\partial G_1}{\partial x_i} = - \frac{\partial F_x}{\partial x_i}, \quad i = 7, 8, \ldots, 14 \tag{10-52}$$

The derivatives of $\dot{F}_x$ are computed numerically. The approximation is

$$\frac{\partial \dot{F}_x}{\partial x_i} = \frac{\dot{F}_x\left(x_{i_o} + \Delta_i\right) - \dot{F}_x\left(x_{i_o}\right)}{\Delta_i} \tag{10-53}$$

where the Δ_i are input constants.

10.6.3 Aerodynamic Coefficients in the M Matrix

Effects of rate of change of wing angle of attack on the lift coefficients of each stabilizing surface are included in the M matrix as $\dot{W}$, or acceleration, derivative in accordance with the analysis in Section 5.5 of Reference 24. As stated in the reference,

> "The $\dot{\alpha}$ derivatives owe their existence to the fact that the pressure distribution on a wing or tail does not adjust itself instantaneously to its equilibrium value when angle of attack is suddenly changed."

The $\dot{\alpha}$ derivatives discussed in Reference 24 are $C_{Z_{\dot{\alpha}}}$ and $C_{M_{\dot{\alpha}}}$ which correspond to $Z_{\dot{w}}$ and $M_{\dot{w}}$ in C81. In the referenced analysis, the spans of both the wing and tail are assumed parallel to a body X-Y plane; consequently, the contributions of $\dot{\alpha}$ to lift affect only the vertical force and the pitching moment. In C81 the $\dot{\alpha}$ derivative is replaced by the $\dot{W}$ derivative and the stabilizing surface does not necessarily lie in a body X-Y plane; i.e., the surface may have a large dihedral angle. Therefore, the $\dot{W}$ increment is resolved from the body to wind axis reference system, the change in lift calculated, and the force resolved back to body axis which yields both a Z and a Y force. The result is that in addition to the conventional $Z_{\dot{w}}$ and $M_{\dot{w}}$ derivatives, side force, rolling moment, and yawing moment derivatives ($Y_{\dot{w}}$, $L_{\dot{w}}$, and $N_{\dot{w}}$) are also included.

10.6.4 Tabulation of the Partial Derivatives

The entire set of partial derivatives is given in Figures 10-1, 10-2, and 10-3. Figure 10-1 is the M matrix. The elements in this matrix are all determined analytically, and the elements are zero where not otherwise indicated.

The C matrix, Figure 10-2, contains analytical terms as well as derivatives of the applied forces and moments. The symbol $-\partial$ indicates that $\frac{-\partial F_i}{\partial \dot{x}_j}$ is included in the element in the i^{th} row, j^{th} column.

In the K matrix, Figure 10-3, $-\frac{\partial F_i}{\partial x_j}$ is indicated in the same manner.

10.7 THE OUTPUT

The Stability Analysis section in Program C81 produces output in the form of eigenvalues and eigenvectors which is immediately useful to the user. Also, the control power derivatives are computed and listed. With these values, complete information for control transfer function parameters is listed. A detailed explanation of the STAB output is given in Section 4.11 of Volume II.

$\ddot{x}$ / G	$\dot{u}$ 1	$\dot{w}$ 2	$\dot{q}$ 3	$\dot{v}$ 4	$\dot{p}$ 5	$\dot{r}$ 6	$\ddot{a}_{FM}$ 7	$\ddot{a}_{LM}$ 8	$\ddot{a}_{1M}$ 9	$\ddot{b}_{1M}$ 10	$\ddot{a}_{FT}$ 11	$\ddot{a}_{LT}$ 12	$\ddot{a}_{1T}$ 13	$\ddot{b}_{1T}$ 14
1	m													
2		$m - Z_{\dot{w}}$												
3		$-M_{\dot{w}}$	I_Y											
4		$-Y_{\dot{w}}$		m										
5		$-L_{\dot{w}}$			I_X	$-I_{XZ}$								
6		$-N_{\dot{w}}$			$-I_{XZ}$	I_Z								
7			$-I_{FM} T_{M22}$		$-I_{FM} T_{M12}$	$-I_{FM} T_{M32}$	I_{FM}							
8					$I_{LM} T_{M11}$	$I_{LM} T_{M31}$		I_{LM}						
9			$-I_{RM} T_{M22}$		$-I_{RM} T_{M12}$	$-I_{RM} T_{M32}$			$-I_{RM}$					
10					$-I_{RM} T_{M11}$	$-I_{RM} T_{M31}$				$-I_{RM}$				
11			$-I_{FT} T_{T22}$		$-I_{FT} T_{T12}$	$-I_{FT} T_{T32}$					I_{FT}			
12					$I_{LT} T_{T11}$	$I_{LT} T_{T31}$						I_{LT}		
13			$-I_{RT} T_{T22}$		$-I_{RT} T_{T12}$	$-I_{RT} T_{T32}$							$-I_{RT}$	
14					$-I_{RT} T_{T11}$	$-I_{RT} T_{T31}$								$-I_{RT}$

Figure 10. Inertial Matrix $\left(M_{ij} = \frac{\partial G_i}{\partial \ddot{x}_j} \right)$.

$\dot{x}$ / G	u 1	w 2	q 3	v 4	p 5	r 6	a_{FM} 7	a_{LM} 8	a_{1M} 9	b_{1M} 10	a_{FT} 11	a_{LT} 12	a_{1T} 13	b_{1T} 14
1	$-\partial$	$mq_o-\partial$	$mw_o-\partial$	$-mr_o-\partial$	$-\partial$	$-mv_o-\partial$	$-\partial$	$-\partial$	$-\partial$	$-\partial$	$-\partial$	$-\partial$	$-\partial$	$-\partial$
2	$-mq_o-\partial$	$-\partial$	$-mu_o-\partial$	$mp_o-\partial$	$mv_o-\partial$	$-\partial$	$-\partial$	$-\partial$	$-\partial$	$-\partial$	$-\partial$	$-\partial$	$-\partial$	$-\partial$
3	$-\partial$	$-\partial$	$-\partial$	$-\partial$	$(I_x-I_z)r_o$ $+2I_{xz}p_o-\partial$	$(I_x-I_z)p_o$ $-2I_{xz}r_o-\partial$	$-\partial$	$-\partial$	$-\partial$	$-\partial$	$-\partial$	$-\partial$	$-\partial$	$-\partial$
4	$mr_o-\partial$	$-mp_o-\partial$	$-\partial$	$-\partial$	$-mw_o-\partial$	$mu_o-\partial$	$-\partial$	$-\partial$	$-\partial$	$-\partial$	$-\partial$	$-\partial$	$-\partial$	$-\partial$
5	$-\partial$	$-\partial$	$(I_z-I_y)r_o$ $-I_{xz}p_o-\partial$	$-\partial$	$-I_{XZ}q_o-\partial$	$(I_z-I_y)q_o-\partial$	$-\partial$	$-\partial$	$-\partial$	$-\partial$	$-\partial$	$-\partial$	$-\partial$	$-\partial$
6	$-\partial$	$-\partial$	$(I_y-I_x)p_o$ $+I_{xz}r_o-\partial$	$-\partial$	$(I_Y-I_X)q_o-\partial$	$I_{XZ}q_o-\partial$	$-\partial$	$-\partial$	$-\partial$	$-\partial$	$-\partial$	$-\partial$	$-\partial$	$-\partial$
7	$-\partial$	$-\partial$	$-\partial$	$-\partial$	$-\partial$	$-\partial$	$C_{FM}-\partial$	$-\partial$	$-\partial$	$-\partial$				
8	$-\partial$	$-\partial$	$-\partial$	$-\partial$	$-\partial$	$-\partial$	$-\partial$	$C_{LM}-\partial$	$-\partial$	$-\partial$				
9	$-\partial$	$-\partial$	$-\partial$	$-\partial$	$-2\Omega_M I_{RM}T_{M11}-\partial$	$-2\Omega_M I_{RM}T_{M31}-\partial$	$-\partial$	$-\partial$	$-\partial$	$-2\Omega_M I_{RM}-\partial$				
10	$-\partial$	$-\partial$	$2\Omega_M I_{RM}T_{M22}-\partial$	$-\partial$	$2\Omega_M I_{RM}T_{M12}-\partial$	$2\Omega_M I_{RM}T_{M32}-\partial$	$-\partial$	$-\partial$	$2\Omega_M I_{RM}-\partial$	$-\partial$				
11	$-\partial$	$-\partial$	$-\partial$	$-\partial$	$-\partial$	$-\partial$					$C_{FT}-\partial$	$-\partial$	$-\partial$	$-\partial$
12	$-\partial$	$-\partial$	$-\partial$	$-\partial$	$-\partial$	$-\partial$					$-\partial$	$C_{LT}-\partial$	$-\partial$	$-\partial$
13	$-\partial$	$-\partial$	$-\partial$	$-\partial$	$-2\Omega_T I_{RT}T_{T11}-\partial$	$-2\Omega_T I_{RT}T_{T31}-\partial$					$-\partial$	$-\partial$	$-\partial$	$-2\Omega_T I_{RT}-\partial$
14	$-\partial$	$-\partial$	$2\Omega_T I_{RT}T_{T22}-\partial$	$-\partial$	$2\Omega_T I_{RT}T_{T12}-\partial$	$2\Omega_T I_{RT}T_{T32}-\partial$					$-\partial$	$-\partial$	$2\Omega_T I_{RT}-\partial$	$-\partial$

Note: $-\partial$ indicates $-\dfrac{\partial F_i}{\partial x_j}$

Figure 10-2. Damping Matrix $\left(C_{ij} = \dfrac{\partial G_i}{\partial \dot{x}_j} \right)$.

G \ x	$\int$ udt 1	$\int$ wdt 2	$\int$ qdt 3	$\int$ vdt 4	$\int$ pdt 5	$\int$ rdt 6	a_{FM} 7	a_{LM} 8	a_{IM} 9	b_{IM} 10	a_{FT} 11	a_{LT} 12	a_{T} 13	b_{LT} 14
1			W_Z			$-W_Y$	-∂	-∂	-∂	-∂	-∂	-∂	-∂	-∂
2			$-W_X$		W_Y		-∂	-∂	-∂	-∂	-∂	-∂	-∂	-∂
3							-∂	-∂	-∂	-∂	-∂	-∂	-∂	-∂
4					$-W_Z$	W_X	-∂	-∂	-∂	-∂	-∂	-∂	-∂	-∂
5							-∂	-∂	-∂	-∂	-∂	-∂	-∂	-∂
6							-∂	-∂	-∂	-∂	-∂	-∂	-∂	-∂
7							K_{FM} -∂	-∂	-∂	-∂				
8							-∂	K_{LM} -∂	-∂	-∂				
9							-∂	-∂	-∂	-∂				
10							-∂	-∂	-∂	-∂				
11											K_{FT}-∂	-∂	-∂	-∂
12											-∂	K_{LT}-∂	-∂	-∂
13											-∂	-∂	-∂	-∂
14											-∂	-∂	-∂	-∂

Note: $-\partial$ indicates $-\dfrac{\partial F_i}{\partial x_j}$ Figure 10-3. Stiffness Matrix $\left(K_{ij} = \dfrac{\partial G_i}{\partial x_j} \right)$

11. MANEUVER SIMULATION

11.1 INTRODUCTION

Ever since the capability of simulating maneuvers was first added to C81, the four-cycle Runge-Kutta method has been used to numerically integrate the equations of motions during such simulations. Over the years, several new methods of numerical integration have been developed and some previously existing methods have come into more prevalent use. Consequently, a study was conducted to determine which of the available techniques of numerical integration is most suitable to the system of differential equations used in C81.

Four criteria were used to assess each method:

(1) Compatibility with the type of differential equations in C81

(2) Accuracy of the integration

(3) Computer time required to perform the integration

(4) Computer storage requirements for the algorithm

With regard to the first criterion, certain techniques of numerical integration are unstable or otherwise unsuitable when applied to certain types of differential equations. For example, the system of equations in C81 includes many differential equations, some of which have little harmonic content and some of which have relatively high harmonics. This situation automatically eliminated from consideration several techniques which are known to have difficulty when simultaneously integrating both types of equations.

The second and third criteria had to be considered as trade-offs and in most cases as a single criterion. That is, given an unlimited amount of computer time, almost any method could meet any prescribed accuracy requirement. However, given a limited, or specified, amount of computer time, the accuracy of a method could be adversely affected. In view of the historical use of the Runge-Kutta method, its accuracy and time requirements were taken as baseline values for evaluating other methods.

Only minor emphasis was placed on the fourth criterion. The reasoning was (1) that the Runge-Kutta technique was only responsible for about 5 percent of the total program storage for the AGAJ72 version of C81 and would account for an even smaller percent of the storage requirements for AGAJ73, and (2) that the advent of larger computers and virtual memory systems reduces the importance of storage requirements. Hence, numerical techniques which would require up to twice the storage of the Runge-Kutta method were still considered acceptable.

11.2 EVALUATION OF TECHNIQUES OF NUMERICAL INTEGRATION

Ten methods of numerical integration were examined during the study. The following procedure was used to evaluate the methods. The fore-and-aft and lateral flapping rate equations from C81 were chosen as a typical set of equations which any method would need to solve.

$$\frac{dp}{dt} = - \Omega q - F_A \qquad (11\text{-}1)$$

$$\frac{dq}{dt} = \Omega p - F_B \qquad (11\text{-}2)$$

where F_B and F_A are forcing functions,

Ω is rotor speed, and
p and q are rotor roll and pitch rates respectively.

These equations were programmed on an analog computer, and the responses to several forcing functions such as those shown in Figure 11-1 were computed. Response data to the same forcing functions were also computed with a very small error tolerance on the Runge-Kutta numerical method. The resulting analog and digital data (which were within the accuracy limitations of the respective computations) were then defined to be the baseline against which the remaining nine methods of numerical integration would be compared.

Where possible, existing computer subroutines for the methods studied were used to compute the response of Equations (11-1) and (11-2) to the same forcing functions used in the baseiine case. Some of the simplier methods for which programming did not exist were programmed and evaluated in a similar manner.

This initial phase of the study indicated that of the methods which were examined and are currently available, Hamming's predictor-corrector method was the best method with respect to the four criteria stated above. The current Runge-Kutta method was judged next best. Seven other methods were deemed not suitable. The tenth technique (the Adams-Krogh method) was judged to show much promise but was considered to be too experimental, not yet checked out thoroughly enough by the originator of the method, and not sufficiently documented to be included as one of the two best methods. However, it was felt that the Adams-Krogh method should be reconsidered sometime in the future.

A brief description (including some equations) and a few remarks about each of the ten methods evaluated follow. The sources for most of the methods can be found in the selected bibliography given in Section 14.

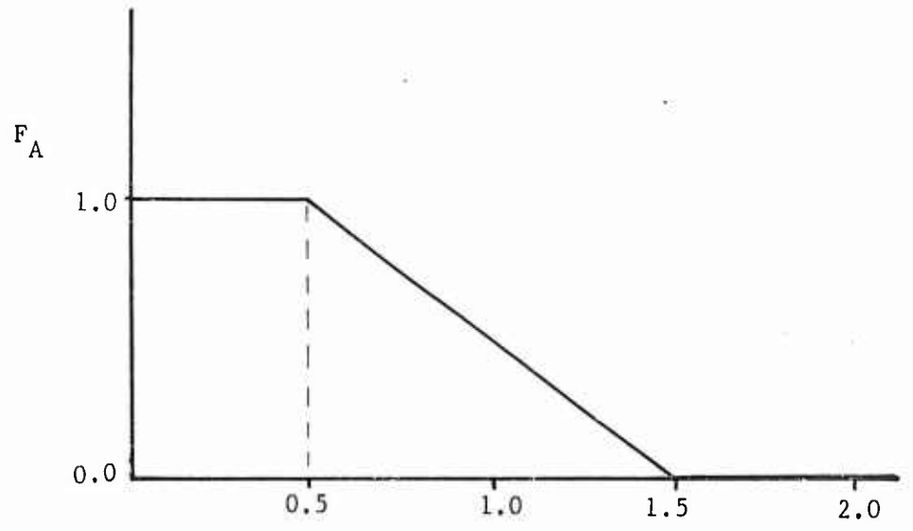

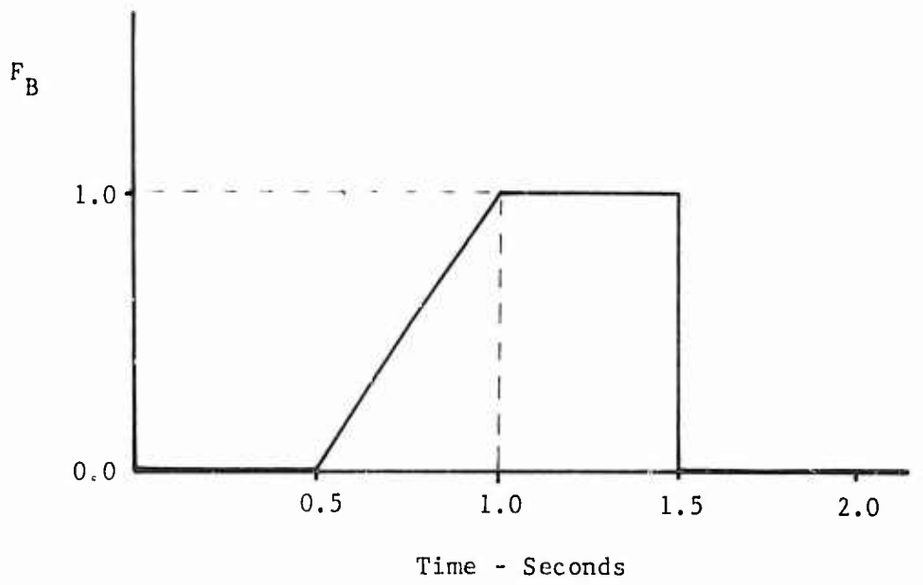

Figure 11-1. Forcing Functions Used in Study of Techniques.

11.2.1 Runge-Kutta Method

Consider a first-order differential equation

$$\frac{dy}{dt} = f(t,y) \tag{11-3}$$

with initial values t_o and y_o. The increment for advancing the dependent variable is given in

$$\Delta y = \frac{\Delta t}{6} (f_1 + 2f_2 + 2f_3 + f_4) \tag{11-4}$$

where Δt is the time step (independent variable) and

$$f_1 = f(t_o, y_o) \tag{11-5}$$

$$f_2 = f(t_o + \frac{\Delta t}{2}, y_o + \frac{\Delta t}{2} f_1) \tag{11-6}$$

$$f_3 = f(t_o + \frac{\Delta t}{2}, y_o + \frac{\Delta t}{2} f_2) \tag{11-7}$$

$$f_4 = f(t_o + \Delta t, y_o + \Delta t\, f_3) \tag{11-8}$$

The values at (t_1, y_1) are then given by

$$t_1 = t_o + \Delta t \tag{11-9}$$

and

$$y_1 = y_o + \Delta y. \tag{11-10}$$

The increment on y for the second interval is computed by the same formulas with (t_o, y_o) replaced by (t_1, y_1).

This is one of the most widely used methods of numerical integration. It is stable and self-starting; step size is easy to change at any step in the calculations; its computational routine has fewer formulas; and the routine is easily programmed. It requires four function evaluations per time step. This method was judged the second best of the methods studied.

11.2.2 Treanor's Method

This method, in general, is similar to the Runge-Kutta method with the exception that evaluation of f_4 in Equation (11-8) is modified as shown below.

$$f_4 = f(t_o + \frac{\Delta t}{2}, y_o + \Delta t\ f_m) \tag{11-11}$$

where

$$f_m = 2f_3\ g_2 + (g_1 - 2g_2)f_1 + pf_2g_2\Delta t \tag{11-12}$$

$$p = \text{Max} \begin{cases} \dfrac{2(f_2 - f_3)}{\Delta t(f_2 - f_1)} \\ \\ 0 \end{cases} \tag{11-13}$$

$$g_1 = \frac{-1}{p\Delta t}\ e^{-p\Delta t} \tag{11-14}$$

$$g_2 = \frac{g_1 - 1}{-p\Delta t} \tag{11-15}$$

By using this method to solve a set of stiff equations, bigger step size can be applied and more accurate results can be obtained than those from the Runge-Kutta method. However, for harmonic functions it can lead to dividing by zero. In view of the harmonic nature of many parameters in C81, this method was rejected.

11.2.3 Hamming's Predictor-Corrector Method

This is a stable fourth-order integration procedure that requires the function evaluation only twice per time step. This is a great advantage compared with other methods of the same order of accuracy. Another advantage is that at each step the calculation procedure gives an estimate for the local truncation error. Thus, the procedure is able to automatically change the step size. However, this is not a self-starting method. To obtain the starting values, a special Runge-Kutta procedure followed by one iteration step is added to the predictor-corrector method. This special procedure is also used to take care of any discontinuities which may cause trouble to the predictor-corrector method.

To evaluate the function at $(n+1)^{th}$ time point, it is necessary to go through the formulas below.

Predictor: $$P_{n+1} = y_{n-3} + \frac{4\Delta t}{3}(2y'_n - y'_{n-1} + 2y'_{n-2}) \tag{11-16}$$

Modifier: $$M_{n+1} = P_{n+1} - \frac{112}{121}(P_n - C_n) \tag{11-17}$$

$$M'_{n+1} = f(t_{n+1}, M_{n+1}) \tag{11-18}$$

Corrector: $$C_{n+1} = \frac{1}{8}[9y_n - y_{n-2} + 3\Delta t(M'_{n+1} + 2y'_n - y'_{n-1})] \tag{11-19}$$

Final Values: $$y_{n+1} = C_{n+1} + \frac{9}{121}(P_{n+1} - C_{n+1}) \tag{11-20}$$

$$y'_{n+1} = f(t_{n+1}, y_{n+1}) \tag{11-21}$$

Note that

$$y' = dy/dt = f(t,y) \text{ with } y(t_o) = y_o \tag{11-22}$$

11.2.4 Finite Difference Method

This is one of the most stable methods. It is self-starting and easy to change step size.

For a system of this form,

$$a\ddot{y} + b\dot{y} + cy = f(t) \tag{11-23}$$

The first step is to define a guessed value for the second time derivative of y, $\ddot{y}_g(t)$.

Next initial values of $y(0)$, $\dot{y}(0)$, and $\ddot{y}(0)$ are used to solve for guessed values of $y(t)$ and $y(t)$:

$$\dot{y}_g(t) = \dot{y}(0) + \frac{\Delta t}{2}[\ddot{y}(0) + \ddot{y}_g(t)] \tag{11-24}$$

$$y_g(t) = y(0) + \frac{\Delta t}{2}[\dot{y}_g(t) + \dot{y}(0)] + \frac{(\Delta t)^2}{6}[\ddot{y}_g(t) - \ddot{y}(0)] \tag{11-25}$$

where Δt is the step size.

Equation (11-23) can then be solved for a computed value of $\ddot{y}$, i.e., $\ddot{y}_c(t)$:

$$\ddot{y}_c(t) = [r(t) - b\dot{y}_g(t) - cy_g(t)]/a \tag{11-26}$$

Finally, if

$$\left|\frac{\ddot{y}_c(t) - \ddot{y}_g(t)}{\ddot{y}_c(t)}\right| = \left|\frac{\Delta\ddot{y}(t)}{\ddot{y}_c(t)}\right| \leq \varepsilon \tag{11-27}$$

where ε is some preassigned accuracy limit, the system can be regarded as solved at the time point t. If the above convergence criterion is not met, a new guessed value of $\ddot{y}_g(t)$ is provided by a procedure which uses previous $\Delta\ddot{y}$ and $\ddot{y}_g$ values to find a solution which minimizes $\Delta\ddot{y}$. The process repeats itself until the convergence criterion is met. Since this is an iterative procedure, it may take considerable computer time to solve a large system of equations. Considering the size of the system of equations in C81, this method was also rejected.

11.2.5 Milne Method

This is a predictor-corrector type method. It uses

$$y_{n+1} = y_{n-3} + \frac{4}{3}\Delta t\,(2y'_n - y'_{n-1} + 2y'_{n-2}) \tag{11-28}$$

as a predictor and

$$y_{n+1} = y_{n-1} + \frac{\Delta t}{3}\,(y'_{n+1} + 4y'_n + y'_{n-1}) \tag{11-29}$$

as a corrector. It requires four previous values to start the method. For systems with positive damping, equations solved by this method are unstable because each single error is magnified exponentially while the exact solution decays. Since nothing precludes positive damping in C81, this method was rejected.

11.2.6 Adams Method

This is also a predictor-corrector type method. It uses

$$y_{n+1} = y_n + \frac{\Delta t}{24}\,(55y'_n - 59y'_{n-1} + 37y'_{n-2} - 9y'_{n-3}) \tag{11-30}$$

as a predictor and

$$y_{n+1} = y_n + \frac{\Delta t}{24} (9y'_{n+1} + 19y'_{n-5}y'_{n-1} + y'_{n-2}) \qquad (11\text{-}31)$$

as a corrector. Although it needs four previous values to start, the method is stable. This method was programmed for comparison to the analog-ditial baseline response data discussed previously. Based on time and accuracy criteria, Adam's method was inferior to Runge-Kutta and was consequently rejected.

11.2.7 Gear's Method

This is a multistep predictor-corrector method. The step size may be specified by the user, but is changed by the subroutine DIFSUB (Reference 26) to limit the estimated error to a specified tolerance. The orders of the predictor-corrector formulas are automatically chosen by the subroutine as the integration proceeds. Up to three corrector iterations can be taken.

In highly damped systems this method can use large time steps through most of the integration region, as shown in Reference 26 where this method is compared with Adam's. When forcing functions are of harmonic forms, which are typical helicopter equations, test runs of subroutine DIFSUB indicated that Adam's method discussed in the previous section is more efficient. Since Adam's method was inferior to Runge-Kutta, Gear's method being inferior to Adams method was considered sufficient grounds for rejecting Gear's method.

11.2.8 A Predictor-Corrector Method

In Hamming's method, the predictor is calculated first, then modifier, corrector, and final value. Before proceeding to the next time point, it evaluates derivatives. In the type of predictor-corrector method considered here, the concept is to try to replace derivative evaluation by numerical differentiation. Thus, at each time point only one function value is needed. Unfortunately, the numerical differentiation is unstable and its result is not accurate enough. Hence, this method was also rejected.

11.2.9 Euler Method

This is one of the simplest predictor-corrector type methods. The predictor formula is

$$y_{n+1} = y_n + \Delta t\, y'_n \qquad (11\text{-}32)$$

and the corrector formula is

$$y_{n+1} = y_n + \frac{\Delta t}{2} (y'_n + y'_{n+1}) \qquad (11\text{-}33)$$

It requires only one previous function value. Therefore, it is easier to incorporate into any system. Unfortunately, the step size must be kept small to assure sufficient accuracy. To match the accuracy of Runge-Kutta, the required time step is so small that the computation time becomes too great with respect to Runge-Kutta computation time. Hence, this method was rejected.

11.2.10 Adams-Krogh Method

This method is a self-starting, predictor-corrector type method with variable orders and variable step size. The change in step size is carried out by using modified divided differences. Although this method appeared to combine some of the better features of several of the techniques examined, it is a very new technique and not yet thoroughly checked out. Hence, this method was rejected primarily because of its unknown characteristics rather than any adverse qualities. It is felt that the method shows considerable promise and should be reconsidered as a new or alternate technique for numerical integration in C81 when the method is better known and more thoroughly documented.

11.3 CURRENT PROGRAM OPTIONS

As a result of the study discussed in the previous section, Hamming's predictor-corrector method of numerical integration was programmed into C81. The test cases during the study had indicated that Hamming's method required fewer function evaluations than the Runge-Kutta method and that it should reduce the run time of a maneuver by 25 to 40 percent as compared to runs with Runge-Kutta.

When Hamming's method was chosen for incorporation into C81, the decision was also made to retain the Runge-Kutta method in the program until the checkout of Hamming's method was complete. Hence, Hamming's method was installed as a programmer option. The logic was structured such that the two methods of numerical integration were completely independent of each other. Although this parallel logic was originally intended to simplify the removal of the second best method at the end of the comparison phase of the study, it greatly facilitated switching from one method to the other during checkout.

The comparison phase of the study concluded that Hamming's method did not live up to expectation. In particular, run times with Hamming's method were 20 to 30 percent longer than the corresponding Runge-Kutta runs. Curiously enough, the cause of the longer than anticipated run time with Hamming's method was traced to the integration of the rotor flapping equations given by Equations (11-1) and (11-2) in this report. Specifically, the C81 program found it necessary to halve the time increment more often than in the test case run outside of C81. The reason for the increased number of step size reduction was apparently the presence of aerodynamic damping in the C81 equation and lack of it in the external test cases. Efforts to reduce the run time of Hamming's method to less

than those with Runge-Kutta failed. However, it was concluded that the increased accuracy with Hamming's method and the relatively small difference in run times between the two methods could not justify the removal of either method. Also, it was felt that with additional work, more decreases in the run time of cases using Hamming's method could eventually be accomplished. Therefore, it was decided to retain the Runge-Kutta techniques as the normal method of numerical integration and to provide Hamming's method as a programmer option. Another reason for retaining Hamming's method was that its logic and storage requirements appeared similar to those of the Adams-Krogh method. At such time as incorporation of this method is attempted, the retention of Hamming's method should simplify the installation.

12. CONCLUSIONS AND RECOMMENDATIONS

The modifications made to the Rotorcraft Flight Simulation Computer Program C81 under contract DAAJ02-72-C-0098 were the most extensive ever made during a single contractual or independent development effort. The new and revised mathematical models of rotorcraft components added during this contract have expanded the variety of configurations which can be simulated and provided more precise simulation for every major model in the program. The revised and expanded User's Manual (Volume II of this report) and the reorganization of the input data make the program easier for the new C81 user to set up an input data deck. For the experienced user the program is more flexible and adaptable for setting up simulations of unusual configurations, flight conditions, or maneuvers. Except for the proprotor collective governor (which model has become outdated), all abilities of previous versions of the program have been maintained.

The development of AGAJ73 impacted on almost every subroutine and mathematical model previously incorporated in the program. As a consequence, a thorough review of the strong and weak points of the program, both in terms of analysis and usability, was made. From this review, six recommendations for future improvements to the program are made:

(1) Aeroelastic Fuselage: Previous studies have shown the rotor support system to have a significant effect on loads and frequencies. Preliminary investigations have shown that the rotor support system (fuselage or wind tunnel support) can be included in the C81 program by using the modal method, which would be compatible with the elastic rotor analysis.

(2) Rotor Control System: Review of the current model for the rotor control system indicated that it contains some small angle assumptions and restrictions which are not compatible with the coupled, mixing and nonlinear control systems currently being developed. A method of more rigorously defining the control system geometry is desirable and would be mandatory in conjunction with an aeroelastic fuselage.

(3) Rotor Wake Analysis: The program currently has the logic for defining the induced velocity distribution over the rotor disc with inputs from a data table. At present, data for the table must be generated by a program which is external to C81 and then processed to be input to the table. The obvious shortcut is to include such an analysis in C81. Concurrently with the installation of such a model, the present simplified model for the effects of rotor wake on the aerodynamic surfaces should be updated.

(4) Aerodynamic Model of Wing and Stabilizing Surfaces: Considering the data which would be available from a rotor wake analysis, it is suggested that the representation for aerodynamic forces acting on the wing and stabilizing surfaces be changed from the current lifting line model to a lifting surface segmented model, i.e., treated in much the same manner as the rotor aerodynamics. A modification of this type could permit a more accurate representation of rotor wake effects on aerodynamic surfaces than that referred to in the preceding recommendation.

(5) Trim at Commanded Power: For a user to trim in autorotation or a maximum power climb, it is currently necessary first to compute trims at several rates of climb (or descent), then interpolate or extrapolate the data to determine the rate which gives the desired power condition, and finally to run another trim to verify the predicted results. An option should be provided for trimming at a prescribed power level with rate of climb (or climb angle) being added to the trim procedure as an independent variable.

(6) Numerical Integration: The study of techniques of numerical integration performed during this contract led to the incorporation of Hamming's predictor-corrector method as a programmer option to the Runge-Kutta technique previously used. The performance of Hamming's method within the program was not up to expectations and deserves additional investigation. Also, the study indicated that in the next 1 to 5 years, one or more methods currently under development may emerge as a superior method for use in C81. Hence, the method of integration programmed should be reviewed again in the future.

13. REFERENCES

1. Harvey, K. W., Blankenship, B. L., and Drees, J. M., ANALYTICAL STUDY OF HELICOPTER GUST RESPONSE AT HIGH FORWARD SPEEDS, Bell Helicopter Company, USAAVLABS Technical Report 69-1, U. S. Army Aviation Materiel Laboratories, Fort Eustis, Virginia, September 1969, AD862594.

2. Livingston, C. L., A STABILITY AND CONTROL PREDICTION METHOD FOR HELICOPTER AND STOPPABLE ROTOR AIRCRAFT, Bell Helicopter Company Technical Report AFFDL-TR-69-123, Volumes I - IV, Air Force Flight Dynamics Laboratory, Air Force Systems Command, Wright-Patterson AFB, Ohio, 1970.

3. Houbolt, John C., and Brooks, George W., DIFFERENTIAL EQUATIONS OF MOTION FOR COMBINED FLAPWISE BENDING, CHORDWISE BENDING, AND TORSION OF TWISTED NONUNIFORM ROTOR BLADES, NACA Report 1346, 1958.

4. Scanlan, R. H., and Rosenbaum, R., AIRCRAFT VIBRATION AND FLUTTER, New York, N. Y., Macmillan Co., 1951.

5. Oette, H., BERECHNUNG DER SCHLAGBIEGE-, SCHWENKBIEGE-UND TORSIONSSCHWINGUNGEN VON ROTORBLÄTTERN MIT GEKOPPELTEN EIGENFORMEN UND -FREQUENZEN, Deutsche Luft-und Raumfahrt, DLR - Forschungsbericht 71-108, 1971.

6. Velkoff, Henry, INTRODUCTION TO HELICOPTER ANALYSIS AND DESIGN, Columbus, Ohio, Ohio State University, 1965.

7. Gessow, Alfred and Myers, Garry C., Jr., AERODYNAMICS OF THE HELICOPTER, New York, N. Y., The Macmillan Company.

8. Livingston, C. L., ROTOR INDUCED VELOCITY, Bell Helicopter Company IOM 81:CLL:am-838, October 7, 1966.

9. Drees, J. M., A THEORY OF AIRFLOW THROUGH ROTORS AND ITS APPLICATIONS TO SOME HELICOPTER PROBLEMS, The Journal of The Helicopter Society of Great Britian, Vol. 3, No. 2, 1949.

10. Harris, F. D., Tarzanin, F. J. Jr., and Fisher, Richard K. Jr., ROTOR HIGH SPEED PERFORMANCE, THEORY VS. TEST, Journal of the American Helicopter Society, Volume 15, No. 3, July 1970.

11. Hoerner, Signard F., FLUID-DYNAMIC DRAG, New York, N. Y., Published by the Author, 1958.

12. Loewy, R. G., A TWO-DIMENSIONAL APPROXIMATION TO THE UNSTEADY AERODYNAMICS OF ROTARY WINGS, J. Aeron. Sci.24(2), 1957.

13. Timman, R., and Van de Vooren, A. I., FLUTTER OF A HELICOPTER ROTOR ROTATING IN ITS OWN WAKE, J. Aeron. Sci., 1957.

14. Drees, J. M., AEROELASTIC ROTOR PHENOMENA AND NONSTEADY ROTOR AERODYNAMICS, Annals of the New York Academy of Sciences, Volume 154, Art. 2., pp. 481-504, New York, N. Y., 1968.

15. Carta, F. O., Casellini, L. M., Arcidiacono, P. J., and Elman, H. L., ANALYTICAL STUDY OF HELICOPTER ROTOR STALL FLUTTER, Paper presented at the 26th Annual National Forum of the American Helicopter Society, Washington, D. C., 1970.

16. Arcidiacono, P. J., Carta, F. O., Casellini, L. M., and Elman, H. L., INVESTIGATION OF HELICOPTER CONTROL LOADS INDUCED BY STALL FLUTTER, USAAVLABS Technical Report 70-2, U. S. Army Air Mobility Research and Development Laboratory, Fort Eustis, Virginia, March 1970, AD869823.

17. Bisplinghoff, R. L., Ashley, H., and Halfman, R. L., AEROELASTICITY, Cambridge, Massachusetts, Addison-Wesley Publishing Company, 1955.

18. Gormont, R. E., A MATHEMATICAL MODEL OF UNSTEADY AERODYNAMICS AND RADIAL FLOW FOR APPLICATION TO HELICOPTER ROTORS, Boeing-Vertol, USAAMRDL Technical Report 72-67, U. S. Army Air Mobility Research and Development Laboratory, Fort Eustis, Virginia, May 1973, AD767240.

19. Hildebrand, F. B., INTRODUCTION TO NUMERICAL ANALYSIS, New York, McGraw-Hill, 1956.

20. Jorgensen, L. H., PREDICTION OF STATIC AERODYNAMIC CHARACTERISTICS FOR SPACE-SHUTTLE-LIKE AND OTHER BODIES AT ANGLES OF ATTACK FROM 0° to 180°, NASA TN D-6996, January 1973.

21. Jorgensen, L. H., A METHOD FOR ESTIMATING STATIC AERODYNAMIC CHARACTERISTICS FOR SLENDER BODIES OF CIRCULAR AND NONCIRCULAR CROSS SECTION ALONE AND WITH LIFTING SURFACES AT ANGLES OF ATTACK FROM 0° to 90°, NASA TN D-7228, April 1973.

22. Polhamus, E. C., and Sleeman, W. C., Jr., THE ROLLING MOMENT DUE TO SIDESLIP OF SWEPT WINGS AT SUBSONIC AND TRANSONIC SPEEDS, NASA TN D-209, February 1960.

23. USAF STABILITY AND CONTROL DATCOM, U. S. Air Force Flight Dynamics Laboratory, Wright-Patterson Air Force Base, Ohio, February 1972.

24. Etkin, Bernard, DYNAMICS OF FLIGHT, New York, N. Y., John Wiley and Sons, 1967.

25. Young, A. D., THE AERODYNAMIC CHARACTERISTICS OF FLAPS, British Aeronautical Research Council RM No. 2622, February 1947 (also printed as R.A.E. Report Aero. 2185, August 1947).

26. Wilkinson, J. H., THE ALGEBRAIC EIGENVALUE PROBLEM, Oxord Clarendon Press, 1965.

27. SYSTEM/360 SCIENTIFIC SUBROUTINE PACKAGE, Version III, Programmer's Manual, H20-0205-3, IBM, 1968, pp. 337-341.

14. SELECTED BIBLIOGRAPHY FOR TECHNIQUES OF NUMERICAL INTEGRATION

1. Ralston, Anthony, and Wolf, Herbert S., MATHEMATICAL METHODS FOR DIGITAL COMPUTERS, New York, Wiley, 1967, pp.95-120.

2. Treanor, Charles E., A METHOD FOR THE NUMERICAL INTEGRATION OF COUPLED FIRST-ORDER DIFFERENTIAL EQUATIONS WITH GREATLY DIFFERENT TIME CONSTANTS, Mathematics of Computing No. 20, January 1966, pp.39-45.

3. Losey, H. E., and Hsieh, P. Y., A STUDY OF FOLDING PROPROTOR VTOL AIRCRAFT DYNAMICS, Vol. II. Bell Helicopter Company; AFFDL Technical Report 71-7, U. S. Air Force Flight Dynamics Laboratory, Wright-Patterson Air Force Base, Ohio, Sept. 1971, pp.63-65.

4. Gear, C. W., THE AUTOMATIC INTEGRATION OF ORDINARY DIFFERENTIAL EQUATIONS, Communications of the ACM, Vol. 14, No. 3, March 1971, pp.176-179.

5. Gear, C. W., DIFSUB FOR SOLUTION OF ORDINARY DIFFERENTIAL EQUATIONS, Communications of the ACM, Vol. 14, No. 3, March 1971, pp.185-190.

6. Hamming, R. W., NUMERICAL METHODS FOR SCIENTISTS AND ENGINEERS, New York, McGraw-Hill Book Company, 1962, pp.202-204.

7. Krogh, Fred T., CHANGING STEPSIZE IN THE INTEGRATION OF DIFFERENTIAL EQUATIONS USING MODIFIED DIVIDED DIFFERENCES, California Institute of Technology; JPL Internal Document, Section 914 TM No. 312, Jet Propulsion Laboratory, Pasadena, Calif., Oct. 1972.

15. LIST OF SYMBOLS

A	unsteady pitching moment parameter proportional to $\dot{\alpha}$ used with Carta's tables
$A_1,..,A_5$	constants used to calculate the aerodynamic pitching moment coefficient
$\vec{A}$	aerodynamic force vector, lb
A_{1M}	main (first) rotor fore-and-aft flapping displacement, positive down aft with respect to vertical shaft, rad
A_{1T}	tail (second) rotor fore-and-aft flapping displacement, positive down aft with respect to vertical shaft, rad
A_{FM}	main (first) pylon fore-and-aft vibratory angular displacement, positive forward, rad
A_{FT}	tail (second) pylon fore-and-aft vibratory angular displacement, positive forward, rad
A_j	total applied load on blade j, lb
A_{LM}	main (first) pylon lateral vibratory angular displacement, positive right, rad
A_{LT}	tail (second) pylon lateral vibratory angular displacement, positive right, rad
A_x	component of aerodynamic force in the $\vec{i}$ direction, lb
A_y	component of aerodynamic force in the $\vec{j}$ direction, lb
A_z	component of aerodynamic force in the $-\vec{k}$ direction, lb
A_θ	component of aerodynamic pitching moment about the $\vec{i}$ direction axis, right hand positive, ft-lb
a	distance from midchord to elastic axis divided by semichord
$\underline{a}$	slope of lift curve
ab	distance from midchord to elastic axis, positive aft of the elastic axis, ft
a_F	fore-and-aft pylon displacement, rad

$\dot{a}_F$	fore-and-aft pylon vibration velocity, rad/sec
a_L	lateral pylon displacement, rad
$\dot{a}_L$	lateral pylon vibratory velocity, rad/sec
a_m	total mast tilt angle, rad
$\vec{a}_p$	acceleration of P relative to an inertial reference system, ft/sec^2
B	unsteady pitching moment parameter proportional to $\overline{\theta}$ used with Carta's tables
B	tip loss factor
B_{lM}	main (first) rotor lateral flapping displacement, positive down right with respect to vertical shaft, rad
B_{lT}	tail (second) rotor lateral flapping displacement, positive down left with respect to vertical shaft, rad
b	blade semichord, ft
[C]	velocity coefficient matrix in the stability analysis
C_B	corrected thrust coefficient
C_d	aerodynamic drag coefficient
C_{d_N}	aerodynamic coefficient for determining drag force in the $\vec{j}_b$ direction
C_{d_R}	aerodynamic drag coefficient for determining drag force in the $\vec{i}_b$ direction
C_{ij}	element of the velocity coefficient matrix in the stability analysis
C_l	aerodynamic lift coefficient
$C_{L_{max}}$	maximum lift coefficient
C_{l_s}	steady state aerodynamic lift coefficient
C_{l_T}	lift coefficient with unsteady effects included

C_m	aerodynamic pitching moment coefficient
C_T	thrust coefficient
C(k)	Theodorsen circulation function
c	blade chord, ft
c	lead-lag damper coefficient, ft-lb-sec/rad
d	length dependent on the blade chord and pitch axis location
$\bar{d}$	constant used to calculate the aerodynamic pitching moment coefficient
$\vec{d}$	blade deformation vector
E	expression involving the Theodorsen circulation function
EI_z	out-of-plane stiffness distribution, lb-ft^2
$\vec{F}$	aerodynamic force vector
F_F	forcing function for fore-and-aft pylon motion, ft-lb
F_L	forcing function for lateral pylon motion, ft-lb
F_N	function for determining the value of induced velocity, normalized by $\bar{V}_i$
F_{damp}	lead-lag damper force, lb
F_i	i^{th} applied force or moment in the stability analysis
F_n	forcing function for the n^{th} blade mode, ft-lb
F_x	fore-and-aft (X) component of applied force in fuselage body reference, lb
F_y	lateral (Y) component of applied force in fuselage body reference, lb
F_z	vertical (Z) component of applied force in fuselage body reference, lb
F(k)	real components of C(k)
G	ground effect factor

G_i	functional notation used in representing the equations of motion in the stability analysis
$\left.\frac{\partial G_i}{\partial x_j}\right\|_o$	partial derivative of the i^{th} motion expression with respect to the j^{th} perturbation variable, evaluated at the initial condition
$G(k)$	imaginary component of $C(k)$
h	undersling distance, ft
$\dot{h}$	vertical (heaving) velocity of blade segment, positive down, ft/sec
$\ddot{h}$	vertical (heaving) acceleration, positive down, ft/sec^2
$\dot{h}_o$	"steady" (frequency less than Ω) part of the inflow velocity, positive down, ft/sec
$\dot{h}_v$	vibratory part of the inflow velocity, positive down, ft/sec
HTC	hub transfer coefficient matrix
I_F	fore-and-aft pylon inertia (about pivot point), slug-ft^2
I_L	lateral pylon inertia (about pivot point), slug-ft^2
I_n	generalized inertia of n^{th} blade mode, ft-lb-sec^2
I_s	total torsional inertia at top of flexible shaft, slug-ft^2
I_y	inplane inertial force distribution, lb/ft
I_z	out-of-plane inertial force distribution, lb/ft
I_θ	inertial pitching moment distribution, ft-lb/ft
I_∞	total torsional inertia at bottom of flexible shaft, slug-ft^2
IBM_n	inplane bending moment distribution on n^{th} mode, ft-lb
IBM_T	total inplane bending moment distribution, ft-lb
IS_n	inplane shear distribution of n^{th} mode, lb
IS_T	total inplane shear distribution, lb

$\vec{i}, \vec{j}, \vec{k}$	unit vectors in rotating coordinate system
$\vec{i}_b$, $\vec{j}_b$, $\vec{k}_b$	unit vectors in the blade reference system
$[K]$	displacement coefficient matrix in the stability analysis
K_{ij}	element of the displacement coefficient matrix in the stability analysis
k	reduced frequency in the Theodorsen circulation function
k_F	fore-and-aft pylon spring rate, ft-lb/rad
k_L	lateral pylon spring rate, ft-lb/rad
k_s	mast torsional spring rate, ft-lb/rad
k_1	flapping stop spring rate, ft-lb/rad
k_2	flapping spring rate, ft-lb/rad
L	roll component of applied moment in fuselage reference, ft-lb
L'	lift per unit span, positive down, lb/ft
L_{PM}	roll component of applied moment in main (first) pylon reference, ft-lb
L_{PT}	roll component of applied moment in tail (second) pylon reference, ft-lb
L_{RM}	roll component of applied moment in main (first) rotor reference, ft-lb
L_{RT}	roll component of applied moment in tail (second) rotor reference, ft-lb
$L_w^{\bullet}$	roll component of aerodynamic moment caused by vertical acceleration of the fuselage, (ft-lb)/(ft-sec)
l_F	fore-and-aft pylon focal length, ft
l_L	lateral pylon focal length, ft
ℓ	distance from shear center to blade cg distribution, ft
M	blade mass distribution, slug/ft

M	Mach number
$[M]$	acceleration coefficient matrix in the stability analysis
$\vec{M}_A$	aerodynamic moment vector, ft-lb
M_{blade}	three-dimensional Mach number with yawed flow effect
M_{ij}	element of the acceleration coefficient matrix in the stability analysis
M_{PM}	pitch component of applied moment in main (first) pylon reference, ft-lb
M_{PT}	pitch component of applied moment in tail (second) pylon reference, ft-lb
M_{RM}	roll component of applied moment in main (first) rotor reference, ft-lb
M_{RT}	roll component of applied moment in tail (second) rotor reference, ft-lb
M_s	flapping moment due to flapping spring, ft-lb
$M_{\dot{w}}$	pitch component of aerodynamic moment caused by vertical acceleration of the fuselage, (ft-lb)/(ft-sec)
M_y	component of aerodynamic pitching moment about the $\vec{j}$ direction axis, ft-lb
M_z	component of aerodynamic pitching moment about the $\vec{k}$ direction axis, ft-lb
M_θ	total torsional pitching moment distribution, ft-lb/ft
MM	Mach number parameter
mg	gross weight of the rotorcraft, lb
N	yaw component of applied moment in fuselage reference, ft-lb
$N_{\dot{w}}$	yaw component of aerodynamic moment caused by vertical acceleration of the fuselage, (ft-lb)/(ft-sec)
NB	number of blades
NM	total number of modes used in elastic rotor representation

P	a designated point on the rotor blade, as in Figures 3-1 and 3-17
P	roll component of fuselage angular velocity in fuselage body reference, rad/sec
P_{SM}	roll component of fuselage angular velocity in main (first) rotor shaft reference, rad/sec
P_{ST}	roll component of fuselage angular velocity in tail (second) rotor shaft reference, rad/sec
PA	location of pitch axis, normalized on the chord length, positive aft of the leading edge (Reference 18)
PMOM	pitch moment at top of shaft, ft-lb
p	roll component of fuselage angular velocity perturbations, rad/sec
p_b	roll angular velocity of rotating (blade) coordinate system, rad/sec
p_n	value of a polynomial p at time point t_n
$p_n^{(r)}$	value of the r^{th} derivative of the polynomial p at t_n
p_o	initial value of the fuselage roll angular velocity in the stability analysis, rad/sec
Q	pitch component of the fuselage angular velocity in fuselage body reference, rad/sec
Q_{SM}	pitch component of fuselage angular velocity in main (first) rotor shaft reference, rad/sec
Q_{ST}	pitch component of fuselage angular velocity in tail (second) rotor shaft reference, rad/sec
q	pitch component of fuselage angular velocity perturbations, ft/sec
q	dynamic pressure, lb/ft^2
$\bar{q}$	dynamic pressure with vibratory velocity included, lb/ft^2
q_b	pitch angular velocity of rotating (blade) coordinate system, rad/sec

q_o	initial value of the fuselage pitch angular velocity (q) in the stability analysis, rad/sec
q_1, q_2	constants used to calculate Mach number with yawed flow effect
R	components of the fuselage angular velocity in fuselage body reference, rad/sec
R	rotor radius
$\vec{R}_H$	radius vector from fuselage cg to top of mast, ft
RMOM	rolling moment at top of shaft, ft-lb
R_{SM}	yaw component of fuselage angular velocity in main (first) rotor shaft reference, rad/sec
R_{ST}	yaw component of fuselage angular velocity in tail (second) rotor shaft reference, rad/sec
r	yaw component of fuselage angular velocity perturbations, rad/sec
r_b	yaw angular velocity of rotating (blade) coordinate system, rad/sec
$\vec{r}_p$	displacement vector from the hub to the point P on the rotor blade, ft
r_o	initial value of fuselage yaw angular velocity (r) in the stability analysis, rad/sec
r_1	radial attachment point of lead-lag damper, ft
S_x	fore-and-aft shear at top of mast, lb
S_y	lateral shear at top of mast, lb
T	thrust, lb
$T_{M_{ij}}$	element of the Euler angle transformation matrix relating fuselage body reference to main (first) rotor shaft reference
$T_{T_{ij}}$	element of the Euler angle transformation matrix relating fuselage body reference to tail (second) rotor shaft reference
$T[\Psi,\Theta,\Phi]$	Euler angle transformation matrix

TBM_n	torsional moment distribution on n^{th} mode, ft-lb
TBM_T	total torsional moment distribut on, ft-lb
U	magnitude of relative wind, ft/sec
U	fore-and-aft (X) component of fuselage linear velocity in fuselage body reference, ft/sec
$\overline{U}$	magnitude of relative wind with vibratory velocity included, ft/sec
U_P	component of relative wind velocity at P perpendicular to U_T and U_R, positive up, ft/sec
U_R	component of relative wind velocity at P in radial direction, positive outboard, ft/sec
U_T	component of relative wind velocity at P perpendicular to blade-span axis and shaft axis, positive toward trailing edge, ft/sec
$\overline{U}_R$, $\overline{U}_T$, $\overline{U}_P$	components of relative wind at P with blade vibration velocity included, ft/sec
u	fore-and-aft (X) component of fuselage velocity perturbations, ft/sec
u_o	initial value of the fuselage fore-and-aft velocity (u) in the stability analysis, ft/sec
V	lateral (Y) component of fuselage linear velocity in fuselage body reference, ft/sec
V	flight path velocity, ft/sec
$\overline{V}_i$	average value of induced velocity, ft/sec
V_n	component of free-stream velocity in the plane perpendicular to the rotor shaft, ft/sec
V_z	component of free-stream velocity along the centerline to the rotor shaft, positive up, ft/sec
v	resultant wind velocity
v	lateral (Y) component of fuselage velocity perturbations, ft/sec
$\vec{v}_h$	linear velocity of the hub, ft/sec

$\vec{v}_i$	induced velocity at a point on the rotor blade, ft/sec
v_o	initial value of the fuselage lateral velocity (v) in the stability analysis, ft/sec
$\vec{v}_p$	the relative wind velocity at a point P on the rotor blade, ft/sec
v_{sound}	velocity of sound, ft/sec
VBM_n	out-of-plane bending moment distribution on the n^{th} mode, ft-lb
VBM_T	total out-of-plane bending moment distribution, ft-lb
VS_n	out-of-plane shear distribution on n^{th} mode, lb
VS_T	total out-of-plane shear distribution, lb
W	virtual work, ft-lb
W	vertical component of fuselage linear velocity in fuselage body reference, ft/sec
W_x	fore-and-aft component of the weight vector in fuselage body reference, lb
W_y	lateral component of the weight vector in fuselage body reference, lb
W_z	vertical component of the weight vector in fuselage body reference, lb
w	vertical (Z) component of fuselage velocity perturbations, ft/sec
w_o	initial value of the fuselage vertical velocity (w) in the stability analysis, ft/sec
X	component of $\vec{r}_p$ along $\vec{i}$ vector, ft
X_H	fore-and-aft hub displacement, ft
x	radial station, ft
x_h	hub extent (limited by the rotor radius), ft
x_i	i^{th} basic perturbation variable in the stability analysis

$\bar{x}_i$ — i^{th} basic variable in the stability analysis

x_{i_o} — i^{th} basic variable initial value in the stability analysis

$x_{j_{oo}}$ — amplitude of the j^{th} perturbation variable

Y — component of $\vec{r}_p$ along $\vec{j}$ vector, ft

Y_H — lateral hub displacement, ft

Y_n — inplane displacement distribution of n^{th} mode, ft

$\dot{Y}_p$ — component of blade vibration velocity at P in the $\vec{j}_b$ direction, ft/sec

$Y_{\dot{W}}$ — side force component of aerodynamic force caused by vertical acceleration of the fuselage, lb/(ft-sec)

y_i — i^{th} auxiliary perturbation variable in the stability analysis

$\bar{y}_i$ — i^{th} auxiliary variable in the stability analysis

y_{i_o} — initial value of i^{th} auxiliary variable in the stability analysis

Z — component of $\vec{r}_p$ along $-\vec{k}$ vector, ft

Z — out-of-plane displacement of n^{th} mode, ft

$\dot{Z}_p$ — component of blade vibration velocity at P in the $-\vec{k}_b$ direction, ft/sec

$Z_{\dot{W}}$ — vertical component of aerodynamic force caused by vertical acceleration of the fuselage, lb/(ft-sec)

α — angle of attack, rad

$\bar{\alpha}$ — angle of attack with vibratory velocity included, rad

$\underline{\alpha}$ — angle of attack excluding the effect of vertical velocity, rad

α_B — angle of attack at which the aerodynamic pitching moment coefficient curve breaks sharply, rad

α_{Carta} — angle of attack modified for Mach number effect before entering Carta tables

α_{EQU} — the equivalent angle of attack including effects from the circulation function (Reference 18), rad

α_{mod}	angle of attack modified for yawed flow, rad
α_{RD}	reference angle of attack for drag
α_{RL}	reference angle of attack for lift
β	flapping angle, positive up, rad
β_o	"steady" (frequency less than Ω) part of β, rad
β_v	vibratory part of the flapping angle, rad
γ	blade tip sweep angle, rad
Δ a.c.	offset of the blade tip segment aerodynamic center, ft
ΔC_l	increment in lift coefficient due to unsteady aerodynamic effects
ΔC_m	increment in pitching moment coefficient due to unsteady effects
$\Delta\vec{D}_N$	normal drag vector for a blade segment, lb
$\Delta\vec{D}_R$	radial drag vector for a blade segment, lb
Δ_i	i^{th} constant in numerical evaluation of partial derivatives
ΔL	incremental lift, lb
$\Delta\vec{L}$	lift vector for a blade segment, lb
$\Delta\vec{M}$	pitching moment vector for a blade segment, ft-lb
Δr	blade segment length, ft
Δt	increment of time, sec
$\Delta\alpha$	angle of attack increment for stall hysteresis, rad
Θ	Euler pitch angle relating the fuselage body axis system to an inertial axis system, rad
Θ_M	main (first) rotor fore-and-aft tilt angle, positive forward, rad
Θ_T	tail (second) rotor fore-and-aft tilt angle, positive forward, rad

θ	fuselage Euler pitch angle perturbation in the stability analysis, rad
ϑ	total elastic torsion deflection, rad
$\overline{\vartheta}$	geometric pitch with blade vibtation velocity included, rad
ϑ_c	total blade cyclic pitch, rad
$\vartheta_{F/A}$	fore-and-aft cyclic pitch angle, rad
ϑ_{LAT}	lateral cyclic pitch angle, rad
ϑ_n	torsion mode shape, rad
ϑ_o	collective pitch angle, rad
θ_o	initial value of the fuselage Euler pitch angle in the stability analysis, rad
ϑ_o	"steady" (frequency less than Ω) part of the pitch angle, rad
ϑ_p	rigid blade geometric pitch at P, rad
ϑ_{tw}	total twist angle, rad
ϑ_v	vibratory part of the pitch angle, rad
Λ	angle of the relative wind to blade-span axis (yawed flow angle), rad
$\overline{\Lambda}$	Λ with vibratory velocity included, rad
λ	local inflow ratio
λ	eigenvalue of the stability determinant
$\overline{\lambda}$	average inflow ratio
$\overline{\lambda}_i$	average induced velocity divided by the blade tip tangential speed
μ	advance ratio
$\overline{\mu}$	average advance ratio
ρ	air density, slugs/ft^3

Φ	Euler roll angle relating the fuselage body axis system to an inertial axis system, rad
Φ_M	main (first) rotor lateral tilt angle, positive right, rad
Φ_T	tail (second) rotor lateral tilt angle, positive right, rad
ϕ	fuselage Euler roll angle perturbation in the stability analysis, rad
φ	inflow angle, rad
$\bar{\varphi}$	inflow angle with blade vibration velocity included, rad
φ_o	initial value of the fuselage Euler roll angle in the stability analysis, rad
Ψ	Euler yaw angle relating the fuselage body axis system to an inertial axis system, rad
ψ	azimuth of blade-span axis, rad
ψ	fuselage Euler yaw angle perturbation in the stability analysis, rad
ψ_o	initial value of the fuselage Euler yaw angle in the stability analysis, rad
$\dot{\psi}_T$	mast windup velocity, rad/sec
Ω	rotor angular velocity, rad/sec
Ω_k	response frequency used in computing the reduced frequency argument for the circulation function, rad/sec
ω	frequency of oscillation, rad/sec
$\bar{\omega}_b$	angular velocity of the rotating shaft reference system relative to an inertial reference system, rad/sec
∇	backward difference operator
∇^r	operator indicating the r^{th} backward difference